Nonlinear Acoustic Wave Propagation with Diffusion and Relaxation

A thesis submitted to the School of Mathematics at the University of East Anglia in partial fulfilment of the requirements for the degree of Doctor of Philosophy

Eman Aljabali

February/2020

Abstract

A sonic boom is the sound associated with the pressure shock wave generated by disturbances in the atmosphere that lead to rapid increases in pressure over a short time. This research considers the propagation of the finite-amplitude plane waveform involving a balance of nonlinear steepening and other physical dissipation mechanisms. These dissipation mechanisms include the effect of viscosity and molecular relaxation associated with the vibration of polyatomic molecules. When the shock is controlled solely by thermoviscous diffusion the disturbance is governed by Burgers' equation. A comprehensive study is undertaken with the emphasis on shock position, amplitude and thickness. This study is concerned with the applications of the combined approaches of matched asymptotic expansions, Cole-Hopf transformation, the method of characteristics, and numerical schemes such as Fourier pseudo-spectral method and the fourth-order Runge-Kutta method. The augmented Burgers' equation is used when thermoviscosity and relaxation processes are taken into account. An asymptotic analysis of the shock profile is conducted governing the cases of one and two relaxation modes. This analysis reached a descriptive classification of the shock structure based upon the variations in relaxation parameters. The numerical schemes are adopted to simulate the propagation through the relaxing medium, and comparisons are made with the asymptotic findings. Asymptotic predications of the shock thickness, which is controlled by various physical mechanisms, are presented and compared with numerical results.

Contents

List of Figures

List of Tables

Acknowledgements

The first place in these acknowledgements belongs to my supervisor Dr Paul Hammerton for his profuse assistance and dedicated involvement in every step throughout the process. This achievement would not have been possible without his always excellent guidance, priceless advices, continuous support, and the way he responded to my questions and queries so promptly throughout the experimental and thesis work. For which I'm deeply thankful. It was a real privilege and an honour for me to share of his exceptional knowledge but also of his extraordinary human qualities.

Secondly, my deepest gratitude goes to my second supervisor Dr Richard Purvis, whom his insightful notes and simplicity of explanation contributed to notable advancements in my thesis. Furthermore, I mostly grateful for him in helping me learn LaTeX.

I would like to thank my collogues for their rich discussions and constant encouragement, especially Dane Grundy for our scientific discussions, his friendly and noble personality made them enjoyable.

I am also thankful to the University of East Anglia for allowing me the chance to study the PhD program in Mathematics, offering the Personal and Professional Development (PPD) courses, and for all the programs and tools

that they provided.
I would also like gratefully to acknowledge the IT staff for their continuous cooperation. In addition, I would like to thank the staff of the local Support office of the Mathematics department, especially Mrs. Nadia Mobbs for her assistance and consultations. My gratitude is extended to the PGR office team. Moreover, I would like to acknowledge the honourable faculty members who taught me throughout my courses, it has been great working with them.

I would like to acknowledge Imam Muhammad Bin Saud University for providing this opportunity to pursue my post graduate studies, and the Saudi Arabian Cultural Bureau for the graduate Scholarship .

To my mother Fouz Almonee and my family for being my guiding light, inspiration, support, motivation, and especially for always believing in me.

1

Introduction

1.1 Physical Description

1.1.1 Shock Waves

Shock waves are initiated from high amplitude pressure waves that propagate with supersonic velocities through a medium such as earth's atmosphere. Such disturbances are produced, for example, by a supersonic aircraft, explosions, lightning strokes.
Shock waves can be described to be very narrow zones in the fluid where the fluid properties (pressure, density, temperature) chanumericalnge abruptly [55]. The distinctive physical features that make shock waves different from regular sound waves are their supersonic propagation speed and the steep fronts with sharp change. This sudden change in flow properties labels shock waves as discontinuities [54]. For a shock wave that is created by a supersonic aircraft, it is usually followed with an expansion wave. This attached wave known as a rarefaction wave approaches the shock pulse to merge with it eventually and attenuates it.

If a pressure wave with high amplitude is propagating through a medium, nonlinear effects naturally occur. An explanation for the appearance of nonlinear convection is when the pressure amplitude rises: it causes the wave speed to increase. Thus, the wavelets at high pressure are travelling faster than

those at lower pressure [91]. If the initial pressure difference is high enough, the sinusoidal waveform transforms into a sawtooth-shaped wave, and hence the pressure wave becomes a shock wave. Therefore, the cumulative pressure reaches a level where it can not build up any more. Eventually, this compressed disturbance converts to a shock wave. At this point, the wave front slope is tending to infinity; however, the infinitesimal energy absorption prevents the wave from breaking over as in shallow water waves [91]. The sound energy is absorbed by the air due to friction, as air molecules collide with each other. This classical absorption, known as thermoviscosity is one of the dominant mechanisms by which sound energy is absorbed by the air. Therefore, nonlinear steepening of the shock front is competing with the dissipative actions associated with viscosity that smooths this front [55]. At some point, the pressure peak value known as shock amplitude will decrease as some of the energy carried by the wave is absorbed in the air by thermoviscosity and relaxation processes. The width (thickness) of the shock is inversely proportional to its amplitude and can be considered constant as long as the nonlinearity and thermoviscosity effects are balanced [58].

1.1.2 Shock Waves in Relaxing Gas

Molecular relaxation processes are physical influences in which the energy is exchanged between the internal structure of molecules in the fluid [21].
Relaxation processes are equilibrium phenomena, and the presence of an acoustic wave can prevent the process from being in equilibrium. for physical description of a relaxation process, let us assume that a shock front is moving into a molecular gas, then the energy (or temperature) of the gas molecules is altered. The total energy goes initially to increase the translational energy, and it is followed by relaxation from translational mode to rotational mode and also from translational mode to vibrational mode until the equilibrium between these modes is reattained [55]. Each relaxation mode has a characteristic time-scale, and if this time-scale is comparable with the disturbance time-scale,

then the effect of relaxation must be taken into account in the evolution of the disturbance. In polyatomic gases, the molecular vibration would not adjust instantly as in the molecular rotations, this finite time is called relaxation time. Sound frequency is another contributor in determining how close the relaxation process is to the equilibrium state. For linear propagation of harmonic disturbance with relaxation effects included, the phase velocity increases monotonically with signal frequency from the low frequency or equilibrium state of sound speed to the high frequency or frozen sound speed. Therefore, each relaxation process is subject to two parameters; the increment of frozen and equilibrium speeds, and the relaxation time.

In air, the internal vibrational and rotational energies of Nitrogen and Oxygen molecules dominate the relaxation absorption of sound frequencies in the audible range. In seawater, the prime components are Boric acid and Magnesium sulphate which contribute to the acoustic relaxation absorption by seawater over the range of low sound frequencies [21].

1.2 Literature Review

In this section we begin by shedding some light on historical researches and contributions in studying the shock waves phenomena. Then we review the foundations of Burgers' equations in acoustics.

The shock waves' theoretical concept was first tackled in 1759, Euler [30] without mentioning the term shock wave, discussed in his article on the propagation of sound waves the "size of disturbance" of a sound wave referring to the wave amplitude.

In 1808 Poisson [75] settled the foundation of shock theory in his paper "One dimensional movement of air in the case that the velocities of the molecule velocities are no longer very small". Poisson examined mathematically the one-dimensional plane waves of finite amplitude without dissipation and he

determined the solution for the particle velocity as $u = f\big(x - (c+u)t\big)$, with f being an arbitrary function.

Stokes [85] in 1848 pursued the implications of Poisson's solution. He presented the term "surface of discontinuity", to indicate the appearance of a discontinuity and described how the wave became distorted as a result of large values of velocity propagation more rapidly than small values. A discontinuity begins at the time when $\frac{\partial u}{\partial x}$ is infinite.

Earnshaw [28] from his observations of thunder was the first to comment on the time delay between thunder and lightening and he assumed the possibility of thunder propagating at supersonic speeds. Earnshaw [28] in 1858 derived a simple exact solution of the gas motion equation in an implicit form.

The terminology "shock waves" was first introduced by Riemann [80] to describe sound waves of finite amplitude. Riemann [80] in 1858 proposed a practical solution of the gas flow problem by introducing his variables known as "Riemann invariants". He introduced the term "shock compression" and "compression wave" to describe the abrupt steepening of the shock front. Riemann was also the first to attempt to obtain conditions on the jump discontinuity of physical quantities passing through the surface. However, he did not succeed in this matter. The correct relations were later deduced by Rankine [77] and Hugoniot [41].

The first visualization of shock waves in air was by Ernst Mach [59]. He took the historic photograph of a bullet travelling in air and captured the shock wave cone which was later named Mach cone. The experiments of Ernst Mach in acoustics (1878) [60], used electric discharge to generate shock waves, and they proved that the waves generated by an electric spark travels faster than the sound speed.

The detailed analysis of shock wave theory began with the work of Rankine, Hugoniot and Rayleigh. Rankine [77] in 1869 and Hugoniot [41] in 1887 deduced from the conservation laws three fundamental relations governing the

formation of shock waves. Rankine [77] pointed out that the flow process across the shock is irreversible as a consequence of no additional heat from outside the shock and thus the entropy increases across the shock. Hugoniot [41] showed that for non-viscous flow crossing a shock, three relations between the values of density, pressure and velocity on the two sides of the shock can be obtained from the conservation of mass, momentum and energy. Rayleigh [78] in 1910 deduced that in perfect gases the entropy across the shock must be increasing. The classical work by Taylor [88] in 1910 was the first to view the role that viscous effects plays in which the shock discontinuity would be smoothed by viscous dissipative effects. Taylor presented his famous solution describing the steady shock where dissipation and nonlinearity are balanced. The establishment of the modern theory for shock waves waited until the notable work of Whitham [93, 91, 92], and Lighthill [55].

The Hungarian physicist Gyozy Zemplen [94] was first to present this modern and descriptive definition of shock waves in 1905 " A Shock wave is a surface of discontinuity propagating in a gas at which density and velocity experience abrupt changes. One can imagine types of shock waves:(positive) compression shocks which propagate into the direction where the density of the gas is minimum, and (negative) rarefaction waves which propagate into the direction of maximum density."

Many model equations were used for nonlinear acoustical shock waves and one of the well known model equations is Burgers' equation, which this project will consider for the nonlinear propagation of sonic booms. In the next paragraph we present some of the first uses of Burgers' equation, and some the contributions of this equation.

The Burgers' equation characteristic feature, is its simple mathematical form that combines a low-order nonlinear convection term with a higher-order linear diffusion term. Burgers' equation was first introduced by Bateman [3] in 1915.

Later the equation emerged in a mathematical model of turbulence [12, 13] after whom this equation is named.
Burgers' equation is one of the main model equations for the propagation of finite amplitude dissipative waves, many authors attempted successfully to modify equations of finite amplitude sound propagation to be fitted in Burgers' equation type, for example, [6], [7], [47]. Mendousse [65] was first to note the similarity between the acoustic equation and Burgers' equation and introduced it as a model equation in nonlinear acoustics, but his effort was not recognised until a decade later.

Cole [23] and Hopf [40] introduced independently the solution to Burgers' equation by making a transformation which is now known as the Cole-Hopf Transformation to the linear heat equation. Implications of this solution for initial waveforms were studied by Lighthill [55] , Hays [38], Blackstock [18], Whitham [92] and others. Crighton [26] in his survey on nonlinear acoustics, classified Burgers' equation as one of the model equations that has been derived to represent the propogation of nonlinear sound waves. Benton and Platzman [4] presented a tabular survey of thirty five distinct solutions of the one-dimensional Burgers' equation. While Moran and Shen [67] and Leibovich and Seebass [53] showed that Burgers' equation arises from the mathematical techniques of matched asymptotic expansions and multiple scales.

Many of the studies relevant to the effects of nonlinearity in a relaxing medium arise. The early theory of how relaxation processes are established and its role on the relaxed shock is proposed by Lighthill [55] and Pierce [72]. The generalized Burgers' equation which includes geometrical spreading effects and inhomogeneous mediums has been explored by Lighthill [55], Carlton and Blackstock [18], and Fridman [33]. Crighton and Scott [25] implemented the method of matched asymptotic expansions to generate an approximation for the more general case of Burgers' equation including geometric effects. Lighthill [55] suggested that the behaviour for finite small amplitude propagation in a

relaxing gas is governed by Burgers' equation. He presented two classifications for the relaxed shock waves, which is still used to date. The first class is the fully-dispersed shock in which the whole waveform is supported by the relaxing process. The second, partially-dispersed class of shock, begins with a classical viscous shock at its head, followed by a region controlled by the relaxation process.

Clarke and Rodgers [20] analysed the structure of plane shock waves in a gas with several relaxing internal energy modes, and showed with numerical illustrations that internal mode energy contents may overshoot their local equilibrium values. Polyakova, Soluyan and Khokhlov [76] derived simplified equations describing the propagation of small nonlinearity and energy dissipation for slow relaxation processes. Blythe [9] and Ockenden and Spence [69] studied the case for a single relaxation mode, and obtained travelling wave solutions implicitly. They deduced that for some range of parameter values, a single relaxation mode alone is insufficient to support the shock and a narrow sub-shock arises controlled by other mechanisms. Hodgson [39] was first to find that the relaxation is a dominant mechanism in controlling the shock width and showed that the structure of the waves depends on shock strength, ambient pressure, temperature and humidity.

1.3 Aim and Outline

In this thesis we investigate the phenomena of shocks, focusing on the structure of the shock and its amplitude and thickness. We begin by using Burgers' model for waves of small but finite pressure amplitude, restricting attention to one-dimensional propagation. We begin by considering the physical effects of nonlinearity attenuation and viscous dissipation, studying how the solution changes as it progresses. This investigation advances to study the nonlinear propagation in a viscous relaxing gas. In the second part of the thesis we

consider the augmented Burgers' equation accompanied with a set of relaxation equations for the study of the finite-amplitude nonlinear propagation in a relaxing medium.

In the second chapter, we look at Burger's equation in the plane for the nonlinear finite amplitude flow propagating in thermoviscous medium. Each section is devoted to a different technique used to find solution of Burgers' equation.

We begin in section §2.2 by neglecting the viscous effects on the shock wave and Burger's equation is then reduced to the inviscid version. We apply the method of characteristics to look for the exact solutions of the inviscid Burgers' equation. Such solutions resemble wave propagation in a nondissipative medium. Depending on the initial conditions, the method of characteristics may predict the appearance of multivalued solutions as a result of the intersection of characteristic curves. Thus, using the weak shock theory, we consider a weak solution that is associated with these characteristic curves to recover the single-valued solutions by fitting a discontinuity in the waveform which propagates as time advances [7]. This discontinuity that appears after a certain time is called a shock, where the characteristic curves on both sides intersect for the first time with the shock curve. We focus on investigating the dynamics of shock waves such as shock formation, shock location and the interaction of multiple shocks. The Rankine-Hugoniot relation which includes the particle velocity on both sides of the shock can be applied to ascertain the shock location and amplitude (see for instance, Pierce [72] section 11-3). The theory is concluded with an alternative method referred to as equal area rule to fit the shock.

We then include in the second section §2.3 a very small viscous effect in Burgers' equation. In this case we implemented a perturbation method to look for the analytical approximation of the solution. The asymptotic analysis follows the perturbation method proposed by Crighton and Scott [25], and the

shock profile is analysed. An outer solution is deduced form the characteristic solution and for the inner solution a Taylor viscous shock is obtained. The inner and outer expansions are matched to second order and an expression is obtained for the location of the thermoviscous shock. We end the section with results on the shock width which is associated with shock wave asymptotic solutions.

In section §2.4 we use the well known Cole-Hopf transformation to determine an analytical solution of the viscid Burgers' model. We then derive a detailed explanation for the case of significantly small viscosity using the stationary phase method.

Finally in §2.5 we conclude this chapter with a numerical implementation to approximate the solution of the non-linear Burgers' equation. We choose a pseudo-spectral method for spatial discretization using truncated Fourier modes, and the fourth-order Runge-Kutta for time marching. A rectangular unit pulse is defined as the initial representative waveform of the nonlinear problem. The Fourier pseudo-spectral scheme is modified to improve the numerical stability of the solution. We validate the outcomes of the numerical scheme by comparisons with the asymptotic and Cole-Hopf solutions.

In the third chapter, the augmented Burgers' equation is stated for the propagation in viscous and relaxing gases. Each relaxation process is characterised by two parameters, and these parameters are accommodated in a governing equation (Pierce [72] Ch 10-7). Travelling waves in dimensionless form are considered in §3.4 for a single relaxation mode. The asymptotic behaviour of the shock solution is analysed and conditions depending on the order of magnitude of the relaxation parameters are obtained for different classes of shock structure. The analysis clarified that for particular values of the relaxation parameters, the relaxation mode does not fully control the shock and a finer sub-shock controlled by viscosity arises, otherwise the shock is totally governed by the relaxation process. Lighthill [55] referred to the former shock

as partially dispersed and fully-dispersed for the latter shock. We then seek the inner and outer expansions, which are matched to second order to obtain an expression for the shock position. The asymptotic analysis is summed up with a calculations of the shock width by looking at the maximum values of the velocity gradient.

In §3.4.7 we generate a numerical approximation of the travelling wave solution to validate the asymptotic solutions. In §3.5 we seek a numerical solution for the augmented Burgers' equation by applying the numerical approach described earlier in §2.5, with a simple modification to include the relaxation terms. Thus, we use the Fourier pseudo-spectral (FPS) numerical method for discretizing the problem and we then apply fourth-order Runge-Kutta for time marching. We compare the outcomes of this scheme with both numerical and asymptotic solutions of the travelling wave.

The chapter is summed up in §3.5.2 with comparisons between the delicate asymptotic measurements of the maximum slope and the numerically computed results of the FPS method.

In the fourth chapter, we look at one-dimensional small amplitude sound wave propagation subject to thermoviscous dissipation and two vibrational relaxation modes. Since for propagation through the atmosphere, it is believed that the vibrational states of N_2 and O_2 molecules are significant. This chapter therefore is an in-depth analysis where we obtain analytical and numerical solutions in the presence of two relaxation modes. In this chapter, once again, we follow the analysis presented earlier in the third chapter to bring asymptotic and numerical solutions for the travelling wave in the nondimensional form in §4.2. We examine how the shock structure is affected by this combination of thermoviscosity, nonlinearity and the two relaxation processes. In the presence of thermoviscous dissipation and two molecular relaxation modes, in this case the shock may consist of three regimes [44] depending on the relaxation parameters. In §4.2.2 the sensitive shock width with this multiple layers is studied by looking at highest value of the gradient. In §4.3 the Fourier

pseudo-spectral numerical (FPS) method proposed earlier in §3.5 is used with the inclusion of the second relaxation mode. The analysis of augmented Burgers' equation coupled with two relaxation modes ends in §4.3.3 with comparison results of the asymptotic suggestions of the maximum gradient together with the FPS outputs.

In the fifth chapter, we look at the parametric example proposed by Pierce and Kang [73] to estimate the shock waveform of sonic boom shocks on the ground. We use the atmospheric measured values in Pierce and Kang's example to compare our predictions of the pressure profile and shock width with their results. The thesis is then summed up with some conclusion remarks.

2

The Finite-Amplitude Plane Burgers' Equation

2.1 Introduction

The objective of this chapter is to investigate the structure of the shock wave. For this investigation we study the model of plane non-linear finite-amplitude Burgers' equation propagating in a thermoviscous medium. The classical Burgers' equation is expressed as

$$u_t + u\,u_x = \epsilon\,u_{xx}, \qquad \epsilon \ll 1,\ x \in \mathbb{R},\ t \geq 0,$$

combining both non-linear propagation effects and diffusive effects. Here $u(x,t)$ is a particle velocity for position x and time t and the parameter $\epsilon > 0$ represents viscosity. The subscripts u_t and u_x denote the partial differentiation $\frac{\partial u}{\partial t}$, $\frac{\partial u}{\partial x}$ and $u_{xx} = \frac{\partial^2 u}{\partial x^2}$. We explore several analytical and numerical techniques to solve this non-linear PDE. We begin in section §2.2 with the case of vanishing viscosity $\epsilon = 0,$ that is the use of the inviscid Burgers' equation

$$u_t + u\,u_x = 0, \qquad x \in \mathbb{R},\ t \geq 0.$$

We apply the method of characteristics to look for the exact solutions of the inviscid Burgers' equation. Such solutions $u = f(x - u\,t)$ resemble wave propagation in a non-dissipative medium. Depending on the initial conditions,

the method of characteristics may predict the appearance of multivalued solutions as a result of the intersection of characteristic curves. Thus, using the weak shock theory, we consider a weak solution that is associated with these characteristic curves to recover the single-valued solutions by fitting a discontinuity in the waveform which propagates as time advances [7]. This discontinuity that appears after a certain time is called a shock where the characteristic curves on both sides intersect with the shock curve. We focus on investigating the dynamics of shock waves such as shock formation, shock location and the interaction of multiple shocks. The Rankine-Hugoniot relation which includes the particle velocity on both sides of the shock can be applied to ascertain the shock location and amplitude (see for instance, Pierce [72] section 11-3). The Rankine-Hugoniot condition does not determine the waveform uniquely. Using an entropy condition which is obtained from the second law of thermodynamics, the entropy of a gas can only increase as it passes through a shock and therefore the uniqueness can be guaranteed (see for example, Ockendon and Tayler [70]). The theory is concluded with an alternative method referred to as equal area rule to fit the shock.

We then include in the second section §2.3 a very small viscous effect in Burgers' model. Following the analysis presented by Crighton and Scott [25] we implemented the method of matched asymptotic expansions to look for the analytical approximation of the solution. In addition, we explore the shock width which is associated with shock wave asymptotic solutions.

In section §2.4 we use the well known Cole-Hopf transformation to determine an analytical solution of the viscid Burgers' model. We derive a detailed explanation for the case of significantly small viscosity using the stationary phase method. Finally in §2.5 we conclude this chapter with a numerical implementation to approximate the solution of the non-linear Burgers' equation numerically. The numerical chosen method is a combination of the Fourier pseudo-spectral (FPS) method for discretization and the fourth-order Runge-Kutta method for integration. The FPS method is modified to improve the numerical stability of the solution. We validate the outcomes of the numerical scheme by comparisons with the asymptotic solutions.

To understand the Burgers' equation properties such as shock and rarefaction waves which appear as a characteristic features of shock waves, we look for the solutions of three initial value problems of the viscid and inviscid Burgers' model. The three piecewise constant initial profiles are denoted by $\phi_1(x_0)$, $\phi_2(x_0)$ and $\phi_3(x_0)$. The first initial condition $\phi_1(x_0)$ is formed as a rectangular unit pulse and for $\phi_2(x_0)$ and $\phi_3(x_0)$ they consist of two rectangular regions with amplitudes, 2 and 1.

We introduce the first initial condition $\phi_1(x_0)$ with two discontinuities at the points -2 and 2, one of which is an instant shock. The propagation of the disturbance, including the position of the shock for $t > 0$ is explained in detail in the next section. The second and third initial conditions $\phi_2(x_0)$, $\phi_3(x_0)$ are very similar in form with three discontinuities, -2,-1,2 in $\phi_2(x_0)$ and -2,1,2 in $\phi_3(x_0)$. The idea of choosing these two initial profiles in which the disturbance evolves two shocks, is to show the difference in interaction of the two shocks.

$$\phi_1(x_0) = \begin{cases} 0, & x_0 < -2, \\ 1, & -2 < x_0 < 2, \\ 0, & 2 < x_0. \end{cases} \tag{2.1.1}$$

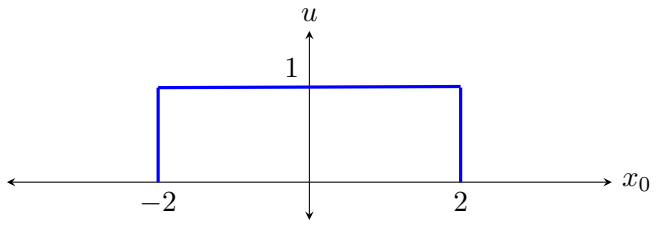

Figure 2.1.1: First initial condition $\phi_1(x_0)$.

$$\phi_2(x_0) = \begin{cases} 0, & x_0 < -2, \\ 2, & -2 < x_0 < -1, \\ 1, & -1 < x_0 < 2, \\ 0, & 2 < x_0. \end{cases} \tag{2.1.2}$$

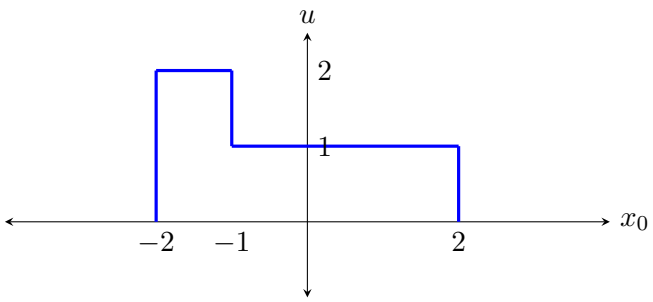

Figure 2.1.2: Second initial condition $\phi_2(x_0)$.

$$\phi_3(x_0) = \begin{cases} 0, & x_0 < -2, \\ 2, & -2 < x_0 < 1, \\ 1, & 1 < x_0 < 2, \\ 0, & 2 < x_0. \end{cases} \tag{2.1.3}$$

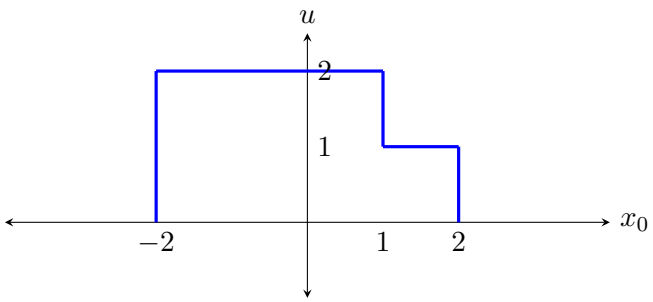

Figure 2.1.3: Third initial condition $\phi_3(x_0)$.

2.2 The Method of Characteristics

2.2.1 Introduction

The aim of the characteristics method is to transform the governing partial differential equation to a set of coupled ordinary differential equations along certain curves known as characteristic curves or simply characteristics in the x and y plane. Many authors covered characteristics theory, for example Liepmann and Roshko [54], Emanuel [29] and Landau and Lifschitz [52]. We followed the analysis in [79] in describing characteristic method. Let us demonstrate a brief algebraic description of the method

2.2.2 General Theory

Consider the first order quasi-linear equation for $u = u(x, y)$:

$$P(x, y, u)\,\frac{\partial u}{\partial x} + Q(x, y, u)\,\frac{\partial u}{\partial y} = R(x, y, u), \tag{2.2.1}$$

where P, Q and R are continuous functions of x, y and u. Suppose that $u = u(x, y)$ represents a surface in the space (x, y, u) which can be written implicitly

$$F(x, y, u) = u(x, y) = u. \tag{2.2.2}$$

Instead of solving the surface we look for spatial curves on which the PDE (2.2.1) is reduced to set of ODEs along these curves. Suppose we choose an arbitrary one-dimension curve $x(s)$, $y(s)$, and want to determine $u(s)$ where s is a parameter that increases along the curve. Applying the chain rule to the rate of change of u we have

$$\frac{\mathrm{d}u}{\mathrm{d}s} = \frac{\partial u}{\partial x}\,\frac{\mathrm{d}x}{\mathrm{d}s} + \frac{\partial u}{\partial y}\,\frac{\mathrm{d}y}{\mathrm{d}s}. \tag{2.2.3}$$

We then rearrange (2.2.3) in order to eliminate the partial derivative $\partial u/\partial x$ from equation (2.2.1). So equation (2.2.3) becomes

$$\frac{\partial u}{\partial x} = \frac{1}{x'(s)}\left[u'(s) - \frac{\partial u}{\partial y}\,y'(s)\right]. \tag{2.2.4}$$

Substituting in (2.2.1) gives

$$\frac{\partial u}{\partial y}\left[Q(x,y,u) - P(x,y,u)\,\frac{y'(s)}{x'(s)}\right] + P(x,y,u)\,\frac{u'(s)}{x'(s)} = R(x,y,u), \tag{2.2.5}$$

where $x'(s)$, $y'(s)$ and $u'(s)$ denote the derivatives of x, y along the arbitrary chosen curve. Equation (2.2.5) is still a PDE due to the remaining partial derivative is $\partial u/\partial y$, but we can choose a curve $x(s), y(s)$ so that the coefficient of $\partial u/\partial y$ vanishes. Hence, we can choose the curve that satisfies

$$\frac{\mathrm{d}y}{\mathrm{d}x} = \frac{\mathrm{d}y/\mathrm{d}s}{\mathrm{d}x/\mathrm{d}s} = \frac{y'(s)}{x'(s)} = \frac{Q(x,y,u)}{P(x,y,u)}. \tag{2.2.6}$$

Any curve satisfying equation (2.2.6) is called a characteristic curve, and along this characteristic curve, equation (2.2.5) becomes

$$\frac{\mathrm{d}u}{\mathrm{d}x} = \frac{R(x,y,u)}{P(x,y,u)}, \tag{2.2.7}$$

which is the second coupled ODE. Thus we can say that the governing equation (2.2.1) is

$$\frac{\mathrm{d}u}{\mathrm{d}x} = \frac{R}{P} \qquad \text{on characteristics where} \qquad \frac{\mathrm{d}y}{\mathrm{d}x} = \frac{Q}{P}. \tag{2.2.8}$$

These two independent ODEs are known as characteristic equations, which can be also written in the form

$$\frac{\mathrm{d}x}{P} \equiv \frac{\mathrm{d}y}{Q} \equiv \frac{\mathrm{d}u}{R}. \tag{2.2.9}$$

Note that if $R = 0$ then equation (2.2.1) becomes

$$P(x,y,u)\,\frac{\partial u}{\partial x} + Q(x,y,u)\,\frac{\partial u}{\partial y} = 0. \tag{2.2.10}$$

Thus, the derivative $\mathrm{d}u/\mathrm{d}x$ in (2.2.8) is zero and hence u is constant on a characteristic curve.

2.2.3 Inviscid Burgers' Model

We apply the method of characteristics using equation (2.2.13) to convert the Inviscid Burgers' initial value problem

$$u_t + u\,u_x = 0, \qquad x \in \mathbb{R},\ t \geq 0, \tag{2.2.11}$$

with the initial condition

$$u(x,0) = u_0(x), \qquad x \in \mathbb{R}, \tag{2.2.12}$$

into the following two fully coupled characteristic ODEs

$$\begin{cases} \frac{\mathrm{d}x}{\mathrm{d}t} = u\big(x(t),t\big), \quad x(0) = \xi, \\ \\ \frac{\mathrm{d}u}{\mathrm{d}t} = 0, \qquad\qquad\quad u(\xi,0) = u_0. \end{cases} \tag{2.2.13}$$

Since $\frac{\mathrm{d}u}{\mathrm{d}t} = 0$ and so $u = u_0$ is a constant on a characteristic curve. Then the characteristic curves $\frac{\mathrm{d}x}{\mathrm{d}t} = u_0$ are straight lines. We can obtain the equation of a particular characteristic curve $x = x(t)$ in (x,t) plane from equation (2.2.13) as follows

$$\frac{\mathrm{d}x}{\mathrm{d}t} = u(x,t) = u(\xi,0) = u_0(\xi).$$

Direct integration of (2.2.3) gives the characteristic curve $x = x(t)$ as follows

$$x = \xi + u_0(\xi)\,t, \tag{2.2.14}$$

where ξ is the x-intercept of the characteristic line. This equation shows that the characteristics are lines in (x,t) plane emanating from $(\xi,0)$ with slope $\frac{1}{u_0(\xi)}$

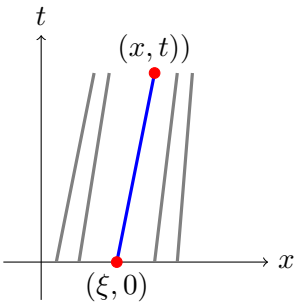

Figure 2.2.1: A characteristic curve for the inviscid Burgers' equation

(see figure 2.2.1). The characteristic equation defines $\xi = \xi(x,t)$ implicitly as a function of x and t. Thus, the solution of the initial value problem (2.2.11), (2.2.12) is given by

$$u(x,t) = u(\xi,0) = u_0(\xi) = u_0(x - u_0\, t), \tag{2.2.15}$$

which we can also present as

$$\begin{cases} u(x,t) = u_0(\xi), \\ \\ x = \xi + u_0(\xi)\, t. \end{cases} \tag{2.2.16}$$

The method of characteristics describes continuous solutions (2.2.16) for the PDE (2.2.11). For a given x, t we look for the characteristic passing through the point (x,t). Then we find the corresponding ξ given implicitly in (2.2.14) and therefore, the solution can be obtain in (2.2.15). However, for some smooth initial waveform u_0, characteristic curves may intersect at a critical time t_b. thus, the point (x_b, t_b) lies on two characteristics with different values of ξ and hence different values of u. The result of this is that the solution u for $t > t_b$ becomes multivalued. In order to define a solution for the PDE (2.2.11) after this critical time we need to allow discontinuities in u. These discontinuities are known as shocks. Let us now derive a detailed description of the shock theory, how they are formed and how to locate them.

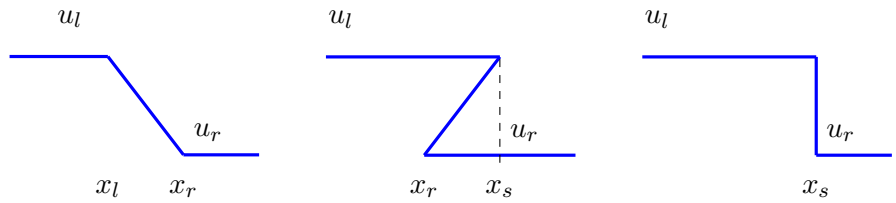

(a) Initial waveform where $u_l > u_r$ and the solution at time t.

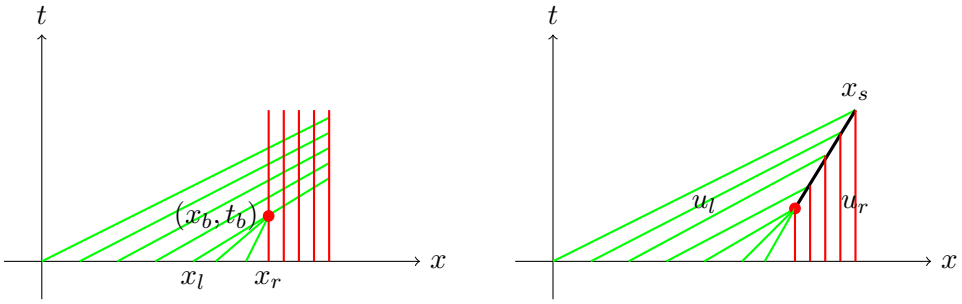

(b) Characteristic curves

Figure 2.2.2: In (a) a plot of initial waveform (left panel), the solution remains single-valued. After such time $t > 0$ the solution becomes multivalued (middle). By fitting a discontinuity at x_s the solution becomes single valued (right panel). In (b) the corresponding characteristic lines emanating from $(\xi, 0)$ with slope $\frac{1}{u_0(\xi)}$. When the green characteristics intersect with the red lines the solution becomes multivalued and then a shock curve $x = x_s$ is fitted.

Shock Wave Formation

To demonstrate the shock appearance let us present a typical initial wave of the inviscid Burgers' equation expressed as

$$u_0(x) = \begin{cases} u_l, & x < x_l, \\ u_l - a\,x, & x_l < x < x_r, \\ u_r, & x_r < x, \end{cases}$$

where $u_0(x), a > 0$ and hence, the wave propagates in the positive direction of x as characteristics have a positive slope. We suppose that the initial profile $u_0(x)$ is decreasing in the interval $[x_l, x_r]$, so $u_0(x_l) > u_0(x_r)$. Figure 2.2.2 (a) shows the propagation of this initial waveform with the corresponding characteristic lines in (b). We can see in figure 2.2.2 (a) that for a fixed x the wave travels faster on the left side of x than the right side of x. This leads to the faster wave overtaking the slower wave, causing the solution to become a multivalued

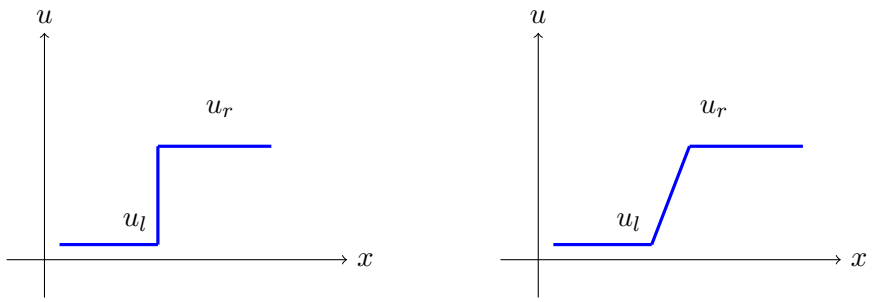

(a) Initial waveform where $u_l < u_r$ and the solution at time t.

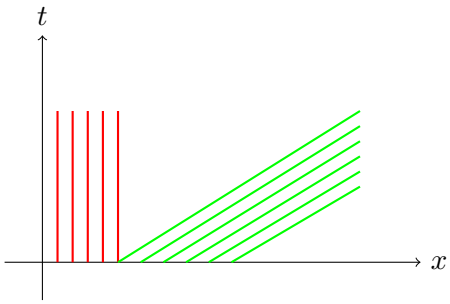

(b) Characteristics for $u_l < u_r$.

Figure 2.2.3: Plot of initial profile for $u_l < u_r$ and the solution propagation for $t > 0$ in (a). In (b) characteristic curves where an area is not covered by characteristics.

at later times (see the middle panel of 2.2.2 (a)). The sketched characteristic lines in figure 2.2.2 (b) (left panel) have the slopes $\frac{1}{u_l(\xi)}$ in the region $\xi < x_l$ and for $\xi > x_r$ have slopes equal to $\frac{1}{u_r(\xi)}$. In the region where $x_l < \xi < x_r$ the characteristic's slope increases with ξ. Thus, for fixed x the characteristics on the right of x are steeper than the left characteristics and so, they must intersect at finite time. Initially the characteristics may not cross and the solution is single-valued (see figure 2.2.2 (b) left panel). However, when characteristics cross say at the point (x_b, t_b), it will lie on two or more different characteristic lines, and thus the solution becomes multivalued at the intersection point. The time at which the first intersection of characteristics happens is a critical time called the breaking time t_b. For some applications a multivalued solution is physically meaningful. For example waves on the surface of a fluid allows overturning of waves. However, in acoustics, where we interpret $u(x,t)$ as the air pressure, multivalued solutions are clearly not meaningful. Therefore the solution $u(x,t)$ is assumed to be unique at each point. So in order that the solution can continue

after passing the breaking time a discontinuity in u is then established. This jump discontinuity is called a shock where the solution suddenly changes values and is formed as follows

$$u(x,t) = \begin{cases} u_l, & x < x_s(t), \\ u_r, & x_s(t) < x, \end{cases} \tag{2.2.17}$$

Here $x = x_s(t)$ represents shock curve. We can see in figure 2.2.2 (b) (right panel) where this situation is treated by fitting the shock jump at x_s. This shock wave will continue to propagate with speed $s(t)$.

This general example showed that for a continuous initial wave of the inviscid Burgers' equation, the solution develops discontinuities. This type of solution is classified with a broader concept than a classical continuously differentiable solution. These types of solutions are referred to as weak solutions. In this case, this solution solves the Burgers' equation (2.2.11) and can contain discontinuities which may not be differentiable [89]. However, in hyperbolic systems, weak solutions do not guarantee uniqueness and it is necessary to support it with an entropy condition to obtain the uniqueness of the weak solution. This entropy condition is valid only when the characteristics enter the shock and the condition becomes invalid if the characteristics are emerging from the shock. Therefore, we can say that the entropy condition is a restriction on weak solutions to eliminate non-physical weak solutions and we can express the entropy condition algebraically

$$f'(u_l) > \frac{f(u_l) - f(u_r)}{u_l - u_r} > f'(u_r) \implies u_l > s > u_r, \tag{2.2.18}$$

where s is the slope of the propagating discontinuity. Thus, a discontinuity in a piecewise continuous weak solution is called a shock if its slope is greater than the slope at u_r but less than the slope at u_l.

We now consider a different initial waveform in which the initial profile $u_0(x)$ is increasing in the interval $[x_l, x_r]$, so $u_0(x_l) < u_0(x_r)$ the characteristic lines do not cross. Also there exists a wedge which is not by any characteristics (see

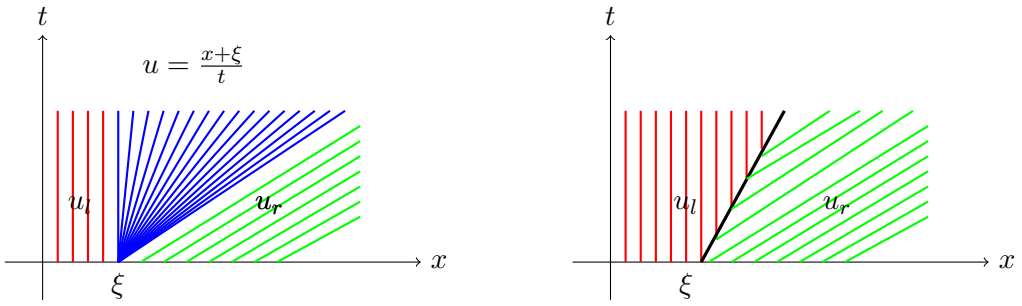

Figure 2.2.4: The characteristics for the rarefaction fan (left) and the rarefaction shock (right). The rarefaction wave is a physically solution, while the rarefaction shock is not.

figure 2.2.3). The method of characteristics does not provide any information about this region, but we have two possibilities for a solution within this region. One possibility is the rarefaction shock [89] (see figure 2.2.4 right panel). This is a weak solution satisfying the PDE (2.2.11). However, since the entropy condition states that for a propagating discontinuity with speed s, the solution must satisfy equation (2.2.18). Thus, this solution will be rejected by the entropy condition. The other possibility, is that characteristic lines emerge out ξ creating a wedged fan called a rarefaction wave

$$u(x,t) = \begin{cases} u_l, & x < \xi + u_l\, t \\ \dfrac{x+\xi}{t}, & \xi + u_l\, t < x < \xi + u_r\, t \\ u_r, & \xi + u_r\, t < x \end{cases} \tag{2.2.19}$$

This rarefaction wave emerges from the point $(\xi, 0)$ into the region $\xi + u_l\, t < x < \xi + u_r\, t$ and spread out as time advances. We can see in figure 2.2.4 (left panel) the rarefaction wave (blue lines). This ends our discussion on the formation of shock and rarefaction waves.

Next we define the concept of the Rankine-Hugoniot jump condition which presents a relation between the shock curve $x_s(t)$ and the solution on the left of the shock u_l and on the right u_r.

The Rankine-Hugoniot jump condition

We introduce the jump condition concept which holds at a discontinuity or a sharp variation in the solution. Let us consider an equation in the form

$$u_t + \Big[\, f(u) \Big]_x = 0, \qquad x \in \mathbb{R},\ t \geq 0, \tag{2.2.20}$$

where $f(u)$ is known as the flux. When the flux is $f(u) = \frac{1}{2}\,u^2$ we obtain the inviscid Burgers' equation (2.2.11). Suppose $x = x_s(t)$ is the shock position where $x_s \in [\xi_l, \xi_r]$. Suppose also that the solution and its derivative are continuous in $\xi_l < x < x_s$ and $x_s < x < \xi_r$. We consider equation (2.2.20) in the integral form by integrating with respect to x over $\xi_l < x < \xi_r$ and hence from (2.2.20), we have

$$\frac{\mathrm{d}}{\mathrm{d}t}\int_{\xi_l}^{\xi_r} u(x,t)\,\mathrm{d}x = -\Big[f(u)\Big]_{\xi_l}^{\xi_r}. \tag{2.2.21}$$

Here Burgers' equation (2.2.20) is written in the conservation law form which states that the rate of change of u is equal to the flux of u across the boundaries. Thus, we can write equation (2.2.21) as

$$\frac{\mathrm{d}}{\mathrm{d}t}\int_{\xi_l}^{\xi_r} u(x,t)\,\mathrm{d}x = f\big(u_l(\xi_l,t)\big) - f\big(u_r(\xi_r,t)\big),$$

where $u_l(x,t)$ is the value of the solution $u(x,t)$ on the left side of the discontinuity and $u_r(x,t)$ is the value of $u(x,t)$ on the right side of the discontinuity i.e $u_l = \lim_{x\to x_s^-} u$ and $u_r = \lim_{x\to x_s^+} u$. Splitting the range of integration at x_s yields

$$\frac{\mathrm{d}}{\mathrm{d}t}\bigg(\int_{\xi_l}^{x_s} u_l(x,t)\,\mathrm{d}x\bigg) + \frac{\mathrm{d}}{\mathrm{d}t}\bigg(\int_{x_s}^{\xi_r} u_r(x,t)\,\mathrm{d}x\bigg) = f\big(u_l(\xi_l,t)\big) - f\big(u_r(\xi_r,t)\big).$$

and by using Leibniz's Rule for differentiation under the integral sign we can write this as

$$\int_{\xi_l}^{x_s} \frac{\partial}{\partial t} u_l \, \mathrm{d}x + \int_{x_s}^{\xi_r} \frac{\partial}{\partial t} u_r \, \mathrm{d}x + \frac{\mathrm{d}x_s}{\mathrm{d}t} \Big(u_l(x_s,t) - u_r(x_s,t) \Big) = f\big(u_l(\xi_l,t)\big) - f\big(u_r(\xi_r,t)\big).$$

In the limit $\xi_l \to x_s^-$ and $\xi_r \to x_s^+$ the two integrals tend to zero and we obtain

$$\begin{aligned} \frac{\mathrm{d}x_s}{\mathrm{d}t} \Big[u_l(x_s,t) \, - \, u_r(x_s,t) \Big] \quad &= \quad \Big[f\big(u_l(x_s,t)\big) - f\big(u_r(x_s,t)\big) \Big] \\ \\ \Longrightarrow \quad \frac{\mathrm{d}x_s}{\mathrm{d}t} \quad &= \quad \frac{f\big(u_l(x_s,t)\big) \, - \, f\big(u_r(x_s,t)\big)}{u_l(x_s,t) \, - \, u_r(x_s,t)}. \end{aligned}$$

This is the general derivation of shock speed. In our case for inviscid Burgers' equation $f(u) = \frac{1}{2}\, u^2$.

$$\begin{aligned} \frac{\mathrm{d}x_s}{\mathrm{d}t} \quad &= \quad \frac{1}{2} \, \frac{{u_l}^2(x_s,t) - {u_r}^2(x_s,t)}{u_l(x_s,t) \, - \, u_r(x_s,t)} \\ \\ &= \quad \frac{1}{2} \Big[\, u_l(x_s,t) + u_r(x_s,t) \, \Big]. \end{aligned} \tag{2.2.22}$$

Therefore, the shock speed is the average of the value of u just in front and behind the shock. Thus, the Rankine-Hugoniot jump condition identifies the shock speed and further determines the shock position at a given time by integrating equation (2.2.22) with respect to t .

Breaking Time

The breaking time is the minimum time at which the first intersection of characteristics occur. So we consider when two characteristic lines cross. Suppose two characteristics emanate initially from the points ξ_l and $\xi_r = \xi_l + \Delta\xi$. For $t \geq 0,$ these characteristics will intersect when

$$\xi_l + u_0(\xi_l)\, t = \xi_r + u_0(\xi_r)\, t.$$

Then the time when intersection happens is

$$t = -\frac{\xi_r - \xi_l}{u_0(\xi_r) - u_0(\xi_l)} = -\frac{\Delta\xi}{u_0(\xi_l + \Delta\xi) - u_0(\xi_l)}.$$

When $\Delta\xi \to 0$ the time will converge to

$$t = \lim_{\Delta\xi \to 0} \left(-\frac{\Delta\xi}{u_0(\xi_r) - u_0(\xi_l)} \right) = \left(-\frac{1}{u'_0(\xi)} \right),$$

over a set of ξ such that $u'_0 < 0$. Hence, the breaking time is at

$$t_b = \min \left(-\frac{1}{u'_0(x)} \right). \tag{2.2.23}$$

Equal Area Rule

The equal area rule is an alternative technique for determining the correct position of the shock. Equal area property is a geometrical technique applied by inserting a discontinuity in the multivalued areas of the wave profile. Since the multivalued curve and the discontinuity curve satisfy the conservation law (2.2.20). Therefore, the equal area rule states that the area under the multivalued curve A_- and the area under the discontinuity curve A_+ must be the same [93]. Figure 2.2.5 shows the discontinuity curve $x_s(t)$ cuts off the area A_- and includes the area A_+ in the waveform in which $A_- = A_+$.

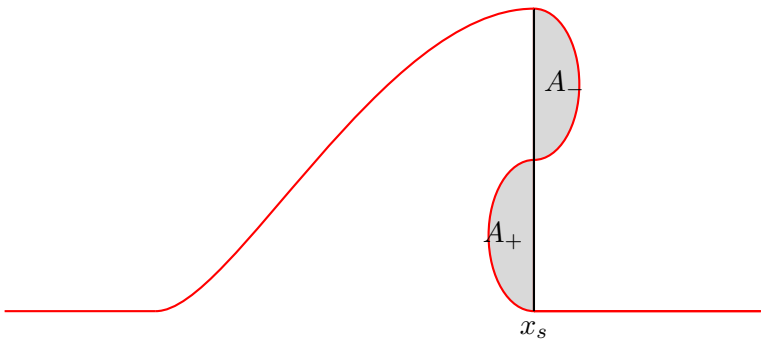

Figure 2.2.5: Equal area establishment of shock position x_s in the multivalued curve where the two areas A_- and A_+ are equal.

The shock in $[\xi_l, \xi_r]$ is constructed with the solution defined in (2.2.16). We consider a continuous solution in $[\xi_l, \xi_r]$. The area under the curve is defined by $A = \int_{\xi_l}^{\xi_r} u(x,t)\,\mathrm{d}x$. We will show that the change in the area as time advances is constant. Using equation (2.2.21) we derive the change of the area as follows

$$\begin{aligned} \frac{\mathrm{d}A}{\mathrm{d}t} &= \frac{\mathrm{d}}{\mathrm{d}t}\int_{\xi_l}^{\xi_r} u(x,t)\,\mathrm{d}x \\ &= \frac{1}{2}\,u^2(\xi_l,t) - \frac{1}{2}\,u^2(\xi_r,t). \end{aligned}$$

If we take ξ_l and ξ_r so that $\frac{1}{2}u^2(\xi_r) = \frac{1}{2}u^2(\xi_l)$ the area then is preserved through time, which means

$$A = \int_{\xi_l}^{\xi_r} u(x,t)\,\mathrm{d}x = \text{Constant in time.}$$

According to this result, the shock line in figure 2.2.6 (a) (right panel) can be mapped back in the initial profile $u_0(\xi)$ as a straight line joining the two points ξ_l and ξ_r (see figure 2.2.6 (a)(left panel). Since the area corresponding to $\xi_l \le \xi \le \xi_r$ is constant, then the equal area rule still holds in the initial curve u_0 and the two shaded areas are equal . Therefore, we can determine the shock position graphically from the initial curve u_0 by drawing chords linking two points in u_0 with the chord cutting off two equal areas.

The equal area rule is also true for the viscous form of Burgers' equation, for certain forms of boundary conditions. So, let us recall the viscous Burgers' equation

$$u_t + u\,u_x = \epsilon\,u_{xx}. \tag{2.2.24}$$

If $\epsilon \neq 0$ the change of the area through time is

$$\begin{aligned}
\frac{\mathrm{d}A}{\mathrm{d}t} &= \frac{\mathrm{d}}{\mathrm{d}t}\int_{\xi_l}^{\xi_r} u(x,t)\,\mathrm{d}x \\
&= -\int_{\xi_l}^{\xi_r} \frac{\partial}{\partial x}\left(\frac{1}{2}\,u^2(x,t)\right)\,\mathrm{d}x + \epsilon\int_{\xi_l}^{\xi_l} \frac{\partial^2}{\partial x^2}\,u(x,t)\,\mathrm{d}x \qquad \text{From (2.2.24)} \\
&= -\left[\,\frac{1}{2}\,u^2(x,t)\,\right]_{\xi_l}^{\xi_r} + \epsilon\left[\,u_x(x,t)\,\right]_{\xi_l}^{\xi_r} \\
\frac{\mathrm{d}A}{\mathrm{d}t} &= \frac{1}{2}\left[\,u^2(\xi_l,t) - u^2(\xi_r,t)\,\right] - \epsilon\left[\,u_x(\xi_l,t) - u_x(\xi_r,t)\,\right]. \qquad (2.2.25)
\end{aligned}$$

If ξ_l and ξ_r are taken so that $\frac{1}{2}u^2(\xi_l,t) = \frac{1}{2}u^2(\xi_r,t)$ and $u_x(\xi_l,t) = u_x(\xi_r,t)$ then the right hand side of equation (2.2.25) is equal to 0 and so the area A is

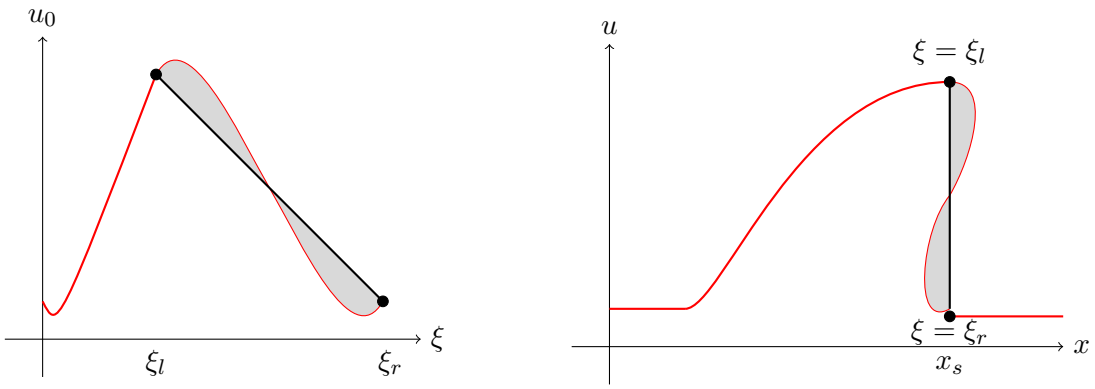

(a) The equal area construction of shock (right panel) in the interval $[\xi_l, \xi_r]$ where the solution is multivalued and (left panel) is the initial waveform

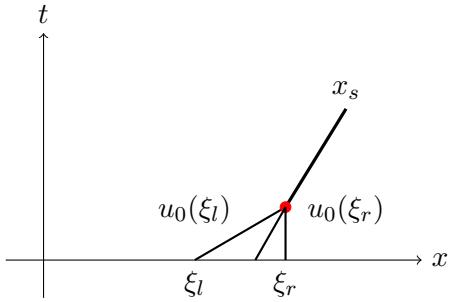

(b) The associated characteristic lines in the (x,t) plane where the two characteristics emerging from ξ_l and ξ_r meet the shock curve xs.

Figure 2.2.6: Equal Area Rule for fitting a shock

constant even if $\epsilon \neq 0$. We consider two classes of waves where this applies. The first class is where $\xi_l = -\infty$ and $\xi_r = \infty$ with $u \to 0$ as $|\xi| \to \infty$. Another class is when the initial wave is periodic with period L, then by the definition of periodic function we can take $\xi_l = \xi_r + L$ the value of the function u at the points ξ_l and ξ_r are the same, and the slope at ξ_l is equal to the slope at ξ_r.

We next apply the method of characteristics to the three types of initial disturbances described earlier in §2.1

Example 1

Let us take the first initial disturbance introduced in §2.1 and deduce the characteristic curves.

$$u(x,0) = \phi_1(x) = \begin{cases} 0, & x < -2, \\ 1, & -2 < x < 2, \\ 0, & 2 < x. \end{cases} \tag{2.2.26}$$

This initial waveform presents an extreme case of wave breaking as this initial state has already a jump discontinuity at $x = 2$ with the value of 1 behind the discontinuity which is greater than that ahead 0. Thus, a shock arises immediately emerging from the point $x = 2$. The characteristic curves are given by $x(t) = \xi + \phi_1(\xi)\, t$ and these are illustrated in figure 2.2.7. If $\xi < -2$, then $\phi_1(\xi) = 0$ which implies $x = \xi$ and $u = 0$ along these curves (see the red lines on the left of figure 2.2.7). If $-2 < \xi < 2$, then $\phi_1(\xi) = 1$ which implies $x = \xi + t$ and $u = 1$ along these curves (black lines in figure 2.2.7). If $\xi > 2$, then $\phi_1(\xi) = 0$ which implies $x = \xi$ and $u = 0$ along these curves (see figure 2.2.7 red lines on the right). Consequently, we have a region $-2 < x < -2 + t$

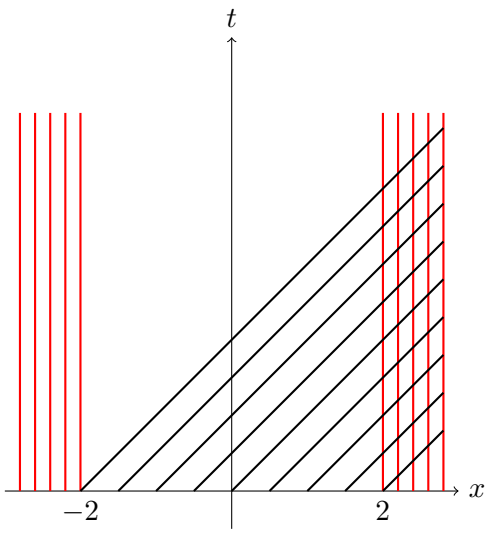

Figure 2.2.7: The projected characteristics for the initial profile ϕ_1.

where no characteristics cross, and the solution forms a rarefaction wave (the

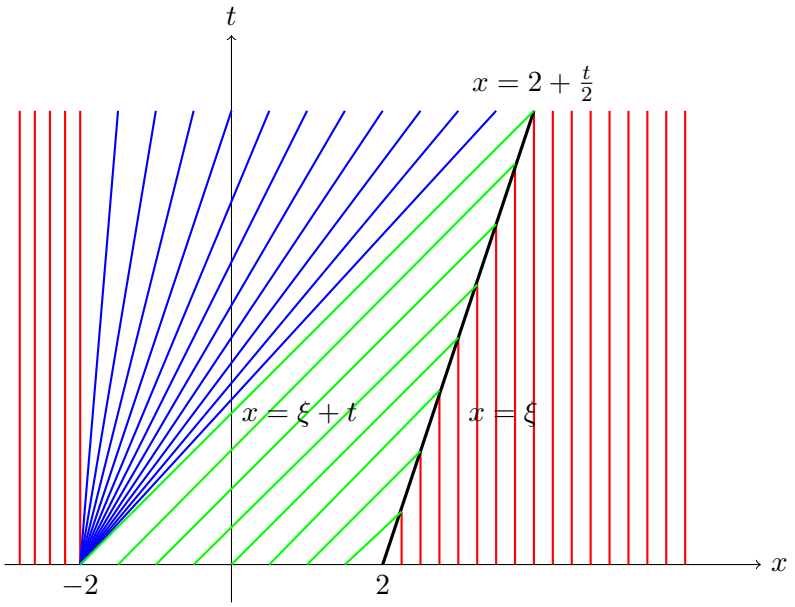

Figure 2.2.8: Characteristics showing shock curve $x = 2 + \frac{t}{2}$ (black) bounded between the characteristics $x = \xi + t$ (green) and $x = \xi$ (red) and rarefaction lines emanating from $\xi = -2$ in blue.

blue lines in figure 2.2.8) as we explained in §2.2.3. The second region where characteristics $x = \xi + t$ (green lines in fig 2.2.8) cross with characteristics $x = \xi$ (red lines) to form a shock curve (black line in figure 2.2.8).

By the Rankine-Hugoniot jump condition, from equation (2.2.22) the speed s_1 of the shock must be

$$\begin{aligned} s_1(t) = \frac{\mathrm{d}x_s}{\mathrm{d}t} &= \frac{1}{2}(u_l(x_s,t) + u_r(x_s,t)) \\ &= \frac{1}{2}(1+0) \\ &= \frac{1}{2} \end{aligned}$$

Therefore, the shock curve is given by

$$x_1 = 2 + \frac{t}{2}. \tag{2.2.27}$$

For simplicity we used the notation x_1 to refer to the position of the first shock

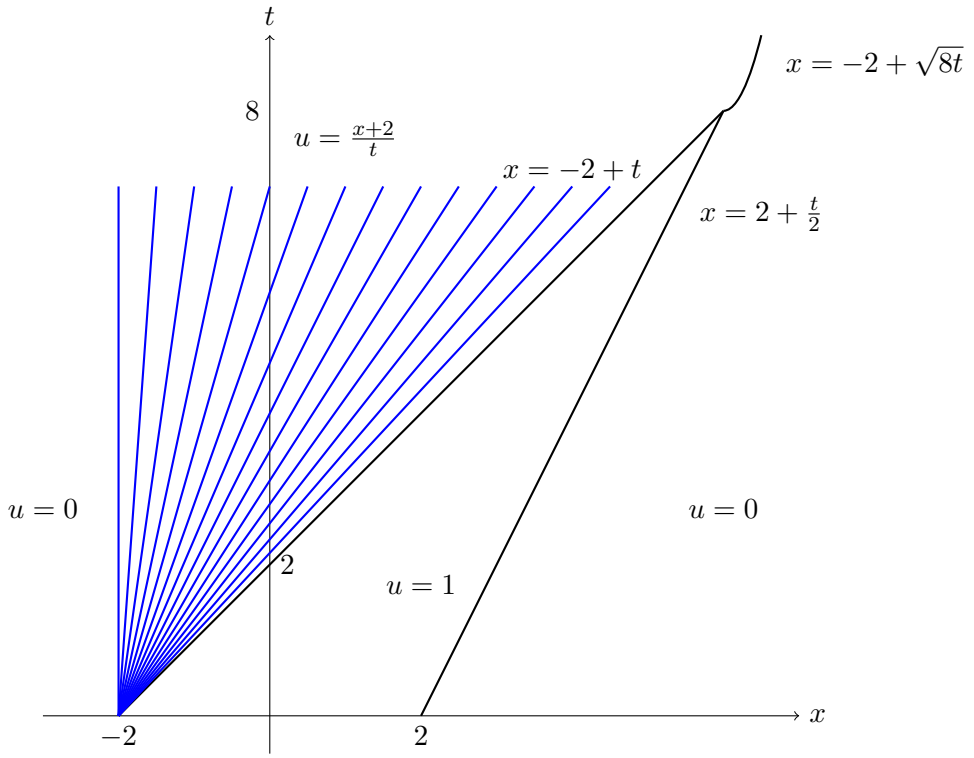

Figure 2.2.9: The characteristics at time $t = 8$, where the rarefaction curve $x = -2 + t$ intersects the shock curve $x_1 = 2 + \frac{1}{2}t$ at the point $(6, 8)$ to form the second shock curve $x_2 = -2 + \sqrt{8t}$.

x_{s_1}. The weak solution of equation (2.2.11) is given by

$$u(x,t) = \begin{cases} 0, & x < -2 \\ \dfrac{x+2}{t}, & -2 < x < -2 + t, \\ 1, & -2 + t < x < 2 + \frac{1}{2}t, \\ 0, & 2 + \frac{1}{2}t < x. \end{cases} \tag{2.2.28}$$

After some time, the rarefaction wave with leading edge $x = -2 + t$ hits the shock curve $x = 2 + t/2$. This happens at $t = 8$, at this time, the shock is located at $x = 6$. Figure 2.2.9 shows the rarefaction fan (blue) $x = -2 + t$ intersect with the shock curve $x = 2 + t/2$ to produce a new shock. For $t > 8$, the solution to the left of the jump is $u^- = (x + 2)/t$ and to the right $u^+ = 0$, and so, the

speed is

$$\begin{aligned} s_2(t) &= \frac{1}{2}\left(u_l(x_s,t)+u_r(x_s,t)\right) \\ &= \frac{1}{2}\left(\frac{x+2}{t}+0\right) \\ &= \frac{x+2}{2\,t} \qquad \text{for } t>8. \end{aligned} \tag{2.2.29}$$

We have found a new shock wave starting from the point $(6,8)$ with speed $s_2(t)=\frac{(x+2)}{2\,t}$. Integrating (2.2.29) to obtain the shock curve

$$\frac{\mathrm{d}x_2}{\mathrm{d}t}=\frac{x_2+2}{2\,t} \implies \int\frac{\mathrm{d}x_2}{x_2+2}=\int\frac{\mathrm{d}t}{2\,t} \implies x_2=-2+\sqrt{8\,t} \tag{2.2.30}$$

and the solution $u(x,t)$ is

$$u(x,t)=\begin{cases} 0, & x<-2, \\ \dfrac{x+2}{t}, & -2<x<-2+\sqrt{8\,t}, \\ 0, & -2+\sqrt{8\,t}<x. \end{cases} \tag{2.2.31}$$

We can see in figure 2.2.10(a) and (b) the shock propagation for $0\le t\le 8,$. the shock forms instantly as the initial waveform has a jump discontinuity at $x=2$. This shock is of amplitude 1 and its front is located at $2+\frac{1}{2}\,t$. When time reaches $t=8$ another shock with different speed is formed, for $t>8$ this shock is located at $x_2=-2+\sqrt{8\,t}$. The wave then changes to the permanent triangular-shaped wave that decays to 0 as time passes with the shock amplitude:

$$u_s(t)=\frac{x_s+2}{t}=\frac{-2+\sqrt{8\,t}+2}{t}=\sqrt{\frac{8}{t}}.$$

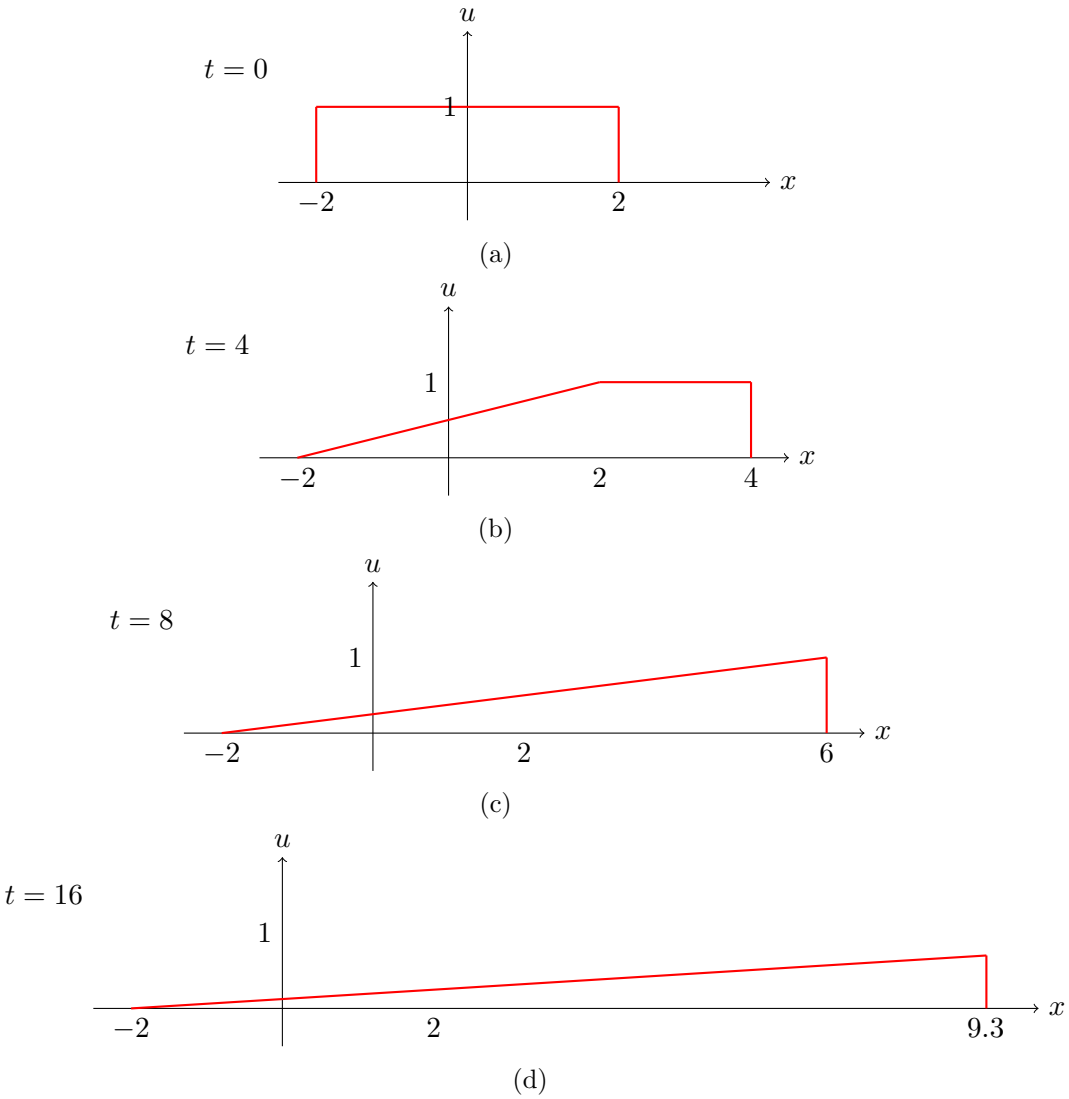

Figure 2.2.10: Plots of the solution $u(x,t)$ for initial condition $u(x,0) = \phi_1(x)$ at times $t = 0, 4, 8, 16$.

We earlier in §2.2.3 described the equal area rule as a geometrical alternative method to find the shock position. According to the equal area rule, if we let A be the area under the curve u when $0 < t < 8$ the solution for this period of time is defined in equation (2.2.28). The equal area rule states that the area A is constant in time, let us now check this statement

$$\begin{aligned} A &= \int_{-\infty}^{\infty} u(x,t)\,\mathrm{d}x \\ &= \int_{-2}^{-2+t} \frac{x+2}{t}\,\mathrm{d}x + \int_{-2+t}^{2+t/2} \mathrm{d}x \\ &= \frac{1}{t}\left[\frac{\big(-2+t\big)^2-4}{2} + 2\Big(\big(-2+t\big)+2\Big)\right] + 4 - \frac{t}{2} \\ &= \frac{1}{t}\left[\frac{1}{2}\Big(4-4\,t+t^2-4\Big)+2\,t\right] + 4 - \frac{t}{2} \\ &= \frac{1}{t}\left[\frac{1}{2}\,t^2\right] + 4 - \frac{t}{2} = 4. \end{aligned}$$

Therefore, the area is constant. For $t > 8$ the solution $u(x,t)$ is defined in equation (2.2.31) and the area is calculated as follows

$$\begin{aligned} A &= \int_{-\infty}^{\infty} u(x,t)\,\mathrm{d}x \\ &= \int_{-2}^{-2+\sqrt{8\,t}} \frac{x+2}{t}\,\mathrm{d}x \\ &= \frac{1}{t}\left[\frac{\big(-2+\sqrt{8\,t}\big)^2-4}{2} + 2\Big(\big(-2+\sqrt{8\,t}\big)+2\Big)\right] \\ &= \frac{1}{t}\left[\frac{1}{2}\Big(4-4\sqrt{8\,t}+8\,t-4\Big)+2\sqrt{8\,t}\right] \\ &= \frac{1}{t}\Big[4\,t\Big] = 4. \end{aligned}$$

Hence, the area is constant and which is the same constant for $t < 8$. Thus, the area under u is $A = 4$.

Example 2

We now look at the characteristics for the second initial waveform

$$u(x,0) = \phi_2(x) = \begin{cases} 0, & x < -2, \\ 2, & -2 < x < -1, \\ 1, & -1 < x < 2, \\ 0, & 2 < x. \end{cases} \tag{2.2.32}$$

The characteristics curves are given by the equation $x_s(t) = \xi + \phi_2(\xi)\, t$. This initial waveform has three discontinuities located at $x = -2, -1, 2$. From our analysis of Example 1, we expect for $t > 0$ to have two instant shocks initially at the points -1 and -2 propagating to the right in addition to a rarefaction wave at -2. Let us focus on the characteristics of these interesting points A, B, C and D positioned at x_1, x_2, x_3 and x_4 illustrated in figure 2.2.11. From the method of characteristics, at time $t > 0$ these points will be located at

$$x_A = -2 + 2t, \quad x_B = -1 + 2t, \quad x_C = -1 + t, \quad x_D = 2 + t.$$

Applying the Rankine-Hugoniot condition defined in (2.2.22) we can determine

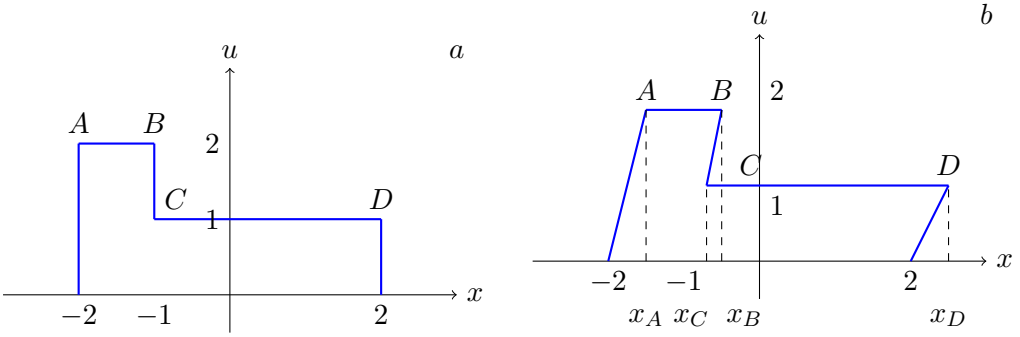

Figure 2.2.11: Initial Waveform $\phi_2(x)$ at $t = 0$ in plot (a), and for $t > 0$ in plot (b)

firstly the speeds for the two shocks and then derive the positions of the two shocks. The speed for the first shock at the point B denoted by s_1 and the

speed for the shock at D denoted by s_2. The values for the two speeds are

$$s_1 = \frac{1}{2}(2+1) = \frac{3}{2} \qquad \text{and} \qquad s_2 = \frac{1}{2}(1+0) = \frac{1}{2}.$$

Thus, the shock curves are $x_1 = -1 + \frac{3}{2}t$ and $x_2 = 2 + \frac{1}{2}t$ and the weak solution is stated as

$$u(x,t) = \begin{cases} 0, & x < -2, \\ \frac{x+2}{t}, & -2 < x < -2+2t, \\ 2, & -2+2t < x < -1+\frac{3}{2}t, \\ 1, & -1+\frac{3}{2}t < x < 2+\frac{1}{2}t, \\ 0, & 2+\frac{1}{2}t < x. \end{cases} \tag{2.2.33}$$

However, since we have two shocks and a rarefaction wave we expect another intersection at finite time, one possibility is the rarefaction wave first intersects with the shock located at $x = x_1$. The second possibility is that the first two shocks cross since the first shock at $x = x_1$ has a larger speed and it will catch the second one. To determine which happens first we look for the time of these intersections, the time when the rarefaction wave crosses the first shock is

$$-2 + 2t = -1 + \frac{3}{2}t \implies t = 2,$$

and the two shocks cross when time t is at

$$-1 + \frac{3}{2}t = 2 + \frac{t}{2} \implies t = 3.$$

Therefore, at $t = 2$, the rarefaction wave hits the first shock curve $x = -1 + \frac{3}{2}t$ at the point (2,2), and a third shock wave is formed emanating from the point $(2, 2)$ with speed $s_3(t)$. Figure 2.2.12 shows the rarefaction fan (blue) collide with the shock curve x_1 (red) to form a third shock. We now consider the position of this new shock for $t \geq 2$. The jump across the shock will satisfy the Rankine-Hugoniot jump condition (2.2.22). Since the solution to the left of the jump is

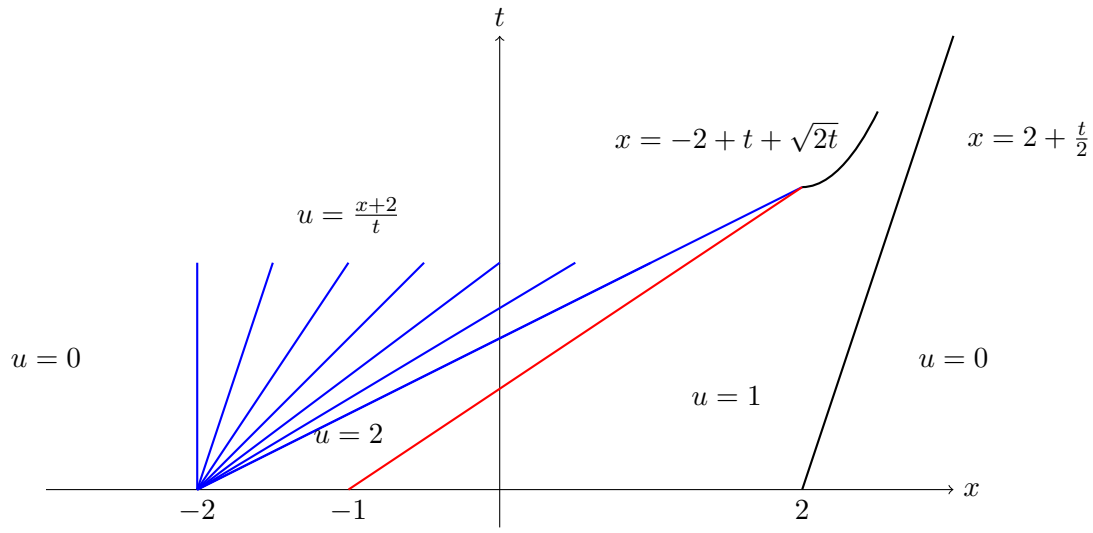

Figure 2.2.12: The rarefaction wave $x = -2 + 2\,t$ (blue lines) intersects with the first shock curve $x_1 = -1 + \frac{3}{2}\,t$ (red curve) at the point $(2, 2)$ to produce the shock curve $x_3 = -2 + t + \sqrt{2\,t}$ which will later intersect with the second shock curve $x_2 = 2 + \frac{t}{2}$.

$u_l = \frac{x+2}{2}$ and to the right $u_r = 1$, the speed is

$$\begin{aligned} s_3(t) &= \frac{1}{2}\Big(u_l(x_3,t) + u_r(x_3,t)\Big) \\ &= \frac{1}{2}\Big(\frac{x_3+2}{t} + 1\Big) \\ &= \frac{x_3+2+t}{2\,t}. \end{aligned}$$

Direct integration of the speed gives the third shock curve as follows

$$\frac{\mathrm{d}x_3}{\mathrm{d}t} = \frac{x_3+2+t}{2\,t} \implies \frac{\mathrm{d}x_3}{\mathrm{d}t} - \frac{1}{2\,t}\,x_3 = \frac{2+t}{2\,t},$$

this is a linear first order ordinary differential equation which can be solved by using the integrating factor $\exp\left(-\int \frac{1}{2t}\,dt\right)$ to obtain

$$\begin{aligned} x_3(t) &= \exp\Big(\int \frac{1}{2t}\,\mathrm{d}t\Big) \int \exp\Big(-\int \frac{1}{2t}\,\mathrm{d}t\Big)\,\frac{2+t}{2\,t}\,\mathrm{d}t \\ &= \sqrt{t}\int \frac{1}{\sqrt{t}}\cdot\frac{2+t}{2\,t}\,\mathrm{d}t \\ &= \sqrt{t}\int \Big(t^{-3/2} + \frac{1}{2}t^{-1/2}\Big)\,\mathrm{d}t \\ &= \sqrt{t}\,\Big(-2t^{-1/2} + t^{1/2} + C\Big). \end{aligned}$$

We can determine the constant C by substituting the point $(2,2)$ in the equation and hence, the third shock curve is

$$x_3 = -2 + t + \sqrt{2\,t} \qquad \text{for } t \geq 2. \tag{2.2.34}$$

The weak solution for $t \geq 2$ is

$$u(x,t) = \begin{cases} 0, & x < -2, \\ \frac{x+2}{t}, & -2 < x < -2 + t + \sqrt{2\,t}, \\ 1, & -2 + t + \sqrt{2\,t} < x < 2 + \frac{t}{2}, \\ 0, & 2 + \frac{t}{2} < x. \end{cases} \tag{2.2.35}$$

Once more the new shock curve $x_3 = -2 + t + \sqrt{2t}$ collides with the second shock curve $x_2 = 2 + \frac{t}{2}$ at some time t resulting a fourth shock. We find the time for the two shocks to intersect which is given by

$$-2 + t + \sqrt{2\,t} = 2 + \frac{t}{2} \implies \sqrt{8\,t} = 8 - t \implies t = 4\big(3 - \sqrt{5}\big) \approx 3.0557.$$

The corresponding position of the shock x_4 is

$$\xi_4 = 2 + \frac{t}{2} = 2 + 2(3 - \sqrt{5}) = 2(4 - \sqrt{5}) \approx 3.55.$$

Thus, at $t = 4\big(3 - \sqrt{5}\big)$ a fourth shock occurs emerges from $\xi_4 = 2(4 - \sqrt{5})$. The speed of the shock is given by equation (2.2.22), where the solution to the left of the jump is $u_l = \frac{x+2}{t}$ and to the right is $u_r = 0$. Hence, the speed of the shock is

$$\begin{aligned} s_4(t) &= \frac{1}{2}\Big(\frac{x_4 + 2}{t} + 0\Big) \\ &= \frac{x_4 + 2}{2\,t}, \qquad \text{for } t > 4\big(3 - \sqrt{5}\big). \end{aligned}$$

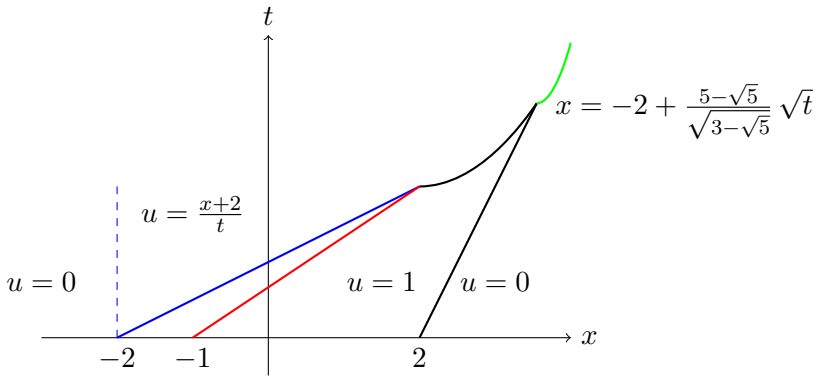

Figure 2.2.13: The shock curve $x = -2 + t + \sqrt{2\,t}$ intersects with the second shock curve $x = 2 + \frac{t}{2}$ at the time $t_1 = 4\big(3 - \sqrt{5}\big)$ a new shock wave (green curve) $x = -2 + \frac{5-\sqrt{5}}{\sqrt{3-\sqrt{5}}}\,\sqrt{t}$ located at $\xi_4 = 2\big(4 - \sqrt{5}\big)$ will be formed.

Direct integration to the speed gives the shock curve position

$$\begin{aligned}
\frac{\mathrm{d}x_4}{\mathrm{d}t} = \frac{x_4 + 2}{2\,t} \quad &\Longrightarrow \quad \int \frac{\mathrm{d}x_4}{x_4 + 2} = \int \frac{\mathrm{d}t}{2\,t} \\
&\Longrightarrow \quad \log\big(x_4 + 2\big) = \frac{1}{2}\log(t) + C_1 \\
&\Longrightarrow \quad x_4 + 2 = C_1\sqrt{t} \\
&\Longrightarrow \quad x_4 = -2 + C_1\sqrt{t}.
\end{aligned}$$

The constant C_1 is determined by inserting the point $\big(2(4-\sqrt{5}), 4(3-\sqrt{5})\big)$ in the above equation as follows

$$C_1 = \frac{x_4 + 2}{\sqrt{t}} = \frac{2(4-\sqrt{5}) + 2}{\sqrt{4(3-\sqrt{5})}} = \frac{(5-\sqrt{5})}{\sqrt{(3-\sqrt{5})}},$$

and hence, the fourth shock curve is

$$x_4 = -2 + \frac{(5-\sqrt{5})}{\sqrt{(3-\sqrt{5})}}\,\sqrt{t} \tag{2.2.36}$$

The weak solution for $t > 4(3-\sqrt{5})$, is given by

$$u(x,t)=\begin{cases}0, & x<-2,\\ \frac{x+2}{t}, & -2<x<-2+\frac{5-\sqrt{5}}{\sqrt{3-\sqrt{5}}}\sqrt{t}\,,\\ 0, & -2+\frac{5-\sqrt{5}}{\sqrt{3-\sqrt{5}}}\sqrt{t}<x.\end{cases} \tag{2.2.37}$$

The solution of the initial value problem of Burgers' equation for the initial condition (2.2.32) is illustrated in figure 2.2.14. We can see in figure 2.2.14 (a), that for $0\le t\le 2$, we have a shock with amplitude 1 located at $x_1=-1+\frac{3}{2}\,t$, and another shock with the same amplitude located at $x_2=2+\frac{t}{2}$. When $2\le t\le 4\big(3-\sqrt{5}\big)$ a new shock located at $x_3=-2+t+\sqrt{2t}$ with amplitude 1 arises together with the second shock mentioned earlier (see figure 2.2.14, (b)). When the time is about $t=4\big(3-\sqrt{5}\big)$ the wave becomes a triangular wave with a shock front located at $x_4=-2+\frac{5-\sqrt{5}}{\sqrt{3-\sqrt{5}}}\sqrt{t}$ (see figure 2.2.14, (c)) and its amplitude is given by

$$u_s(t)=\frac{x_4+2}{t}=\frac{1}{t}\Big(-2+\frac{5-\sqrt{5}}{\sqrt{3-\sqrt{5}}}\sqrt{t}+2\Big)=\frac{5-\sqrt{5}}{\sqrt{t\big(3-\sqrt{5}\big)}}.$$

For large t the solution $u(x,t)$ decays to zero.

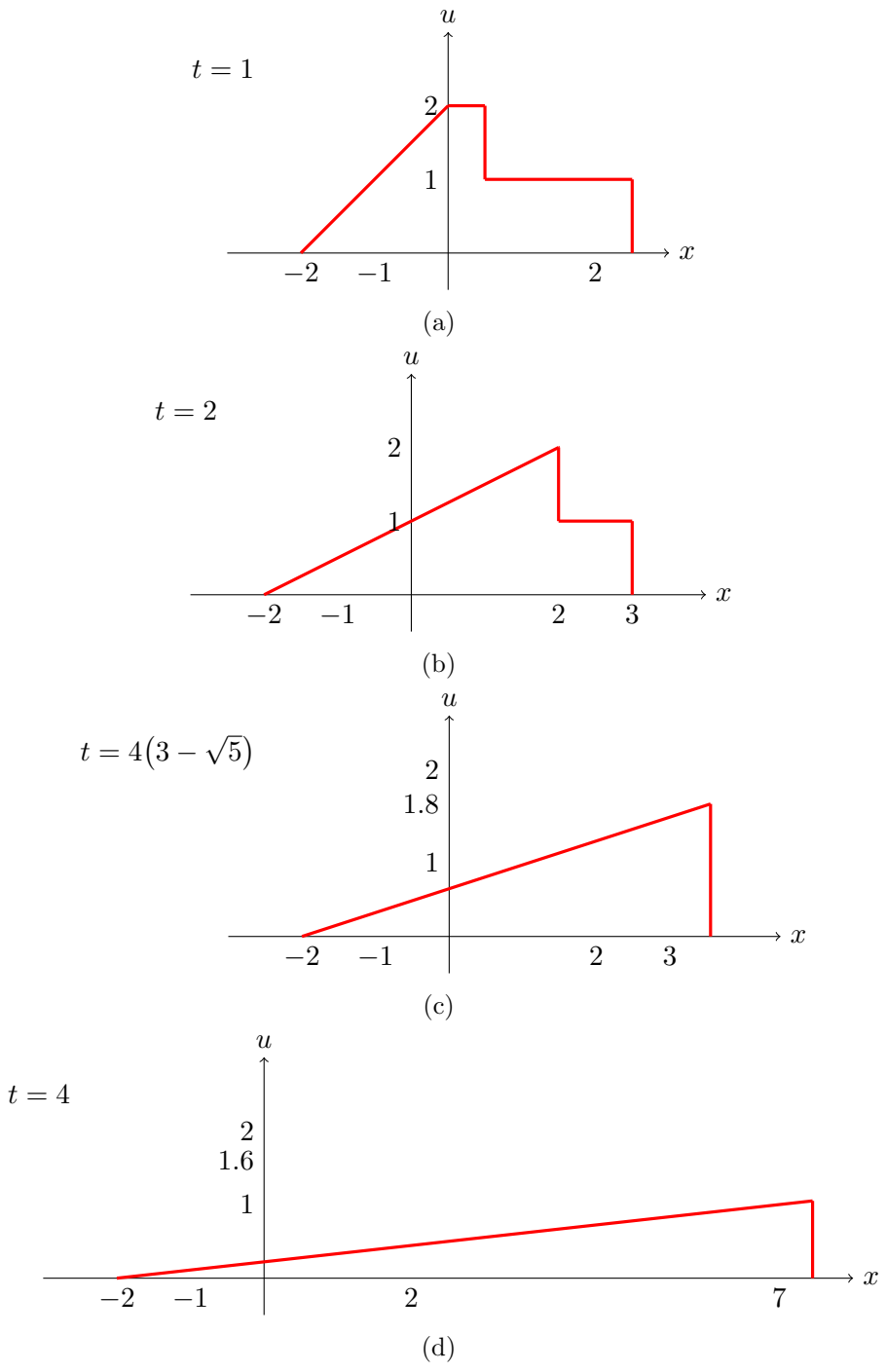

Figure 2.2.14: Plots of the solution $u(x,t)$ for initial condition $u(x,0) = \phi_2(x)$ at times $t = 1,\ 2,\ 4\big(3 - \sqrt{5}\big),\ 4$.

Example 3

We end this section by looking at the third initial waveform. Despite the similarity in form for this example and example 2, however, we will demonstrate how the interaction between shocks differs from an initial profile to another even if the initial curves are similar. Let us remind with the third initial waveform

$$u(x,0) = \phi_3(x_0) = \begin{cases} 0, & x < -2, \\ 2, & -2 < x_< 1, \\ 1, & 1 < x < 2, \\ 0, & 2 < x. \end{cases} \tag{2.2.38}$$

This is similar to the previous example where the initial waveform has three jump discontinuities located at $x = -2,\, 1,\, 2$. The characteristics curves are given by the equation $x(t) = \xi + \phi_3(\xi)\, t$. Thus, we expect to have two instant shocks emerging from these two points in addition to a rarefaction wave at -2. As before let us focus on the characteristics of these interesting points A, B, C and D positioned at x_A, x_B, x_C and x_D. These characterise curves for some time t are located at

$$x_A = -2 + 2t, \quad x_B = 1 + 2t, \quad x_C = 1 + t, \quad x_D = 2 + t. \tag{2.2.39}$$

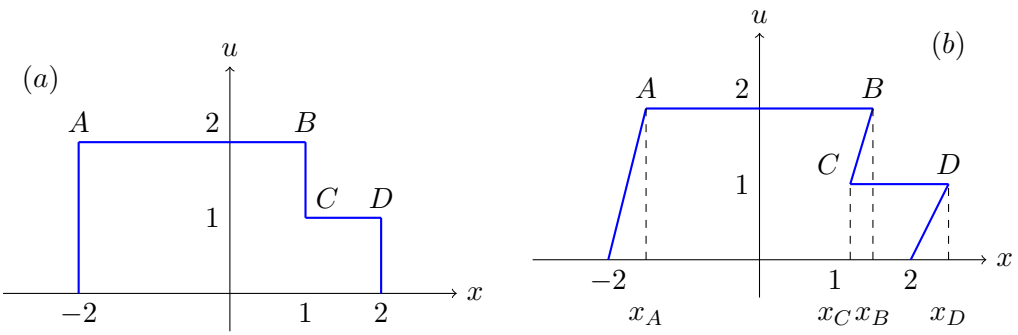

Figure 2.2.15: Initial wave for the initial disturbance $\phi_3(x)$.

In this case, initially the behaviour of solution is similar to the second initial

condition ϕ_2 although we will see how this similarity will change later in time. A rarefaction wave emerges from the point $(-2, 0)$ between $x = -2$ and $x = -2 + 2t$ and two shocks. The Rankine-Hugoniot condition determines the first shock curve located at $x_1 = 1 + \frac{3}{2}t$ travailing in the x direction at speed $s_1 = \frac{3}{2}$ and a second shock in front $x_2 = 2 + \frac{1}{2}t$ travailing at speed $s_2 = \frac{1}{2}$. Thus the solution is given by

$$u(x,t) = \begin{cases} 0, & x < -2, \\ \frac{x+2}{t}, & -2 < x < -2 + 2t, \\ 2, & -2 + 2t < x < 1 + \frac{3}{2}t, \\ 1, & 1 + \frac{3}{2}t < x < 2 + \frac{1}{2}t, \\ 0, & 2 + \frac{1}{2}t < x. \end{cases} \tag{2.2.40}$$

Once again, as we did in second initial waveform, we study the motion of these two shocks and rarefaction through time. Previously, in the second example, when we considered all possible scenarios for those three curves to cross, the first collide was between the rarefaction wave and the first shock. For this example the other possibility will happen first. Thus, the two shocks will cross and they will intersect when the time is at

$$1 + \frac{3}{2}t = 2 + \frac{1}{2}t \implies t = 1, \tag{2.2.41}$$

and the rarefaction wave intersects with the first shock at

$$-2 + 2t = 1 + \frac{3}{2}t \implies t = 6. \tag{2.2.42}$$

Thus, the solution (2.2.40) is valid for $0 \le t \le 1$. At $t = 1$, the first shock curve $x_1 = 1 + \frac{3}{2}t$ will intersect with the second shock curve $x_2 = 2 + \frac{1}{2}t$ at the point $(\frac{5}{2}, 1)$. Figure 2.2.16 shows that before the rarefaction wave at $x = -2 + 2t$ (blue lines) can intersect with any of the two shocks, the shock x_1 collides (red) with shock x_2 (green) to form a third shock. The jump across the shock will satisfy

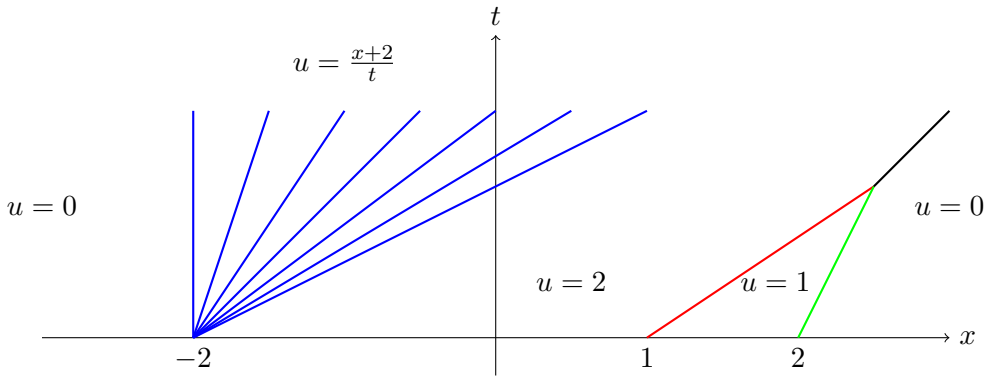

Figure 2.2.16: The first shock curve (red line) hits the second shock curve (the green line) at the point $(\frac{5}{2}, 1)$. A new third shock curve is then produced $x_3 = \frac{3}{2} + t$ (black line) which will later intersect with the rarefaction curve.

the Rankine-Hugoniot jump condition if the solution to the left of the jump is $u_l = 2$ and to the right $u_r = 0$. The speed is obtained

$$\begin{aligned} s_3(t) &= \frac{1}{2}(u_l(x_s, t) + u_r(x_s, t)) \\ &= \frac{1}{2}(2 + 0) = 1. \end{aligned} \tag{2.2.43}$$

Therefore, a third shock wave emanating from the point $(\frac{5}{2}, 1)$ with speed $s_3(t) = 1$. The shock curve is given by

$$\frac{\mathrm{d}x_3}{\mathrm{d}t} = 1 \implies x_3 = \frac{3}{2} + t. \tag{2.2.44}$$

We can write the solution for $t > 1$ as follows

$$u(x,t) = \begin{cases} 0, & x < -2, \\ \frac{x+2}{t}, & -2 < x < -2 + 2\,t, \\ 2, & -2 + 2\,t < x < \frac{3}{2} + t, \\ 0, & \frac{3}{2} + t < x. \end{cases} \tag{2.2.45}$$

We can notice from solution (2.2.45) that the waveform has not reached the triangular form yet, and as time advances we expect a development of another shock. So, once more the rarefaction wave $-2+2t$ hits the new third shock curve

$x_3 = \frac{3}{2} + t$ at

$$-2 + 2\,t = \frac{3}{2} + t \implies t = \frac{7}{2}.$$

Hence, solution (2.2.45) is valued for $1 < t < \frac{7}{2}$ and the newly fourth shock emerges initially from

$$\xi_4 = -2 + 2\,t = -2 + 2\,(\frac{7}{2}) = 5.$$

Figure 2.2.17 shows the intersection between the rarefaction fan (blue) and the third shock (green) to form a fourth shock. We apply the Rankine-Hugoniot jump condition (2.2.22) to give the speed of the shock with the solution to the left of the jump is $u_l = (x+2)/t$ and to the right $u_r = 0$.

$$\begin{aligned} s_4(t) &= \frac{1}{2}\left(\frac{x_4 + 2}{t} + 0\right) \\ s_4(t) &= \frac{x_4 + 2}{2\,t} \end{aligned} \tag{2.2.46}$$

and the shock curve is given by

$$\begin{aligned} \frac{\mathrm{d}x_4}{\mathrm{d}t} = \frac{x+2}{2\,t} \quad &\implies \quad \int \frac{\mathrm{d}x_4}{x+2} = \int \frac{\mathrm{d}t}{2\,t} \\ &\implies \quad \log(x_4 + 2) = \frac{1}{2}\log(t) + C \\ &\implies \quad x_4 + 2 = C\sqrt{t} \\ &\implies \quad x_4 = -2 + C\sqrt{t}. \end{aligned}$$

The constant C can be determined from substituting the point $(5, \frac{7}{2})$ and hence, the position of the fourth shock curve is

$$x_4 = -2 + \sqrt{14\,t}. \tag{2.2.47}$$

Thus, the solution for $t > \frac{7}{2}$ is given by

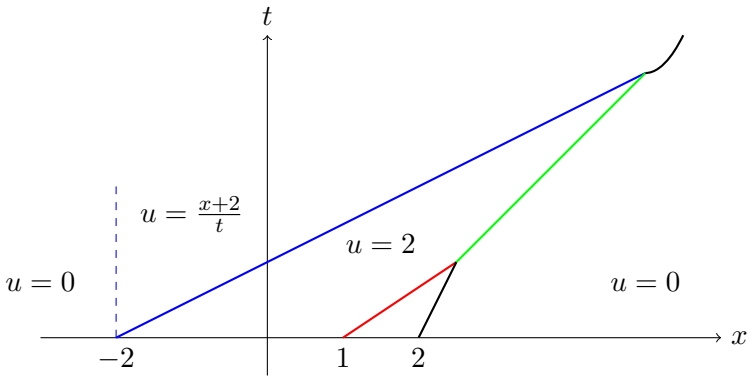

Figure 2.2.17: The rarefaction curve $x = -2+2\,t$ intersects with the third shock curve $x_3 = \frac{3}{2} + t$ (green line) at time $t_1 = 3.5$ and a new fourth shock wave (black curve) $x = -2 + \sqrt{14\,t}$ will emerge from $(5, \frac{7}{2})$.

$$u(x,t) = \begin{cases} 0, & x < -2, \\ \dfrac{x+2}{t}, & -2 < x < -2 + \sqrt{14t}, \\ 0, & -2 + \sqrt{14\,t} < x. \end{cases} \tag{2.2.48}$$

To summarize we can see in figure 2.2.18 (a) that for $0 \le t \le 1$, we have two instant shocks located at $x_1 = 1 + \frac{3}{2}\,t$ and $x_2 = 2 + \frac{1}{2}\,t$ with amplitude 1. When $1 \le t \le \frac{7}{2}$ we have a new third shock located at $x_3 = \frac{3}{2} + t$ with amplitude 2 shown in figure 2.2.18 (b). For $t \ge \frac{7}{2}$ the wave becomes a triangular wave with the shock front at $x_4 = -2 + \sqrt{14\,t}$ and its amplitude is given by

$$u_4(x,t) = \frac{x_4 + 2}{t} = \frac{-2 + \sqrt{14\,t} + 2}{t} = \frac{\sqrt{14}}{\sqrt{t}}. \tag{2.2.49}$$

As in the previous cases when $t \to \infty$ the solution u decays to zero. We can use the equal area property to check the shock curves positions as we demonstrated in example 1.

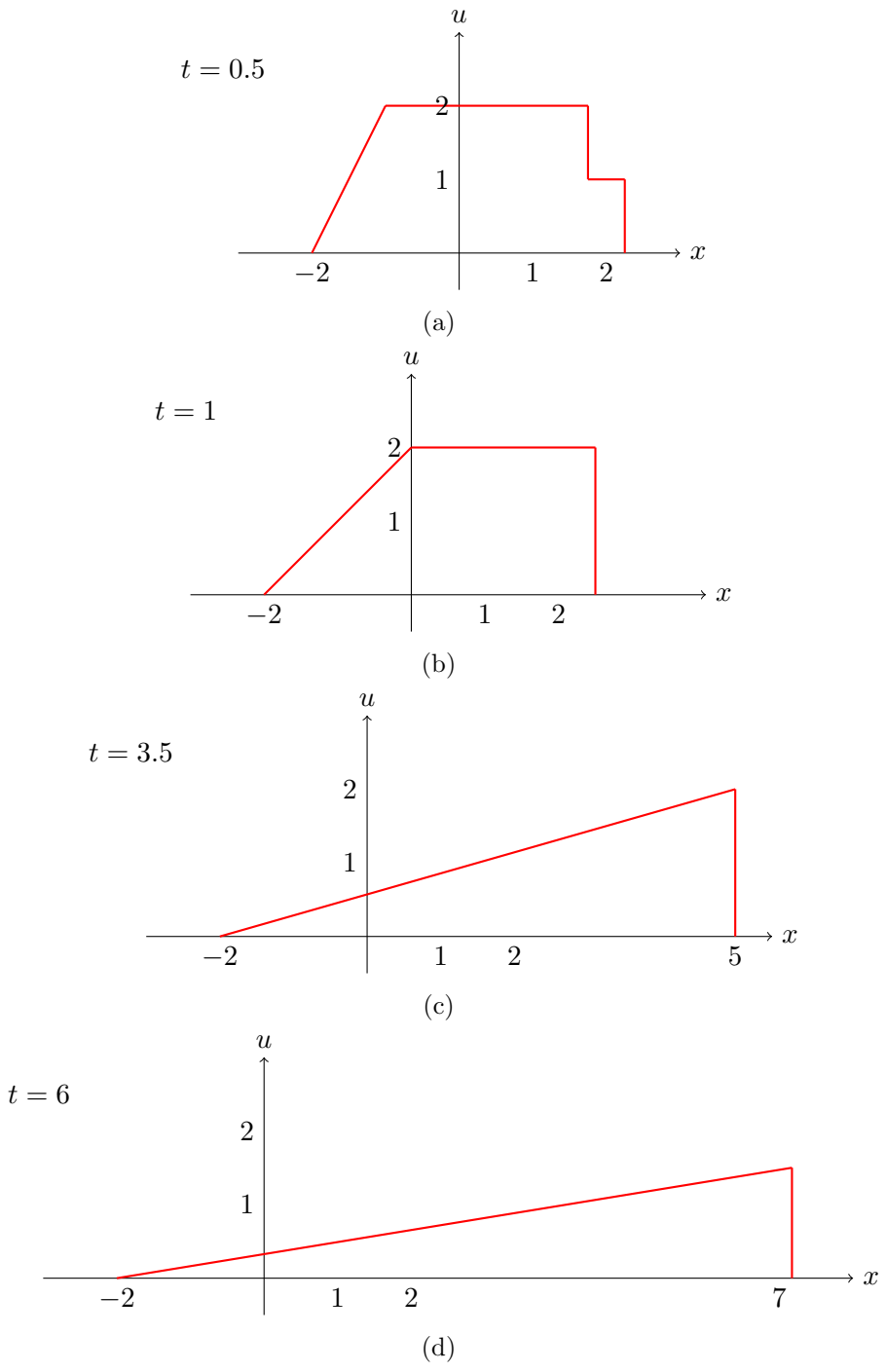

Figure 2.2.18: Plots of the solution $u(x,t)$ for initial condition $u(x,0) = \phi_3(x)$ at time $t = 0.5, 1, 3.5, 6$.

2.2.4 Summary

In this section we illustrated one of the methods to solve the initial value problem of the non-linear inviscid Burgers' equation

$$u_t + u\,u_x = 0, \qquad x \in \mathbb{R},\ t \geq 0, \tag{2.2.50}$$

with the initial condition

$$u(x,0) = u_0(x), \qquad x \in \mathbb{R}. \tag{2.2.51}$$

The method of characteristics provides a solution given by

$$u(x,t) = u(\xi,0) = u_0(\xi) = u_0(x - u_0\,t), \tag{2.2.52}$$

which may be written in the parametric form as follows

$$\begin{cases} u(x,t) = u_0(\xi), \\ x = \xi + u_0(\xi)\,t. \end{cases} \tag{2.2.53}$$

Each point (x,t) for $t \geq 0$ lies on a unique characteristic with velocity u. Since u here is constant along each characteristic, the slope $\frac{\mathrm{d}x}{\mathrm{d}t}$ of each characteristic is constant. Therefore, these characteristics are straight lines with different slopes $\frac{1}{u_0(x_0)}$ which can be determined by the position of the characteristic ξ and the initial data. We looked at solutions of the initial value problem coupled with the three initial profiles ϕ_1 , ϕ_2 and ϕ_3 in each case we showed how the waveform develops a sequences of shocks for such time. The Rankine-Hugoniot jump condition determined the position of these shock discontinuities. An alternative method, the equal area rule can be also used to determine shock position and this was demonstrated for example 1. The formation of the sharp front of the shock wave comes as an abrupt change in flow velocity u followed by a rarefaction wave which travels faster than the shock front and

consequently overtakes the shock. As time progresses each wave developed to a permanent sawtooth-shaped wave. This triangular wave will continue propagating with decreasing amplitude with rate of order $u = O(t^{-1/2})$ and as $t \to \infty$ the wave decays to 0.

In the next sections we will continue exploring more analytical solutions, but with the inclusion of thermoviscous effects (i.e $\epsilon \neq 0$). The next section deals with the method of matched asymptotic expansions for $0 < \epsilon \ll 1$, where we will deduce asymptotic approximations for the first example.

2.3 Asymptotic Solutions of Burgers' Equation

2.3.1 Introduction

In singular perturbations, matched asymptotic expansions is a common analytical approach to approximate the exact solutions. The domain of the differential equation is divided into two or more sub-domains. In one sub-domain the outer expansion is founded by setting $\epsilon = 0$. In the other sub-domains, consisting of inner or boundary layers, this approximation is not adequate for accurate solutions and the perturbations terms are taken into account.

Previously, in the assumption of vanishing viscosity $\epsilon = 0$, we saw in §2.2 how characteristic lines collide resulting a shock. Once the shock is developed the solution then becomes discontinuous. This does not mean that discontinuities will appear in gases, it is rather a simple view to understand the dynamics of the solution. In physical reality, the viscous coefficient has an important role in shock formation. For $\epsilon > 0$ instead of having a discontinuity, the wave is smoothed out by the viscus effects. An interesting results occur in the limit of small viscosity $\epsilon \ll 1$. the convection will cause the wave to steepen and eventually a shock is formed in a very narrow region in which a balance with viscosity is reached [25]. In this section we consider asymptotic solutions in the limit of small viscosity $\epsilon \ll 1$. We utilize the method of matched asymptotic expansions results to study shock structure and shock width. We will show the major role that dissipation processes plays in the thin shock, which also has an effect on the shock width. The increase in viscosity increases shock front width. The shock front width or shock front thickness, is defined to be the range in the spatial variable x in which the solution decreases from 90% of its amplitude to 10% of its amplitude (see for example [88], [3] and [12]), while the shock centre is value of x in which the solution is at 50% of its amplitude [81] see figure 2.3.1.

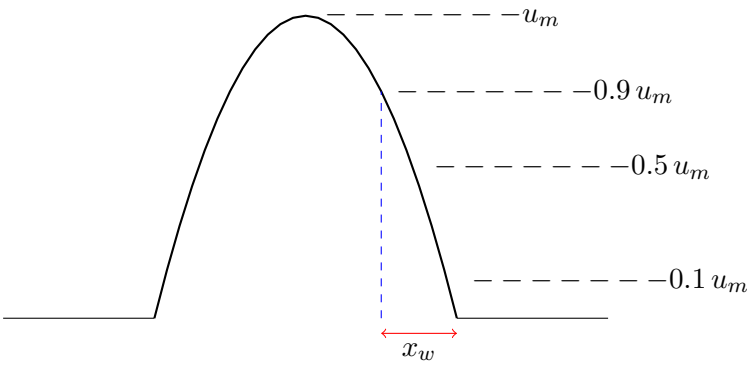

Figure 2.3.1: This figure shows shock wave amplitude u_m ,centre of the shock $x(0.5\,u_m)$ and the shock width $x_w = x(0.1\,u_m) - x(0.9\,u_m)$

2.3.2 General Theory

We now look at the novel work of Crighton and Scott [25] and Schofield and Hammerton [81]. They implemented the method of matched asymptotic expansions to generate an approximation for more general case of Burgers' equation including geometric effects. We introduce a brief explanation of their techniques separately due to the slight difference between them. We begin with the work of Crighton and Scott [25], then consider Schofield and Hammerton [81]. We compare the solutions from the two methods.

Burgers' equation can be generalized to include the effects of cylindrical and spherical spreading:

$$\frac{\partial u}{\partial t} + \frac{j\,u}{2t} + u\frac{\partial u}{\partial x} = \epsilon\frac{\partial^2 u}{\partial x^2}.$$

The integer $j = 0, 1, 2$ corresponds to the cases of plane, cylindrical and spherical wave spreading, respectively. With suitable transformation of variables Crighton and Scott [25] derived the generalised Burgers' equation in dimensionless form as follows

$$\frac{\partial u}{\partial t} + u\frac{\partial u}{\partial x} = \epsilon g(t)\frac{\partial^2 u}{\partial x^2}, \tag{2.3.1}$$

where ϵ is an inverse Reynolds number and

$$g(t) = 1, \quad g(t) = \frac{1}{2}(t + t_0 - 1), \quad g(t) = \exp\Big(\frac{t}{t_0}\Big), \tag{2.3.2}$$

represents the curvature effects for motion with plane, cylindrical and spherical symmetry, respectively in terms of the dimensionless time t and initial time t_0. Crighton and Scott [25] considered the asymptotic solutions of (2.3.1) as $\epsilon \to 0$ for the N-wave problem defined by

$$u(x,1) = \begin{cases} x, & \text{for } |x| < 1, \\ 0, & \text{otherwise.} \end{cases}$$

This standard N-wave is anti-symmetric about $x = 0$ with sharp thin shocks at $x = \pm 1$. Crighton and Scott considered the solutions governing only the region for $x > 0$ and the initial time t_0 is fixed at 1 so that the wave has developed to the sawtooth form as we saw earlier in §2.2.3 that for any attained positive pulse, will eventually approach the form of triangular wave.

We look at the outer expansion for $\epsilon = 0$, the leading term of the outer expansion can be derived by the method of characteristic as follows

$$U_0(x,t) = \begin{cases} \frac{x}{t}, & 0 < x < x_s, \\ 0, & \text{otherwise,} \end{cases} \tag{2.3.3}$$

where $x = x_s$ locates the shock and can be determined by applying the Rankine-Hugoniot jump condition defined in §2.2.3. The Rankine-Hugoniot equation involves the solution to the left of the discontinuity $u^- = \frac{x}{t}$ and to the right $u^+ = 0$, and so, the speed is defined by

$$\begin{aligned} s(T) = \frac{\mathrm{d}x_s}{\mathrm{d}t} &= \frac{1}{2}\Big(u^-(x_s,t) + u^+(x_s,t)\Big) \\ &= \frac{1}{2}\Big(\frac{x}{t} + 0\Big) \\ &= \frac{x}{2\,t}, \end{aligned}$$

and hence, integrating the speed equation we obtain the shock position

$$\frac{\mathrm{d}x}{\mathrm{d}t} = \frac{x_s}{2t} \implies \int \frac{\mathrm{d}x}{x_s} = \int \frac{\mathrm{d}t}{2\,t} \implies x_s(t) = \sqrt{t},$$

where the integration constant is fixed at 1 as $x_s(1) = 1$. This shock has amplitude $t^{-\frac{1}{2}}$ and hence, when $\epsilon = 0$ the solution is defined by

$$U(x,t) = \begin{cases} \frac{x}{t}, & 0 < x < \sqrt{t}, \\ 0, & \text{otherwise.} \end{cases} \tag{2.3.4}$$

For small ϵ the outer expansion is given in the following expression

$$u_{outer}(x,t) = U(x,t) + O(\epsilon).$$

This solution has a jump discontinuity at $x = t^{1/2}$ which must be smoothed off by including the thermoviscous effects in the shock head using some scaling. Crighton and Scott [25] set $X = (x - t^{1/2})/\epsilon$ as the inner variable and the inner expansion is defined as the following expression

$$u_{inner}(x,t) = \widehat{U}(X,t) + \epsilon\,\widehat{V}(X,t) + O(\epsilon^2). \tag{2.3.5}$$

The generalized Burgers' equation (2.3.1) can be written in terms of the inner variable X to become

$$\epsilon u = \frac{1}{2}\,t^{-\frac{1}{2}}\,u_X - u\,u_X + u_{XX}. \tag{2.3.6}$$

Substituting the inner solution (2.3.5) in the generalized Burgers' equation (2.3.2) and hence, the leading order term of the inner expansion can be deduced in the form

$$O(1) \qquad \widehat{U}_{XX} - \widehat{U}\,\widehat{U}_X + \frac{1}{2}t^{-\frac{1}{2}}\,\widehat{U}_X = 0.$$

Solving for $\widehat{U}$, Crighton and Scott [25] derived the leading order term as follows

$$\widehat{U}(X,t) = \frac{1}{2}\,t^{-\frac{1}{2}}\left[1 - \tanh\left(\frac{X - A(t)}{4\,t^{\frac{1}{2}}\,g(t)}\right)\right]. \tag{2.3.7}$$

This is the Taylor's solution [88] describing the thermoviscous shock which combines a balance of convection and diffusion effects. The shock is of

amplitude $t^{-1/2}$ and width $4\,t^{1/2}\,g(t)$ and in terms of the outer variable x it is $4\,\epsilon\,t^{1/2}\,g(t)$ while function $A(t)$ locates the centre of the shock. Crighton and Scott [25] explained two procedures to find $A(t)$. First method is by the integral conservation law, they take the $x-$integral from 0 to $x > t^{1/2}$

$$\frac{\mathrm{d}}{\mathrm{d}t}\int_0^x u\,\mathrm{d}x = \epsilon\,g(t)\Big[\frac{\partial u}{\partial x}(x,t) - \frac{\partial u}{\partial x}(0,t)\Big] + \frac{1}{2}\Big[u^2(x,t) - u^2(0,t)\Big].$$

The second method, which we are interested in, is applying the matched asymptotic expansions. To locate the shock we look at the $O(\epsilon)$ correction term of the inner expansion. Substituting u_{inner} in equation (2.3.1) yields the $O(\epsilon)$ terms

$$\frac{\partial \widehat{V}}{\partial t} + \frac{\partial}{\partial X}\Big(\widehat{U}\,\widehat{V}\Big) - \frac{1}{2}\sqrt{t}\,\frac{\partial \widehat{V}}{\partial X} = g(t)\,\frac{\partial^2 \widehat{U}}{\partial X^2}.$$

Crighton and Scott [25] deduced $\widehat{V}$ explicitly in p.110 equation (3.13) as follows

$$\begin{aligned}
\widehat{V} \quad = \quad & A'(t) - t^{-\frac{1}{2}}\,g(t)\,(y^2\,\operatorname{sech}^2\,y + 2\,y\,\tanh\,y - 1 - 2\,y) \\
& +\ 4\,t^{\frac{1}{2}}\,g'(t)\,\Bigg(y - \tanh\,y\ln(\cosh\,y) + \tanh\,y \\
& +\ \operatorname{sech}^2\,y\,\Big(\frac{y^2}{2} + y\,\ln 2 + \frac{1}{2}\,\mathrm{diln}\big(1+\mathrm{e}^2 y\big)\Big)\Bigg) \\
& +\ G(t)\,\Big(y\,\operatorname{sech}^2\,y + \tanh\,y\Big) + K(t)\,\operatorname{sech}^2\,y.
\end{aligned}$$

Here the variable y is set as $y = \big(X - A(t)\big)/4\,t^{\frac{1}{2}}\,g(t)$ and diln denotes the dilogarithm function, defined by

$$\mathrm{diln}(x) = -\int_1^x \frac{\ln(z)}{z-1}\,\mathrm{d}z,$$

(see Abramowitz and Stegun [1] p 1004). $G(t)$, $K(t)$ are arbitrary functions to be determined by matching.

We now determine $A(t)$ by matching outer and inner solutions, thus, letting

$y \to \pm\infty$ the outer solution becomes

$$\begin{aligned} \lim_{y\to\infty} u_{\text{outer}}(y,t) &\sim t^{-\frac{1}{2}} + \epsilon\, A(t)\, t^{-1}, \qquad x < \sqrt{t}, \\ \lim_{y\to-\infty} u_{\text{outer}}(y,t) &\sim 0, \qquad\qquad\qquad\quad x > \sqrt{t}, \end{aligned}$$

where $x = 4\,\epsilon\, t^{-\frac{1}{2}}\, g(t) + t^{-\frac{1}{2}} + \epsilon\, A(t)\, t^{-1}$ and for the inner expansion we obtain for $x < \sqrt{t}$ and $x > \sqrt{t}$ respectively

$$\begin{aligned} \lim_{y\to-\infty} u_{\text{inner}}(y,t) &\sim t^{-\frac{1}{2}} + \epsilon\Big(A'(t) + t^{-\frac{1}{2}}\, g(t) - 4\, t^{\frac{1}{2}}\, g'(t)\big(1+\ln 2\big) - G(t)\Big), \\ \lim_{y\to\infty} u_{\text{inner}}(y,t) &\sim 0 + \epsilon\Big(A'(t) + t^{-\frac{1}{2}}\, g(t) + 4\, t^{\frac{1}{2}}\, g'(t)\big(1+\ln 2\big) + G(t)\Big). \end{aligned}$$

The first $O(1)$ terms matches automatically and for the $O(\epsilon)$ terms we equate them to zero to have

$$\begin{aligned} A'(t) - A(t)\, t^{-1} + t^{-\frac{1}{2}}\, g(t) - 4\, t^{\frac{1}{2}}\, g'(t)\big(1+\ln 2\big) - G(t) = 0, \qquad x < \sqrt{t}, \\ A'(t) + t^{-\frac{1}{2}}\, g(t) + 4\, t^{\frac{1}{2}}\, g'(t)\big(1+\ln 2\big) + G(t) = 0, \qquad x > \sqrt{t}. \end{aligned}$$

Eliminating the function $G(t)$ yields

$$\frac{\mathrm{d}A}{\mathrm{d}t} - \frac{1}{2} A\, t^{-1} + t^{-\frac{1}{2}}\, g(t) = 0.$$

This is a first order linear ODE and can be solved by the integrating factor method with choosing the integrating factor as t^{-1}, and hence,

$$A(t) = -t^{\frac{1}{2}} \int_1^t \frac{g(t)}{t}\, \mathrm{d}t, \tag{2.3.8}$$

as long as the function $G(t)$ is fixed as

$$G(t) = -4\, t^{\frac{1}{2}}\, g'(t)\big(1+\ln 2\big) - \frac{1}{2} A\, t^{-1}.$$

The function $K(t)$ can be found by looking at the next term of the inner expansion.

This is the Crighton and Scott [25] approach in deriving the outer and inner

expansions and determining shock center.

The second approach by Schofield and Hammerton [81] where they chose to rescale the variables $x^* = t^{-1/2}\,x\,, u^* = t^{1/2}\,u$ and $t^* = \log t$ so that the position and the amplitude of the shock are fixed at the leading order. They then derived the modified generalized Burgers' equation

$$u^*_{t^*} = \frac{u^*}{2} + \left(\frac{x^*}{2} - u^*\right) u^*_{x^*} + \epsilon\, g(t^*)\, u^*_{x^*x^*}, \tag{2.3.9}$$

where in this case the curvature effects for flow in plane, cylindrical and spherical symmetry are

$$g(t^*) = 1, \quad g(t^*) = \frac{1}{2}\exp(t^*), \quad g(t^*) = \exp\Big(\exp(t^*)\Big).$$

Schofield and Hammerton deduced the outer solution as

$$u^*_{outer}(x^*, 0) = \begin{cases} x^*, & \text{for } |x^*| < 1, \\ 0, & \text{otherwise.} \end{cases} \tag{2.3.10}$$

which is identical to the outer solution that Crighton and Scott [25] in (2.3.4) if we inserted the scaling in Crigthon and Scott's outer solution (2.3.4). For the inner expansion, the inner variable was defined as $X^* = (x^* - 1)/\epsilon$ and the inner expansion that Schofield and Hammerton [81] derived is

$$u^*_{inner} = \frac{1}{2}\left[1 - \tanh\left(\frac{X^* + f(t^*)}{4\,g(t^*)}\right)\right] + \epsilon\,\widehat{V}^* + O(\epsilon^2). \tag{2.3.11}$$

The leading term of the inner expansion represents a shock of width $\epsilon\, g(t^*)$ and located at $x^* = 1 - \epsilon\, f(t^*)$ where the function $f(t^*)$ is the $O(\epsilon)$ shift in shock centre. Schofield and Hammerton [81] determined the shock centre $f(t^*)$ by solving for the $O(\epsilon)$ perturbation and determined $\widehat{V}$. For simplicity, they let $\theta =$

$[X^* + f(t^*)]/4\,g(t^*)$ and the $O(\epsilon)$ correction term is deduced as

$$\widehat{V}^* = \frac{1}{8\cosh^2(\theta)}\left[2\,\tilde{A}(t^*)\,p_1(\theta) + \tilde{B}(t^*)\,p_2(\theta) + \tilde{C}(t^*)\,p_3(\theta) + K(t^*)\right]. \quad (2.3.12)$$

where the functions $\tilde{A}$, $\tilde{B}$, $\tilde{C}$ in terms of time are

$$\tilde{A}(t^*) = 4g + 8g', \qquad \tilde{B}(t^*) = -2f' - f, \qquad \tilde{C}(t^*) = 8g',$$

and the functions p_1, p_2, p_3 are defined as

$$\begin{aligned} p_1(\theta) &= \big(2\theta + 1\big)\mathrm{e}^{-2\theta} - 2\theta^2, \\ p_2(\theta) &= 2\mathrm{e}^{-2\theta} - 4\theta + 2, \\ p_3(\theta) &= \Big[2\theta - \ln\Big(2\cosh\theta\Big)\Big]\,\sinh 2\theta - 2\,\mathrm{diln}\big(-\mathrm{e}^{-2\theta}\big) - 2\theta - \mathrm{e}^{-2\theta}. \end{aligned}$$

Matching the inner and the outer expansions as $\theta \to \pm\infty$ produced a composite solution and fixed $f(t^*)$ as

$$f(t^*) = \int_0^{t^*} g(T)\;\mathrm{d}T. \quad (2.3.13)$$

We can Compare the shift the shock center $f(t^*)$ with what Crighton and Scott [25] derived in equation (2.3.8) by substituting $t^* = \log t$ and $\mathrm{d}t^* = \frac{1}{t}\,\mathrm{d}t$ in the function $f(t^*)$

$$f(t^*) = \int_0^{t^*} g(\tau)\,\mathrm{d}\tau = \int_1^{t} \frac{g(\tau)}{\tau}\,\mathrm{d}\tau = -\,t^{-\frac{1}{2}}\,A(t).$$

Next we will apply the matched asymptotic expansions technique to the first initial disturbance considered in §2.1.

2.3.3 Asymptotic Solutions of Rectangular Pulse

We now investigate some interesting results in the limit of small viscosity by employing the method of matched asymptotic expansions to the first initial profile defined in §2.1. In this case when the wave becomes steepened due to convection and a shock is formed in a narrow region which is also controlled by viscosity. We will follow the asymptotic theory of the generalized Burgers' equation discussed in Crighton and Scott [25] together with Schofield and Hammerton [81], dealing only with the plane wave $g(T) = 1$. We will construct the outer and the inner expansions and with suitable combination of the two expansions to find the shock centre.

Previously, in §2.2.3 we derived the characteristic method solutions when $\epsilon = 0$. We now investigate the asymptotic solutions when $\epsilon \to 0$ using matched asymptotic expansions techniques. Away from shock regions the solution for $\epsilon = 0$ is given by the characteristic solutions. Let us recall from §2.1 the initial condition for the rectangular pulse.

$$u(x,0) = \phi_1(x) = \begin{cases} 0, & x < -2, \\ 1, & -2 < x < 2, \\ 0, & 2 < x. \end{cases}$$

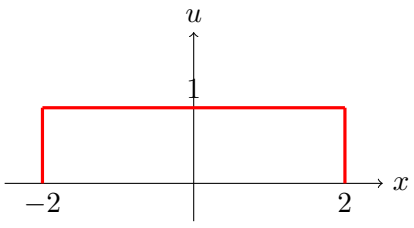

Figure 2.3.2: First initial profile $\phi_1(x,0)$.

In section §2.2.3 we used the method of characteristics for the initial waveform $\phi_1(x)$ and deduced two forms of solution. Since the wave for $0 < t < 8$ takes the shape shown in figure 2.3.3 and subsequently for $t > 8$ it develops the permanent triangular form shown in figure 2.3.4.

Let us begin with the consideration of the solution for $0 < t < 8$.

Asymptotic Solutions of Rectangular Pulse for $0 < t < 8$

For $\epsilon = 0$ in §2.2.3 we obtained the characteristic solution when $0 < t < 8$ as follows

$$U(x,t) = \begin{cases} 0, & x < -2 \\ \frac{x+2}{t}, & -2 < x < -2+t, \\ 1, & -2+t < x < 2+\frac{1}{2}t, \\ 0, & 2+\frac{1}{2}t < x. \end{cases}$$

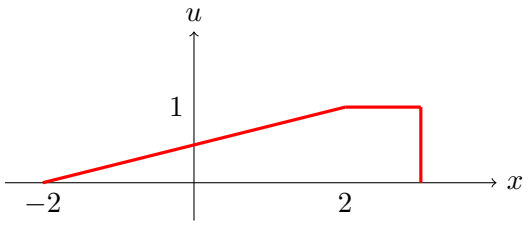

Figure 2.3.3: Wave profile of $\phi_1(x)$ for typical time $t < 8$.

The outer expansion is expressed as

$$u_{outer}(x,t) \sim U(x,t) + o(\epsilon^n), \qquad \text{for all} \quad n > 0. \tag{2.3.14}$$

The outer solution (2.3.3) has a discontinuity at $x = 2 + t/2$ and the solution immediately behind the discontinuity is $U = 1$. In the thin region of discontinuity we use the following rescaling to smooth out this region by a shock

$$X = \frac{1}{\epsilon}\Big(x - 2 - \frac{1}{2}t\Big), \qquad T = t.$$

We then match an inner solution to the outer solution $U = 1$. In the inner region of the shock, the inner expansion is defined by

$$u_{inner} = \widehat{U} + \epsilon\,\widehat{V} + O(\epsilon^2). \tag{2.3.15}$$

For these new variables we have to reform the Burgers' equation and transform the derivatives in terms of X, T.

$$\frac{\partial}{\partial x} = \frac{1}{\epsilon}\frac{\partial}{\partial X}$$

and

$$\begin{aligned}\frac{\partial}{\partial t} &= \frac{\partial T}{\partial t}\frac{\partial}{\partial T} + \frac{\partial X}{\partial t}\frac{\partial}{\partial X} \\ &= \frac{\partial}{\partial T} - \frac{1}{2\epsilon}\frac{\partial}{\partial X}\end{aligned}$$

Substituting these partial derivatives in equation (2.3.1) gives

$$\epsilon\, u_T = \frac{1}{2}u_X - uu_X + u_{XX} \tag{2.3.16}$$

with the boundary conditions $U \to 1$ as $X \to -\infty$ and $U \to 0$ as $X \to \infty$. Substituting inner solution definition (2.3.15) in equation (2.3.16) to obtain

$$\widehat{U}_{XX} - \widehat{U}\widehat{U}_X + \frac{1}{2}\widehat{U}_X + \epsilon\left(\widehat{V}_{XX} - (\widehat{U}\widehat{V})_X + \frac{1}{2}\widehat{V}_X - \widehat{U}_T\right) + O(\epsilon^2) = 0. \tag{2.3.17}$$

Neglecting the $O(\epsilon)$ terms, the $O(\epsilon^0)$ terms determine the leading order of the inner expansion

$$O(1) \qquad \widehat{U}_{XX} - \widehat{U}\widehat{U}_X + \frac{1}{2}\widehat{U}_X = 0.$$

Integrating with respect to X yields

$$\widehat{U}_X - \frac{1}{2}\widehat{U}^2 + \frac{1}{2}\widehat{U} = C_1,$$

with the matching conditions $\widehat{U} \to 1$ as $X \to -\infty$ and $\widehat{U} \to 0$ as $X \to \infty$. Thus, the integration constant fixed at $C_1 = 0$. Once again, we integrate with

respect to X to obtain the inner solution at leading order

$$\begin{aligned}\frac{\partial \widehat{U}}{\partial X} = \frac{1}{2}\Big(\widehat{U}(\widehat{U}-1)\Big) \quad &\Longrightarrow \quad \int \frac{\mathrm{d}\widehat{U}}{\widehat{U}(\widehat{U}-1)} = \int \frac{1}{2}\mathrm{d}X \\ &\Longrightarrow \quad \int \left(\frac{1}{\widehat{U}-1} - \frac{1}{\widehat{U}}\right)\mathrm{d}\widehat{U} = \int \frac{1}{2}\mathrm{d}X \\ &\Longrightarrow \quad \ln\left|\frac{\widehat{U}-1}{\widehat{U}}\right| = \frac{1}{2}\Big(X - A(T)\Big),\end{aligned}$$

where $A(T)$ is an arbitrary function of T. Since we have $0 < \widehat{U} < 1$, this then gives

$$\begin{aligned}\ln\left(\frac{1-\widehat{U}}{\widehat{U}}\right) &= \frac{1}{2}\Big(X - A(T)\Big) \\ \Longrightarrow \frac{\widehat{U}-1}{\widehat{U}} &= \exp\left[\frac{1}{2}\Big(X - A(T)\Big)\right] \\ \Longrightarrow \widehat{U} &= \frac{1}{1+\exp(y)}, \qquad \text{where } y = \frac{1}{2}\Big(X - A(T)\Big).\end{aligned}$$

We multiply the numerator and the denominator by $\exp(-\frac{y}{2})$ to obtain

$$\begin{aligned}\widehat{U} &= \frac{1}{2}\cdot\frac{2\,\exp\left(\frac{-y}{2}\right)}{\exp\left(\frac{-y}{2}\right)+\exp\left(\frac{y}{2}\right)} \\ &= \frac{1}{2}\left[1 - \frac{\exp\left(\frac{y}{2}\right) - \exp\left(\frac{-y}{2}\right)}{\exp\left(\frac{y}{2}\right) + \exp\left(\frac{-y}{2}\right)}\right], \\ &= \frac{1}{2}\left[1 - \tanh\left(\frac{y}{2}\right)\right],\end{aligned}$$

using the definition of the hyperbolic function $\tanh(x) = \frac{\mathrm{e}^x - \mathrm{e}^- x}{\mathrm{e}^x + \mathrm{e}^- x}$. Thus, the leading order term of the inner expansion equation (2.3.15) can be expressed as

$$\widehat{U}(X,T) = \frac{1}{2}\left[1 - \tanh\left(\frac{X - A(T)}{4}\right)\right], \tag{2.3.18}$$

which is a Taylor thermoviscous shock with amplitude 1 and centre $A(T)$, and in terms of the outer variable it is centred at $x = 2 + t/2 + \epsilon\, A(t)$. We can locate the unknown $O(\epsilon)$ shift in shock centre the function $A(T)$ in (2.3.18), by looking for $O(\epsilon)$ correction term to the inner solution and so we will able to identify $A(T)$.

The $O(\epsilon)$ correction term in equation (2.3.17) is

$$O(\epsilon) \qquad \widehat{V}_{XX} - (\widehat{U}\widehat{V})_X + \frac{1}{2}\widehat{V}_x - \widehat{U}_T = 0. \tag{2.3.19}$$

Before integrating (2.3.19) we look for the derivative of $\widehat{U}$ with respect to T and substitute in the fourth term of equation (2.3.19). Thus, the derivative $\widehat{U}_T$ is

$$\begin{aligned} \frac{\partial \widehat{U}}{\partial T} &= \frac{1}{2}\,\frac{\partial}{\partial T}\left[1 - \tanh\left(\frac{X - A(T)}{4}\right)\right] \\ &= \frac{1}{8}\,A'(T)\,\operatorname{sech}^2\left(\frac{X - A(T)}{4}\right). \end{aligned}$$

We now integrate equation (2.3.19) with respect to X, to have

$$\widehat{V}_X - \widehat{U}\widehat{V} + \frac{1}{2}\widehat{V} - \frac{1}{2}\,A'\,\tanh\left(\frac{X - A(T)}{4}\right) = C_2. \tag{2.3.20}$$

Since $\widehat{V} \to 0$ as $X \to \pm\infty$ this yields $A' = 2C_2$ and $-A' = 2\,C_2$, therefore, $A' = C_2 = 0$. Thus we can say the centre of the shock is a constant for all T, i.e. $A(T) = A_0$. We fix the value of the shock centre and then substitute $\widehat{U}$ given in (2.3.18) into equation (2.3.20) to deduce the ODE of $\widehat{V}$ as follows

$$\begin{aligned} \widehat{V}_X &= \frac{1}{2}\left[1 - \tanh\left(\frac{X - A_0}{4}\right)\right]\widehat{V} - \frac{1}{2}\widehat{V} \\ &= -\frac{1}{2}\tanh\left(\frac{X - A_0}{4}\right)\widehat{V}, \end{aligned}$$

solving the ODE for $\widehat{V}$ using the method of separable variable, we arrive at the $O(\epsilon)$ correction term of the inner expansion

$$\widehat{V} = K(T)\,\operatorname{sech}^2\left(\frac{X - A_0}{4}\right). \tag{2.3.21}$$

Substituting $\widehat{U}$ in (2.3.18) and $\widehat{V}$ in (2.3.21) into (2.3.15) gives an expression for the inner expansion formula

$$u_{inner} \sim \frac{1}{2}\left[1 - \tanh\left(\frac{X - A_0}{4}\right)\right] + \epsilon\,K(T)\,\operatorname{sech}^2\left(\frac{X - A_0}{4}\right) + O(\epsilon^2). \tag{2.3.22}$$

The undetermined function $K(T)$ interprets a correction to $A(T)$ or an arbitrary shift in the shock centre. Using a Taylor expansion for tanh and letting $y_0 = \frac{X-A(T)}{4}$

$$\tanh\left(y_0+\epsilon y_1\right) = \tanh\left(y_0\right) + \epsilon y_1 \operatorname{sech}^2\left(y_0\right) + O(\epsilon^2). \tag{2.3.23}$$

The term $K\ \operatorname{sech}^2(y_0)$ just corresponds to replacing A_0 by $A_0 - 2\,\epsilon\,K$, in (2.3.22) so we can absorb this term in $\widehat{U}$.

The Width of Shock Front for $0 < t < 8$

We defined the shock width in §2.3.1 as the range in the spatial variable x in which the shock amplitude decreases from 90% of its value to 10% of its value. We now predict the width of the shock front for the short time period $0 < t < 8$. Then later we make comparisons with numerical results.

Suppose that $u(X_1) = 0.9\,u_m$ and $u(X_2) = 0.1\,u_m$ where u_m represents shock amplitude which is 1. Therefore, the width is defined as $x_{width} = \epsilon(X_2 - X_1)$. Let us now locate X_1 using the knowledge of $u(X_1) = 0.9\,u_m$. The leading order in the inner expansion (2.3.18) defines the shock solution and we have

$$u(X_1) = 0.9\,u_m, \implies u(X_1) = 0.9 \implies \frac{1}{2}\left[1 - \tanh\left(\frac{X_1 - A_0}{4}\right)\right] = 0.9,$$

and hence, X_1 is given by

$$X_1 = 4\,\tanh^{-1}\Big(1 - 2\,(0.9)\Big) + A_0 = -4\,\tanh^{-1}\big(0.8\big) + A_0.$$

We will also locate X_2 by using $u(X_2) = 0.1\,u_m$ as follows

$$u(X_2) = 0.1\,u_m, \implies u(X_2) = 0.1 \implies \frac{1}{2}\left[1 - \tanh\left(\frac{X_2 - A_0}{4}\right)\right] = 0.1,$$

and we deduce X_2 as

$$X_2 = 4\,\tanh^{-1}\Big(1-2\,(0.1)\Big) + A_0 = 4\,\tanh^{-1}\big(0.8\big) + A_0.$$

Hence, the width of the shock front $x_{width} = 8\,\epsilon\,\tanh^{-1}(0.8) \approx 8.78890\,\epsilon$. This width is proportional to the viscosity coefficient, and the width increases with the increase of ϵ.

Asymptotic Solutions of Rectangular Pulse for $t \geq 8$

Following the previous techniques in the case of time is between $0 < t < 8$, we now look for the outer and the inner expansions when $t > 8$. We begin with the derivation of outer solution for $\epsilon = 0$ by recalling the characteristic solution when $t > 8$. This was deduced in §2.2.3 as follows

$$\hat{u}(x,t) = \begin{cases} 0, & x < -2, \\ \frac{x+2}{t}, & -2 < x < x_s, \\ 0, & x_s < x, \end{cases}$$

with the shock located at $x_s = -2 + \sqrt{8t}$.

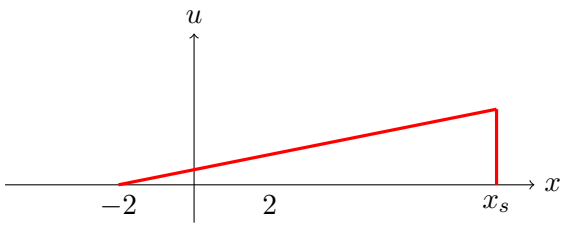

Figure 2.3.4: The propagating shock wave of $\phi_1(x)$ for a typical time $t > 8$.

The outer expansion formula is

$$u_{outer}(x,t) \sim U(x,t) + \epsilon\,V + O(\epsilon^2). \tag{2.3.24}$$

For matching purposes we express the outer expansion in terms of the inner variable X, using the scaling $x = x_s + \epsilon\,X$ and hence, $X = \frac{1}{\epsilon}(x + 2 - \sqrt{8t})$ and

$T = t$. Thus, the outer solution in terms of inner variables is

$$\begin{aligned} u_{outer}(X,T) &= \frac{x+2}{t} \\ &= \frac{x_s + \epsilon\, X + 2}{T} \\ &= \frac{-2+\sqrt{8T}+2}{T} + \epsilon\,\frac{X}{T} \\ &= \sqrt{\frac{8}{T}} + \epsilon\,\frac{X}{T}. \end{aligned} \tag{2.3.25}$$

The inner expansion expressed as

$$u_{inner} \sim \widehat{U} + \epsilon\widehat{V} + O(\epsilon^2). \tag{2.3.26}$$

For these new variables we have to reform the Burgers' equation and rewrite the derivatives in terms of X, T which are

$$\frac{\partial}{\partial x} = \frac{1}{\epsilon}.\frac{\partial}{\partial X}, \qquad \text{and} \qquad \begin{aligned} \frac{\partial}{\partial t} &= \frac{\partial T}{\partial t}.\frac{\partial}{\partial T} + \frac{\partial X}{\partial t}.\frac{\partial}{\partial X}, \\ &= \frac{\partial}{\partial T} - \frac{1}{\epsilon}\,\frac{1}{2}\sqrt{\frac{8}{T}}\cdot\frac{\partial}{\partial X}. \end{aligned}$$

Employing these derivatives in equation (2.3.1) gives Burgers' equation in terms of the inner solution using the notation $u = u_{inner}$

$$\epsilon\, u_T - \frac{1}{2}\sqrt{\frac{8}{T}}u_X + uu_X - u_{XX} = 0, \tag{2.3.27}$$

with the boundary conditions $u \to \sqrt{\frac{8}{T}} + \epsilon\frac{X}{T}$ as $X \to -\infty$ and $u \to 0$ as $X \to \infty$. Substituting the inner expansion (2.3.26) in Burger' equation gives

$$\widehat{U}_{XX} - \widehat{U}\widehat{U}_X + \frac{1}{2}\sqrt{\frac{8}{T}}\,\widehat{U}_X + \epsilon\left(\widehat{V}_{XX} - \left(\widehat{U}\widehat{V}\right)_X + \frac{1}{2}\sqrt{\frac{8}{T}}\,\widehat{V}_X - \widehat{U}_T\right) + O(\epsilon^2) = 0.$$

Eliminating the $O(\epsilon)$ terms, the leading order term of the inner solution can be expressed as

$$\widehat{U}_{XX} - \widehat{U}\widehat{U}_X + \frac{1}{2}\sqrt{\frac{8}{T}}\,\widehat{U}_X = 0.$$

Integrating with respect to X we find

$$\widehat{U}_X - \frac{1}{2}\widehat{U}^2 + \frac{1}{2}\sqrt{\frac{8}{T}}\,\widehat{U} = C_3.$$

Using the far field conditions and balancing for $\widehat{U}$ gives us $\widehat{U} \to \sqrt{\frac{8}{T}}$ as $X \to -\infty$ and $\widehat{U} \to 0$ as $X \to \infty$. Therefore $C_3 = 0$. Integrating once more to obtain the leading order term of the inner solution

$$\begin{aligned}
\frac{\partial \widehat{U}}{\partial X} &= \frac{1}{2}\widehat{U}\left(\widehat{U} - \sqrt{\frac{8}{T}}\right) \\
\Longrightarrow \int \frac{\mathrm{d}\widehat{U}}{\widehat{U}\Big(\widehat{U} - \sqrt{\frac{8}{T}}\Big)} &= \int \frac{1}{2}\mathrm{d}X \\
\Longrightarrow \int \sqrt{\frac{T}{8}}\left(\frac{1}{\widehat{U} - \sqrt{\frac{8}{T}}} - \frac{1}{\widehat{U}}\right)\mathrm{d}\widehat{U} &= \int \frac{1}{2}\mathrm{d}X \\
\Longrightarrow \ln\left|\frac{\widehat{U} - \sqrt{\frac{8}{T}}}{\widehat{U}}\right| &= \frac{1}{2}\sqrt{\frac{8}{T}}\Big(X - A(T)\Big).
\end{aligned}$$

Since the solution $0 < \widehat{U} < \sqrt{\frac{8}{T}}$ this yields

$$\begin{aligned}
\ln\Big(\frac{\sqrt{\frac{8}{T}} - \widehat{U}}{\widehat{U}}\Big) &= \frac{1}{2}\sqrt{\frac{8}{T}}\Big(X - A(T)\Big) \\
\Longrightarrow \frac{\sqrt{\frac{8}{T}} - \widehat{U}}{\widehat{U}} &= \exp\left[\frac{1}{2}\sqrt{\frac{8}{T}}\Big(X - A(T)\Big)\right] \\
\Longrightarrow \widehat{U} &= \sqrt{\frac{8}{T}}\,\frac{1}{1 + \exp(y)},
\end{aligned}$$

where $y = \frac{1}{2}\sqrt{\frac{8}{T}}\,\big(X - A(T)\big)$. Multiplying with $\exp(-\frac{y}{2})$ to drive an expression of the solution in terms of the hyperbolic tangent function $\tanh$ as follows

$$\begin{aligned}
\widehat{U} &= \frac{1}{2}\sqrt{\frac{8}{T}} \cdot \frac{2\,\exp\left(\frac{-y}{2}\right)}{\exp\left(\frac{-y}{2}\right) + \exp\left(\frac{y}{2}\right)} \\
&= \frac{1}{2}\sqrt{\frac{8}{T}}\left[1 - \frac{\exp\left(\frac{y}{2}\right) - \exp\left(\frac{-y}{2}\right)}{\exp\left(\frac{y}{2}\right) + \exp\left(\frac{-y}{2}\right)}\right] \\
&= \frac{1}{2}\sqrt{\frac{8}{T}}\Big[1 - \tanh\theta\Big], \qquad \text{where} \quad \theta = \sqrt{\frac{8}{T}}\Big(\frac{X - A(T)}{4}\Big).
\end{aligned}$$

Therefore, the leading order of the inner expansion can be given as

$$\widehat{U}(X,T) = \frac{1}{2}\sqrt{\frac{8}{T}}\left[1 - \tanh\left(\sqrt{\frac{8}{T}}\Big(\frac{X - A(T)}{4}\Big)\right)\right], \tag{2.3.28}$$

and in terms of the outer spatial variable

$$\widehat{U}(x,t) = \frac{1}{2}\sqrt{\frac{8}{t}}\left[1 - \tanh\left(\frac{1}{4\,\epsilon}\sqrt{\frac{8}{t}}\Big(x + 2 - \sqrt{8\,t} - \epsilon\,A(t)\Big)\right)\right]. \tag{2.3.29}$$

This solution represents the Taylor shock of amplitude $\sqrt{\frac{8}{t}}$ and the shock centre is located at $x = -2 + \sqrt{8\,t} + \epsilon\,A(t)$, where $A(t)$ is the $O(\epsilon)$ shift in shock centre. To determine the function $A(T)$ we consider the $O(\epsilon)$ correction of the inner expansion (2.3.26). But first we write (2.3.27) in terms of θ, where $\theta = \sqrt{\frac{8}{T}}\Big(\frac{X-A(T)}{4}\Big)$, and the derivatives in terms of θ are

$$\frac{\partial}{\partial X} = \frac{1}{4}\sqrt{\frac{8}{T}}.\frac{\partial}{\partial\theta}, \qquad \text{and} \qquad \begin{aligned}\frac{\partial}{\partial T} &= \frac{\partial T}{\partial T}.\frac{\partial}{\partial T} + \frac{\partial\theta}{\partial T}.\frac{\partial}{\partial\theta} \\ &= \frac{\partial}{\partial T} - \Big(\frac{\theta}{2\,T} + \sqrt{\frac{8}{T}}\,\frac{A'(T)}{4}\Big)\,\frac{\partial}{\partial\theta}.\end{aligned}$$

Thus, the governing equation of the inner solution defined in (2.3.27) can be presented in terms of θ as following

$$\epsilon\left[u_T - \left(\frac{\theta}{2\,T} + \frac{1}{4}\sqrt{\frac{8}{T}}\,A'(T)\right)u_\theta\right] - \frac{1}{T}\,u_\theta + \frac{1}{4}\sqrt{\frac{8}{T}}\,uu_\theta - \frac{1}{2\,T}\,u_{\theta\theta} = 0.$$

Substituting $u = \widehat{U} + \epsilon\widehat{V} + O(\epsilon^2)$ then gives

$$\begin{aligned}\epsilon\Big[\widehat{V}_{\theta\theta} + \Big(\theta + A'\sqrt{2\,T}\Big)\,\widehat{U}_\theta \;&-\; \sqrt{2\,T}\,\Big(\widehat{U}\widehat{V}\Big)_\theta + 2\,\widehat{V}_\theta - 2\,T\,\widehat{U}_T\Big] \\ &+\; \widehat{U}_{\theta\theta} - \sqrt{2\,T}\,\widehat{U}\widehat{U}_\theta + 2\,\widehat{U}_\theta + O(\epsilon^2) = 0.\end{aligned}$$

Since we are looking for $O(\epsilon)$ correction we choose the first term in square brackets and neglect the rest of the terms. Then we integrate the $O(\epsilon)$ term

with respect to θ, to obtain

$$\widehat{V}_\theta + \Big(\theta + A'\sqrt{2\,T}\Big)\widehat{U} - \int \widehat{U}\ \mathrm{d}\theta - \sqrt{2\,T}\,\widehat{U}\widehat{V} \quad + \\ 2\,\widehat{V} - 2T\int \frac{\partial \widehat{U}}{\partial T}\ \mathrm{d}\theta \quad = \quad 0. \tag{2.3.30}$$

In order to solve equation (2.3.30) for $\widehat{V}$, we first compute the last term of the equation, which is the integral of $\widehat{U}_T$ with respect to θ. But first let us deduce the derivative of $\widehat{U}$ with respect to T, with θ held fixed

$$\begin{aligned} \frac{\partial \widehat{U}}{\partial T} &= \frac{\partial}{\partial T}\left\{\sqrt{\frac{2}{T}}\Big(1 - \tanh\theta\Big)\right\} \\ &= -\frac{T^{-3/2}}{\sqrt{2}}\Big(1 - \tanh\theta\Big). \end{aligned} \tag{2.3.31}$$

Integrating equation (2.3.31) with respect to θ then yields

$$2\,T\int \frac{\partial \widehat{U}}{\partial T}\ \mathrm{d}\theta = -\sqrt{\frac{2}{T}}\left[\theta - \ln\Big(\cosh\theta\Big)\right] + C_4.$$

For the other integral in (2.3.30), it can be evaluated as follows

$$\begin{aligned} \int \widehat{U}\ \mathrm{d}\theta &= \sqrt{\frac{2}{T}}\int \Big(1 - \tanh\theta\Big)\ \mathrm{d}\theta \\ &= \sqrt{\frac{2}{T}}\left[\theta - \ln\Big(\cosh\theta\Big)\right] + C_5. \end{aligned}$$

The two integration constants will be determined in the following equation. We substitute these two evaluated integrals in equation (2.3.30), and since they are of the same value with opposite signs the first integral will cancel the other, yielding (2.3.30) to be

$$\widehat{V}_\theta + 2\,\widehat{V}\ \tanh\theta = -\Big(\sqrt{\frac{2}{T}}\ \theta + 2A'\Big)\Big(1 - \tanh\theta\Big) + C. \tag{2.3.32}$$

The constant $C = C_4 + C_5$ which can be determined by taking the limit $\widehat{V} \to 0$ as $\theta \to \infty$ gives $C = 0$. Equation (2.3.32) is a first-order linear ODE, and can be

solved for $\widehat{V}$ by using an integrating factor method. Consider $\widehat{V} = \operatorname{sech}^2\theta$, and its derivative is $\widehat{V}_\theta = -2\tanh\theta\,\operatorname{sech}\theta$, therefore, we can say that $\widehat{V} = \operatorname{sech}^2\theta$ is a solution to the homogeneous equation

$$\widehat{V}_\theta + 2\,\widehat{V}\,\tanh\theta = 0.$$

Taking the integrating factor $\cosh^2\theta$, equation (2.3.32) consequently becomes

$$\frac{\mathrm{d}}{\mathrm{d}\theta}\Big(\widehat{V}\cosh^2\theta\Big) = -\Big[f_1(\theta) + f_2(\theta)\Big], \tag{2.3.33}$$

where the functions $f_1(\theta)$ and $f_2(\theta)$ are defined by

$$\begin{aligned} f_1(\theta) &= \sqrt{\frac{2}{T}}\;\theta\Big(1-\tanh\theta\Big)\,\cosh^2\theta, \\ f_2(\theta) &= 2A'\Big(1-\tanh\theta\Big)\,\cosh^2\theta. \end{aligned}$$

We integrate (2.3.33) with respect to θ to have

$$\widehat{V}\cosh^2\theta = -\int f_1(\theta)\,\mathrm{d}\theta - \int f_2(\theta)\,\mathrm{d}\theta.$$

For simplicity we deal with the two integrals individually, the first integral for $f_1(\theta)$ gives

$$\begin{aligned} \int f_1(\theta)\,\mathrm{d}\theta &= \sqrt{\frac{2}{T}}\int \theta\,\cosh^2\theta\Big(1-\tanh\theta\Big)\,\mathrm{d}\theta \\ &= \sqrt{\frac{2}{T}}\int \Big(\theta\,\cosh^2\theta - \theta\,\cosh\theta\,\sinh\theta\Big)\,\mathrm{d}\theta \\ &= \frac{1}{8}\sqrt{\frac{2}{T}}\,\Big(2\,\theta^2 + \big(2\,\theta+1\big)\,\big(\sinh(2\theta) - \cosh(2\theta)\big)\Big) \\ &= \frac{1}{8}\sqrt{\frac{2}{T}}\,\Big(2\,\theta^2 - \mathrm{e}^{-2\,\theta}\big(2\,\theta+1\big)\Big), \end{aligned}$$

and the second integral for $f_2(\theta)$ gives

$$\begin{aligned}\int f_2(\theta)\,\mathrm{d}\theta &= 2A'\int \cosh^2\theta\Big(1-\tanh\theta\Big)\,\mathrm{d}\theta\\ &= 2A'\int \Big(\cosh^2\theta-\cosh\theta\,\sinh\theta\Big)\,\mathrm{d}\theta\\ &= \frac{1}{8}\,2A'\Big(4\,\theta+2\,\sinh(2\theta)-4\cosh^2\theta\Big)\\ &= \frac{1}{8}\,2A'\Big(4\,\theta-2\mathrm{e}^{-2\,\theta}-2\Big).\end{aligned}$$

Thus the solution for $\widehat{V}$ can be represented as follows

$$\widehat{V}=\sqrt{\frac{2}{T}}\;p_1(\theta)+2\,A'\,p_2(\theta)+K(T),$$

where $K(T)$ is an arbitrary function and can be determined by looking at the $O(\epsilon^2)$ terms and $p_{1,2}$ are expressed as

$$\begin{aligned}p_1(\theta) &= \frac{1}{8\cosh^2\theta}\Big[\mathrm{e}^{-2\,\theta}\big(2\,\theta+1\big)-2\,\theta^2\Big],\\ p_2(\theta) &= \frac{1}{8\cosh^2\theta}\Big[2\mathrm{e}^{-2\,\theta}+2-4\,\theta\Big].\end{aligned}$$

To identify the $O(\epsilon)$ shift in the shock centre $A(T)$, for the period of time $t>8$, we start matching the inner solution with the outer by letting $\theta\to-\infty$. We first study the behaviour of the functions p_1 and p_2 as $\theta\to-\infty$, let us observe how $\cosh\theta$ behaves in this limit

$$\text{For}\quad \theta\to-\infty,\quad \cosh(\theta)\sim\frac{1}{2}\mathrm{e}^{-\theta}\quad\Longrightarrow\quad\frac{1}{8\,\cosh^2\,\theta}\sim\frac{1}{2}\,\mathrm{e}^{2\,\theta}.$$

We can use this in the study of the behaviour of the functions $p_1(\theta)$ and $p_2(\theta)$ when $\theta\to-\infty$ which yields

$$\text{For}\quad \theta\to-\infty\qquad p_1(\theta)\sim\frac{1}{2}\,\mathrm{e}^{2\,\theta}\,\Big[\,\mathrm{e}^{-2\,\theta}\big(2\,\theta+1\big)-2\,\theta^2\,\Big]\sim\theta+\frac{1}{2},$$

since $\theta^2\mathrm{e}^{2\,\theta}\to 0$ when $\theta\to-\infty$. For the second function $p_2(\theta)$

$$\text{For}\quad \theta\to-\infty\qquad p_2(\theta)\sim\frac{1}{2}\,\mathrm{e}^{2\,\theta}\,\Big[\,2\mathrm{e}^{-2\,\theta}+2-4\,\theta\,\Big]\sim 1.$$

where the two terms $\mathrm{e}^{2\,\theta}(2-4\theta)$ vanishes as $\theta \to -\infty$. Matching the inner and the outer solutions, we arrive at

$$\lim_{\theta\to-\infty} \widehat{V} = \sqrt{\frac{2}{T}}\left(\theta + \frac{1}{2}\right) + 2\,A',$$

and so,

$$\lim_{\theta\to-\infty}(\widehat{U} + \epsilon\,\widehat{V}) = \sqrt{\frac{8}{T}} + \epsilon\left[\sqrt{\frac{2}{T}}\Big(\theta + \frac{1}{2}\Big) + 2\,A'\right]. \tag{2.3.34}$$

The outer solution

$$\lim_{\theta\to\infty}(U + \epsilon V) = \sqrt{\frac{8}{T}} + \epsilon\left[\ \sqrt{\frac{2}{T}}\,\theta + \frac{A(T)}{T}\ \right]. \tag{2.3.35}$$

Hence, the matching for the inner and outer solutions in (2.3.34) and (2.3.35) to obtain the function $A(T)$ as follows

$$\begin{aligned}
\frac{1}{\sqrt{2\,T}} + 2\,A' = \frac{A}{T} \quad &\Longrightarrow \quad \frac{\mathrm{d}A}{\mathrm{d}T} - \frac{1}{2}\,T^{-1}\,A = -\frac{1}{2}\,(2\,T)^{-\frac{1}{2}} \\
&\Longrightarrow \quad \frac{\mathrm{d}A}{\mathrm{d}T}\,T^{-\frac{1}{2}} - \frac{1}{2}\,T^{-\frac{3}{2}}\,A = -\frac{1}{\sqrt{8}}\,T^{-1} \\
&\Longrightarrow \quad \frac{\mathrm{d}}{\mathrm{d}T}\left(T^{-\frac{1}{2}}\,A\right) = -\frac{1}{\sqrt{8}}\,T^{-1} \\
&\Longrightarrow \quad A(T) = A(8) - \sqrt{\frac{T}{8}}\int_8^T \frac{1}{t}\,\mathrm{d}t.
\end{aligned} \tag{2.3.36}$$

The constant $A(8)$ evaluates the shift at the evolution time $t = 8$ which was determined earlier for shock solution in the period $0 < t < 8$ as A_0. Fixing A_0 and calculating the integral, the $O(\epsilon)$ shift in the shock centre is fixed at

$$A(T) = A_0 - \sqrt{\frac{T}{8}}\ \ln\Big(\frac{T}{8}\Big). \tag{2.3.37}$$

Inserting equation (2.3.37) into the Taylor shock solution (2.3.28), the inner expansion in term of only the leading order is expressed as

$$u_{inner} \sim \frac{1}{2}\sqrt{\frac{8}{T}}\left\{1 - \tanh\left[\frac{1}{4}\sqrt{\frac{8}{T}}\ \Big(X - A_0 + \sqrt{\frac{T}{8}}\ \ln\Big(\frac{T}{8}\Big)\Big)\right]\right\} + O(\epsilon).$$

We can write the shock solution in terms of the outer variables x and t as

$$u_{inner} \sim \frac{1}{2}\sqrt{\frac{8}{t}}\left[1 - \tanh\,\theta\right] + O(\epsilon), \tag{2.3.38}$$

where

$$\theta = \frac{1}{4\,\epsilon}\sqrt{\frac{8}{t}}\left(x + 2 - \sqrt{8\,t} - \epsilon\,A_0 + \epsilon\sqrt{\frac{t}{8}}\,\ln\left(\frac{t}{8}\right)\right)$$

We further would like to verify our results with proposed work of Crighton and Scott [25]. In particular we check if the approximated shock solution and the shift $A(T)$ in shock centre for the case of time $t > 8$ agrees with the illustrated shock solution in [25]. This case of solution where $t > 8$ is chosen because the shock adjusts its form to the triangular shape and the physical problem is then very similar to the initial waveform described in [25]. Since in the presented example the initial evolution time is $t = 8$ and initial position $x = -2$, we make the following rescaling

$$x^* = \frac{x+2}{8}, \qquad\qquad T^* = \frac{T}{8}.$$

Introducing the new variables to the generalized Burgers' equation reduces to

$$\frac{1}{8}\,u_{T^*} + \frac{1}{8}\,uu_{x^*} = \frac{\epsilon}{64}\,g(T^*)u_{x^*x^*} \implies u_{T^*} + uu_{x^*} = \epsilon^* u_{x^*x^*},$$

where $\epsilon^* = \frac{\epsilon}{8}$ and $g(T^*) = 1$ since in our study we focus on the one-dimensional wave.

In terms of the new variables the initial time is $T^* = 1$ which corresponds to the initial time for N-wave in Crighton and Scott's paper. Inserting the new variable in equation (2.3.37) then gives

$$\begin{aligned} A(T^*) &= A(1) - \sqrt{\frac{8\,T^*}{8}}\int_1^{T^*}\frac{1}{t}\,\mathrm{d}t \\ &= A(1) - \sqrt{T^*}\int_1^{T^*}\frac{1}{t}\,\mathrm{d}t. \end{aligned}$$

Which corresponds to the shift of shock location obtained by Crighton and Scott

(see [25] p. 110 equation (3.15)). Similarly, these new variables can be introduced to the leading order of the inner expansion in equation (2.3.28). But first note that the new inner variable X^* is given as

$$\begin{aligned} X^* &= \frac{1}{\epsilon}\left(x^* - \sqrt{T^*}\right) \\ &= \frac{1}{\epsilon}\left(\frac{x+2}{8} - \sqrt{\frac{T}{8}}\right) \\ &= \frac{1}{\epsilon}\left(\frac{x+2-\sqrt{8\,T}}{8}\right) \\ &= \frac{X}{8}. \end{aligned}$$

Considering the Taylor shock solution Crighton and Scott derived (2.3.7) in terms of the new variables, we then have

$$\begin{aligned} \widehat{U}^*(X^*,T^*) &= \frac{1}{2}\,\frac{1}{\sqrt{T^*}}\left[1 - \tanh\left(\frac{X^* - A(T^*)}{4\sqrt{T^*}}\right)\right] \\ &= \frac{1}{2}\sqrt{\frac{8}{T}}\left[1 - \tanh\left(\frac{\frac{X}{8} - A(\frac{T}{8})}{4\sqrt{\frac{T}{8}}}\right)\right]. \end{aligned}$$

Hence, the Taylor thermoviscus shock solution we obtained in equation (2.3.28) corresponds to the shock solution Crighton and Scott derived for the N-wave for $x > 0$ (see [25] p. 108 equation(3.8)).

The Width of Shock Front for $t > 8$

Once again we end this asymptotic investigation of the shock solution for $t > 8$ by calculating the width of the shock front for $t > 8$. Let us suppose that $u(X_1) = 0.9\,u_m$ and $u(X_2) = 0.1\,u_m$ are the 90% and 10% of shock solution where u_m is the shock amplitude, which is in this case is $\sqrt{\frac{8}{T}}$. Thus, the width is defined as $x_{width} = \epsilon(X_2 - X_1)$, and we begin calculating for the spatial variable

X_1 by using the relation

$$\begin{aligned} & u(X_1) = 0.9\sqrt{\frac{8}{T}}, \\ \Longrightarrow \quad & \frac{1}{2}\sqrt{\frac{8}{T}}\left[1 - \tanh\Big(\frac{1}{4}\sqrt{\frac{8}{T}}\Big(X_1 - A(T)\Big)\Big)\right] = 0.9\sqrt{\frac{8}{T}}, \end{aligned}$$

and we can deduce X_1 as

$$\begin{aligned} X_1 &= \sqrt{\frac{T}{8}}\left[4\,\tanh^{-1}\Big(1 - 2(0.9)\Big)\right] + A(T) \\ &= \sqrt{\frac{T}{8}}\left[-4\,\tanh^{-1}\big(0.8\big)\right] + A(T). \end{aligned}$$

and for the second value we have the relation

$$\begin{aligned} & u(X_2) = 0.1\sqrt{\frac{8}{T}}, \\ \Longrightarrow \quad & \frac{1}{2}\sqrt{\frac{8}{T}}\left[1 - \tanh\Big(\frac{1}{4}\sqrt{\frac{8}{T}}\Big(X_2 - A(T)\Big)\Big)\right] = 0.1\sqrt{\frac{8}{T}}, \end{aligned}$$

and the value of X_2 is

$$\begin{aligned} X_2 &= \sqrt{\frac{T}{8}}\left[4\,\tanh^{-1}\Big(1 - 2(0.1)\Big)\right] + A(T) \\ &= \sqrt{\frac{T}{8}}\left[4\,\tanh^{-1}\big(0.8\big)\right] + A(T). \end{aligned}$$

Hence, the shock front width for $t > 8$ is

$$x_{width} = \epsilon\Big(X_2 - X_1\Big) = \epsilon\sqrt{\frac{T}{8}}\Big(8\,\tanh^{-1}\big(0.8\big)\Big). \tag{2.3.39}$$

2.3.4 Summary

In this section we have attempted to show how the method of asymptotic expansions can be applied to the one-dimensional viscid Burgers equation with the initial condition of rectangular pulse defined in §2.1. We formulated an asymptotic solution based on the method the matched asymptotic expansion for generalized Burgers' equation proposed by Crighton and Scott in [25], and Schofield and Hammerton in [81].

The matched asymptotic expansions method is used for solving singularly perturbed problems where the domain consists of one or more sub-domains. We first treat the differential equation as a regular perturbed problem, so we make the approximation $\epsilon = 0$ to the governing equation and find the solution which is called the outer solution. However, the outer expansion cannot describe the physical structure of the shock wave where the transition of the solution occurs, and to cope with this situation an inner region is needed. This inner region describes the shock solution where ϵ is no more negligible. In fact x and ϵ are of comparable sizes, and so we define a new variable X and rescale the original problem. We match the shock solution with the surrounding outer regions, and an approximate solution for the whole domain is obtained. To verify the uniqueness of the $O(\epsilon^0)$ shock solution which often contains unknown functions, we look for the small $O(\epsilon)$ perturbations which fixes the unknowns and the matching can be then accomplished.

We began investigating the evolution of the shock in the time $0 < t < 8$ where the shock takes the form illustrated in figure 2.3.3. The deduced thermoviscous shock solution is

$$u_{inner} \sim \frac{1}{2}\left[1 - \tanh\left(\frac{x - 2 - \frac{t}{2} - \epsilon\, A(t)}{4\,\epsilon}\right)\right].$$

representing the Taylor shock wave of amplitude 1 and centred at $x = 2 + \frac{t}{2} + \epsilon\, A(t)$ where the unknown function describes the $O(\epsilon)$ shift in the shock centre. We then looked for the $O(\epsilon)$ perturbations to identify $A(t)$ which in this

case was constant $A(t) = A_0$. Then we continued studying shock structure by investigating the shock width $x_{width} = 8\,\epsilon\,\tanh^{-1}(0.8) \approx 8.78890\,\epsilon$.

We then studied the evolution of the permanent triangular shock wave when $t > 8$. For this case we once again deduced the $O(\epsilon^0)$ solution represented by the Taylor shock as follows

$$u_{inner} \sim \frac{1}{2}\sqrt{\frac{8}{t}}\left[1 - \tanh\left(\sqrt{\frac{8}{t}}\left(\frac{x + 2 - \sqrt{8\,t} - \epsilon\,A(t)}{4\,\epsilon}\right)\right)\right].$$

For this shock the amplitude is $\sqrt{\frac{8}{t}}$ and the $O(\epsilon)$ shift in shock center is defined as

$$A(t) = A_0 - \sqrt{\frac{t}{8}}\,\log\left(\frac{t}{8}\right).$$

and the shock width

$$x_{width} = \epsilon\sqrt{\frac{t}{8}}\left(8\,\tanh^{-1}\left(0.8\right)\right).$$

Next we demonstrate the use of the Cole-Hopf transformation on the initial value problem of Burgers' equations coupled with the three initial profiles defined in §2.1 to linearise the problems and evaluate the explicit solutions. Further we will show how the Cole-Hopf solution in the limit of small viscosity $\epsilon \to 0$ leads to the Taylor thermoviscous shock we presented earlier in this discussion.

2.4 Cole-Hopf Transformation

2.4.1 General Theory

The first full general solution of the one-dimensional Burgers' equation for arbitrary initial conditions was introduced independently in 1950 by Eberhard Hopf [40] and in 1951 by Julian D. Cole [23]. The Cole-Hopf transformation converts the nonlinear Burgers' equation

$$u_t + \left(\frac{u^2}{2}\right)_x = \epsilon u_{xx}, \qquad -\infty < x < \infty,\ t > 0, \tag{2.4.1}$$

into the linear heat equation

$$\psi_t = \epsilon \psi_{xx}. \tag{2.4.2}$$

This technique has been used in a range of fields such as astrophysics [46], [49] and other fields in which the one dimensional Burgers' equation appears. In this section we employ the nonlinear Cole-Hopf transformation to obtain the solution of Burgers' equation for a general initial condition

$$\begin{cases} u_t + \left(\frac{u^2}{2}\right)_x = \epsilon u_{xx}, & -\infty < x < \infty,\ t > 0, \\ \\ u(x,0) = u_0(x), & -\infty < x < \infty, \end{cases} \tag{2.4.3}$$

where $u_0 \to 0$ as $|x| \to \infty$. The Cole-Hopf transformation is performed in two steps. First we introduce $\psi(x,t)$ by the relation

$$u = -2\epsilon \frac{\partial}{\partial x}(\log \psi) = -2\epsilon \frac{\psi_x}{\psi}, \tag{2.4.4}$$

then integrating equation (2.4.1) with respect to x and substituting (2.4.4) to obtain

$$\begin{aligned}
\frac{\partial}{\partial t}\left(\int_0^x u(y)\,\mathrm{d}y\right)+\frac{u^2}{2} &= \epsilon u_x \\
\frac{\partial}{\partial t}(-2\,\epsilon\,\log\psi)+2\epsilon^2\,\frac{\psi_x^2}{\psi^2} &= -2\epsilon^2\left(\frac{\psi_{xx}}{\psi}-\frac{\psi_x^2}{\psi^2}\right) \\
-2\epsilon\,\frac{\psi_t}{\psi} &= -2\epsilon^2\frac{\psi_{xx}}{\psi} \\
\psi_t &= \epsilon\psi_{xx}. \qquad (2.4.5)
\end{aligned}$$

This is the linear heat equation. The initial value problem for the heat equation for $x\in\mathbb{R}$ and $t\geq 0$ is

$$\begin{cases} \psi_t=\epsilon\psi_{xx}, \\ \\ \psi(x,0)=\psi_0(x) \end{cases} \qquad (2.4.6)$$

where the initial data for u is transformed using relation (2.4.4) into initial data for the heat equation ψ_0 as the following

$$\psi_0(x)\equiv\exp\left(-\frac{1}{2\epsilon}\int_0^x u_0(s)\,\mathrm{d}s\right).$$

The general solution to the initial value problem for the heat equation (2.4.6) is given in [17] as

$$\psi(x,t)=\frac{1}{\sqrt{4\pi\,\epsilon\,t}}\int_{-\infty}^{\infty}\psi_0(y)\exp\left[-\frac{(x-y)^2}{4\epsilon t}\right]\mathrm{d}y, \qquad (2.4.7)$$

where $|\psi_0(y)|$ is bounded above by some constant as $|y|\to 0$. Substituting equation (2.4.7) in (2.4.4) results a formula for the solution of viscous Burgers' equation as

$$u(x,t)=\frac{\displaystyle\int_{-\infty}^{\infty}\frac{x-y}{t}\,\exp\left[\frac{-\big(x-y\big)^2}{4\epsilon\,t}\right]\psi_0(y)\,\mathrm{d}y}{\displaystyle\int_{-\infty}^{\infty}\exp\left[\frac{-\big(x-y\big)^2}{4\epsilon\,t}\right]\psi_0(y)\,\mathrm{d}y}\,, \qquad (2.4.8)$$

or in a more compact form

$$u(x,t) = \frac{\displaystyle\int_{-\infty}^{\infty} \frac{x-y}{t} \exp\left(\frac{-G}{2\epsilon}\right) \mathrm{d}y}{\displaystyle\int_{-\infty}^{\infty} \exp\left(\frac{-G}{2\epsilon}\right) \mathrm{d}y}\ , \tag{2.4.9}$$

where

$$G(y;x,t) = \frac{(x-y)^2}{2t} + \int_0^y u_0(z)\,\mathrm{d}z. \tag{2.4.10}$$

Therefore, the Cole-Hopf transformation represents an explicit form of the solution to initial value problem for the Burgers' equation. The reader can return to the Cole-Hopf solution of Burgers' equation demonstrated by Whitham [93] (equations 4.10,4.11 p 98).

For the three initial conditions previously considered in §2.1 we next evaluate the integrals in (2.4.9) and present illustrating figures of the initial value problem. But first we derive an asymptotic analysis discussing the Cole-Hopf solution in the case of the limit $\epsilon \to 0$.

Asymptotic Behaviour of Cole-Hopf Solution

We now consider the asymptotic behaviour of the Cole-Hopf solution (2.4.9) as $\epsilon \to 0$ while x , t and $u_0(x)$ are held fixed. Much literature has covered the theory of the asymptotic behaviour of the Cole-Hopf solution such as Whitham [93], Kida [48] and Tatsumi and Kida [87] and others in [82] and [56].

As $\epsilon \to 0$, the dominant contribution to the integrals in (2.4.9) comes from the immediate neighbourhood of the minimum points of $G(y;x,t)$ with respect to y. One way to look for minimums of $G(y;x,t)$ is to find the stationary points of G at which $\frac{\partial^2 G}{\partial y^2} > 0$. A stationary point for $G(y;x,t)$ say $y = \xi$ is when the first derivative vanishes, i.e, for fixed x and t the derivative

$$\left.\frac{\partial G}{\partial y}\right|_{y=\xi} = \frac{\xi - x}{t} + u_0(\xi) = 0 \tag{2.4.11}$$

Hence, G assumes a minimum value when $y = \xi(x,t)$, implicitly given by

$$x = \xi + u_0(\xi)\, t. \tag{2.4.12}$$

In the stationary phase method (see for example [8]), the contribution from the neighbourhood of a minimum point ξ to an integral is given by

$$I(\xi) = \int_{-\infty}^{\infty} h(y)\, \exp\!\left(-\frac{G(y)}{2\epsilon} \right) \mathrm{d}y \sim I_m(\xi),$$

where the integral $I_m(\xi)$ is defined by

$$I_m(\xi) = h(\xi)\, \sqrt{\frac{2\,\pi}{\frac{1}{2\,\epsilon}\left|G''(\xi)\right|}}\, \exp\!\left(-\frac{G(\xi)}{2\epsilon} \right). \tag{2.4.13}$$

So if we suppose there is a single minimum point $y = \xi(x,t)$ for G then the contribution to the integrals in $u(x,t)$ is given by

$$u(x,t) \sim \frac{\dfrac{x-\xi}{t}\, \sqrt{\dfrac{4\,\pi\,\epsilon}{\left|G''(\xi)\right|}}\, \exp\!\left(-\dfrac{G}{2\epsilon} \right)}{\sqrt{\dfrac{4\,\pi\,\epsilon}{\left|G''(\xi)\right|}}\, \exp\!\left(-\dfrac{G}{2\epsilon} \right)} + O(\epsilon)$$

which simplifies to

$$u(x,t) \sim \frac{x-\xi}{t} + O(\epsilon), \tag{2.4.14}$$

where $\xi(x,t)$ is defined implicitly in equation (2.4.12). Thus, the asymptotic behaviour of the solution at leading order in the limit $\epsilon \to 0$ can be written as

$$\begin{cases} u(x,t) = u_0(\xi), \\ \\ x = \xi + u_0(\xi)\, t. \end{cases} \tag{2.4.15}$$

This is consistent with the characteristic method solution given in (2.2.16) of inviscid Burgers' model in §2.2.3. The initial condition $u_0(\xi)$ propagates along

the characteristic curve $x = \xi + u_0(\xi)\, t$ where x denotes the particle location at time t at location ξ and moving with velocity $u_0(\xi)$.

If the initial condition is smooth and continuous then for very small time there will be a single solution for ξ. In general as t increases multiple values for ξ arise and so this solution is not valid for all x. At this stage, there will be more than one minimum ξ_1 and ξ_2, then the dominant behaviour is included when taking

$$I(\xi) = \int_{-\infty}^{\infty} h(y)\, \exp\!\left(-\frac{G(y)}{2\epsilon}\right) \mathrm{d}y \sim I_m(\xi_1) + I_m(\xi_2), \qquad \text{For} \qquad G(\xi_1) \neq G(\xi_2).$$

If the value of G at these two minimums is different, then the behaviour of $I(\xi)$ is dominated by the behaviour close to the global minimum. Say for the cases $G(\xi_1) < G(\xi_2)$ and $G(\xi_1) > G(\xi_2)$ the solution is given as

$$u(x,t) \sim \begin{cases} \dfrac{x-\xi_1}{t}, & \text{for} \quad G(\xi_1) < G(\xi_2), \\ \\ \dfrac{x-\xi_2}{t}, & \text{for} \quad G(\xi_1) > G(\xi_2). \end{cases} \tag{2.4.16}$$

In each of these two cases the solution (2.4.15) applies. For the case $G(\xi_1) = G(\xi_2)$ the contribution from both minimums is comparable. Additional discussion of this type of solution is conducted later in detail for a specific initial profile.

Now we consider a specific example of u_0 choosing the example ϕ_1 in equation (2.1.1) as a study case for Hopf-Cole solutions.

2.4.2 Cole-Hopf Solution for the Rectangular Pulse, $\phi_1(x)$

We consider the Cole-Hopf approach to find solutions for viscous Burgers' equation i.e $\epsilon > 0$, by applying Cole-Hopf transformation and comparing asymptotic results for small ϵ with results from the method of characteristics. We focus on the initial condition $u(x,0) = \phi_1(x)$ described in §2.1 as follows,

$$\phi_1(x) = \begin{cases} 0, & x < -2, \\ 1, & -2 < x < 2, \\ 0, & 2 < x. \end{cases} \tag{2.4.17}$$

The function $G_1(\eta; x, t)$ defined in (2.4.10) can be then written as

$$G_1(y; x, t) = \frac{(x-y)^2}{2t} + \widetilde{G}_1(y; x, t),$$

where

$$\widetilde{G}_1(y; x, t) = \begin{cases} 0, & y < -2, \\ \displaystyle\int_{-2}^{y} 1 \, \mathrm{d}y, & -2 < y < 2, \\ \displaystyle\int_{-2}^{2} 1 \, \mathrm{d}y, & 2 < y. \end{cases}$$

Thus, the function G_1 is obtained as follows

$$G_1(y; x, t) = \frac{(x-y)^2}{2t} + \begin{cases} 0, & y < -2, \\ y + 2, & -2 < y < 2, \\ 4, & 2 < y. \end{cases} \tag{2.4.18}$$

Introducing the function $G_1(y; x, t)$ for the initial value problem (2.4.3) along with the initial data ϕ_1 gives an expression for the solution $u_1(x,t)$.

$$u_1(x,t) = \frac{\displaystyle\int_{-\infty}^{-2} \frac{x-y}{t} \, \mathrm{e}^{\frac{-G_1}{2\epsilon}} \, \mathrm{d}y + \int_{-2}^{2} \frac{x-y}{t} \, \mathrm{e}^{\frac{-G_1}{2\epsilon}} \, \mathrm{d}y + \int_{2}^{\infty} \frac{x-y}{t} \, \mathrm{e}^{\frac{-G_1}{2\epsilon}} \, \mathrm{d}y}{\displaystyle\int_{-\infty}^{-2} \mathrm{e}^{\frac{-G_1}{2\epsilon}} \, \mathrm{d}y + \int_{-2}^{2} \mathrm{e}^{\frac{-G_1}{2\epsilon}} \, \mathrm{d}y + \int_{2}^{\infty} \mathrm{e}^{\frac{-G_1}{2\epsilon}} \, \mathrm{d}y}. \tag{2.4.19}$$

The integrals in (2.4.19) can then be evaluated numerically to obtain a Cole-Hopf solution. Later we will present plots of this solution where we numerically evaluated these integrals via MATLAB. But first, we continue our derivation of the solution $u_1(x,t)$ by expressing the integrals in (2.4.19) as error functions $\mathrm{erf}(x)$ and $\mathrm{erfc}(x)$. So, to calculate these integrals in the Cole-Hopf solution we write (2.4.19) in the form

$$u_1 = \frac{I_1 \ + \ I_2 \ + \ I_3}{I_4 \ + \ I_5 \ + \ I_6} \ . \tag{2.4.20}$$

We begin with computing the integrals in the denominator. Lets begin with the integral I_4

$$I_4 \ = \ \int_{-\infty}^{-2} \exp\Big[- \frac{G_1}{2\epsilon} \Big] \, \mathrm{d}y \ = \ \int_{-\infty}^{-2} \exp\Big[- \frac{\big(x-y\big)^2}{4\epsilon \, t} \Big] \, \mathrm{d}y \ .$$

We define the variable $\eta = \frac{x-y}{\sqrt{4\epsilon \, t}}$ then $\mathrm{d}y = -\sqrt{4\epsilon \, t} \, \mathrm{d}\eta$ and the integral limits are $\eta = \infty$ for $y = -\infty$ and $\eta = \frac{x+2}{\sqrt{4\epsilon \, t}}$ for $y = -2$. The integral in terms of the new variable can be calculated as

$$I_4 \ = \sqrt{4\epsilon \, t} \int_{\frac{x+2}{\sqrt{4\epsilon \, t}}}^{\infty} \mathrm{e}^{-\eta^2} \, \mathrm{d}\eta = \sqrt{\pi \epsilon \, t} \ \mathrm{erfc}\left(\frac{x+2}{\sqrt{4\epsilon \, t}} \right), \tag{2.4.21}$$

ht where the complimentary error function is defined by

$$\mathrm{erfc}(z) \equiv 1 - \mathrm{erf}(z) = \frac{2}{\sqrt{\pi}} \int_z^{\infty} \mathrm{e}^{-\eta^2} \, \mathrm{d}\eta, \tag{2.4.22}$$

see for example Abramowitz and Stegun [1]. The second integral to compute is I_5 ,

$$I_5 \ = \ \int_{-2}^{2} \exp\Big[- \frac{G_1}{2\epsilon} \Big] \, \mathrm{d}y \ = \ \int_{-2}^{2} \exp\Big[- \frac{\big(x-y\big)^2}{4\epsilon \, t} - \frac{\big(y+2\big)}{2\epsilon} \Big] \, \mathrm{d}y \, .$$

We aim to write the integral in terms of the error function and to obtain this we reform the exponential function as follows

$$\begin{aligned}\Big[-\frac{\big(x-y\big)^2}{4\epsilon\,t}-\frac{\big(y+2\big)}{2\epsilon}\Big], &= -\frac{1}{4\epsilon\,t}\Big[x^2-2xy+y^2+2ty+4t\Big],\\ &= -\frac{1}{4\epsilon\,t}\Big[y^2+2\,(t-x)\,y+x^2+4t\Big],\\ &= -\frac{1}{4\epsilon\,t}\Big[\Big(y+(t-x)\Big)^2-t^2+2xt+4t\Big],\\ &= -\frac{1}{4\epsilon\,t}\Big[\Big(y+(t-x)\Big)^2+\Big(4+2x-t\Big)\,t\Big].\end{aligned}$$

Thus, the integral I_5 is given by

$$\begin{aligned}I_5 &= \int_{-2}^{2}\exp\Big[-\frac{\Big(y+(t-x)\Big)^2}{4\epsilon\,t}\Big].\exp\Big[\frac{t-2x-4}{4\epsilon}\Big]\,\mathrm{d}y,\\ &= \exp\Big(\frac{t-2x-4}{4\epsilon}\Big)\ \int_{-2}^{2}\exp\Big[-\frac{\Big(y+(t-x)\Big)^2}{4\epsilon\,t}\Big]\,\mathrm{d}y\ .\end{aligned}$$

We define $\eta=\frac{y+t-x}{\sqrt{4\,\epsilon\,t}}$ and then $\mathrm{d}y=\sqrt{4\,\epsilon\,t}\,\mathrm{d}\eta$ and for the integral limits if $y=-2$ then $\eta_1=\frac{t-x-2}{\sqrt{4\,\epsilon\,t}}$ and if $y=2$ then $\eta_2=\frac{t-x+2}{\sqrt{4\,\epsilon\,t}}$. Hence,

$$\begin{aligned}I_5 &= \sqrt{4\,\epsilon\,t}\ \exp\Big(\frac{t-2x-4}{4\epsilon}\Big)\ \int_{\eta_1}^{\eta_2}\mathrm{e}^{-\eta^2}\,\mathrm{d}\eta,\\ &= \sqrt{4\,\epsilon\,t}\ \exp\Big(\frac{t-2x-4}{4\epsilon}\Big)\ \Big[\int_{\frac{t-x-2}{\sqrt{4\,\epsilon\,t}}}^{0}\mathrm{e}^{-\eta^2}\,\mathrm{d}\eta\ +\ \int_{0}^{\frac{t-x+2}{\sqrt{4\,\epsilon\,t}}}\mathrm{e}^{-\eta^2}\,\mathrm{d}\eta\Big],\\ &= \sqrt{\pi\,\epsilon\,t}\ \exp\Big(\frac{t-2x-4}{4\epsilon}\Big)\ \Big[\mathrm{erf}\,\Big(\frac{t-x+2}{\sqrt{4\,\epsilon\,t}}\Big)-\mathrm{erf}\,\Big(\frac{t-x-2}{\sqrt{4\,\epsilon\,t}}\Big)\Big],\end{aligned}$$

where the error function is defined in [1] as

$$\mathrm{erf}(z)\equiv\frac{2}{\sqrt{\pi}}\int_0^z\mathrm{e}^{-\eta^2}\,\mathrm{d}\eta\,. \tag{2.4.23}$$

For the third integral in the dominator of equation (2.4.20) I_6 is computed as follows

$$\begin{aligned} I_6 &= \int_2^\infty \exp\Big[-\frac{\big(x-y\big)^2}{4\epsilon\, t} - \frac{2}{\epsilon}\Big]\,\mathrm{d}y \\ &= \mathrm{e}^{-\frac{2}{\epsilon}} \int_2^\infty \exp\Big[-\frac{\big(x-y\big)^2}{4\epsilon\, t}\Big]\,\mathrm{d}y\ . \end{aligned}$$

We define the variable $\eta = \frac{y-x}{\sqrt{4\epsilon\, t}}$ then $\mathrm{d}y = \sqrt{4\epsilon\, t}\,\mathrm{d}\eta$ and the integral limits are $\eta = \frac{2-x}{\sqrt{4\epsilon\, t}}$ for $y = 2\,.$ and $\eta = \infty$ for $y = \infty$ and integral in terms of η is calculated as

$$I_6 = \sqrt{4\epsilon\, t}\ \mathrm{e}^{-\frac{2}{\epsilon}} \int_{\frac{2-x}{\sqrt{\pi\epsilon\, t}}}^\infty \mathrm{e}^{-\eta^2}\,\mathrm{d}\eta = \sqrt{\pi\epsilon\, t}\ \mathrm{e}^{-\frac{2}{\epsilon}}\ \mathrm{erfc}\Big(\frac{2-x}{\sqrt{4\epsilon\, t}}\Big), \tag{2.4.24}$$

where the complimentary error function defined in equation (2.4.22). We have now computed the three integrals in the denominator. We now consider the integrals in the numerator beginning with I_1

$$\begin{aligned} I_1 &= \int_{-\infty}^{-2} \frac{x-y}{t}\ \exp\Big[\frac{\big(x-y\big)^2}{4\epsilon\, t}\Big]\,\mathrm{d}y \\ &= 2\epsilon \int_{-\infty}^{-2} \mathrm{d}\Big[\exp\Big(-\frac{\big(x-y\big)^2}{4\epsilon\, t}\Big)\Big], \\ &= 2\epsilon\ \exp\Big(-\frac{\big(x+2\big)^2}{4\epsilon\, t}\Big)\,. \end{aligned}$$

For the second integral in the numerator

$$I_2 = \int_{-2}^{2} \frac{x-y}{t}\ \exp\Big[-\frac{\big(x-y\big)^2}{4\epsilon\, t} - \frac{y+2}{2\epsilon}\Big]\,\mathrm{d}y,$$

we apply the integration by parts method by defining U and $\mathrm{d}V$ in the following

$$U = \exp\Big(-\frac{y+2}{2\epsilon}\Big), \qquad \mathrm{d}U = -\frac{1}{2\epsilon}\exp\Big(-\frac{y+2}{2\epsilon}\Big)\,\mathrm{d}y,$$

$$\mathrm{d}V = \frac{x-y}{t}\ \exp\Big(-\frac{\big(x-y\big)^2}{4\epsilon\, t}\Big)\,\mathrm{d}y, \qquad V = 2\epsilon\ \exp\Big(-\frac{\big(x-y\big)^2}{4\epsilon\, t}\Big).$$

The integral I_2 is then written as

$$\begin{aligned} I_2 &= U\,V\Big|_{-2}^{2} - \int_{-2}^{2} V\,\mathrm{d}U \\ &= 2\,\epsilon\,\exp\!\Big(-\frac{\big(x-y\big)^2}{4\epsilon\,t} - \frac{y+2}{2\epsilon}\Big)\Big|_{-2}^{2} + \widetilde{I}_2\,, \end{aligned}$$

where

$$\widetilde{I}_2 = \int_{-2}^{2} \exp\!\Big[-\frac{\big(x-y\big)^2}{4\epsilon\,t} - \frac{\big(y+2\big)}{2\epsilon}\Big]\,\mathrm{d}y,$$

which is the same as integral I_5, and hence

$$\begin{aligned} I_2 \;= 2\epsilon\;&\Big[\mathrm{e}^{-\frac{2}{\epsilon}}\;\exp\!\Big(-\frac{\big(x-2\big)^2}{4\epsilon\,t}\Big) - \exp\!\Big(-\frac{\big(x+2\big)^2}{4\epsilon\,t}\Big)\Big] \\ &+ \sqrt{\pi\,\epsilon\,t}\;\exp\!\Big(\frac{t-2x-4}{4\epsilon}\Big)\;\Big[\mathrm{erf}\,\Big(\frac{t-x+2}{\sqrt{4\,\epsilon\,t}}\Big) - \mathrm{erf}\,\Big(\frac{t-x-2}{\sqrt{4\,\epsilon\,t}}\Big)\Big], \end{aligned}$$

where the error function is defined in equation (2.4.23). Integrating I_3 is similar to I_1

$$\begin{aligned} I_3 &= \int_2^{\infty} \frac{x-y}{t}\;\exp\!\Big[-\frac{\big(x-y\big)^2}{4\epsilon\,t} - \frac{2}{\epsilon}\Big]\,\mathrm{d}y, \\ &= \mathrm{e}^{-\frac{2}{\epsilon}}\;\int_2^{\infty} \frac{x-y}{t}\;\exp\!\Big[-\frac{\big(x-y\big)^2}{4\epsilon\,t}\Big]\,\mathrm{d}y, \\ &= 2\epsilon\;\mathrm{e}^{-\frac{2}{\epsilon}}\;\exp\!\Big(-\frac{\big(x-2\big)^2}{4\epsilon\,t}\Big)\,. \end{aligned}$$

To sum up these calculations we put the Cole-Hopf solution expressed in equation (2.4.19) in the form

$$u_1 = \frac{I_1\;+\;I_2\;+\;I_3}{I_4\;+\;I_5\;+\;I_6}\,.$$

Defining the function $Q(y;x,t)$ as

$$Q(y;x,t) = \exp\!\Big(\frac{t-2x-4}{4\epsilon}\Big)\;\Big[\mathrm{erf}\,\Big(\frac{t-x+2}{\sqrt{4\,\epsilon\,t}}\Big) - \mathrm{erf}\,\Big(\frac{t-x-2}{\sqrt{4\,\epsilon\,t}}\Big)\Big],$$

the integrals I_i for $i = 1, 2, ..., 6,$ are as follows

$$
\begin{aligned}
I_1 &= 2\epsilon \ \exp\Big(- \frac{\big(x+2\big)^2}{4\epsilon\, t}\Big), \\
I_2 &= 2\epsilon \left[\mathrm{e}^{-\frac{2}{\epsilon}} \ \exp\Big(- \frac{\big(x-2\big)^2}{4\epsilon\, t}\Big) - \exp\Big(- \frac{\big(x+2\big)^2}{4\epsilon\, t}\Big)\right] + \sqrt{\pi\,\epsilon\, t}\ \ Q(y;x,t) \\
I_3 &= 2\epsilon \ \mathrm{e}^{-\frac{2}{\epsilon}} \ \exp\Big(- \frac{\big(x-2\big)^2}{4\epsilon\, t}\Big) \\
I_4 &= \sqrt{\pi\epsilon\, t}\ \ \mathrm{erfc}\left(\frac{x+2}{\sqrt{4\epsilon\, t}}\right), \\
I_5 &= \sqrt{\pi\,\epsilon\, t}\ \ Q(y;x,t), \\
I_6 &= \sqrt{\pi\epsilon\, t}\ \ \mathrm{e}^{-\frac{2}{\epsilon}} \ \ \mathrm{erfc}\left(- \frac{x-2}{\sqrt{4\epsilon\, t}}\right).
\end{aligned}
$$

Finally we can derive the solution $u_1(y;x,t)$ in equation (2.4.20) as follows

$$
u_1(y;x,t) = \frac{1}{\sqrt{\pi\,\epsilon\, t}}\ \frac{4\,\epsilon\,\mathrm{e}^{-\frac{2}{\epsilon}} \ \exp\Big(- \frac{\big(x-2\big)^2}{4\epsilon\, t}\Big) + \sqrt{\pi\,\epsilon\, t}\ Q(y;x,t)}{\mathrm{erfc}\left(\frac{x+2}{\sqrt{4\epsilon\, t}}\right) + \mathrm{e}^{-\frac{2}{\epsilon}} \ \ \mathrm{erfc}\left(- \frac{x-2}{\sqrt{4\epsilon\, t}}\right) + Q(y;x,t)}. \tag{2.4.25}
$$

This expression represents the Cole-Hopf solution for the initial value problem (2.4.3) with the initial waveform ϕ_1 .

Next we present our attempts to compute and plot the solution $u_1(x,t)$ given in equation (2.4.25) using a MATLAB program. In addition to those attempts, we will numerically evaluate the integrals in equation (2.4.19) and present figures illustrating all schemes used to evaluate this solution.

Numerical Evaluation of Cole-Hopf Solution for $\phi_1(x)$

Earlier in §2.4.2 we considered the initial value problem of Burgers' equation together with the initial condition $\phi_1(x)$. We looked for the Cole-Hopf solution to the problem and we obtained the solution expressed in (2.4.19) which we can easily evaluate and plot by computing numerically the integrals. We also evaluated the integrals in (2.4.19) and we reached the solution formula in

(2.4.25) in terms of the error functions $\text{erf}(x)$ and $\text{erfc}(x)$.

We now present figures displaying the solution $u_1(x,t)$ using MATLAB programming. We could rely only on demonstrating the computed solution in (2.4.25), but we preferred to numerically calculate the integrals in the solution (2.4.19) using also MATLAB program, and obtain an approximation to the solution. Our intention is to illustrate both schemes of evaluating the solution $u_1(x,t)$ and compare the efficiency and accuracy of each scheme.

Let us now begin describing the first numerical approach, we call it Method 1, which is a Cole-Hopf solution evaluation derived by numerical calculations of the integrals in (2.4.19) using the Trapezoidal rule. We present this method in

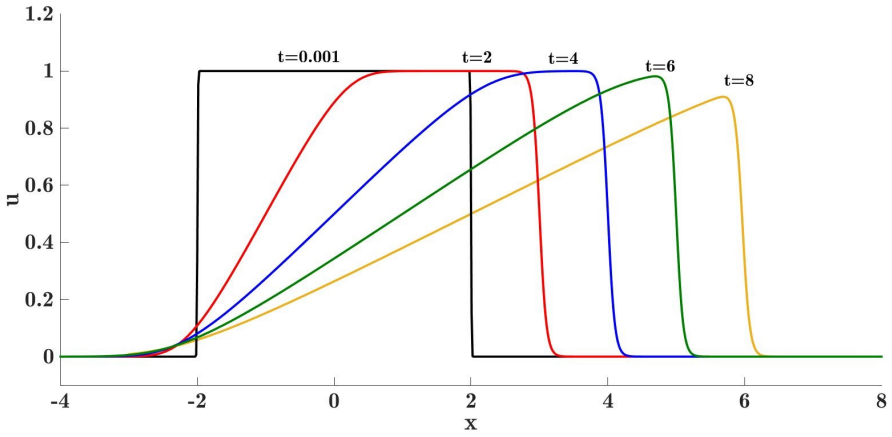

(a) $u_1(x,t)$ $\epsilon = 0.025$

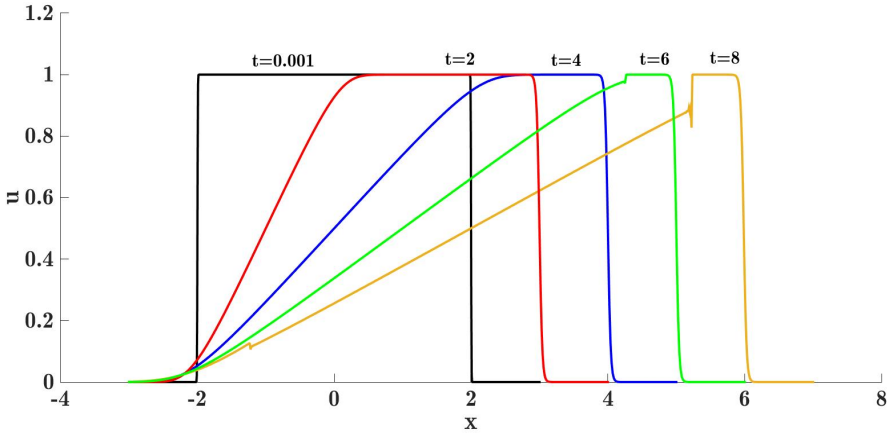

(b) $u_1(x,t)$ $\epsilon = 0.01$

Figure 2.4.1: The propagation of Cole-Hopf solution with numerical computations of integrals in equation (2.4.19) using method 1.

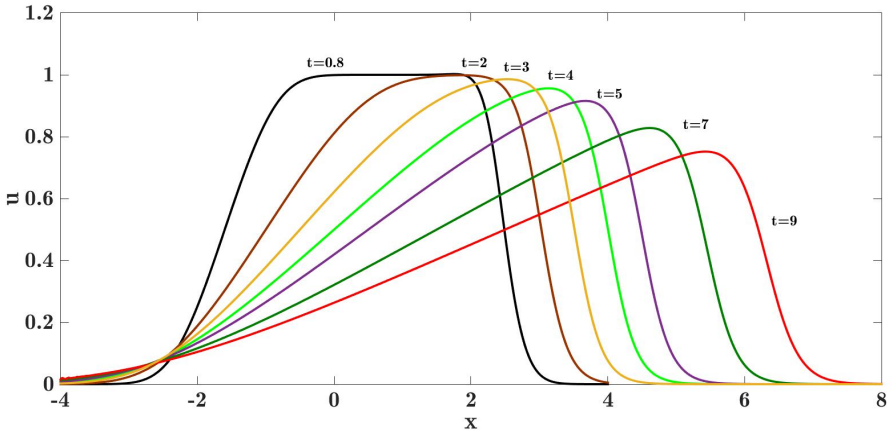

(a) $u_1(x,t) \quad \epsilon = 0.1$

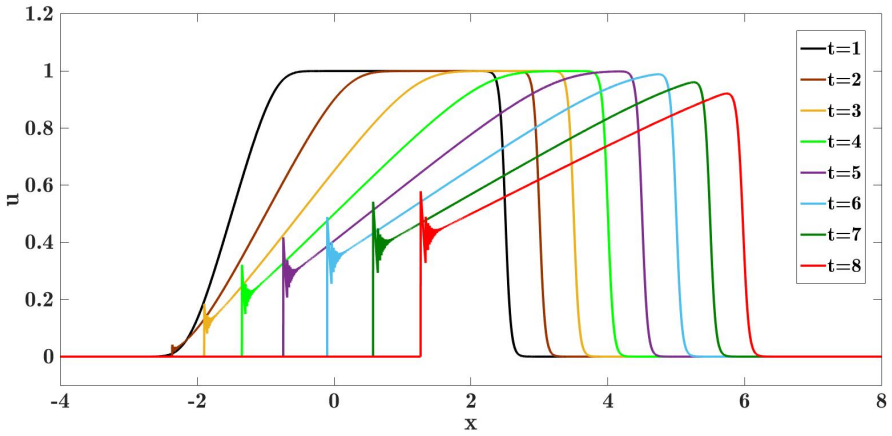

(b) $u_1(x,t) \quad \epsilon = 0.02$

Figure 2.4.2: The evaluated solution of Cole-Hopf solution in terms of error functions $\text{erf}(x)$ and $\text{erfc}(x)$ given in equation (2.4.19) using method 2A.

figure 2.4.1 where we plot the evaluated solution at several times for the two values of viscosity $\epsilon = 0.025$ in (a) and $\epsilon = 0.01$ in (b). Figure 2.4.1 (a) shows the solution which is plotted at consecutive times, as a form of shock wave propagating to the right and which diffuses out as time passes. We can see that the presence of viscosity combined with the effects of non-linearity smooth out the shock front. While previously, in the characteristic method solutions §2.2.3, the solution of inviscid Burgers' equation $\epsilon = 0$ is a propagating wave with sharp discontinuous shock fronts. We see in figure 2.4.1 (a) that for $\epsilon \geq 0.025$, Method 1 produces very accurate results of the solution. However, when viscosity is reduced to $\epsilon = 0.01$ we only could obtain good approximation for the solution up to $t \leq 4$, but for larger t the solution immediately behind the

shock fails and no longer becomes a good approximation to the characteristic solution presented in §2.2.3.

The second approach consists of evaluating the solution (2.4.25) written in terms of error functions $\text{erf}(x)$ and $\text{erfc}(x)$. To evaluate this solution via MATLAB we carried out three different Methods that we named 2A, 2B and 2C. In Method 2A, the arguments in equation (2.4.25) are written in the MATLAB algorithm as numbers, so when we run the calculations of the $\text{erf}(x)$ and $\text{erfc}(x)$ they will return as floating-points results. In Method 2B, we increase the accuracy by converting the arguments into the symbolic form using the command (sym), and after running the calculations we will receive symbolic outcomes. Thus, we use the variable-precision floating-point arithmetic function (vpa,d) to approximate the symbolic results with required number of decimal digits, d, here we fixed at the default value of MATLAB precision, which is 32. Finally, in Method 2C, which is very similar to Method 2B, but with a higher accuracy by choosing the value of d to be inversely dependent on the value of the viscosity.

Figure 2.4.2 represents the solution given in (2.4.25) by applying method 2C at various times. We see in plot (a) that this method works well in generating the solution for several fixed times with relatively small $\epsilon = 0.1$. However, as we reduced viscosity below 0.1, for example $\epsilon = 0.02$ in figure 2.4.2 (b), we see the solution failed in the tail shock region. This failure is more significant as time increases, and we will investigate the cause of this error after we demonstrate the results of Methods 2B and 2C.

Figure 2.4.3 shows the results of Method 2B, we see that this method produce a much accurate solution compared to Method 2A. Since for $\epsilon = 0.02$ in figure 2.4.2 (b) we see the solution fails significantly to meet its exact values, but in figure 2.4.3 (a) we see better results. However, for smaller values of viscosity $\epsilon = 0.01$, the error in the solution at $t = 8$ becomes apparent as shown in figure 2.4.3 (b).

Figure 2.4.4 shows the results of Method 2C, in plot (a) we fixed the decimal of floating-point at $d = 32$, and in plot (b) for reduced viscosity $\epsilon = 0.01$ we increased the digits to $d = 110$ to obtain a higher accuracy in the outputs. Hence, by using Method 2C we can achieve an accurate solution for any small value of ϵ.

We now investigate the cause of the error that leads the solutions of Method 2A and 2B to fail to meet their correct approximated values. We notice that when ϵ is reduced, the error makes the solution to be equal to 0 for small values of x. Followed by some oscillations, then the solution returns back to its accurate values. We believe that studying the behaviour of the error functions

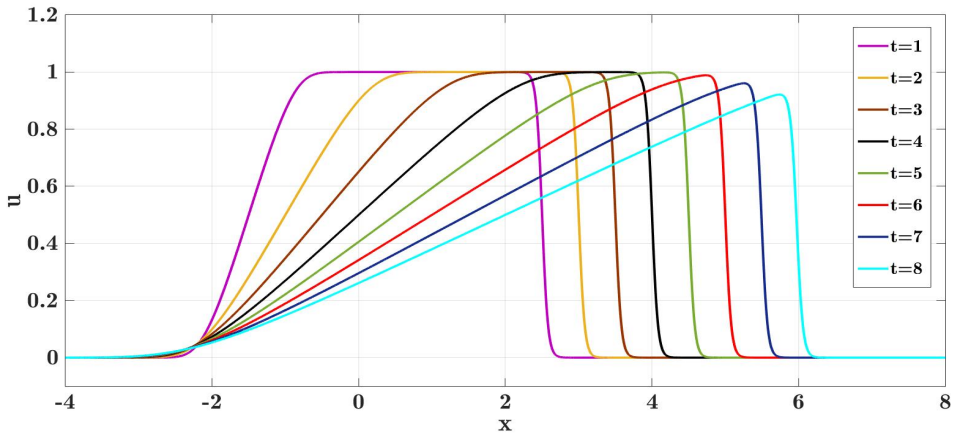

(a) $u_1(x,t) \quad \epsilon = 0.02$

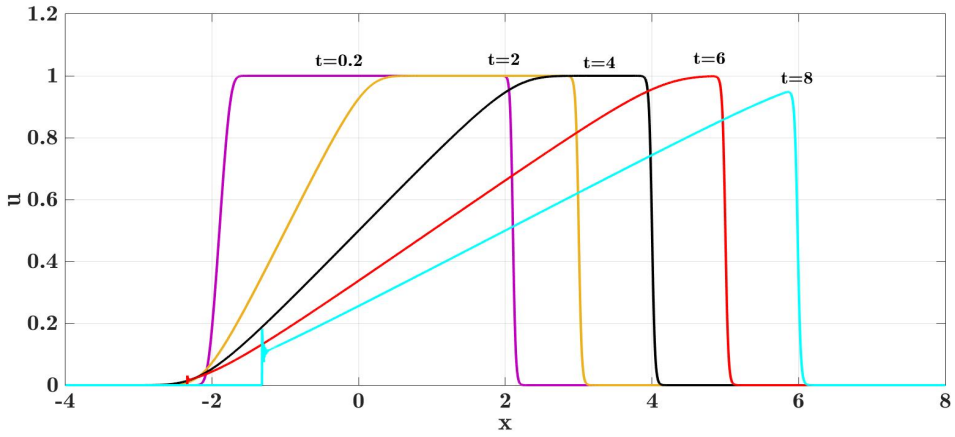

(b) $u_1(x,t) \quad \epsilon = 0.01$

Figure 2.4.3: The evaluated solution of Cole-Hopf solution in terms of error functions $\text{erf}(x)$ and $\text{erfc}(x)$ given in equation (2.4.20) using method 2B.

erf and erfc will give us some answers.

The error functions erf(x) and erfc(x) defined in (2.4.23) and (2.4.22) can be numerically approximated by the expansions defined in Abramowitz and Stegun [1] p 297 as follows

$$\text{erf}(z) = \frac{2}{\sqrt{\pi}} \sum_{n=0}^{\infty} \frac{(-1)^n \, z^{2n+1}}{n! \, (2n+1)}, \tag{2.4.26}$$

$$\text{erfc}(z) = \frac{2}{\sqrt{\pi}} \mathrm{e}^{-z^2} \sum_{n=0}^{\infty} \frac{2^n \, z^{2n+1}}{(2n+1)!!}, \tag{2.4.27}$$

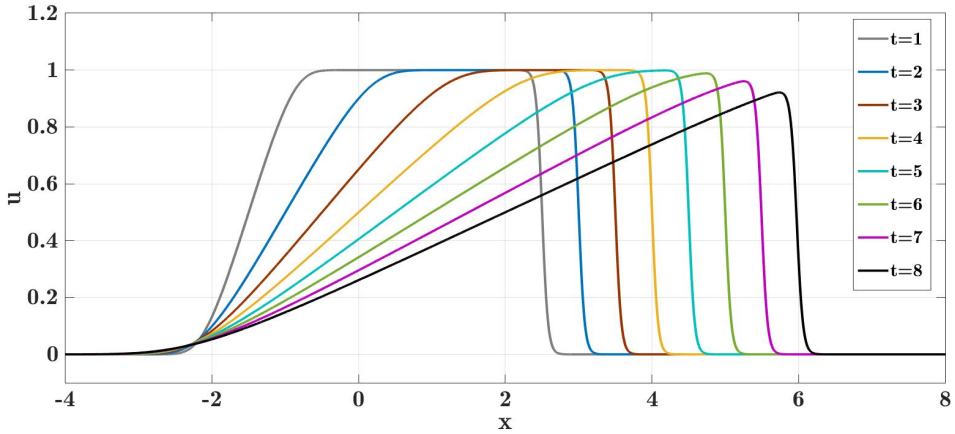

(a) $u_1(x,t) \quad \epsilon = 0.02$

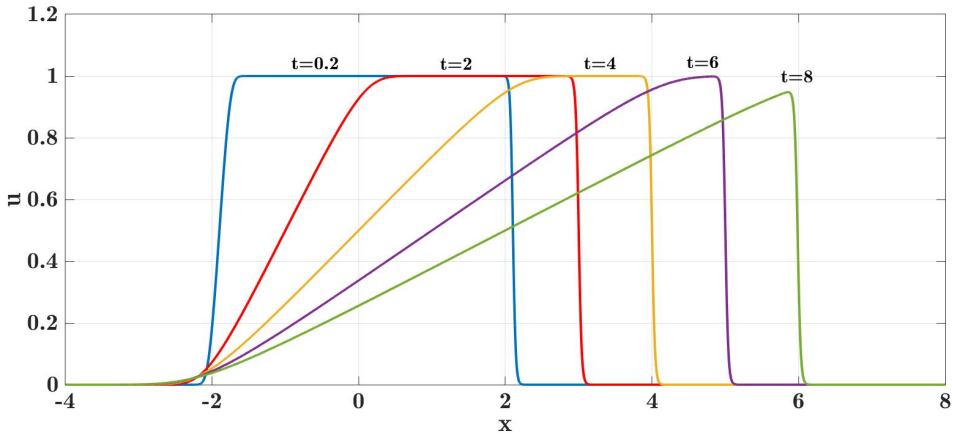

(b) $u_1(x,t) \quad \epsilon = 0.01$

Figure 2.4.4: The evaluated solution of Cole-Hopf solution in terms of error functions erf(x) and erfc(x) given in equation (2.4.20) using method 2C.

for small z and the asymptotic expansion for large z is

$$\operatorname{erfc}(z) = \frac{\mathrm{e}^{-z^2}}{z\sqrt{\pi}}\left\{1 + \sum_{n=1}^{\infty}(-1)^n \frac{(2n-1)!!}{(2z^2)^n}\right\}. \tag{2.4.28}$$

In the MATLAB program, the error function and its complementary function erf and erfc algorithm is a translation of a built-in function in FORTRAN program by W. Cody [22], named SPECFUN, using the rational Chebyshev approximations for error functions $\operatorname{erf}(z)$ and $\operatorname{erfc}(z)$ with maximal error range 6×10^{-19} and 3×10^{-20} [22]. The theoretical approximations used are defined in specified intervals as follows

$$\operatorname{erfc}(z) = 1 - z\,R_{l\,m}(z^2), \qquad |z| \le 0.5 \tag{2.4.29}$$

$$\operatorname{erfc}(z) = \mathrm{e}^{-z^2} R_{l\,m}(z), \qquad 0.5 \le z \le 4.0. \tag{2.4.30}$$

and the asymptotic expansion for large z is

$$\operatorname{erfc}(z) = \frac{\mathrm{e}^{-z^2}}{z}\left\{\frac{1}{\sqrt{\pi}} + \frac{1}{z^2} R_{l\,m}\Big(\frac{1}{z^2}\Big)\right\}, \qquad z \ge 4, \tag{2.4.31}$$

where the $R_{l\,m}(z)$ are rational functions with a polynomial of degree l in the numerator and a polynomial of degree m in the denominator. One can notice that the computations either for erf or erfc for large z contains the evaluation of e^{-z^2} which causes large errors.

We expect this caused error is related to the function $Q(x,t)$ in equation (2.4.25),

$$Q(y;x,t) = \exp\left(\frac{t-2x-4}{4\epsilon}\right)\left[\operatorname{erf}\left(\frac{t-x+2}{\sqrt{4\,\epsilon\,t}}\right) - \operatorname{erf}\left(\frac{t-x-2}{\sqrt{4\,\epsilon\,t}}\right)\right]. \tag{2.4.32}$$

Much care should be taken into account when computing this function. Since it involves a differences between error functions, and any resulting error form this difference will be exponentially enlarged due to the term $\exp\Big(\frac{t-2x-4}{4\epsilon}\Big)$. Thus, for small values of x the arguments z of the error functions becomes large, the error functions are then computed as $\operatorname{erf}(z) = 1 - \operatorname{erfc}(z)$, which is in this case close to 1 (i.e 0.999..), but for small precisions this value is rounded to 1.

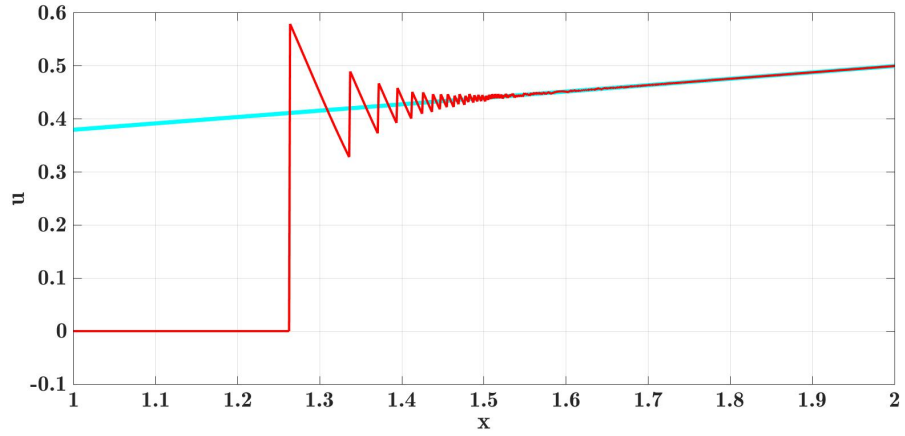

Figure 2.4.5: A blow up plot of the Cole-Hopf solution via Method 2A (red) and 2B covering $1 \leq x \leq 2$ at time $t = 8$ and viscosity $\epsilon = 0.02$.

Consequently, evaluating the difference of the error functions in (2.4.32) is zero, hence, the values of the solution are 0. Then, for moderate values of x some oscillations appear in the solution before it returns to its correct values.

Figure 2.4.5 shows comparisons between Methods 2A and 2B in the spacial interval $[1, 2]$ for $t = 8$ and $\epsilon = 0.02$. It is clear to see the failure of Method 2A (red) to correspond to the correct values of solution in the first half of the interval and gives an accurate approximations in the second half of the interval. In this interval we choose three different spacial points $x = 1,\ 1.264,\ 1.8$ and in table 2.1 we illustrate to seven decimal digits the values of the difference $\sigma(\text{erf})$ where

$$\sigma\big(\,\text{erf}\,\big) = \text{erf}\left(\frac{t-x+2}{\sqrt{4\,\epsilon\,t}}\right) - \text{erf}\left(\frac{t-x-2}{\sqrt{4\,\epsilon\,t}}\right),$$

and the function Q in Methods 2A and 2B for time $t = 8$ viscosity 0.02.

	Method 2A		Method 2B	
x	$\sigma(\text{erf})$	Q	$\sigma(\text{erf})$	Q
1	0	0	$9.672204\,E^{-19}$	$6.96446\,E^{-8}$
1.264	$1.110223\,E^{-16}$	$1.087499\,E^{-9}$	$5.657911E^{-16}$	$5.542102\,E^{-9}$
1.8	$1.131318\,E^{-13}$	$1.679024\,E^{-11}$	$1.131031\,E^{-13}$	$1.678599\,E^{-11}$

Table 2.1: Comparisons of the values of the function Q defined in (2.4.32) for the two Methods 2A and 2B.

The final figures 2.4.6 and 2.4.7 represent comparisons between the first approach, the numerical evaluation of the integral in equation (2.4.19) (method 1) which is represented by blue (o) and two evaluated solutions in terms of error functions erf and erfc given in equation (2.4.25), method 2B represented by red $(*)$ and method 2C represented by green hexagon. This comparison is taken for small values of viscosity $\epsilon = 0.025$ $\epsilon = 0.01$ and the figures show the solutions at times $t = 0.2, 4, 8$. In figure 2.4.6, we see the agreement is very good for this value of ϵ except for the head shock region at small times (see figure 2.4.6 (a)). In figure 2.4.7 when the viscous parameter is reduced to $\epsilon = 0.01$ we see that only method 2C marked by green hexagon gives an accurate results, in contrast method 1 and method 2B, both fail to the accurate values (see plots 2.4.7 (b),(c)) and it is seen that method 2B is the worst among the three. We notify that the errors in evaluation for small times are not considered further.

In conclusion we were able to produce different numerical evaluations of the Cole-Hopf solution. First scheme is by computing numerically the integrals in (2.4.19). The second scheme is carried out through numerical computing of the error functions erf and erfc in solution (2.4.25). For the later implementation we derived three Methods 2A, 2B and 2C where the precisions varies. It appears that Method 2C is of the highest accuracy among all methods, with applying the MATLAB procedure of precision floating-point arithmetic to minimise the effect of round-off errors. The computations in all figures except figure 2.4.6 are taken with the step size $\mathrm{d}x = 0.0012$ to achieve more accuracy which made the calculations costly in time. In particular, Methods 1 and 2C where executing their figures took days.

The key message of this analysis is that while Cole-Hopf provides an exact solution for plane Burgers' equation, considerable care is needed in evaluating the solution for small ϵ, and in this case asymptotic analysis is better. Next we will introduce a higher efficiency numerical approach based on the pseudo-spectral methods and fourth-order Runge-Kutta method

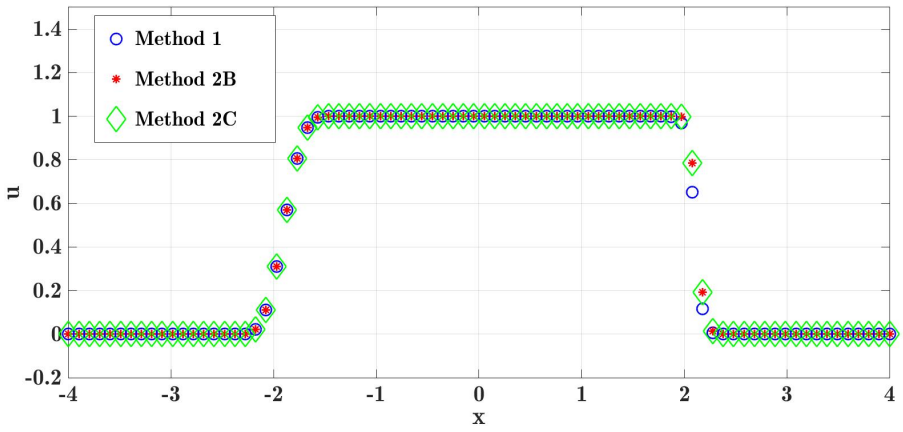

(a) $u_1(x, 0.2)$ $\epsilon = 0.025$

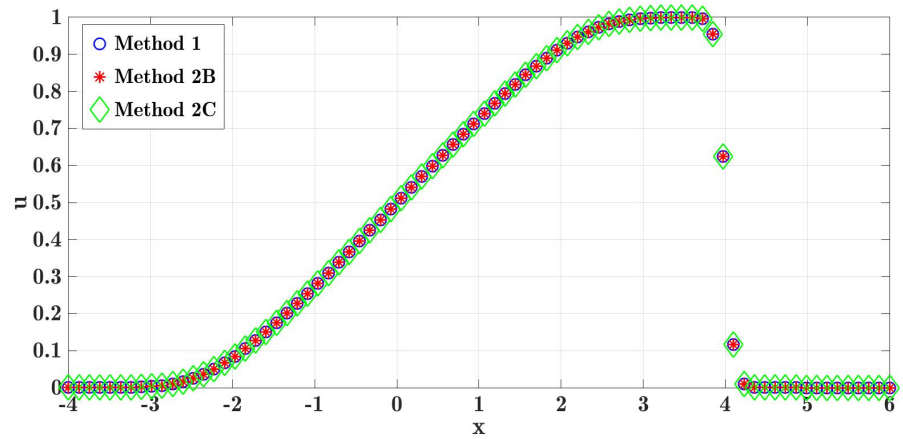

(b) $u_1(x, 4)$ $\epsilon = 0.025$

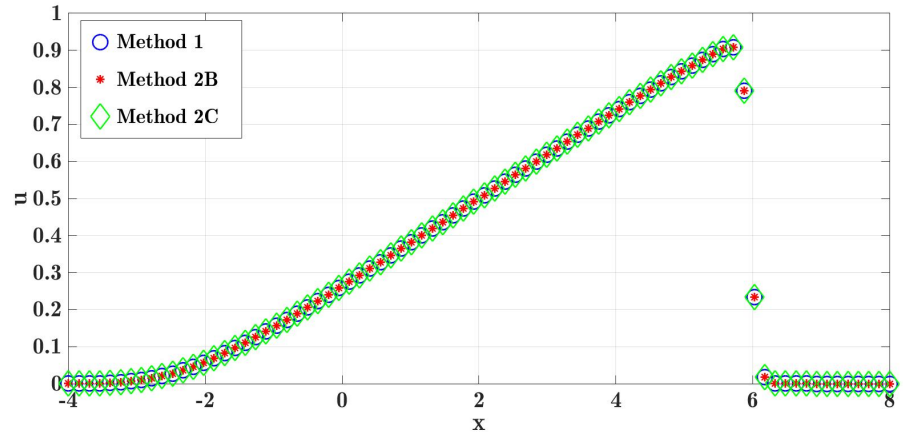

(c) $u_1(x, 8)$ $\epsilon = 0.025$

Figure 2.4.6: Comparisons of the Cole-Hopf solutions for $u_1(x, t)$ one is the numerical evaluations of the integrals (blue o) (method 1) and the two computed solutions in terms of error functions using method 2B (red *) and method 2C green hexagon.

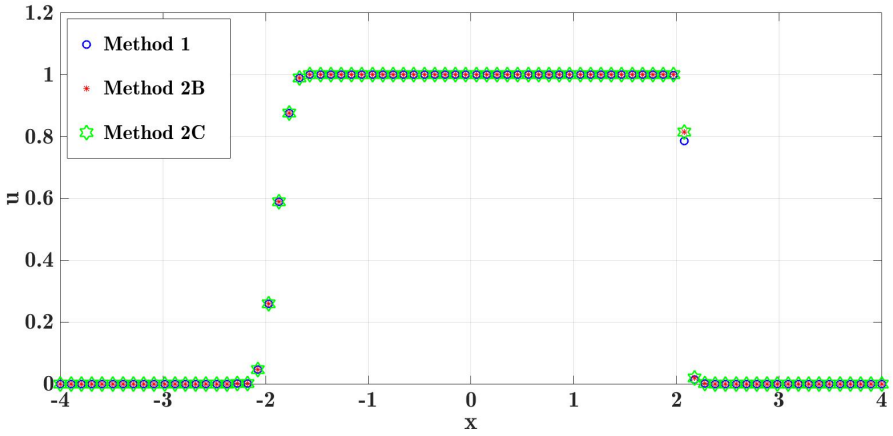

(a) $u_1(x, 0.2) \quad \epsilon = 0.01$

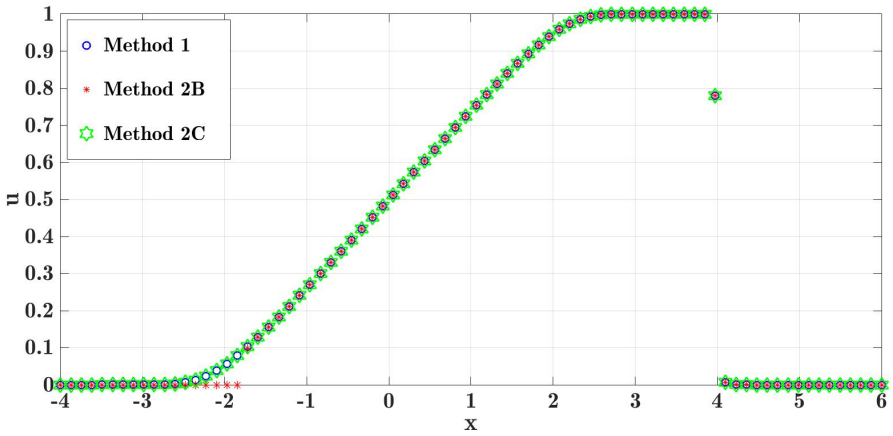

(b) $u_1(x, 4) \quad \epsilon = 0.01$

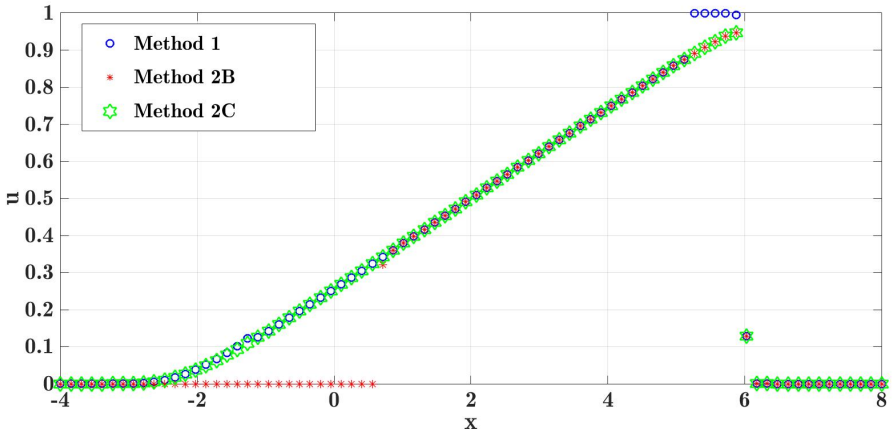

(c) $u_1(x, 8) \quad \epsilon = 0.01$

Figure 2.4.7: Comparisons of the Cole-Hopf solutions for $u_1(x, t)$ one is the numerical evaluations of the integrals (blue o) (method 1) and the two computed solutions in terms of error functions using method 2B (red *) and method 2C green hexagon.

Asymptotic Behaviour of The Solution

Before we consider the asymptotic behaviour of Cole-Hopf solution (2.4.19) in the limit $\epsilon \to 0$, we summarise the results of the characteristics method described earlier in §2.2.3 for the first initial condition $u_0(x) = \phi_1(x)$ defined in equation (2.4.17).

The method of characteristic supplemented by the Rankine-Hugoniot condition ensures the solution is single-valued everywhere and when it becomes multivalued a discontinuity is inserted. In figure 2.4.8 (a) we can see this initial profile has a jump discontinuity at $x = 2$ we expect for $t > 0$ the wave to overturn. Thus, for $t > 0$ we divided the solution into five regions A, B, C, D and E shown in 2.4.8 (b). Region A for $x < -2$, region B when $-2 < x < -2 + t$ and C is between $-2 + t$ and 2. Region D is when the wave is overturning that is when $2 < x < 2 + t$ and finally region E for $2 + t < x$.

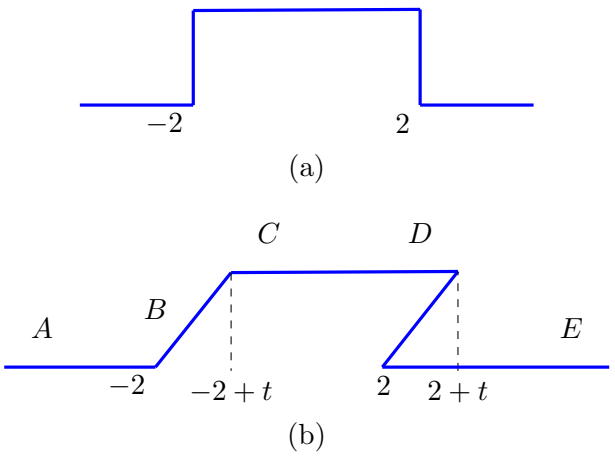

Figure 2.4.8: The solution $u_1(x, t)$ for time $0 < t < 8$ showing regions A, B, C, D and E where the the function $G_1(\xi)$ assumes single minimum value except in region D where G_1 has more than one minimum value as the solution is multivalued in this region.

We now find the small ϵ asymptotic solution and show it is consistent with the characteristic method solution. In particular, the discontinuities and shock positions that were deduced either by the Rankine-Hugoniot condition or Equal Area Rule as explained in §2.2.3. To begin constructing the asymptotic Cole-

Hopf solution $u_1(x,t)$ for $\epsilon \ll 1$, let us recall the importance of minimum values of $G(y;x,t)$ defined in (2.4.10). Previously, in §2.4.1 we mentioned that in order to understand the solution's behaviour, we examined the integrand in equation (2.4.9) using the method of stationary phase. One way to locate the minimums of $G(y)$ is to find the stationary points or in other words the zeros of the derivative $\frac{\partial G}{\partial y}$ at which $\frac{\partial^2 G}{\partial y^2} > 0$. For this example the function G is given as G_1 defined in equation (2.4.18). To locate its minimum values we differentiate G_1 with respect to y and equate the derivative to zero as follows

$$0 = \frac{\partial G_1}{\partial y}\bigg|_{y=\xi} = \frac{\xi - x}{t} + \begin{cases} 0, & \xi < -2, \\ 1, & -2 < \xi < 2, \\ 0, & 2 < \xi, \end{cases} \tag{2.4.33}$$

We denote the zeros of the derivative $G'(y)$ by $y = \xi_i$ for $i = 1, 2, ..., N$ and $\xi_i < \xi_{i+1}$. Then for sufficiently small ϵ the function $\exp\left(-\frac{G_1}{2\,\epsilon}\right)$ is much smaller than its value at $y = \xi_i$ where it peaks. Hence, we can asymptotically evaluate the integrals in (2.4.19) to obtain

$$u_1(x,t) \sim \frac{\displaystyle\sum_{i=1}^{N} \frac{x-\xi_i}{t} \sqrt{\frac{4\,\pi\,\epsilon}{\left|G_1''(\xi_i)\right|}}\, \exp\!\left(-\frac{G_1(\xi_i)}{2\epsilon}\right)}{\displaystyle\sum_{i=1}^{N} \sqrt{\frac{4\,\pi\,\epsilon}{\left|G_1''(\xi_i)\right|}}\, \exp\!\left(-\frac{G_1(\xi_i)}{2\epsilon}\right)}. \tag{2.4.34}$$

Therefore, for very small ϵ the set ξ_i of minimum values of $G_1(y)$ determines completely the asymptotic solution $u_1(x,t)$. In figure 2.4.9, we plot the derivative $\frac{\partial G_1}{\partial y}$ as a function of y for $t = 2$ for various values of x corresponding to the regions illustrated in figure 2.4.8. We begin with analysing regions $\mathrm{A}, \mathrm{B}, \mathrm{C}, \mathrm{E}$ leaving D to a later discussion. In regions A,B,C,E we see from figure 2.4.9, that since there is a single root of $G_1'(y)$, and hence a single minimum of G_1. So from (2.4.34) the solution u_1 is then given by

$$u_1(x,t) \sim \frac{x-\xi}{t}. \tag{2.4.35}$$

This corresponds to the characteristic method solution (2.2.28) for the regions where the solution is single valued (see figure 2.4.8). In region D we see in plot (d) there are three roots of $G_1'(y)$ We return to this case later when we show that there are two minimums and one maximum.

We now look in more detail at the solution in regions A,B,C and E and compare the solutions with characteristic method outputs. In figure 2.4.9 (a), where $x = -3$ corresponding to a point in region A, we have a single root $\xi = x$ and hence from (2.4.14) $u = 0$. In (b) when $x = -1$ we again have a single root $\xi = -2$ and hence, $u = \frac{x+2}{t}$. In (c) for $x = 1$ we have single root $\xi = x - t$, and hence, $u = 1$. Plot (e) is representative of region E which is similar to A. For $x = 4.5$ we have a single root $\xi = x$ and hence $u = 0$. We can sum up the solution for the various regions as follows

$$u_1(x,t) = \begin{cases} 0, & x < -2 \\ \frac{x+2}{t}, & -2 < x < -2 + t \\ 1, & -2 + t < x < 2 \\ f(x,t), & 2 < x < 2 + t \\ 0, & 2 + t < x, \end{cases} \tag{2.4.36}$$

where $f(x,t)$ is the solution in region D which we will now analyse. In region D, $G_1(y)$ contains more than one minimum and then the solution is multivalued as we illustrated in figure 2.4.8. Thus, a shock should be fitted in this region and we will show using the method of stationary phase of the Cole-Hopf solution that we can determine the postion and structure of the shock. Let us look at figure 2.4.9 plot (d) for $x = 3$ and $t = 2$, there exist three roots:

$$\xi_1 = x - t, \qquad \xi_2 = 2, \qquad \xi_3 = x,$$

where the corresponding solution u_1 is given by

$$u_1(\xi_1) = 1, \qquad u_1(\xi_2) = \frac{x-2}{t}, \qquad u_1(\xi_3) = 0.$$

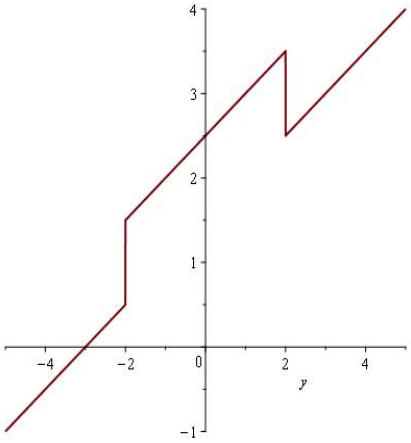

(a) Region A for $G_1'(y, -3, 2)$.

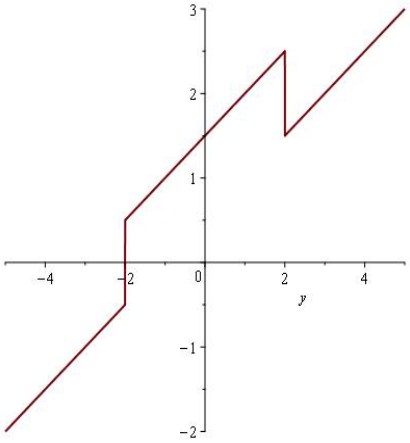

(b) Region B for $G_1'(y, -1, 2)$.

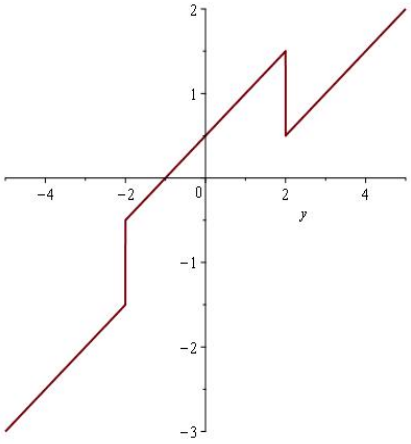

(c) Region C for $G_1'(y, 1, 2)$.

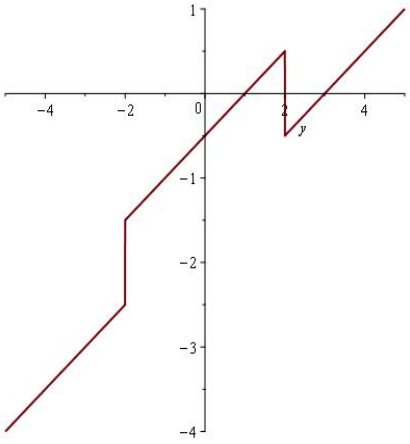

(d) Region D for $G_1'(y, 3, 2)$.

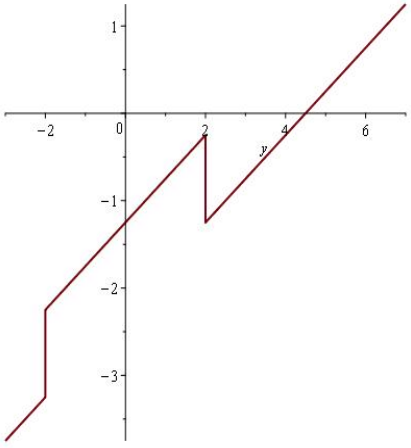

(e) Region E for $G_1'(y, 4.5, 2)$.

Figure 2.4.9: Plots of the derivative $\frac{\partial G_1(y)}{\partial y}$ showing stationary points for fixed x and t.

In figure 2.4.10 we see that ξ_1 and ξ_3 correspond to minimum values of $G_1(y;x,t)$ corresponding to $u=1$ and $u=0$ respectively. Also, ξ_2 corresponds to a maximum in G_1 and so is not relevant to the stationary phase method in §2.4.1.

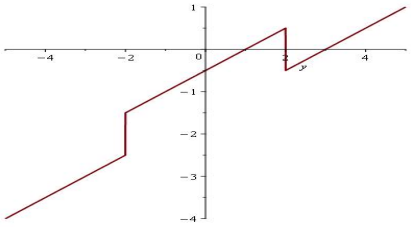

(a) $G_1'(y,-3,2)$

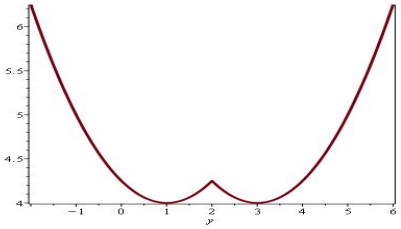

(b) $G_1(y,3,2)$

Figure 2.4.10: Plots of $\frac{\partial G_1}{\partial y}$ in (a) and $G_1(y)$ in (b) in Region D showing the three roots $\xi_1=1$, $\xi_2=2$, $\xi_3=3$ in (a) and in (b) we can see that $\xi_1=1$ and $\xi_1=3$ are minimums while $\xi_2=2$ is maximum which is for $x=3$ and $t=2$.

To determine the solution in region D, we look for the functions $G(\xi)$ in terms of the two roots ξ_1, ξ_3

$$G_1(\xi_1) = \frac{t}{2} + \begin{cases} 0, & x < t-2 \\ x-t+2, & t-2 < x < t+2 \\ 4, & t+2 < x \end{cases}$$

$$G_1(\xi_3) = \begin{cases} 0, & x < -2 \\ x+2, & -2 < x < 2 \\ 4, & 2 < x \end{cases}$$

Since we are interested in region D, thus, we look when $2 < x < 2+t$. In this case we have

$$\begin{aligned} G_1(\xi_1) &= \frac{t}{2} + (x-t+2) = x - \frac{t}{2} + 2 \\ G_1(\xi_3) &= 4. \end{aligned}$$

For given x and t the function $G_1(\xi)$ assumes its minimum values at a set of points $\xi = \xi_i$. Consequently, there exists some ξ_k in which $G_1(\xi_k)$ takes its

lowest value among all ξ_i, and hence for $i \neq k$ we deduce

$$\frac{G_1(\xi_k)}{2\epsilon} \ll \frac{G_1(\xi_i)}{2\epsilon}, \quad \Longrightarrow \quad \exp\bigg(-\frac{G_1(\xi_k)}{2\epsilon}\bigg) \gg \exp\bigg(-\frac{G_1(\xi_i)}{2\epsilon}\bigg).$$

Thus, for $\epsilon \ll 1$ the right hand side of equation (2.4.34) is dominated by the term $i = k$ and all other terms $i \neq k$ will be neglected. In region D we have two ξ_1, ξ_3 and so we study the case if one is lower than the other. For the case $G_1(\xi_1) < G_1(\xi_3)$ i.e $x - \frac{t}{2} + 2 < 4$, this is true when $x < 2 + \frac{t}{2}$. The solution is then dominated by the contributions from the immediate neighbourhood of ξ_1

$$u_1(x,t) \sim \frac{\sqrt{t}\,\dfrac{x-\xi_1}{t}\;\exp\bigg(-\dfrac{G_1(\xi_1)}{2\epsilon}\bigg)}{\sqrt{t}\,\exp\bigg(-\dfrac{G_1(\xi_1)}{2\epsilon}\bigg)},$$

where the second derivative of $G(\xi)$ is calculated $G''(\xi_i) = \frac{1}{t}$. Therefore, we can write the solution as

$$u_1^-(x,t) \sim \frac{x-\xi_1}{t} \sim \frac{x-(x-t)}{t} \sim 1, \tag{2.4.37}$$

which is the solution to the left of the shock. If $G_1(\xi_1) > G_1(\xi_3)$ then $x > 2 + \frac{t}{2}$ and from the method of stationary phase, the solution to the right of the shock is dominated by the contributions from the immediate neighbourhood of ξ_3

$$u_1^+(x,t) \sim \frac{x-\xi_3}{t} \sim \frac{x-x}{t} \sim 0. \tag{2.4.38}$$

We now consider the case when $G_1(\xi_1)$ and $G_1(\xi_3)$ are very close in value. Then $G_1(\xi_1) \approx G_1(\xi_3)$ i.e $x \approx 2 + \frac{t}{2}$. If we let $G_1(\xi_1) = G_1(\xi_3) + \Delta$ where Δ is very small then $G_1(\xi_1) = 4 + \Delta$. Hence, from equation (2.4.34) the solution is then evaluated as the sum of contributions from the immediate neighbourhoods of ξ_1

and ξ_3 as follows

$$\begin{aligned} u_1(x,t) &\sim \frac{\sqrt{t}\left[\frac{x-(x-t)}{t}\exp\left(-\frac{4+\Delta}{2\epsilon}\right)+\frac{x-x}{t}\exp\left(-\frac{4}{2\epsilon}\right)\right]}{\sqrt{t}\left[\exp\left(-\frac{2}{\epsilon}-\frac{\Delta}{2\epsilon}\right)+\exp\left(-\frac{2}{\epsilon}\right)\right]} \\ &\sim \frac{\sqrt{t}\ \exp\left(-\frac{2}{\epsilon}-\frac{\Delta}{2\epsilon}\right)}{\sqrt{t}\left[\exp\left(-\frac{2}{\epsilon}-\frac{\Delta}{2\epsilon}\right)+\exp\left(-\frac{2}{\epsilon}\right)\right]} \\ &\sim \frac{\exp\left(-\frac{\Delta}{2\epsilon}\right)}{\exp\left(-\frac{\Delta}{2\epsilon}\right)+1} \\ &\sim \frac{1}{1+\exp\left(\frac{\Delta}{2\epsilon}\right)}. \end{aligned}$$

Multiplying numerator and denominator by $2\exp(-\frac{\Delta}{4\epsilon})$ and using the definition of the hyperbolic tangent function $\tanh(x)$, gives

$$\begin{aligned} u_1(x,t) &\sim \frac{1}{2}\frac{2\exp\left(-\frac{\Delta}{4\epsilon}\right)}{\exp\left(-\frac{\Delta}{4\epsilon}\right)+\exp\left(\frac{\Delta}{4\epsilon}\right)} \\ &\sim \frac{1}{2}\left[1-\frac{\exp\left(\frac{\Delta}{4\epsilon}\right)-\exp\left(-\frac{\Delta}{4\epsilon}\right)}{\exp\left(\frac{\Delta}{4\epsilon}\right)+\exp\left(-\frac{\Delta}{4\epsilon}\right)}\right] \\ &\sim \frac{1}{2}\left[1-\tanh\left(\frac{\Delta}{4\epsilon}\right)\right]. \end{aligned}$$

Since $\Delta = x-2-\frac{t}{2}$ the solution $u_1(x,t)$ expressed in terms of the hyperbolic tangent function as

$$u_1(x,t) \sim \frac{1}{2}\left[1-\tanh\left(\frac{1}{4\epsilon}\left(x-2-\frac{t}{2}\right)\right)\right]. \tag{2.4.39}$$

This solution is the Taylor's hyperbolic tangent solution which describes thermoviscous shock of amplitude 1 and the shock front is located at $x_s = 2+\frac{t}{2}$ which corresponds to the solution we obtained earlier in the

asymptotic expansions theory in §2.3.3 equation (2.3.18).

This investigation showed that for fixed very small ϵ, the shock wave solution can be approximated by the method of characteristics in the region of shock formation where the solution is a discontinuity. The method of characteristics coupled with the Rankine-Hugoniot condition or the equal area rule has an importance in providing the time and position of shock formation which is of our interest. However, for studying the effects of diffusion on shock structure, the asymptotic expansion theory covers the influence of ϵ on shock width.

We next demonstrate Cole-Hopf solutions for the initial profiles $\phi_2(x)$ and $\phi_3(x)$ given in §2.1.

2.4.3 Cole-Hopf Solution for the Second and Third Initial Profiles

We now present the evaluation of Cole-Hopf solutions for the second and third initial waveforms $\phi_2(x)$ and $\phi_3(x)$ displayed in §2.1. Since these two given initial disturbances are stepwise constant functions, we can consider a more general form of ϕ_1 and ϕ_2 defined by

$$u_0(x) = \begin{cases} 0, & x < a \\ p, & a < x < b \\ q, & b < x < c \\ 0, & c < x \end{cases} \tag{2.4.40}$$

One can notice that fixing the constants $a = -2$, $b = -1$, $c = 2$, $p = 2$ and $q = 1$, the function u_0 corresponds to the second initial condition $u_0 = \phi_2$ and if $b = 1$ then u_0 corresponds to ϕ_3. To obtain the Cole-Hopf solution which is defined in equation (2.4.9) as

$$u_i(x,t) = \frac{\displaystyle\int_{-\infty}^{\infty} \frac{x-y}{t} \exp\left(\frac{-G_i}{2\epsilon}\right) \mathrm{d}y}{\displaystyle\int_{-\infty}^{\infty} \exp\left(\frac{-G_i}{2\epsilon}\right) \mathrm{d}y}, \qquad \text{For } i = 1, 2, \tag{2.4.41}$$

where

$$G_i(y;x,t) = \frac{(x-y)^2}{2t} + \widetilde{G}_(y;x,t),$$

we look for the function $\widetilde{G}_i(y;x,t)$ which represents the integral of the initial condition with respect to y. Thus, we can write $\widetilde{G}_i$ in the following form

$$\widetilde{G}_i(y;x,t) = \begin{cases} 0, & y < a \\ \int_a^y p \, \mathrm{d}y, & a < y < b \\ \int_a^b p \, \mathrm{d}y + \int_b^y q \, \mathrm{d}y, & b < y < c \\ \int_a^b p \, \mathrm{d}y + \int_b^c q \, \mathrm{d}y, & c < y \end{cases}$$

these integrals can be calculated so that $\widetilde{G}$ is in a simpler form to have this stepwise function

$$\widetilde{G}_i(y;x,t) = \begin{cases} 0, & y < a \\ p(y-a), & a < y < b \\ q(y-b) + p(b-a), & b < y < c \\ q(c-b) + p(b-a), & c < y. \end{cases} \tag{2.4.42}$$

Thus, for the initial condition ϕ_2 the function $\widetilde{G}_2$ is given by

$$\widetilde{G}_2(y;x,t) = \begin{cases} 0, & y < -2 \\ 2(y+2), & -2 < y < -1 \\ (y+1) + 2, & -1 < y < 2 \\ 5, & 2 < y \end{cases}$$

and for the initial condition ϕ_3 we have

$$\widetilde{G}_3(y;x,t) = \begin{cases} 0, & y < -2 \\ 2(y+2), & -2 < y < 1 \\ (y-1) + 6, & 1 < y < 2 \\ 7, & 2 < y \end{cases}.$$

Therefore, by inserting $\widetilde{G}_2$ in equation (2.4.41) we have an expression of Cole-Hopf solution u_2 for initial condition ϕ_2, this also applies for the other initial condition ϕ_3 if we inserted $\widetilde{G}_3$. To evaluate the solutions u_2 and u_3 we can apply any of the previous implemented methods described in §2.4.2. Here we choose method 1, to evaluate the integrals in (2.4.41) numerically using MATLAB programming.

The Cole-Hopf solutions u_2 and u_3 are presented in figures 2.4.11 and 2.4.12 (blue curves), compared with the characteristics solutions described in §2.2.3

and §2.2.3, but before we describe the Cole-Hopf solutions in figures 2.4.11, 2.4.12, let us present an overview reminder of the method of characteristics results coupled with Rankine-Hugoinot conditions for the initial value problem of inviscid Burgers' equation together with ϕ_2, ϕ_3.

We begin with the the method of characteristics solution for ϕ_2 described in §2.2.3 where a rarefaction wave at $x = -2$ and an existing two shocks S_1 and S_2 (shown in figure 2.4.11(a) red curve), positioned respectively at $x_1 = -1 + \frac{3}{2}$ and $x_2 = 2 + \frac{1}{2}\,t$ with amplitude 1. At time $t = 2$ as the rarefaction wave is propagating faster than shock S_1 and overtakes this shock to form a new third shock S_3 located at $-2 + t + \sqrt{2\,t}$ with amplitude $1 + \sqrt{\frac{2}{t}}$ (see plot 2.4.11 (b)). When time reaches $t = 3.1$, the two shock S_2 and S_3 will collide resulting a fourth shock S_4 shown in plot (c) figure 2.4.11, this permanent shock front is located at $x_4 = -2 + 3.16\sqrt{t}$ with the amplitude being absorbed into the shock in the rate $\frac{3.16}{\sqrt{t}}$.

Similarly for the other initial wave ϕ_3, the method of characteristics solutions in §2.2.3 indicated that wave has formed two shocks S_1 and S_2 located respectively at $x_{S\,1} = 1 + \frac{3}{2}$ and $x_{S\,2} = 2 + \frac{1}{2}\,t$ with amplitude 1 (see plot (a) in figure 2.4.12 red curve). In plot 2.4.12 (b) shows that these two shocks will collide at time $t = 1$ to produce a shock S_3 located at $x = \frac{3}{2} + t$ and it continues to propagate before the shock changes to the triangular deformation at $t = 3.5$ in figure 2.4.12 (c), and then it decays in a lower rate $\sqrt{\frac{14}{t}}$.

We now return to the Cole-Hopf solutions u_2 and u_3 for the two viscid initial problem of ϕ_2 and ϕ_3. For non-zero small viscosity ϵ, we anticipate the effect of viscosity to be small except in the narrow shock region, and so the Cole-Hopf solution will resemble the $\epsilon = 0$ case, except for the finite shock thickness. We can see that in figure 2.4.11 showing the Cole-Hopf solution u_2 in blue curves for the fixed viscosity $\epsilon = 0.025$ corresponding to the $\epsilon = 0$ solution in red curve except in the thin shock zone where the viscous coefficient smoothed out the shock front. This also true for the other Cole-Hopf solution u_3 illustrated in figure 2.4.12.

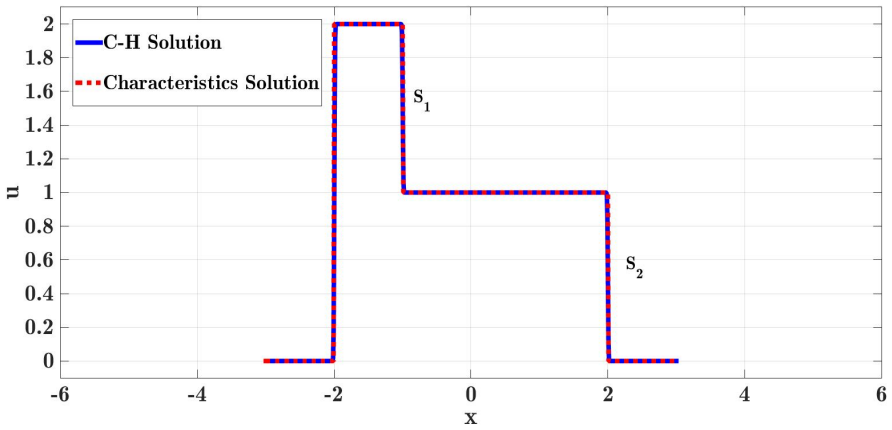

(a) $u_2(x, 0.001) \quad \epsilon = 0.025$

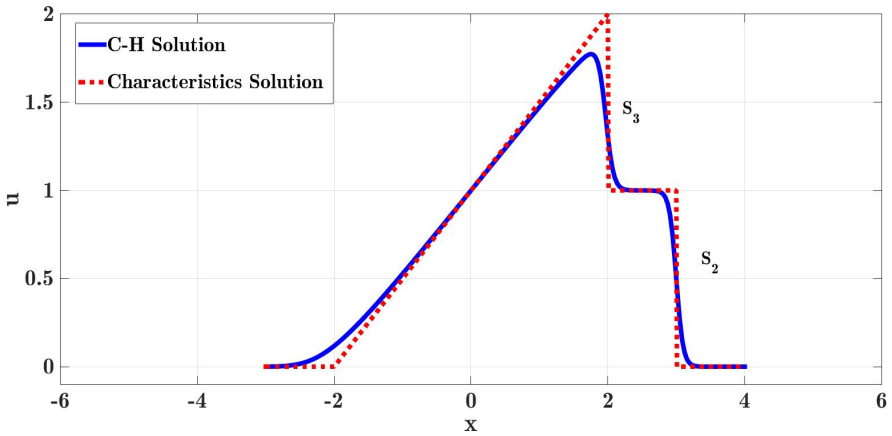

(b) $u_2(x, 2) \quad \epsilon = 0.025$

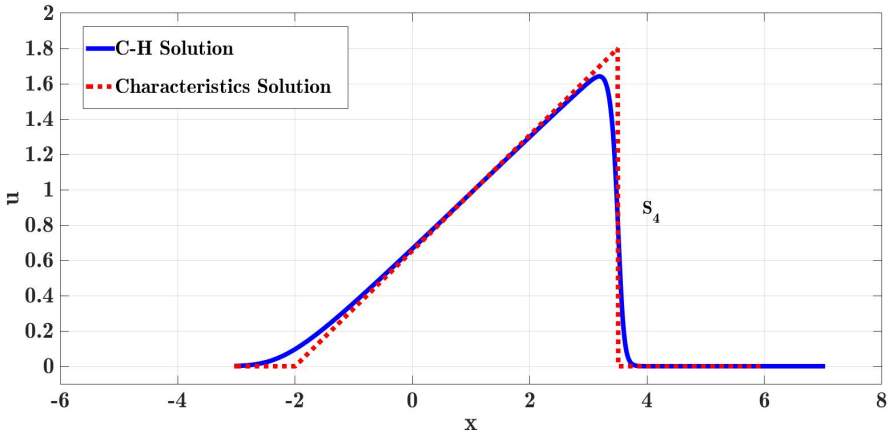

(c) $u_2(x, 3.1) \quad \epsilon = 0.025$

Figure 2.4.11: Cole-Hopf solution $u_2(x,t)$ for the second initial disturbance $\phi_2(x,t)$ at times $t = 0.001,\ 2,\ 3.1$

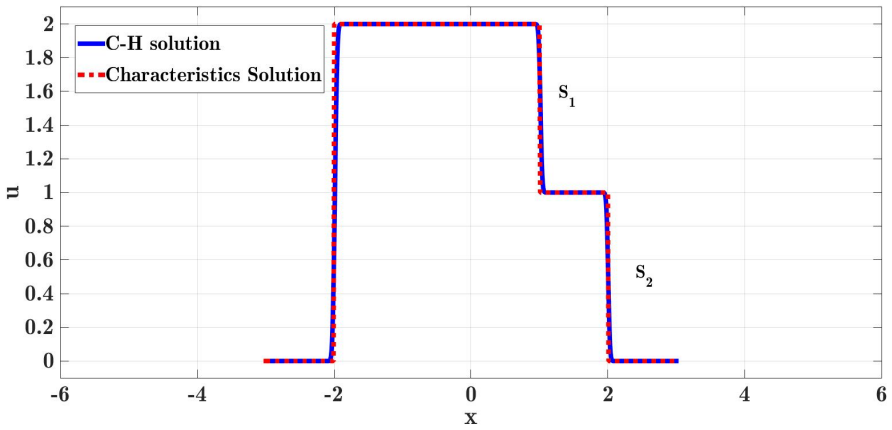

(a) $u_3(x, 0.01)$ $\epsilon = 0.025$

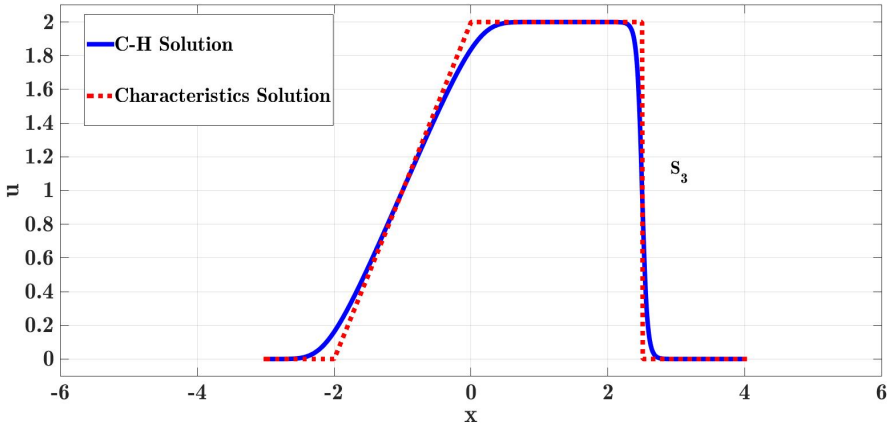

(b) $u_3(x, 1)$ $\epsilon = 0.025$

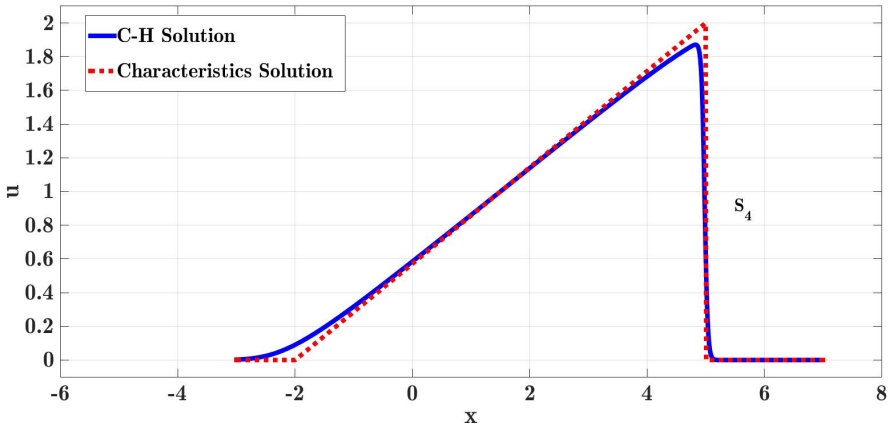

(c) $u_3(x, 3.5)$ $\epsilon = 0.025$

Figure 2.4.12: Cole-Hopf solution $u_3(x, t)$ for the third initial disturbance $\phi_3(x, t)$ at times $t = 0.01$, 1, 3.5

2.4.4 Summary

In this section we used the well known Cole-Hopf transformation that attracted many mathematicians to solve the non-linear Burgers' PDE. We solved the initial value problem of Burgers' equation coupled with three different initial conditions and reached an exact expressions for each disturbance in the form of an integral

$$u_i(y;x,t) = \frac{\displaystyle\int_{-\infty}^{\infty} \frac{x-y}{t}\, \exp\!\left(\frac{-G_i}{2\epsilon}\right) \mathrm{d}y}{\displaystyle\int_{-\infty}^{\infty} \exp\!\left(\frac{-G_i}{2\epsilon}\right) \mathrm{d}y}\,, \qquad i = 1,2,3, \tag{2.4.43}$$

where

$$G(y;x,t) = \frac{(x-y)^2}{2t} + \int_0^y u_0(z)\,\mathrm{d}z.$$

We presented a descriptive study covering two methods to evaluate the Cole-Hopf solution (2.4.43) for the first initial waveform $u_0(x) = \phi_1(x)$. The first method is numerical evaluation of integrals in equation (2.4.43). The second method is derived by writing these integrals in term of error functions $\mathrm{erf}(x)$ and $\mathrm{erfc}(x)$. We derived the two methods outcomes comparing the accuracy and time cost of each method.

We next studied the small ϵ behaviour of the integrals in Cole-Hopf solution, and showed that as $\epsilon \to 0$ the solution approaches the method of characteristic solution for $\epsilon = 0$ and in the shock region it is reduced to the Taylor shock solution given in equation (2.4.39).

We also evaluated the Cole-Hopf expressions for initial functions $\phi_i(x,t)$ where $i = 2,3,$ and compared the two solutions to the $\epsilon = 0$ case illustrated earlier in the characteristic method.

In the next section we carry out a numerical scheme to calculate viscid Burgers' solutions numerically in terms of the three initial conditions $\phi_i(x,t)$ for $i = 1,2,3$ and compare the numerical results with the asymptotic approximations deduced earlier in §2.3 and the Cole-Hopf approximations.

2.5 Numerical scheme

2.5.1 Introduction

The numerical solution of Burgers' equation is of great importance due to two features of this PDE. One feature is the existence of analytical solutions. Burgers' equation is one of the few non-linear partial differential equations that can be solved exactly for arbitrary initial conditions. This is done using Cole-Hopf transformation as we illustrated earlier in §2.4. These analytical solutions are useful to validate the numerical algorithms implemented to solve the Burgers' equation. The other feature which attract many studies is the appearance of the narrow shock for small viscosity ϵ. It was seen in §2.4 that when ϵ is very small, numerical evaluation of the Cole-Hopf solution was difficult. Various studies have developed computational schemes to solve Burgers' equation numerically, these schemes were based on finite difference [15, 31, 42, 43, 57], finite element [16, 68, 19] and spectral methods [36, 62, 63, 86, 64]. Dhawan *et al.* [27] presented a comprehensive review of several numerical techniques used to solve Burgers equation. Spectral methods were developed for incompressible turbulent flows for its accuracy and efficiency. The expectation, as pointed out by Gottlieb [15], that spectral methods will enable us to capture the shock, and the delicate features and structures of the flow. Obviously, spectral approaches will be extremely valuable to a class of aerodynamical problems that involve the interaction of both turbulence and shock [31]. Such an interaction is some of the most challenging problems in computation fluid dynamics. Therefore, a shock-capturing scheme is necessary. The shock-capturing scheme is required to be high-order accurate throughout the computational domain (to properly simulate the evolution of turbulence) as well as to be able to give a smooth and accurate transition across the shock wave. Furthermore in chapter §3 when we include relaxation processes into Burgers' equation, this simulation can be easily modified to accommodate the relaxation effects.

We consider solutions of Burgers equation which decay to 0 as $|x| \to \infty$. Thus, a standard method is to use the truncated Fourier series on the domain $[-L, L]$ with boundary condition of periodicity $2\,L$ [10]. We use the truncated Fourier series for approximating the spatial variable and generating an ODE in terms of time. For numerically solving any time-dependent partial differential equation such as Burgers' equation by spectral methods, it depends on two procedures: spectral differentiation in space and finite differences in time.

In our numerical approach to solve the non-linear Burgers PDE, we implement a spectral technique presented by Lloyd Trefethen in [90](p 110-113) where he solved the Korteweg-de Vries (KDV) equation which is a non-linear dispersive partial differential equation. The KDV equation acts as a model for a scheme that solves time-dependent partial differential equations that combines a non-linear term with a higher order linear term. Therefore, we found that this scheme is appropriate for Burger's equation.

Thus, the first step of the numerical approach is to construct a discrete representation of the Burgers' equation using Discrete Fourier Transform (DFT) which is computed with the Fast Fourier Transform (FFT). For spectral differentiation we apply the pseudospectral procedure for evaluating the derivatives at interpolating points. The procedure consists of computing the discrete coefficients $\hat{u}(k)$ of the interpolating trigonometric polynomials from the interpolating values of $u(x)$ using FFT. Then forming the coefficients of the derivatives by multiplying each Fourier coefficient by its wavenumber. Finally, the derivatives can be recovered from Fourier space to physical space using inverse fast Fourier transform IFFT.
The pseudospectral procedure can be also applied to computing products. A multiplication $w(x) = u(x)v(x)$, corresponds to a convolution sum in Fourier space, but convolution computation requires $O(N^2)$ sums per time step. These sums are costly in time and can be replaced with pseudospectral treatment

using FFT which can considerably speed up the calculations to $O(N \log_2 N)$ calculations per time step, where N is the number of Fourier modes. Thus, to calculate the multiplication $w(x) = u(x)v(x)$, in Fourier space, we transform $\hat{u}$ and $\hat{v}$ to physical space using IFFT. We then perform multiplication uv in the physical space. We then transform back to Fourier space by FFT to obtain $\hat{w} = \widehat{uv}$.

Time marching can be carried out by choosing one of a number of schemes for example, forward step, leap frog, Runge-Kutta [14],[37],[51]. Our choice will be the fourth-order Runge-Kutta (RK4) since it is the most popular time integrating scheme to be combined with high accuracy spectral methods. This is because of the property of its decaying error in terms of the integration steps Δt is of order $O(\Delta t^4)$, and it preserves stability with longer time steps compared to other explicit methods [11].

The presence of the viscous term means that the stability criterion takes the form $\Delta t_{\max} = O(N^{-2})$. Thus, for large number of Fourier modes, the required time step for stability is extremely small. In order to resolve this problem as we march forward in time, we introduce in §2.5.2 the method of integrating factor (IF) to remove the linear term which leads to a strict restriction on the time step for stability [90]. The method of integrating factor for PDEs was introduced by Milewski and Tabak [66], and much literature discusses the use of this method, for example, Maday et al. [61], Smith and Waleffe [83],[84], Fornberg and Driscoll [32], Boyd [11] and Cox and Matthews [24], and the method is well summarised by Trefethen [90].

2.5.2 Spatial Discretization: Fourier Pseudospectral Method

The pseudospectral method is a popular approach to solve non-linear partial differential equations, because it offers a simple treatment of non-linear terms. The spectral and pseudospectral methods were first proposed by Kreiss and Oliger [50] and Gottlieb and Orszag [36], and more of the theory of pseudospectral methods can be found in [11], [5] and [71].

We treat Burgers' equation using the Fourier Discrete Transform DFT. We assume a periodic domain and boundary conditions, which is appropriate for computations, since we are interested in computing the shock that is unrelated to the boundaries [90]. Also the problem of interest u is constant near the left hand and right hand boundaries [34].
We look for a discrete representation $u_N(y)$ of u on the interval $[-\pi, \pi]$, for the differential equation at interpolation points:

$$-\pi =< y_1 < ... < y_{2N-1} < y_{2N} = \pi, \qquad y_j = j\Delta y = j\frac{\pi}{N}, \quad j = -N, ..., N-1. \tag{2.5.1}$$

The Discrete Fourier Transform (DFT) is defined as

$$\mathcal{F}[u] = \hat{u}(k) = \frac{\pi}{N} \sum_{j=-N}^{N-1} u(y_j)\, \exp\big(-i\, k\, y_j\big), \qquad k = -N+1, ..., N, \tag{2.5.2}$$

and the inverse Fourier Transform is:

$$\mathcal{F}^{-1}[\hat{u}] = u(y_j) = \frac{1}{2\pi} \sum_{k=-N+1}^{N} \hat{u}(k)\, \exp\big(i\, k\, y_j\big), \qquad j = 1, ..., 2N, \tag{2.5.3}$$

where $\mathcal{F}[u] = \hat{u}$ and $\mathcal{F}^{-1}[\hat{u}] = u$ are the Fourier transform and inverse Fourier transform operators. The trigonometric functions $\exp\big(i\, k\, y_j\big)$ are the basis functions for the Fourier series where $u(y)$ is assumed to be periodic. The wavenumber k and the spatial index j take integer values and N is the number of Fourier modes. The numerical computations of the formulas (2.5.2)

and (2.5.3) can be carried out efficiently using FFT.

We define the rescale variable as $x = \frac{L}{\pi}\, y$ to replace the interval $[-\pi, \pi]$ with a more general spatial domain $[-L, L]$. Therefore, the discrete Fourier transform expression defined in (2.5.2) becomes:

$$\hat{u}(k) = \frac{\pi}{N} \sum_{j=-N}^{N-1} u(x_j)\, \exp\Big(- i\, k\, \frac{\pi}{L}\, x_j \Big), \qquad k = -N+1, ..., N, \tag{2.5.4}$$

and the inverse Fourier transform and (2.5.3) becomes:

$$u(x_j) = \frac{1}{2\pi} \sum_{k=-N+1}^{N} \hat{u}(k)\, \exp\Big(i\, k\, \frac{\pi}{L}\, x_j \Big), \qquad j = -N, ..., N-1. \tag{2.5.5}$$

To look for the discrete derivatives we use spectral differentiation and we illustrated this in §2.5.1 the pseudospectral treatment for computing the derivatives with the use of FFT. In general, for differentiating in Fourier space we multiply by $(ik)^p$ to calculate the p^{th} derivative $\hat{w}(k) = \frac{\partial^p}{\partial k^p}\, \hat{u}(k)$. Thus, the discrete p^{th} derivative $w(x_j) = \frac{\partial^p}{\partial x^p}\, u(x_j)$ can be obtained by three steps. First, for given data $u_1, ..., u_{2N}$ we use FFT in (2.5.4) to compute $\hat{u}(k)$. Second, define $\hat{w}(k) = (ik\pi/L)^p\, \hat{u}(k)$. Third step is to use the inverse FFT to define the p^{th} derivative $w(x_j)$ as

$$\frac{\partial^p}{\partial {x_j}^p} u = \frac{1}{2\pi} \sum_{k=-N+1}^{N} \Big(i\, \tilde{k} \Big)^p\, \hat{u}(k)\, \exp\big(i\, \tilde{k}\, x_j \big), \qquad j = -N, ..., N-1, \tag{2.5.6}$$

where $\tilde{k} = \frac{\pi}{L}\, k$. We can also compute the product u^2 using the pseudospectral treatment, or it can be evaluated by the convolution

$$u^2(x) = \sum_{k=-N+1}^{N} \sum_{m=-N+1}^{N} \hat{u}(k)\, \hat{u}(m) \exp\Big[i(k+m) x_j \Big]. \tag{2.5.7}$$

The calculations of the nonlinear term in Burgers' equation which is the product u^2 will be illustrated later at the end of the spatial discretzation discussion.

We now introduce the discrete representation of Burgers' equation:

$$u_t + \frac{1}{2}\left(u^2\right)_x - \epsilon u_{xx} = 0, \tag{2.5.8}$$

to discretize the spatial part and obtain the first order ODE in Fourier space

$$\hat{u}_t + \frac{1}{2}\left(i\tilde{k}\right)\widehat{(u^2)} + \epsilon\,\tilde{k}^2\,\hat{u} = 0. \tag{2.5.9}$$

We can continue with any appropriate solver of the ODE (2.5.9). This will generate an approximation for the solution at interpolation points $x_j = j\frac{L}{N}$ successfully but with very small time step Δt as a requirement for the stability of the integration method used on equation (2.5.9). Since the resulting ODE is a classical example of stiff equations where here the stiffness is related to the linear term with high derivative whereas the nonlinear term contains low derivative. This stiffness still exist even in the limit of small viscosity, since for reduced viscosity a higher wavenumber is required to resolve the rapid oscillations [90]. Instead we can apply a commonly used modification of pseudospectral discreteizations. This modification is based on integrating factor method which transforms the problem to solve the linear term in Burgers' equation which involves highest frequency k^2 that constrains stability. This method allows us to take larger time steps while maintaining stability.

We modify equation (2.5.9) by changing the variable $\hat{u}$, then we multiply the converted equation by a determined integrating factor $f(k)$ so that the linear term can be evaluated exactly. Then we integrate the transformed equation with any time forwarding numerical scheme of our choice (see for example Trefethen [90] and Kassam and Trefethen [45]).

The integrating factor method uses a smooth change of variables in an attempt to evaluate the linear term of Burgers' equation. So lets define the variable $\hat{v}$ as

follows

$$\hat{v} = \hat{u}\ \mathrm{e}^{f(k)\,t}. \tag{2.5.10}$$

The term $\mathrm{e}^{f(k)\,t}$ is known as the integrating factor. Differentiating (2.5.10) with respect to time we have

$$\hat{v}_t = \hat{u}_t\ \mathrm{e}^{f(k)\,t} + f(k)\,\hat{u}\ \mathrm{e}^{f(k)\,t}. \tag{2.5.11}$$

Now let us return back to equation (2.5.9) and multiply it by the integrating factor to have

$$\hat{u}_t\ \mathrm{e}^{f(k)\,t} + \frac{1}{2}\left(i\tilde{k}\right)\widehat{(u^2)}\ \mathrm{e}^{f(k)\,t} + \epsilon\,\tilde{k}^2\,\hat{u}\ \mathrm{e}^{f(k)\,t}\ = 0. \tag{2.5.12}$$

Rearranging equation (2.5.12) becomes

$$\left[\hat{u}_t\ \mathrm{e}^{f(k)\,t} + \epsilon\,\tilde{k}^2\,\hat{u}\ \mathrm{e}^{f(k)\,t}\right] + \frac{1}{2}\left(i\tilde{k}\right)\widehat{(u^2)}\ \mathrm{e}^{f(k)\,t} = 0.$$

The two terms in square brackets are the right hand side of (2.5.11) if we fixed $f(k) = \epsilon\,\tilde{k}^2$ and hence, this yields

$$\hat{v}_t = \lambda\,\mathrm{e}^{f(k)\,t}\ \widehat{u^2}. \tag{2.5.13}$$

where $\lambda = -\frac{i}{2}\,\tilde{k}$. The stiff linear term has gone, and the problem is simpler. Working in Fourier space, we discretize the problem in the form

$$\hat{v}_t = \lambda\,\mathrm{e}^{f(k)\,t}\ \mathcal{F}\left(\left(\mathcal{F}^{-1}\big(\mathrm{e}^{-f(k)\,t}\ \hat{v}\big)\right)^2\right). \tag{2.5.14}$$

Once again we apply the pseudospectral treatment in equation (2.5.14) for evaluation the non-linear term $\widehat{u^2}$ in (2.5.13). The pseudospectral calculations of the non-linear term is an efficient method which is done in following three steps. First, we transformed $\hat{u}$ to physical space using FFT to have $u = \mathcal{F}^{-1}(\hat{u})$ expressed in the inner brackets in equation (2.5.14). Second, make the product of $u^2 = \left(\mathcal{F}^{-1}(\hat{u})\right)^2$ in the physical space. Thirdly, transform back to the

spectral space using the Fourier transform operator $\mathcal{F}$.

We now move to the next step which is solving the ODE (2.5.14) numerically with the fourth-order Runge-Kutta ODE solver.

2.5.3 Time Discretization: Fourth-Order Runge-Kutta Method

We apply fourth-order Runge-Kutta formula (RK4) on the transformed equation (2.5.9) which can be written in the form

$$\hat{u}_t = G\big(t,\, \hat{u}\big), \tag{2.5.15}$$

where $G(t, \hat{u}) = -\frac{i\tilde{k}}{2}\widehat{u^2} - \epsilon\tilde{k}^2\hat{u}$. Then the RK4 algorithm for computing $\hat{u}_{n+1}$ from $\hat{u}_n$ in (2.5.15) is defined as follows

$$\begin{aligned}
K_a &= G\Big(t_n,\, \hat{u}_n\Big), \\
K_b &= G\Big(t_a,\, \hat{u}_a\Big), \qquad t_a = t_n + \frac{\Delta t}{2} \qquad \hat{u}_a = \hat{u}_n + \frac{\Delta t}{2}\, K_a, \\
K_c &= G\Big(t_b,\, \hat{u}_b\Big), \qquad t_b = t_n + \frac{\Delta t}{2} \qquad \hat{u}_b = \hat{u}_n + \frac{\Delta t}{2}\, K_b, \\
K_d &= G\Big(t_c,\, \hat{u}_c\Big), \qquad t_c = t_n + \Delta t \qquad \hat{u}_c = \hat{u}_n + \Delta t\, K_c,
\end{aligned}$$

$$\hat{u}_{n+1} = \hat{u}_n + \frac{\Delta t}{6}\,\Big(K_a + 2\,K_b + 2\,K_c + K_d\Big),$$

where Δt is the time step, $t_n = n\,\Delta t$. However, with the earlier modification to equation (2.5.9) made in §2.5.2, the integrating factor method was applied to improve the stiffness of the linear term. We changed the dependent variable $\hat{u}$ to $\hat{v} = \mathrm{e}^{q(t)}\,\hat{u}$ where $q(t) = f(k)\,t$, and hence we now seek an approximation for $\hat{v}_{n+1}$ using the relations

$$\hat{u} = \mathrm{e}^{-q}\,\hat{v} \qquad \text{and} \qquad G\big(t,\, \hat{u}\big) = \mathrm{e}^{-q}\,P\big(t, \mathrm{e}^{q}\,\hat{u}\big), \tag{2.5.16}$$

Thus, we need to identify a RK4 algorithm for $\hat{v}_{n+1}$ by constructing the increments for $\hat{v}$, L_a, L_b, L_c, L_d using the increments K_a, K_b, K_c, K_d defined above.

We begin with the first increment, K_a is given by

$$\begin{aligned} K_a &= G\Big(t_n,\, \hat{u}_n\Big) \\ &= \mathrm{e}^{-q_n}\, P\Big(t_n,\, \mathrm{e}^{q_n}\, \hat{u}_n\Big) \\ &= \mathrm{e}^{-q_n}\, P\Big(t_n,\, \hat{v}_n\Big), \end{aligned}$$

and hence, L_a can be defined as

$$L_a = \mathrm{e}^{q_n}\, K_a = P\Big(t_n,\, \hat{v}_n\Big). \tag{2.5.17}$$

For the second increment L_b, we recall K_b is defined as

$$\begin{aligned} K_b &= G\Big(t_a,\, \hat{u}_a\Big), \qquad t_a = t_n + \frac{\Delta t}{2}, \quad \hat{u}_a = \hat{u}_n + \frac{\Delta t}{2}\, K_a, \\ &= \mathrm{e}^{-q_a}\, P\Big(t_a,\, \mathrm{e}^{q_a}\, \big(\hat{u}_n + \frac{\Delta t}{2}\, K_a\big)\Big) \\ &= \mathrm{e}^{-q_a}\, P\Big(t_a,\, \mathrm{e}^{q_a}\, \mathrm{e}^{-q_n}\big(\hat{v}_n + \frac{\Delta t}{2}\, L_a\big)\Big) \\ &= \mathrm{e}^{-q_a}\, P\Big(t_a,\, E_a\, \big(\hat{v}_n + \frac{\Delta t}{2}\, L_a\big)\Big), \end{aligned}$$

where $E_a = \exp(q_a - q_n)$, and we can define L_b as

$$L_b = \mathrm{e}^{q_a}\, K_b = P\Big(t_a,\, E_a\, \big(\hat{v}_n + \frac{\Delta t}{2}\, L_a\big)\Big). \tag{2.5.18}$$

The third increment is deduced from K_c as follows

$$\begin{aligned} K_c &= G\Big(t_b,\, \hat{u}_b\Big), \qquad t_b = t_n + \frac{\Delta t}{2}, \quad \hat{u}_b = \hat{u}_n + \frac{\Delta t}{2}\, K_b, \\ &= \mathrm{e}^{-q_b}\, P\Big(t_b,\, \mathrm{e}^{q_b}\, \big(\hat{u}_n + \frac{\Delta t}{2}\, K_b\big)\Big) \\ &= \mathrm{e}^{-q_b}\, P\Big(t_a,\, \mathrm{e}^{q_b - q_n}\, \hat{v}_n + \frac{\Delta t}{2}\, L_b\Big), \qquad \text{as} \quad q_a = q_b. \end{aligned}$$

Hence, L_c is defined as

$$L_c = \mathrm{e}^{q_b} K_c = P\Big(t_b,\, E_b\, \hat{v}_n + \frac{\Delta t}{2}\, L_b\Big), \tag{2.5.19}$$

where $E_b = \exp(q_b - q_n)$, and $E_b = E_a$ since $q_b = q_a = t_n + \Delta t/2$. We drive the fourth and final increment from K_d as follows

$$\begin{aligned} K_d &= G\Big(t_c,\, \hat{u}_c\Big), \qquad\qquad t_c = t_n + \Delta t, \quad \hat{u}_c = \hat{u}_n + \Delta t\, K_c, \\ &= \mathrm{e}^{-q_c}\, P\Big(t_c,\, \mathrm{e}^{q_c}\, \big(\hat{u}_n + \Delta t\, K_c\big)\Big) \\ &= \mathrm{e}^{-q_c}\, P\Big(t_c,\, \mathrm{e}^{q_c}\, \big(\mathrm{e}^{-q_n} \hat{v}_n + \Delta t\, \mathrm{e}^{-q_b} L_c\big)\Big) \\ &= \mathrm{e}^{-q_c}\, P\Big(t_c,\, \mathrm{e}^{q_c - q_n}\, \hat{v}_n + \Delta t\, \mathrm{e}^{q_c - q_b}\, L_c\Big). \end{aligned}$$

The fourth increment is defined as

$$L_d = \mathrm{e}^{q_c} K_d = P\Big(t_c,\, E_c\, \hat{v}_n + \Delta t\, \frac{E_c}{E_b}\, L_c\Big), \tag{2.5.20}$$

where $E_c = \exp(q_c - q_n)$ and $\frac{E_c}{E_b} = \exp(q_c - q_n)\ \exp(q_n - q_b) = \exp(q_c - q_b)$. The formula for the approximation $\hat{v}_{n+1}$ can be expressed with the use of the approximation $\hat{u}_{n+1}$ and the relation in equation (2.5.16):

$$\hat{u}_{n+1} = \hat{u}_n + \frac{\Delta t}{6}\, \Big(K_a + 2\, K_b + 2\, K_c + K_d\Big).$$

We apply the relation in equation (2.5.16) and use the increments L_a, L_b, L_c, L_d defined in equations (2.5.17), (2.5.18), (2.5.19) and (2.5.20) respectively to deduce the approximation $\hat{v}_{n+1}$ as

$$\mathrm{e}^{-q_{n+1}}\, \hat{v}_{n+1} = \mathrm{e}^{-q_n}\, \hat{v}_n + \frac{\Delta t}{6}\, \Big(\mathrm{e}^{-q_n} L_a + 2\, \mathrm{e}^{-q_a}\, L_b + 2\, \mathrm{e}^{-q_b}\, L_c + \mathrm{e}^{-q_c}\, L_d\Big).$$

Multiplying both sides of the equation by $\mathrm{e}^{q_{n+1}}$ yields

$$\hat{v}_{n+1} = \mathrm{e}^{q_{n+1} - q_n} \left[\hat{v}_n + \frac{\Delta t}{6}\, \Big(L_a + 2\, \mathrm{e}^{q_n - q_a}\, L_b + 2\, \mathrm{e}^{q_n - q_b}\, L_c + \mathrm{e}^{q_n - q_c}\, L_d\Big)\right].$$

We substitute the notations E_a, E_b and E_c, and define the notation $E_n = \exp(q_{n+1} - q_n)$ and use the relation $E_a = E_b$ to obtain

$$\begin{aligned}\hat{v}_{n+1} &= E_n\left[\hat{v}_n + \frac{\Delta t}{6}\left(L_a + 2\,\frac{1}{E_a}\left(L_b + L_c\right) + \frac{1}{E_c}\,L_d\right)\right] \\ &= E_n\,\hat{v}_n + \frac{\Delta t}{6}\left(E_n\,L_a + 2\,\frac{E_n}{E_a}\left(L_b + L_c\right) + \frac{E_n}{E_c}\,L_d\right).\end{aligned}$$

Recalling that $q = f(k)\,t$ and we introduce the notations

$$E = \exp\Big(\frac{\Delta t}{2}\,f(k)\Big), \qquad\qquad E^2 = \exp(\Delta t\,f(k)).$$

Notice that $E_n = E^2$, $E_n/E_a = E$ and $E_n = E_c$ and the approximation formula for $\hat{v}_{n+1}$ can be written as

$$\hat{v}_{n+1} = E^2\,\hat{v}_n + \frac{\Delta t}{6}\left(E^2\,L_a + 2\,E\left(L_b + L_c\right) + L_d\right).$$

Therefore, we can solve the ODE (2.5.14) numerically with the following constructed RK4 algorithm

$$\begin{aligned}
L_a &= P\Big(t_n,\,\hat{v}_n\Big), \\
L_b &= P\Big(t_a,\,\hat{v}_a\Big), \qquad t_a = t_n + \frac{\Delta t}{2}, \quad \hat{v}_a = E\big(\hat{v}_n + \frac{\Delta t}{2}\,L_a\big), \quad E = \mathrm{e}^{\frac{1}{2}\Delta t\,f(k)}, \\
L_c &= P\Big(t_b,\,\hat{v}_b\Big), \qquad t_b = t_n + \frac{\Delta t}{2}, \quad \hat{v}_b = E\,\hat{v}_n + \frac{\Delta t}{2}\,L_b, \\
L_d &= P\Big(t_c,\,\hat{v}_c\Big), \qquad t_c = t_n + \Delta t, \quad \hat{v}_c = E\big(E\hat{v}_n + \Delta t\,L_c\big), \quad E^2 = \mathrm{e}^{\Delta t\,f(k)},
\end{aligned}$$

$$\hat{v}_{n+1} = E^2\,\hat{v}_n + \frac{\Delta t}{6}\left(E^2\,L_a + 2\,E\left(L_b + L_c\right) + L_d\right), \tag{2.5.21}$$

where Δt is the time step and P is the nonlinear functional of the right hand side of equation (2.5.14). This RK4 algorithm is consistent with the formula that Trefethen deduced in [90] (program 27 p 112). To conclude this analysis, we deduced the RK4 algorithm for equation (2.5.14) to solve numerically for $\hat{v}$ by seeking $\hat{v}_{n+1}$ defined in (2.5.21). [90].

2.5.4 Defining an Initial Function for the Rectangular Pulse

In our problem all the three initial conditions ϕ_1 , ϕ_2 and ϕ_3 mentioned in §2.1 have a jump discontinuity. The Heaviside function $H(x)$ is a step function and can be used to represent the initial functions. However, the high accuracy FFT algorithm when it deals with discontinuous functions, this accuracy weakens because the Fourier method's estimations of derivatives are poor. Nevertheless the initial data can be smoothed so that we can use FFT with a smooth approximation of the step function, the scaled hyperbolic tangent function defined by

$$F(x) = \frac{1}{2}\Big(1 + \tanh\big(\frac{x}{\delta}\big)\Big). \tag{2.5.22}$$

Figure 2.5.1 represents the two functions $F(x+2)$ (left) and $F(2-x)$ (right). We will use a combination of the scaled hyperbolic tangent functions to construct

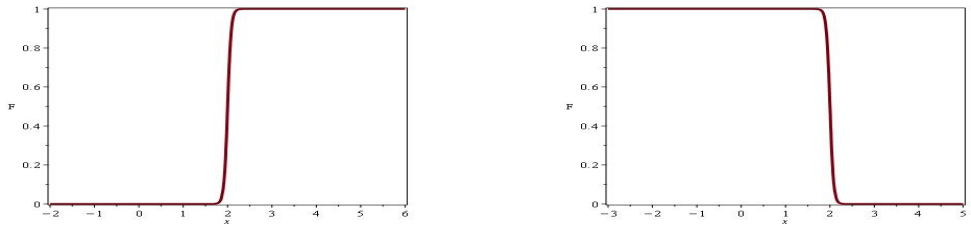

(a) $F(x+2)$ (b) $F(2-x)$

Figure 2.5.1: The curves of the functions $F(x+2)$ in (a) and $F(2-x)$ in (b).

smooth function replica to the discontinuous initial profiles defined in §2.1,

$$u_0 = \frac{1}{2}\Big(1 + \tanh\big(\frac{x-a}{\delta}\big)\Big) . \frac{1}{2}\Big(1 + \tanh\big(\frac{b-x}{\delta}\big)\Big). \tag{2.5.23}$$

The two values a and b decide the size of the pulse and position and the parameter $\frac{1}{\delta}$ where $0 < \delta \ll 1$ determines the slope of the function and for a larger δ the pulse width becomes larger. This combination creates a rectangular unit pulse see figure 2.5.2 for the first initial condition we can define it as

$$\phi_1(x) = F(x+2)\ F(2-x). \tag{2.5.24}$$

We also can apply this procedure to redefine the other initial conditions ϕ_2 and

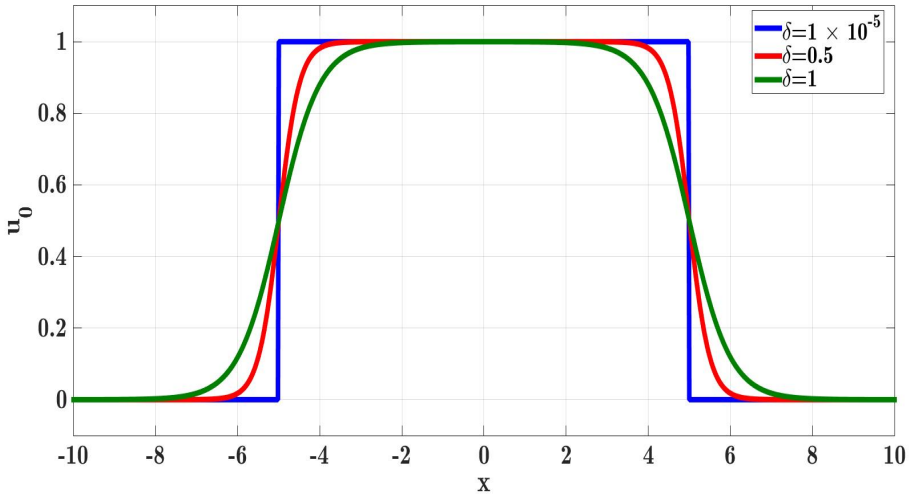

Figure 2.5.2: The tanh-pulse initial disturbance for length $L = 10$ and various slopes $\delta = 0.00001, 0.5, 1$. The values of a and b are $-0.5\,L$ and $0.5\,L$ respectively.

ϕ_3 in terms of combinations of $F(x)$. The second and third initial condition consists of two humps, so we can present the two initial waveforms as

$$\phi_2(x) \;=\; 2\,F(x+2)\;F(-1-x) + F(x+1)\;F(2-x), \qquad (2.5.25)$$

$$\phi_3(x) \;=\; 2\,F(x+2)\;F(1-x) + F(x-1)\;F(2-x). \qquad (2.5.26)$$

The first term creates the hump of amplitude 2 and the second term creates second hump of amplitude 1.

For describing a function with a jump discontinuity, we will take the slope scale $1/\delta$ large to create steep fronts. However, this will destroy the accuracy of the truncated Fourier series as the Fourier series works well except near the discontinuity where the approximation overshoots. This overshooting is known as Gibbs phenomenon which commonly occurs in the inviscid Burgers' equation. This problem is resolved by the inclusion of the viscus term $\epsilon\, u_{xx}$ in Burgers' equation which smooths out the sharp front of high gradient. Thus, the shock wave solution $u(x)$ is now described by a thin region of rapid change in which

the width depends on viscosity. The viscosity coefficient is better chosen to be proportional to the spatial grid size $\epsilon \sim C\Delta x = C\frac{L}{N}$ for some constant C to insure a sufficient number of grid points is covering the narrow shock region [11]. This will improve the spectral accuracy since the Fourier coefficients convergence rate depends on the smoothness of the function but it will also minimize the impact of viscosity which is of our interest to study viscous effects on the shock front. Therefore, as $u(x)$ is decaying exponentially as $|x| \to \infty$, for a sufficiently large L, we increase the number N of Fourier modes and the Fourier pseudospectral algorithm produces a high accuracy as the error decreases [35]. In figure 2.5.3 we can see that for a fixed small value of viscosity, when the number of Fourier coefficients is $N = 2^8$ in 2.5.3 (a) we observe Gibbs oscillations and when $N = 2^{13}$ in 2.5.3(b) the oscillations disappear.

Next we present some numerical results of our proposed Fourier pseudospectral scheme for solving the nonlinear viscid Burgers' equation (2.5.8) associated with three different initial conditions given in (2.5.24), (2.5.25) and (2.5.26).

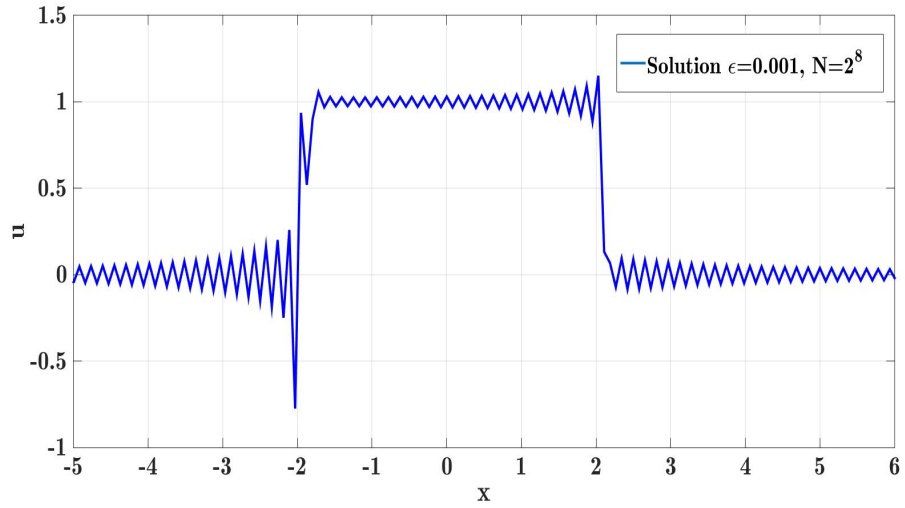

(a) $u_1(x,t)$ $N = 2^8$

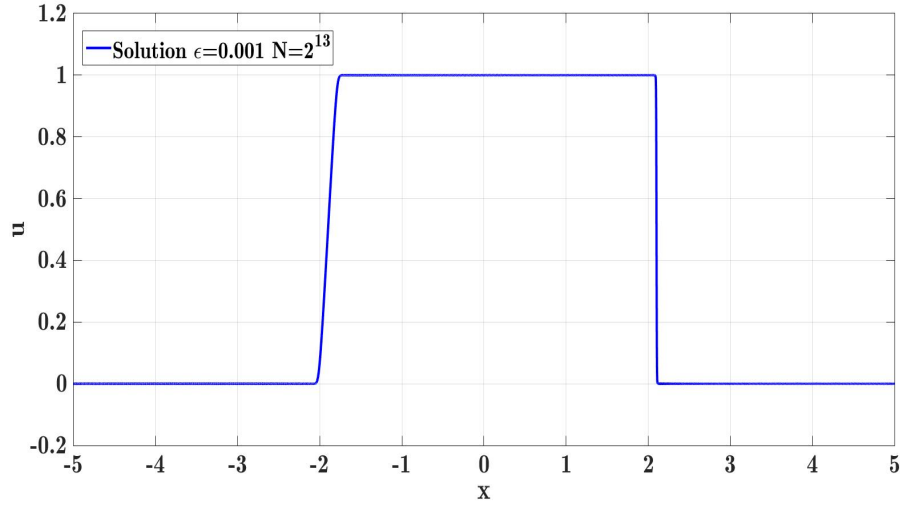

(b) $u_1(x,t)$ $N = 2^{13}$

Figure 2.5.3: Numerical solution at time $t = 0.02$ for $\epsilon = 0.001$ showing Gibbs oscillations when $N = 2^8$ and when $N = 2^{13}$ the solution is free from the oscillations.

2.5.5 Numerical Results

We begin by looking at $u_0(x) = \phi_1(x)$. In figure 2.5.4 the waveform is plotted for various times with $\epsilon = 0.01$ so that the shock regions are narrow. At $t = 4$, we see in figure 2.5.4 (a), the shock centre is located at $x = 4$ and there is a region $2 < x < 3.9$ where $u \approx 1$. This can be compared with the characteristic solution described in §2.2.3, where the shock location is given by $x = 2 + \frac{1}{2}t$ and the maximum amplitude $u = 1$ occurs for $-2 + t < x < 2 + \frac{1}{2}t$. When $t = 8$ the characteristic solution predicted the shock location at $x = -2 + \sqrt{8t}$ with the shock amplitude $\sqrt{\frac{8}{t}}$ and this is compared with numerical solution in figure 2.5.4 (b) where shock is centred approximately at $x = 5.98$ with amplitude $u \approx 0.95$. This shock continues propagating, with decaying amplitude predicted by the method of characteristics $\sqrt{\frac{8}{t}}$. This can be compared to numerical approximations, for example when $t = 16$ the amplitude in figure 2.5.4 (c) is $u_m = 0.7$, compared with $\sqrt{\frac{8}{t}} = 0.707$.

In figure 2.5.5 we compute the absolute error $|u_{\text{exact}} - u_{\text{approx}}|$ where u_{approx} is the approximated solution against the mesh points N for $N = 2^8, ..., 2^{15}$. The error is plotted for three values of integration steps $\Delta t = 0.001$, 0.0001, 0.00001 with viscosity fixed at $\epsilon = 0.001$, time at $t = 1$ and location is at $x = 0$ which is in the outer region of the solution. We see that for higher values of N the error decreases, and for all time steps the error values are very close. In the inner solution, there must be enough mesh points to capture the shock detail. The structure of the shock for different small values of ϵ is illustrated in figure 2.5.6. For $\epsilon = 0.01, 0.005$, choosing $N = 2^{13}$ gives a good resolution but this is not true for $\epsilon = 0.001$ in figure 2.5.6 (c). When the shock region is narrower, the number of points should be increased to capture the shock structure (see figure 2.5.7 showing the difference of the resolution in shock region when $N = 2^{13}$ in (a) and $N = 2^{15}$ in (b)).

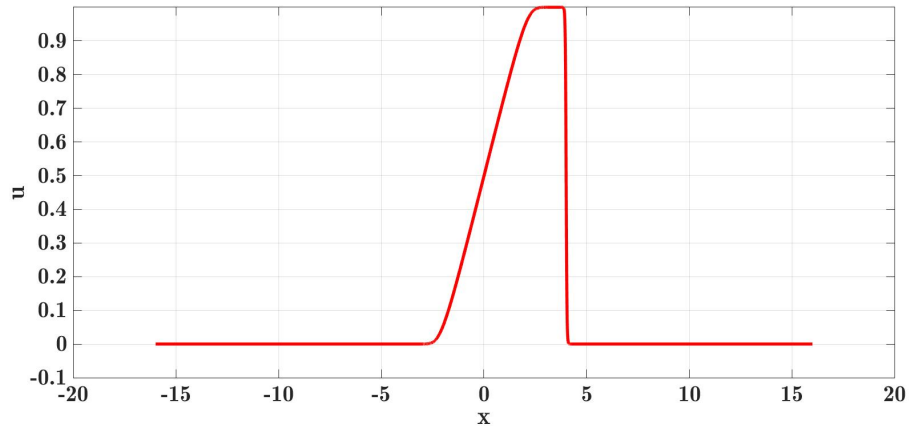

(a) $u_1(x,t)$ $t = 4$

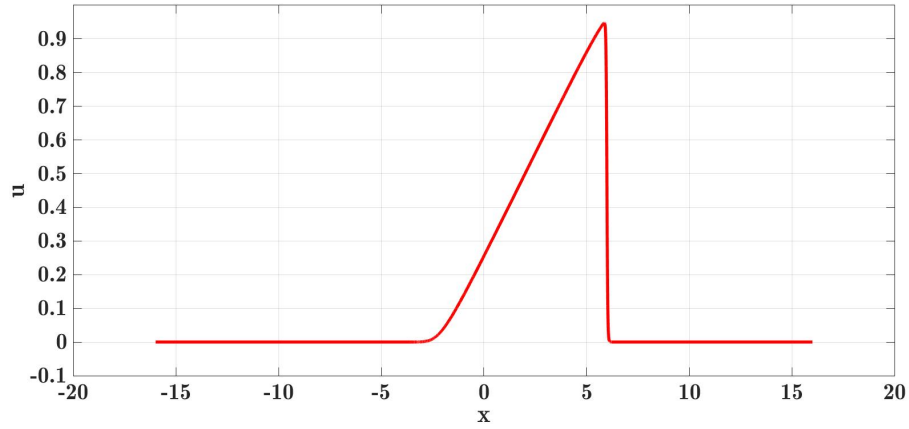

(b) $u_1(x,t)$ $t = 8$

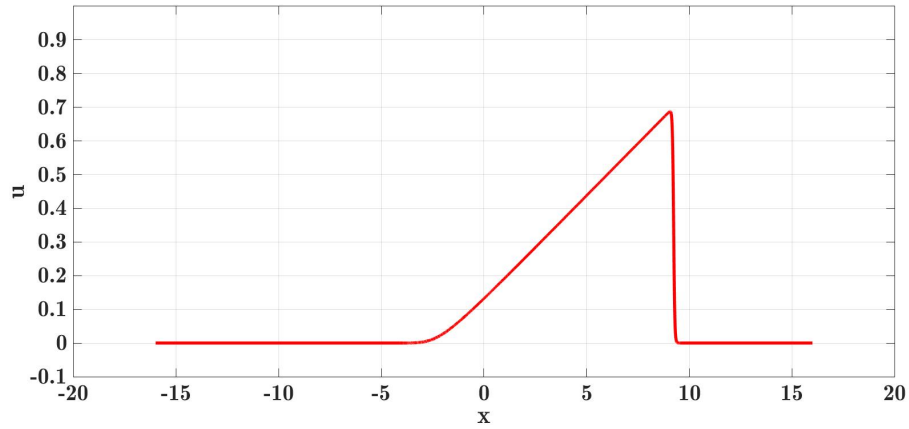

(c) $u_1(x,t)$ $t = 16$

Figure 2.5.4: Numerical approximations of the Burgers' solution $u_1(x,t)$ for the times $t = 4, 8, 16$ for fixed viscosity $\epsilon = 0.01$ and number of points $N = 2^{13}$ and time step $\Delta t = 0.001$.

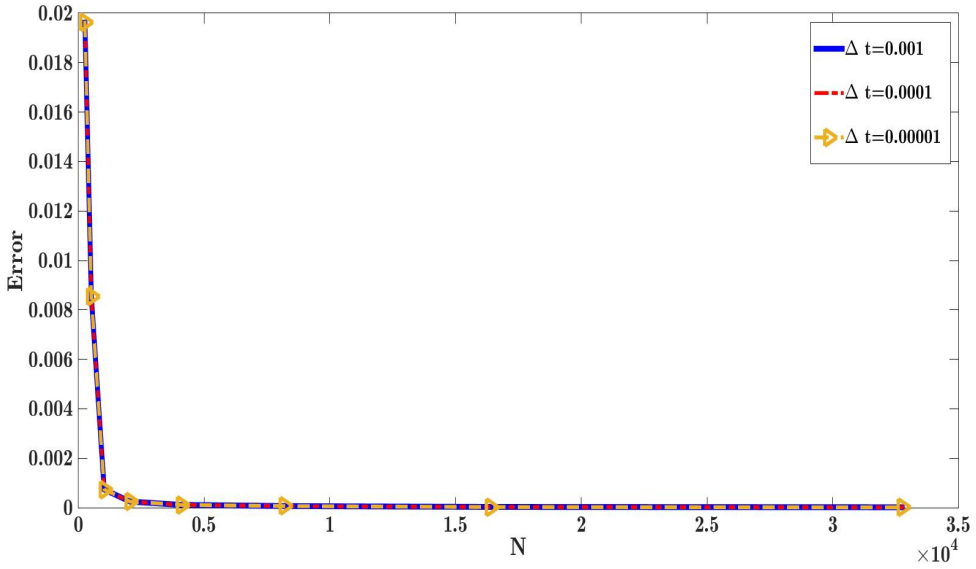

(a) $u_1(x,t)$ $N = 2^{13}$

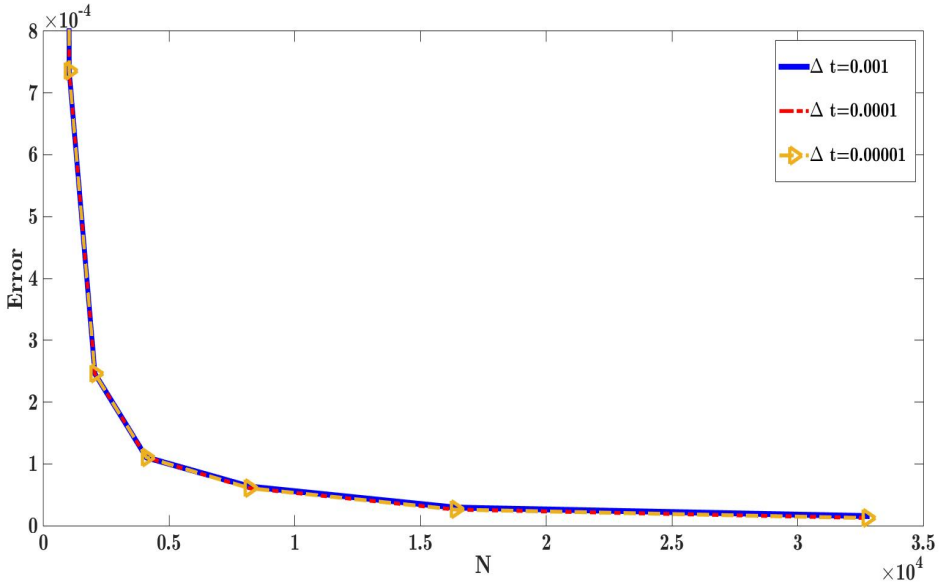

(b) $u_1(x,t)$ $N = 2^{15}$

Figure 2.5.5: The absolute error against N plotted for $u(0,1)$ and $\epsilon = 0.001$ in (a). In (b) a blow-up of the region where N is between 2^{10} and 2^{15}.

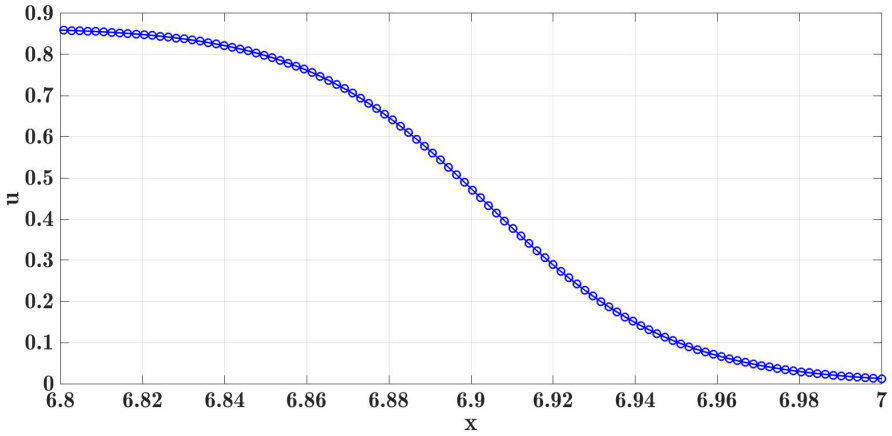

(a) $u_1(x,t)$ $\epsilon = 0.01$

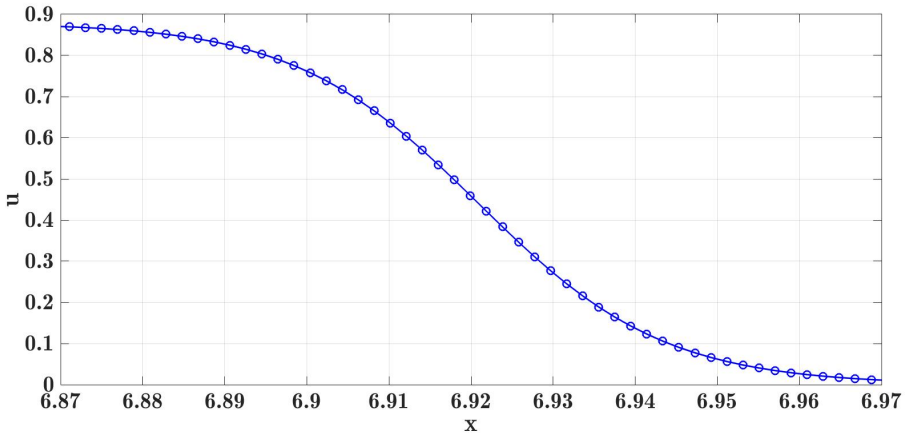

(b) $u_1(x,t)$ $\epsilon = 0.005$

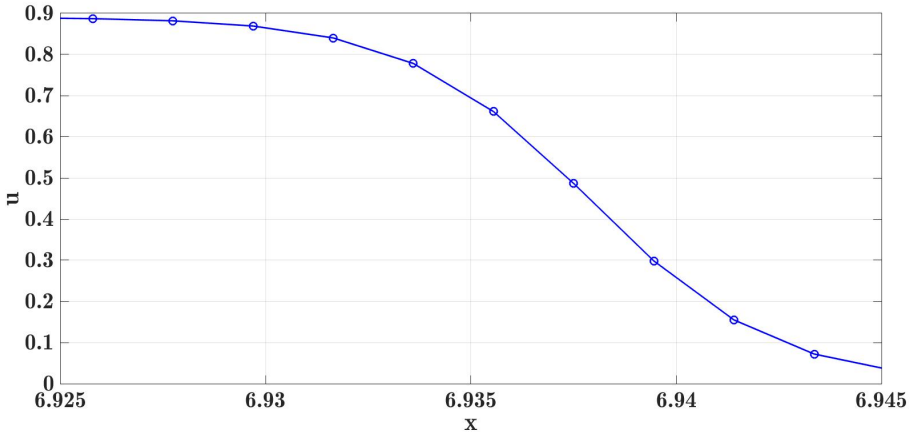

(c) $u_1(x,t)$ $\epsilon = 0.001$

Figure 2.5.6: Blow up figure of the thin shock front region shows the distribution of spatial points in the region of rapid change. The plots are for $t = 10$ and fixed number of spatial points $N = 2^{13}$ with a decreasing values of viscous parameter $\epsilon = 0.01,\ 0.005,\ 0.001$.

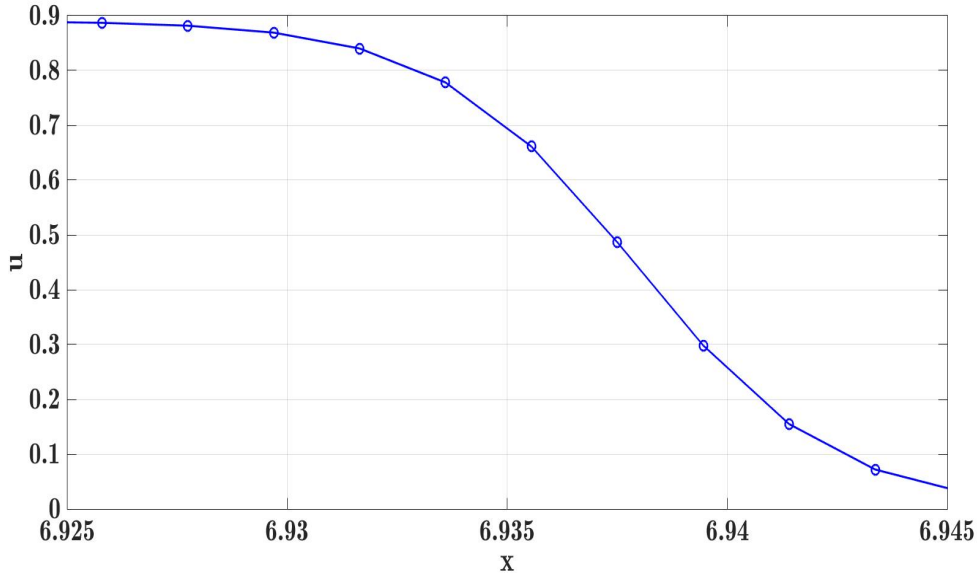

(a) $u_1(x,t) \quad N = 2^{13}$

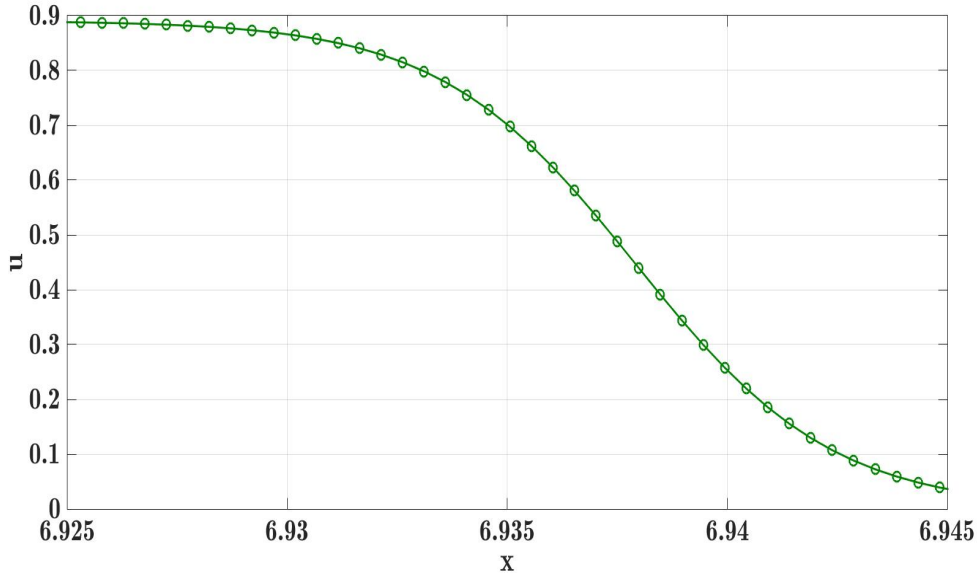

(b) $u_1(x,t) \quad N = 2^{15}$

Figure 2.5.7: Blow up figure of the thin shock front region shows the distribution of points in the region of rapid change. The plots are for $t = 10$ and fixed viscosity $\epsilon = 0.001$ with increasing N from 2^{13} to 2^{15}.

2.5.6 Comparison of Numerical and Analytical Solutions

We conducted some comparisons to show the validation of the numerical solution of Burgers' equation coupled with the first initial condition $u_0(x) = \phi_1(x)$ compared to the analytical solutions discussed earlier in §2.3 and §2.4. The first comparison shown in figure 2.5.8 is with the Cole-Hopf results of evaluation the solution in terms of error functions $\mathrm{erf}(x)$ and $\mathrm{erfc}(x)$ given in equation (2.4.19) with employing MATLAB double precision arithmetic. In these comparisons we captured the shock front for fixed viscosity $\epsilon = 0.01$ at times $t = 5$ and $t = 12$. In figure 2.5.8 (a) we capture the first shock for time $0 < t < 8$ and we can see the close agreement between the two solutions. In figure 2.5.8 (b) we capture the second shock front for $t > 8$ and again the correspondence is very good.

Secondly, we compare this numerical solution to the asymptotic solutions. Figure 2.5.9 represents the numerical solution compared to the asymptotic solution for the case when time $0 < t < 8$:

$$u_{inner} \sim \frac{1}{2}\left[1 - \tanh\left(\frac{x - 2 - \frac{1}{2}t - \epsilon\, A_0(0)}{4\,\epsilon}\right)\right] + O(\epsilon),$$

where the constant A_0 is the $O(\epsilon)$ shift of shock centre. We can see the correspondence of the numerical solution to the asymptotic solution for the two values taken for viscosity $\epsilon = 0.001,\, 0.0005$ at the fixed time $t = 6$. The $O(\epsilon)$ shift A_0 is chosen respectively to be $A_0 = 0$.

When time is $t \geq 8$ the numerical solution is compared to the asymptotic solution for this time which is given as

$$u_{inner} \sim \widehat{U} + \epsilon\, \widehat{V},$$

where the leading order $\widehat{U}$ is given by

$$\widehat{U} = \frac{1}{2}\sqrt{\frac{8}{t}}\left[1 - \tanh\left(\sqrt{\frac{8}{t}}\left(\frac{x + 2 - \sqrt{8\,t} - \epsilon\, A(t)}{4\,\epsilon}\right)\right)\right]. \qquad (2.5.27)$$

The function $A(t)$ here represents the $O(\epsilon)$ shift in shock centre defined by

$$A(t) = A_0 - \sqrt{\frac{t}{8}}\ \ln\left(\frac{t}{8}\right).$$

The $O(\epsilon)$ correction to the shock solution is given by

$$\widehat{V} = \sqrt{\frac{2}{T}}\ p_1(\theta) + 2\,A'\,p_2(\theta),$$

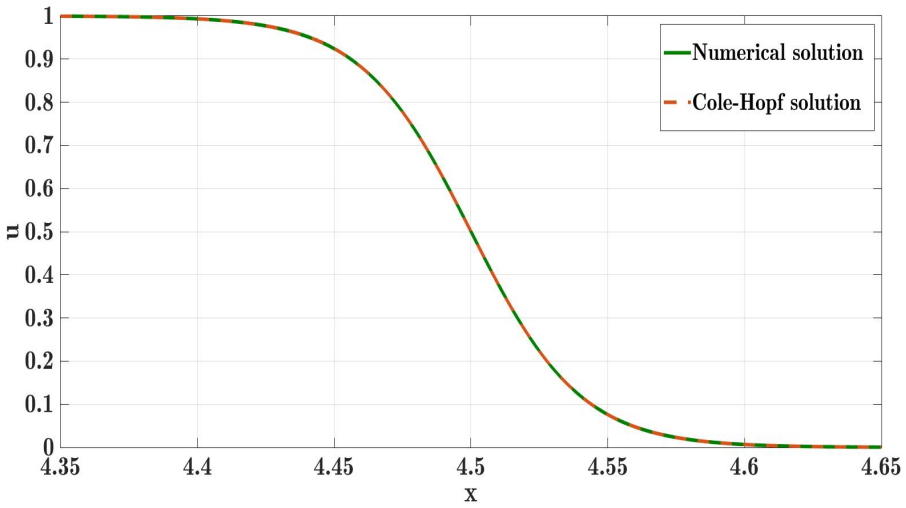

(a) $u_1(x,t)$ $t = 5$

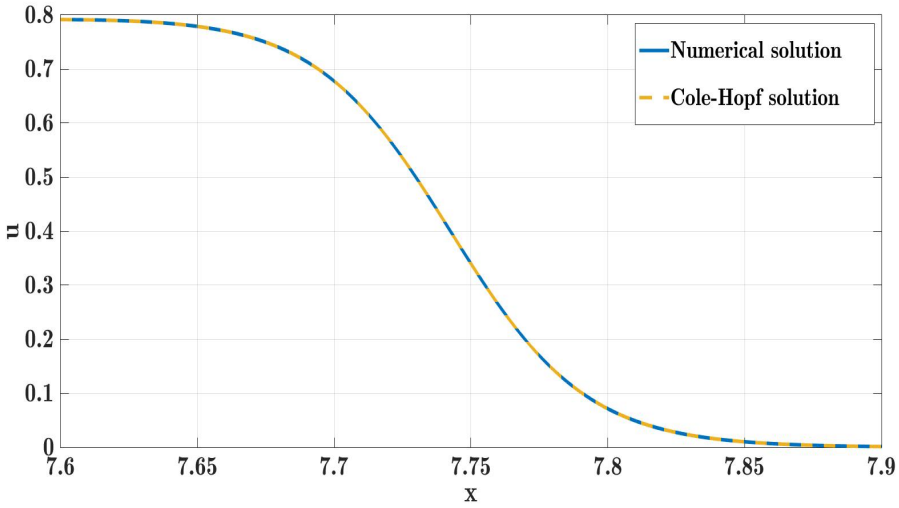

(b) $u_1(x,t)$ $t = 12$

Figure 2.5.8: A comparison between the numerical solution and the Cole-Hopf solution given in equation (2.4.19) for $t = 5,\ 12$ and viscous coefficient $\epsilon = 0.01$.

where

$$
\begin{aligned}
p_1(\theta) &= \frac{1}{8\cosh^2\theta}\Big[\mathrm{e}^{-2\theta}\big(2\theta+1\big)-2\theta^2\Big],\\
p_2(\theta) &= \frac{1}{8\cosh^2\theta}\Big[2\mathrm{e}^{-2\theta}+2-4\theta\Big].
\end{aligned}
$$

Figure 2.5.10 captures the correspondence of the numerical and asymptotic solutions at $t = 12$ for $\epsilon = 0.001$ in 2.5.10 (a) and $\epsilon = 0.0005$ in 2.5.10 (b). To achieve this match we chose the value $A_0 = 0$.

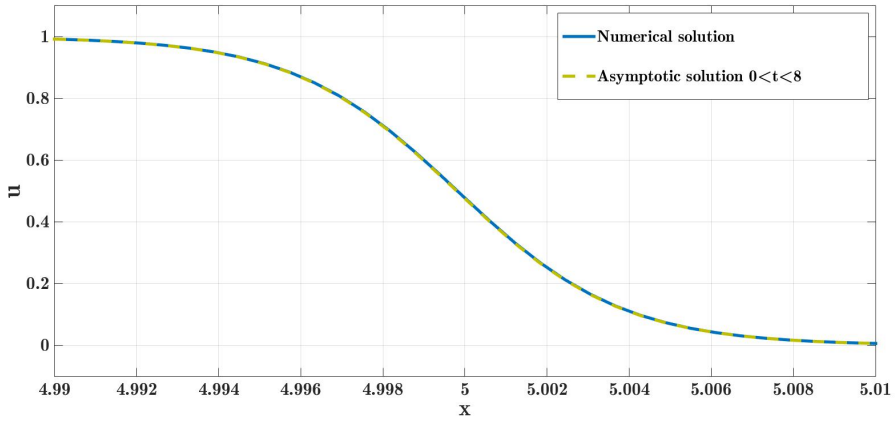

(a) $u_1(x, 6)$ $\epsilon = 0.001$

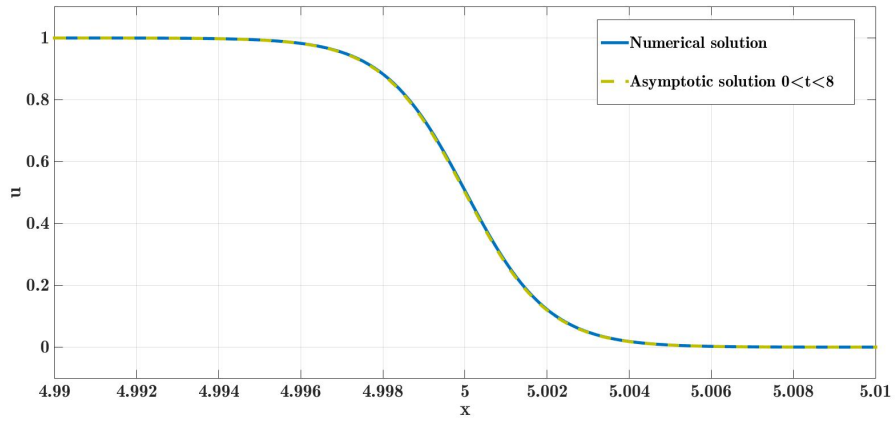

(b) $u_1(x, 6)$ $\epsilon = 0.0005$

Figure 2.5.9: Comparisons of numerical solution (blue) and asymptotic solution (yellow) for the case $0 < t < 8$ taking the time at $t = 6$. Plot (a) is taken for the viscosity parameter $\epsilon = 0.001$ with $N = 2^{15}$ number of points for spatial discretization and time step is $\Delta t = 0.0001$. While for plot (b) the viscosity is reduced to $\epsilon = 0.0005$ with increasing the number of points to $N = 2^{15}$ with a smaller time step $\Delta t = 0.00008$.

The final comparison, illustrated in figure 2.5.11, is made by monitoring the width of the shock pulse for both the asymptotic and numerical shock width for $0 < t < 15$. We recall in §2.3.1 we referred to the shock width to be the difference in spatial coordinate in which u changes from 90% of its amplitude to 10% of its amplitude. In figure 2.5.11 (a) where viscous parameter is $\epsilon = 0.01$, we can see the agreement between numerical and asymptotic width is good for the time $0 < t < 8$ where for this period of time the asymptotic width is $8\,\epsilon\,\tanh^{-1}(0.8)$. But when time reaches $t = 8$ as expected the

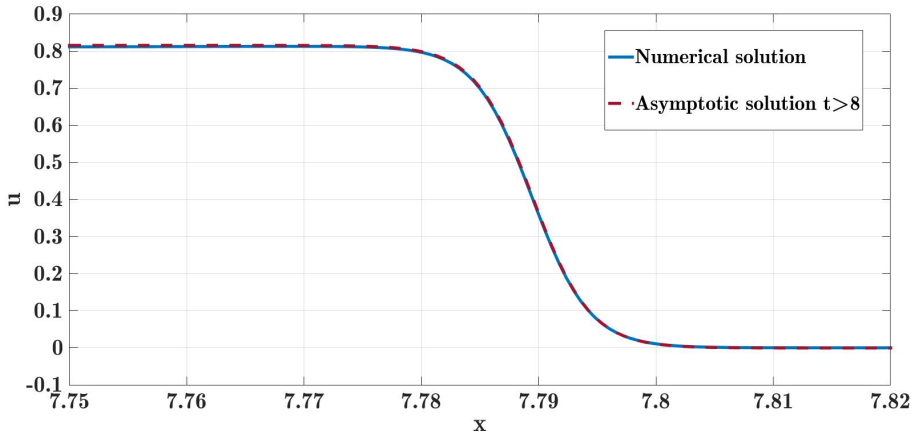

(a) $u_1(x, 12) \quad \epsilon = 0.001$

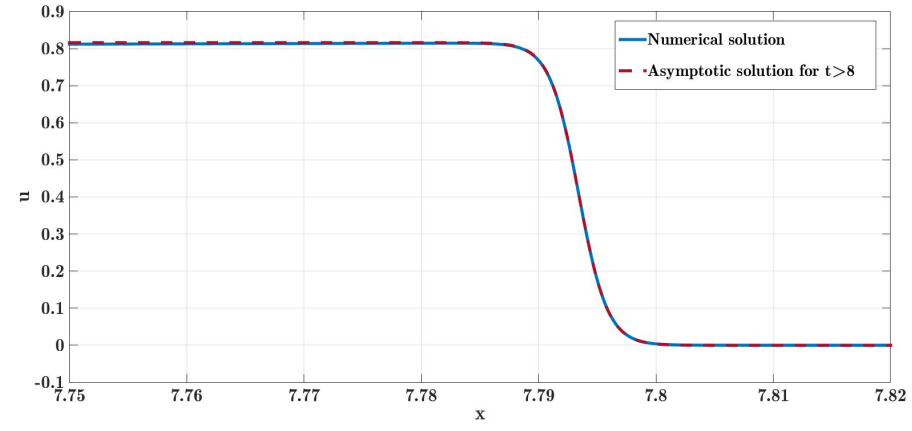

(b) $u_1(x, 12) \quad \epsilon = 0.0005$

Figure 2.5.10: Comparisons of numerical solution (blue) and asymptotic solution (burgundy) for the case $t \geq 8$ taking the time at $t = 12$. Plot (a) is taken for the viscosity parameter $\epsilon = 0.001$ with $N = 2^{15}$ number of points for spatial discretization and time step is $\Delta t = 0.0001$. While for plot (b) the viscosity is reduced to $\epsilon = 0.0005$ with increasing the number of points to $N = 2^{18}$ with a smaller time step $\Delta t = 0.00008$.

correspondence is weaker and this due to the decreasing amplitude, since the asymptotic width for $t > 8$ is $\sqrt{\frac{t}{8}}.8\,\epsilon\,\tanh^{-1}(0.8)$. Reducing the viscosity to 0.001 in figure 2.5.11 (b) results in a much better agreement. We note that the drop in beginning of the numerical width goes back to the value of slope δ given in the described initial condition for the numerical code.

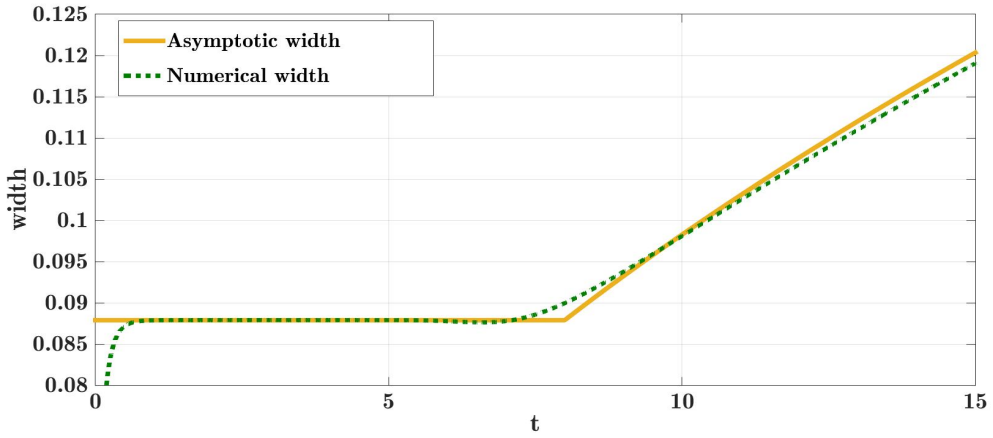

(a) $\epsilon = 0.01$

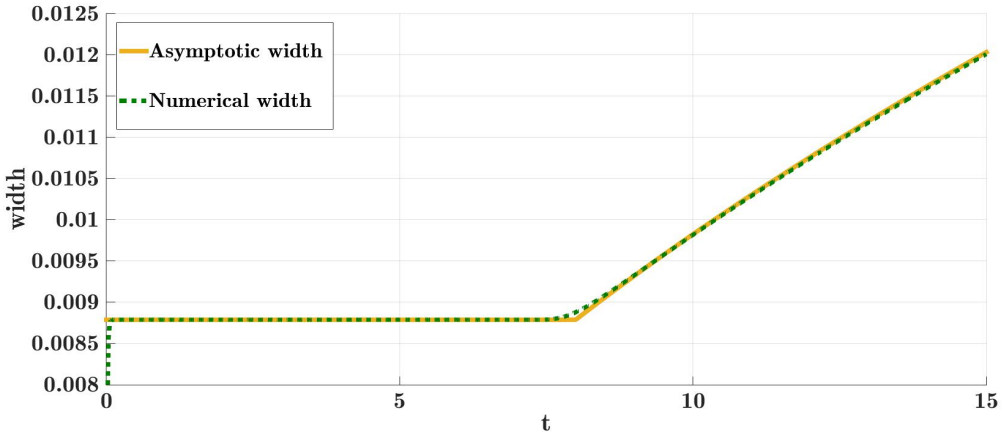

(b) $\epsilon = 0.001$

Figure 2.5.11: Comparison of numerical shock width (green) and asymptotic shock width (yellow) taken for the period of time $0 < t < 15$ and the viscosity parameter is taken $\epsilon = 0.01$ in(a) and $\epsilon = 0.001$ in (b). We see that the correspondence becomes better when the viscosity coefficient is reduced from 0.01 to 0.001 .

2.5.7 Summary

In this section we carried out a numerical scheme to solve Burgers' equation for the initial function $u_0(x) = \phi_1(x)$ which we defined in terms of the scaled hyperbolic tangent function defined as

$$u_0(x) = \frac{1}{2}\left[1 + \tanh\left(\frac{x+2}{\delta}\right)\right] . \frac{1}{2}\left[1 + \tanh\left(\frac{2-x}{\delta}\right)\right].$$

The developed shock wave solution of this initial condition is not a discontinuity, due to the presence of the viscosity coefficient ϵ. Instead it is rather a thin region of rapid change in which the width is controlled by the size of ϵ. For numerically approximating the viscous shock solution of Burgers' equation, we applied the pseudospectral method for discretizing in space and fourth-order Runge-Kutta method for discretizing in time.

The spectral differentiation of a function using Fourier collocation method can be evaluated either by matrix multiplication or by FFT. We chose the FFT technique for its reduced number of operations $O(N \log N)$ which takes "minutes" compared to the matrix multiplication of $O(N^2)$ requires "two days".

For maintaining the stability of the fourth order Runge-Kutta method, we incorporated the integrating factor method into the spectral algorithm to eliminate the linear term with high wavenumber k, since high wavenumbers correspond to wave oscillations. In addition, by this modification we achieve a sufficient enlargement of time step Δt and we employed this property in capturing the shock structure. To validate our numerical experiment we conducted some comparison plots of the numerical shock pulse with the analytical Cole-Hopf solution and with the asymptotic solutions for different values of viscosity.

In this chapter, we presented various analytical and numerical expressions of the viscous shock wave solution of Burger' equation for a rectangular pulse wave. Next we look at some of these techniques when Burgers' equation is

extended to include the relaxation effects.

3

Augmented Burgers' Model in Single Relaxation Mode

3.1 Introduction

Much literature discusses shock waves propagating in mediums in which a single relaxation mode is dominant. Lighthill [55] developed a theory of the interaction of nonlinear steepening and relaxation dispersion in shock waves. He presented two classifications describing the shock wave as fully or partially dispersed. Blythe [9], Ockendon and Spence [69] obtained travelling wave solutions in implicit form describing the propagation of a forward facing step. Their analysis showed the conditions on relaxation parameters for the existence of the solution. For a range of parameters, the relaxation mode does not have a full control on the shock structure and the formation of narrow a viscous sub-shock arises.

In this chapter we study the propagation of a one-dimensional finite-amplitude acoustic disturbance associated with thermoviscous dissipation and a single molecular relaxation process. Our detailed investigation covers the impact of the combination of nonlinearity, thermoviscosity and the relaxation mechanism on the propagating wave, in particular in shock formation. In this investigation we use the augmented Burgers' equation as the governing equation for this disturbance.

We begin with a brief description of the relaxation processes in polyatomic

gases in §3.2. Each relaxation process is characterised by two parameters, τ_r a relaxation time, and Δ_r the difference in linear sound speed between the low and high frequency. We choose a model of the augmented Burgers equation presented by Pierce [72]. In §3.3 we establish a nondimensional form of the augmented Burgers equation for the nonlinear viscous propagation in a medium with n relaxation modes. In §3.4 we present an asymptotic and numerical analysis for the viscous travelling wave solutions controlled by a single relaxation mode with the viscosity $\epsilon \ll \tau$. It is found that the shock structure takes two possible forms depending on the values of the relaxation parameter Δ_r. In §3.5 a numerical pseudo-spectral method using truncated Fourier modes and fourth order Runge-Kutta for time marching is described to solve numerically the nonlinear problem. A subsequent comparison of the numerical and asymptotic results are examined, focusing our attention on the case $\Delta < \frac{1}{2}$ where asymptotic theory predicts the multilayer formation in the shock region. This chapter is summed up with an examination of the asymptotic and numerical maximum negative slope. The maximum negative slope is a technique applied on the multilayer shock to calculate the width which is inversely proportional to the maximum negative slope.

3.2 Dynamics of Relaxing Gas

We present some basics of the modelling of the relaxation mechanism, to understand the molecular collisional relaxation processes associated with molecular internal vibration distribution of acoustics propagation in polyatomic gases. The theory presented here is taken from discussions of gas dynamics relevant to propagation of linear acoustics in a relaxed medium proposed by Pierce [72] in (Ch 10 p 552-562).

The main idea of a relaxation process is establishing a new total equilibrium statistical energy after its distribution due to molecule collisions. So, let us first present Pierce's definition of the internal energy e per unit mass of gas which is the total sum of energies contained in a molecule [72]. Each polyatomic molecule carries a substantial amount of translational mode of energy (defined relative to the average flow velocity since we are concerned with the static energy), and internal modes of motion that arise as rotations of the whole molecule or as vibrations of the molecule's atoms. The sum of the internal energy can be written as

$$e = e_{tr} + e_{rot} + \sum_{v} e_v,$$

where e_{tr} is the translational energy, e_{rot} is the rotational energy and e_v is the sum of vibrational energies of all molecules of species v per unit mass of fluid. For most gases in equilibrium, the apparent temperatures associated with translation T_{tr}, rotation T_{rot} and vibration T_v are the same. Thus, for a given energy e, the ratios of energies should be fixed. However, in a non-equilibrium state, with fluctuating translational temperature, the molecular rotation adjusts instantaneously but molecular vibration with large quantum level spacing is unable to follow these changes, leading to unfixed ratios of energy. Consequently, the vibrational energy is transferred between the various modes until equilibrium is attained. This transfer is known as thermal molecular

relaxation and gives rise to relaxation absorption of acoustic energy. For each mode, there is a characteristic time τ_v, which expresses the rate at which T_v returns from its disturbed non-equilibrium value to its equilibrium condition.

The relaxation process is described by the equation

$$\frac{\mathrm{d}T_v}{\mathrm{d}t} = \frac{1}{\tau_v}\Big(T_0 - T_v\Big).$$

The relaxation time τ_v, relates to the energy exchanged in unit time by a molecule of species v as it collides with other molecules. The relaxation time can therefore be sensitive to the composition of the medium. For air, the relaxation times associated with O_2 and N_2 are dependent on the fraction of air with water molecules. These O_2 and N_2 molecules are much more likely to experience a change in vibrational energy when colliding with an H_2O molecule than when colliding with each other.

The magnitude of the relaxation time relative to the characteristic disturbance time scale is important when considering the effect of relaxation on the propagation of an acoustic disturbance through a medium. If the disturbance time scale is large enough, the effect of relaxation is small since the adjustment to thermal equilibrium is practically instantaneous. However, for a high frequency signal, the internal vibration energy can never adjust to the change in equilibrium and is frozen.

The frequency dependence of absorption α_v by the relaxation processes is shown in figure 3.2.1 (a) where

$$\frac{\alpha_v\,\lambda}{\big(\alpha_v\,\lambda\big)_m} = \frac{2}{\frac{f_v}{f} + \frac{f}{f_v}}, \qquad \frac{f}{f_v} = \omega\,\tau_v, \tag{3.2.1}$$

here the molecular relaxation absorption coefficient $\alpha_v(\omega)$, where $\omega = 2\pi\,f$ is the acoustic angular frequency. While $\lambda = \frac{2\,\pi c}{\omega}$ is the nominal wavelength

of sound of angular frequency ω, $c(\omega)$ is frequency-dependent phase velocity and the ratio $\frac{f}{f_v}$ represents frequency in units of the relaxation frequency f_v. The quantity $(\alpha_v \lambda)_m$ is the absorption due to the v-type relaxation process for propagation in a distance of one wavelength and $\alpha_v \lambda$ is the maximum absorption per wavelength associated with v-type relaxation process. We can see in figure 3.2.1 (a) that the acoustic absorption $\alpha_v \lambda$ reaches its maximum value when the signal frequency is equal to the relaxation frequency. We see in figure 3.2.1 (b) that as the frequency increases, the phase velocity increases monotonically from the low frequency of sound speed c_0 or (equilibrium sound speed) to the high-frequency of sound speed c_∞, (frozen sound speed). This increase is measured with the increment Δc_v which is equal to $(\frac{c_\infty}{\pi})(\alpha_v \lambda)_m$.

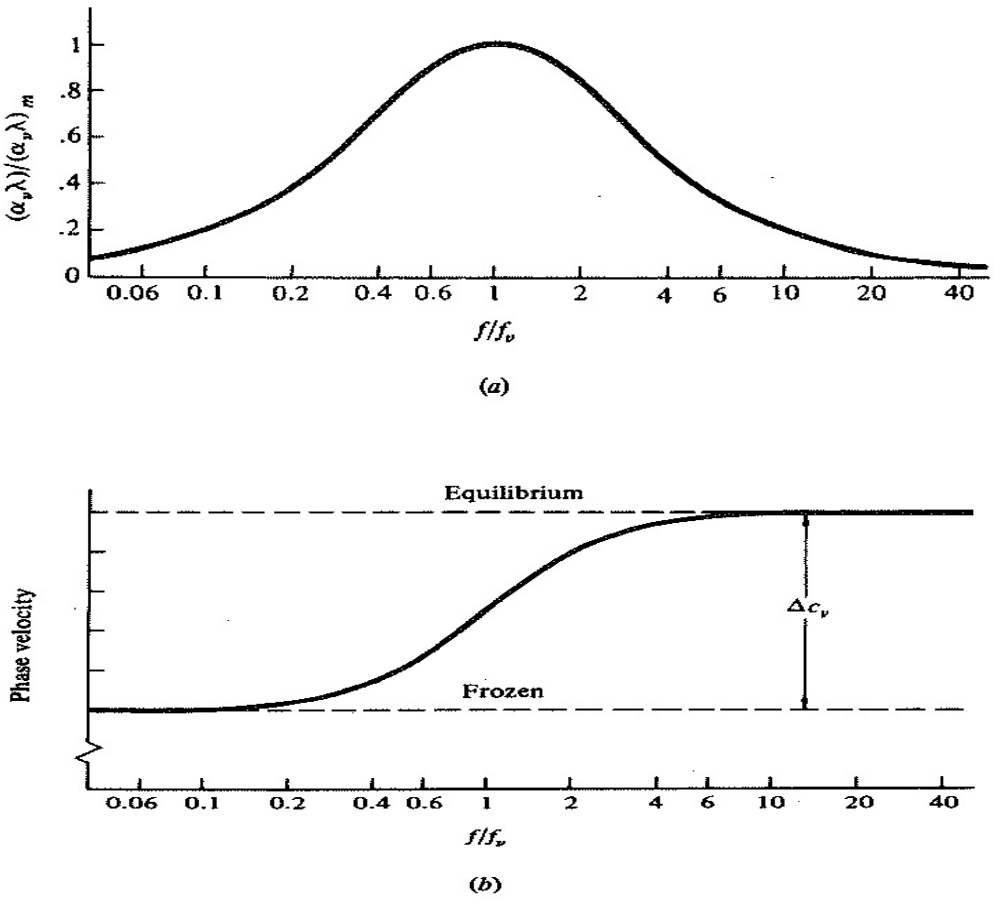

Figure 3.2.1: These two figures are taken from [72] where (a) represents frequency dependence of absorption $\alpha_v \lambda$ per wavelength for a single relaxation process. In (b) we see the increase in phase velocity with frequency from the low frequency or equilibrium sound speed to the high frequency (frozen sound speed), where the increment Δc_v represent this increase.

3.3 Formulation of the Augmented Burgers Equation

Quasi-one-dimensional propagation in an ideal fluid, neglecting viscous and dissipative effects is modelled by

$$\frac{\partial p}{\partial \tilde{t}} + c\frac{\partial p}{\partial \tilde{x}} = 0,$$

where $\tilde{x}$ and $\tilde{t}$ are dimensional variables. Including the thermoviscous dissipation and relaxation effects yields the set of equations

$$\frac{\partial p}{\partial \tilde{t}} + c\frac{\partial p}{\partial \tilde{x}} + \sum_r \tilde{\Delta}_r \frac{\partial p_r}{\partial \tilde{x}} = \tilde{\epsilon}\frac{\partial^2 p}{\partial \tilde{x}^2}, \qquad \tilde{x} \in \mathbb{R},\ \tilde{t} \geq 0,\ \tilde{\epsilon} \ll 1, \tag{3.3.1}$$

$$\left(1 + \tilde{\tau}_r \frac{\partial}{\partial \tilde{t}}\right) p_r = \tilde{\tau}_r \frac{\partial p}{\partial \tilde{t}}, \qquad r = 1, 2, ..., n, \tag{3.3.2}$$

where p represents acoustic pressure, c is the low frequency linear sound speed and $\tilde{\epsilon}$ the thermoviscous coefficient. Each relaxation mode r has an associated partial pressure p_r which is the variation $p - T_r$ where T_r is the apparent vibration temperature associated with the relaxation mode r [72]. The two characteristic parameters are $\tilde{\Delta}_r$ the linear sound speed difference between the high and low frequency signals and $\tilde{\tau}_r$ the relaxation time.

We modify (3.3.1) to include the nonlinear steepening so that the propagating disturbance can be governed by the Burgers' equation defined in §2.3. Therefore, the wave speed changes from c to $c + \frac{\beta p}{\rho c}$. In the study of one dimensional propagation of acoustics in a relaxing medium we consider the equations presented by Pierce [72]. The dimensional equation is referred to as the augmented Burgers equation and coupled with an additional equation for each relaxation mode

$$\frac{\partial p}{\partial \tilde{t}} + c\frac{\partial p}{\partial \tilde{x}} + \left(\frac{\beta p}{\rho c}\right)\frac{\partial p}{\partial \tilde{x}} + \sum_r \tilde{\Delta}_r \frac{\partial p_r}{\partial \tilde{x}} = \tilde{\epsilon}\frac{\partial^2 p}{\partial \tilde{x}^2}, \tag{3.3.3}$$

$$\left(1 + \tilde{\tau}_r \frac{\partial}{\partial \tilde{t}}\right) p_r = \tilde{\tau}_r \frac{\partial p}{\partial \tilde{t}}. \tag{3.3.4}$$

Here the non-linear effects $\frac{\beta p}{\rho c}$ include the air density ρ and volume expansion coefficient $\beta = \frac{\alpha+1}{2}$ where α is ratio of specific heats.

An equivalent representation to (3.3.3) can be found by rewriting it in terms of the particle velocities $v = \frac{\beta}{\rho c}\, p$ and $v_r = \frac{\beta}{\rho c}\, p_r$. Thus, we have

$$\frac{\partial v}{\partial \tilde{t}} + \Big(c + v\Big)\frac{\partial v}{\partial \tilde{x}} + \sum_r \tilde{\Delta}_r \frac{\partial v_r}{\partial \tilde{x}} = \tilde{\epsilon}\, \frac{\partial^2 v}{\partial \tilde{x}^2}, \tag{3.3.5}$$

$$\Big(1 + \tilde{\tau}_r \frac{\partial}{\partial \tilde{t}}\Big) v_r = \tilde{\tau}_r \frac{\partial v}{\partial \tilde{t}}, \qquad r = 1, 2, ..., n. \tag{3.3.6}$$

Notice that if the wave is propagating without the relaxation processes, equation (3.3.5) with $\tilde{\Delta}$ set to zero is reduced to Burgers' equation. We will produce a standard representation of Burgers' equation by regarding v as a function of $X = \tilde{x} - c\,\tilde{t}$ and $T = \tilde{t}$ rather than $\tilde{x}$ and $\tilde{t}$. The aim of this scaling is to eliminate the low frequency speed c so the spatial and time derivatives are

$$\begin{aligned} \frac{\partial}{\partial \tilde{x}} &= \frac{\partial}{\partial X}, \\ \frac{\partial}{\partial \tilde{t}} &= \frac{\partial}{\partial T} - c\,\frac{\partial}{\partial X}. \end{aligned}$$

Thus, the augmented Burgers equation in relaxation media reduces to

$$\frac{\partial v}{\partial T} + v\,\frac{\partial v}{\partial X} + \sum_r \tilde{\Delta}_r \frac{\partial v_r}{\partial X} = \tilde{\epsilon}\, \frac{\partial^2 v}{\partial X^2}, \tag{3.3.7}$$

$$\Big(1 - c\,\tau_r \frac{\partial}{\partial X}\Big)\, v_r = -c\,\tau_r \frac{\partial v}{\partial X} + \tau_r \frac{\partial}{\partial T}\Big(v - v_r\Big). \tag{3.3.8}$$

We now put the equations (3.3.7), (3.3.8) in non-dimensional form as they contains physical quantities. This action is to remove these units using a suitable substitution of variables. Choosing V_∞, L and K as typical velocity, length and time scales, respectively. We start replacing the dependent variables $v = V_\infty\, u$ and $v_r = V_\infty\, u_r$, and the independent variables with the scaled quantities $X = Lx$ and $T = Kt$, where the units of length and time L and K will be determined later. This puts the augmented Burgers equation in dimensionless form

$$\frac{\partial u}{\partial t} + \Big(\frac{K\,V_\infty}{L}\Big)\, u\,\frac{\partial u}{\partial x} + \frac{K}{L}\sum_r \tilde{\Delta}_r \frac{\partial u_r}{\partial x} = \Big(\frac{\tilde{\epsilon}\,K}{L^2}\Big)\frac{\partial^2 u}{\partial x^2}, \tag{3.3.9}$$

and for the relaxation equation

$$\Big(1-\Big(\frac{c\,\tilde{\tau}_r}{L}\Big)\,\frac{\partial}{\partial x}\Big)\,u_r=-\Big(\frac{c\,\tilde{\tau}_r}{L}\Big)\,\frac{\partial u}{\partial x}+\Big(\frac{\tilde{\tau}_r}{K}\Big)\,\frac{\partial}{\partial t}\Big(u-u_r\Big),\qquad r=1,2,..,n. \tag{3.3.10}$$

We chose $K=\frac{L}{V_\infty}$ and define the new parameters as follows

$$\epsilon=\frac{\tilde{\epsilon}}{V_\infty\,L},\qquad \Delta_r=\frac{\tilde{\Delta}_r}{V_\infty},\qquad \tau_r=\frac{c\,\tilde{\tau}_r}{L},\qquad r=1,2. \tag{3.3.11}$$

Therefore, equations (3.3.9), (3.3.10) become

$$u_t+u\,u_x+\sum_r \Delta_r\,u_{r,x} = \epsilon\,u_{xx}, \tag{3.3.12}$$

$$\Big(\tau\,\frac{\partial}{\partial x}-1\Big)\,u_r = \tau_r\,u_x+O\Big(\frac{\tau_r\,V_\infty}{c}\Big), \tag{3.3.13}$$

where u , x , t are the dimensionless wave amplitude, spatial coordinate and time, respectively. The model equation is valid only if the changes in wave shape occur over a large number of wavelengths, which requires that non-linearity effects are weak $\frac{V_\infty}{c}\ll 1$, the energy in each relaxation mode is small $\frac{\tilde{\Delta}_r}{c}\ll 1$ and finally the thermoviscosity is small $\epsilon\ll 1$. Therefore, $O\Big(\frac{\tau_r\,V_\infty}{c}\Big)$ terms are very small and so neglected and we study the system of equations

$$u_t+u\,u_x+\sum_r \Delta_r\,u_{r,x} = \epsilon\,u_{xx}, \tag{3.3.14}$$

$$\Big(\tau_r\,\frac{\partial}{\partial x}-1\Big)\,u_r = \tau_r\,u_x,\qquad r=1,2,...,n. \tag{3.3.15}$$

In the next section we begin by looking at travelling wave solutions of these equations. We will look at at the interesting case which occurs when $\Delta_r=O(1)$ and $\tau_r\ll 1$ with very little viscosity included to smooth out the discontinuity. This choice of parameters will allow us to capture the whole range of the thin relaxation shock waves of hight $O(1)$.

3.4 Travelling Waves for Single Relaxation Mode

3.4.1 Introduction

A travelling wave is a wave that advances in a particular direction with a constant velocity, while retaining a fixed shape through out its course of propagation. Since travelling waves are observed in conservation laws, Burgers' model is considered one of the classical non-linear PDEs that exhibits shock waves which are characterised as travelling wave. Studying such solutions is important in determining the dynamics of shocks. In this section we will provide an asymptotic analysis to obtain a solution for the travelling wave that corresponds to the non-linear augmented Burgers equation. A set of numerical methods are then implemented for obtaining an approximated solution to the travelling wave system. The section is ends with a detailed description of the maximum negative slope, which we will measure the width of the shock.
We begin with the augmented Burgers equation (3.3.14) and the relaxation process equation (3.3.15) for a single relaxation mode:

$$u_t + u\,u_x + \Delta\,u_{r,x} = \epsilon\,u_{xx}, \tag{3.4.1}$$

$$\left(1 - \tau\,\frac{\partial}{\partial x}\right) u_r = -\tau\,u_x. \tag{3.4.2}$$

3.4.2 Asymptotic Approaches of Travelling Waves

We consider the governing equations in (3.4.1), (3.4.2) subject to the boundary conditions $u \to 1$, $u_x \to 0$ as $x \to -\infty$ and $u \to 0$, $u_x \to 0$ as $x \to \infty$. In dimensional quantities this corresponds to an increase of magnitude V_∞.
We define the substitutions

$$u(t,x) = F(\theta) = F(x - st) \qquad u_r(t,x) = \tilde{F}(\theta) = \tilde{F}(x - st), \qquad \theta = x - st,$$

with the boundary conditions

$$F, F_\theta, \tilde{F}, \tilde{F}_\theta \to 0, \qquad \text{as} \qquad \theta \to \infty, \tag{3.4.3}$$

$$F \to 1, \qquad F_\theta, \tilde{F}, \tilde{F}_\theta \to 0, \qquad \text{as} \qquad \theta \to -\infty. \tag{3.4.4}$$

Upon replacing the partial derivatives of u and u_r in equations (3.3.12), (3.3.13) with the appropriate derivatives in F and $\tilde{F}$, we get

$$-s\,F_\theta + \Big(\tfrac{1}{2}F^2\Big)_\theta + \Delta\,\tilde{F}_\theta = \epsilon\,F_{\theta\,\theta}, \tag{3.4.5}$$

$$\Big(1 - \tau\,\frac{\mathrm{d}}{\mathrm{d}\theta}\Big)\tilde{F} = -\tau\,F_\theta. \tag{3.4.6}$$

The travelling wave (3.4.5) advances to the right at a constant speed. To represent the travelling wave we first eliminate $\tilde{F}$. Integrating (3.4.5) once puts it into the form

$$-s\,F + \frac{1}{2}F^2 + \Delta\,\tilde{F} = \epsilon\,\frac{\mathrm{d}F}{\mathrm{d}\theta} + C.$$

The boundary condition (3.4.3) implies the integration constant $C = 0$. Applying the second boundary condition requires the wave speed to be $s = \frac{1}{2}$. Substituting

$$\Delta\,\tilde{F} = \epsilon\,F_\theta + \frac{1}{2}\Big(F - F^2\Big),$$

in equation (3.4.6) gives

$$\Big(1 - \tau\,\frac{\mathrm{d}}{\mathrm{d}\theta}\Big)\left(\frac{1}{2}\left(F^2 - F\right) - \epsilon\,F_\theta\right) - \Delta\,\tau\,F_\theta = 0,$$

$$\implies F\Big(F-1\Big) - \tau\left(2\,F - 1\right)F_\theta - 2\,\Delta\,\tau\,F_\theta + 2\,\epsilon\left(\tau\,F_{\theta\,\theta} - F_\theta\right) = 0,$$

$$\implies \Big(F-1\Big)\,F - \Big(\tau\left(2\,F - 1 + \phi\right) + 2\,\epsilon\Big)\,F_\theta + 2\,\tau\,\epsilon\,F_{\theta\,\theta} = 0,$$

where $\phi = 2\Delta$. If we set $\gamma = \frac{1-\phi}{2}$, this yields

$$2\,\tau\,\epsilon\,F_{\theta\,\theta} - 2\Big(\tau\left(F - \gamma\right) + \epsilon\Big)F_\theta + \Big(F-1\Big)\,F = 0, \tag{3.4.7}$$

which is the travelling wave ODE deduced from the augmented Burgers' PDE. Next we use the matched asymptotic expansions scheme to evaluate the travelling wave solution when $\epsilon \ll \tau \ll 1$, i.e when the effect of viscosity is much less than that of relaxation over the main part of the disturbance.

3.4.3 Asymptotic Solutions: Outer Expansion

We begin by expressing the outer solution as follows

$$F_{out} = F_0 + \epsilon\, F_1 + O(\epsilon^2). \tag{3.4.8}$$

Substituting the outer expansion (3.4.8) in the travelling wave equation (3.4.7) to derive the leading order and the first correction as follows.
The leading order of the outer expansion is given by

$$O(1) \qquad \Big(F_0 - 1\Big)\, F_0 - 2\,\tau\,\Big(F_0 - \gamma\Big)\frac{\mathrm{d}F_0}{\mathrm{d}\theta} = 0, \tag{3.4.9}$$

and the first correction by

$$O(\epsilon) \quad 2\,\tau\,\frac{\mathrm{d}^2 F_0}{\mathrm{d}\theta^2} - 2\,\left[\Big(\tau\, F_1 + 1\Big)\frac{\mathrm{d}F_0}{\mathrm{d}\theta} + \tau\Big(F_0 - \gamma\Big)\frac{\mathrm{d}F_1}{\mathrm{d}\theta}\right] + \Big(2\,F_0 - 1\Big)F_1 = 0. \tag{3.4.10}$$

The relevant limiting conditions are $F_0(-\infty) = 1$ and $F_0(\infty) = F_1(\pm\infty) = 0$.
Before integrating the leading order term we rewrite (3.4.9) as

$$\begin{aligned}
\Big(F_0 - 1\Big)\, F_0 &= 2\,\tau\,\Big(F_0 - \gamma\Big)\frac{\mathrm{d}F_0}{\mathrm{d}\theta}, \\
\implies \tau\,\frac{\mathrm{d}F_0}{\mathrm{d}\theta} &= \frac{F_0(F_0 - 1)}{2\Big(F_0 - \gamma\Big)}, \\
\implies \frac{1}{\tau}\,\frac{\mathrm{d}\theta}{\mathrm{d}F_0} &= \frac{2\,F_0 - (1-\phi)}{F_0(F_0 - 1)}, \qquad \text{where} \quad \gamma = \frac{1-\phi}{2},
\end{aligned}$$

applying the partial fraction decomposition yields

$$\frac{1}{\tau}\,\frac{\mathrm{d}\theta}{\mathrm{d}F_0} = \frac{1+\phi}{F_0 - 1} + \frac{1-\phi}{F_0}. \tag{3.4.11}$$

This integrates to

$$\frac{\theta-\theta_0}{\tau} = (1+\phi)\ln\Big|1-F_0\Big| + (1-\phi)\ln\Big|F_0\Big|,$$

where θ_0 is an arbitrary constant. Applying the exponential function yields an implicit equation for F_0

$$\exp\left[\frac{\theta-\theta_0}{\tau}\right] = \Big(1-F_0\Big)^{1+\phi}\Big(F_0\Big)^{1-\phi}, \qquad 0<F_0<1, \tag{3.4.12}$$

where θ_0 describes the arbitrary horizontal shift of the travelling wave solution. If we fix the position of the wave such that $F_0(\theta_0) = F^*$, for some $0<F^*<1$, then

$$\exp\left[\frac{\theta-\theta_0}{\tau}\right] = \left(\frac{1-F_0}{1-F^*}\right)^{1+\phi}\left(\frac{F_0}{F^*}\right)^{1-\phi}. \tag{3.4.13}$$

We now distinguish between the cases $0<\phi<1$, $\phi=1$ and $\phi>1$, where $\phi = 2\Delta$.

Asymptotic Travelling Wave Solution: $\phi > 1$

Applying the boundary conditions to the implicit solution (3.4.12) gives

$$\begin{aligned} &\text{for} \qquad F_0 \to 1 \implies \exp\left(\tfrac{\theta-\theta_0}{\tau}\right) \to 0 \implies \theta \to -\infty, \\ &\text{for} \qquad F_0 \to 0 \implies \exp\left(\tfrac{\theta-\theta_0}{\tau}\right) \to \infty \implies \theta \to \infty. \end{aligned}$$

Thus, F_0 satisfies the required boundary conditions when $\phi > 1$ and the waveform of the outer solution remains single-valued. This is known as the fully dispersed relaxing shock (see Lighthill [55]) and represents a physically realistic solution for F_{out} over the whole range $0<F_{out}<1$. In this case, the viscosity ϵ has little effect on the shape of the waveform [55]. Figure 3.4.1 illustrates the fully dispersed travelling wave taken for several values of ϕ where $\phi>1$, we can see as ϕ increases the tail in front of the shock becomes longer.

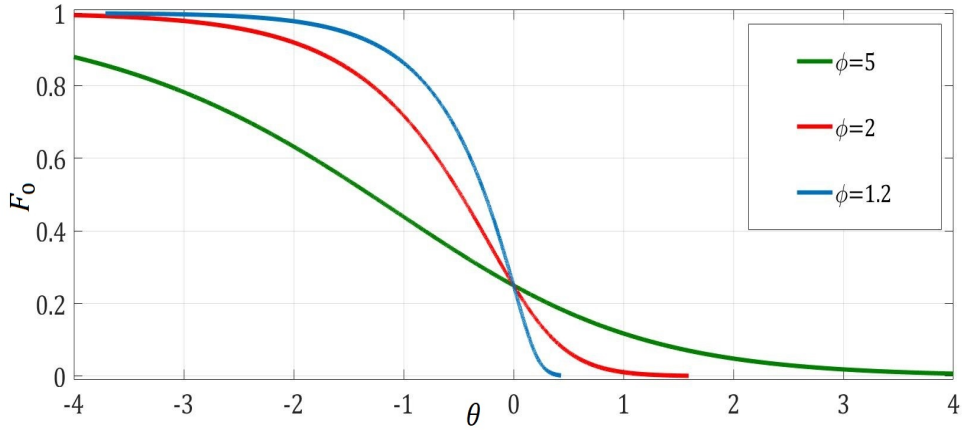

Figure 3.4.1: Asymptotic travelling wave solution at leading order for various values of $\phi > 1$

Asymptotic Travelling Wave Solution: $\phi = 1$

This is a special case, as the solution (3.4.12) becomes

$$\frac{\theta - \theta_0}{2\,\tau} = \ln\left(\frac{1 - F_0}{1 - F^*}\right).$$

This can be expressed explicitly as

$$F_0 = 1 - \left(1 - F^*\right) \mathrm{e}^{\frac{\theta - \theta_0}{2\,\tau}}. \tag{3.4.14}$$

We apply the boundary conditions on this explicit solution to have

$$\text{for} \qquad \theta \to -\infty \implies F_0 = 1 - \left(1 - F^*\right) \mathrm{e}^{-\infty} \implies F_0 \to 1,$$
$$\text{for} \qquad \theta \to \infty \implies F_0 = 1 - \left(1 - F^*\right) \mathrm{e}^{\infty} \implies F_0 \to -\infty.$$

For $\phi = 1$ the solution has a discontinuity in gradient at $F = 0$. The presence of viscosity smooths out this discontinuity in slope without altering the full waveform.

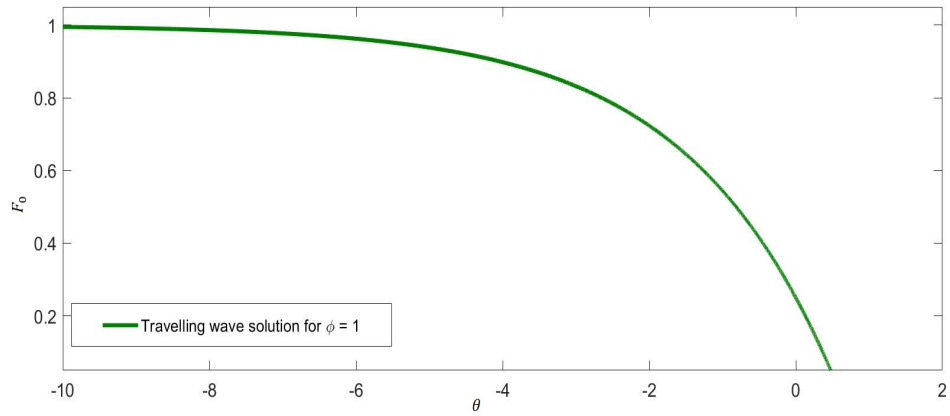

Figure 3.4.2: Asymptotic travelling wave solution at leading order when $\phi = 1$

Asymptotic Travelling Wave Solution: $0 < \phi < 1$

If ϕ falls below the critical value, 1 , then the boundary conditions become

$$\text{for} \qquad F_0 \to 1 \implies \exp\left(\tfrac{\theta-\theta_0}{\tau}\right) \to 0 \implies \theta \to -\infty,$$
$$\text{for} \qquad F_0 \to 0 \implies \exp\left(\tfrac{\theta-\theta_0}{\tau}\right) \to 0 \implies \theta \to -\infty.$$

Therefore, when $\phi < 1$ the second boundary condition is no longer satisfied, the outer solution is now multi-valued as can be seen in Figure 3.4.3, hence, in this case when $\epsilon = 0$ no such travelling wave solution exists. In other words, the relaxation mode is insufficient to support the shock, but for small ϵ, thermoviscosity insures a single-valued solution. An inner Taylor type sub-shock, controlled by the ϵ term, must be inserted at $\theta = \theta_0$, describing the transition from the outer solution for $\theta < \theta_0$ to zero ahead of the inner shock. The waveform is known as partly dispersed [55],[9], [69]. If we identify $F_0(\theta_0) = 1 - \phi$, thus, from equation (3.4.13) we see that when $\phi < 1$ the outer solution for $\theta < \theta_0$ is

$$\exp\left[\frac{\theta - \theta_0}{\tau}\right] = \left(\frac{1 - F_0}{\phi}\right)^{1+\phi} \left(\frac{F_0}{1-\phi}\right)^{1-\phi}, \qquad 1 - \phi < F_0 < 1. \quad (3.4.15)$$

However, before considering this inner region, we obtain the $O(\epsilon)$ correction to the outer solution that will be used later in the matching process. Rearranging

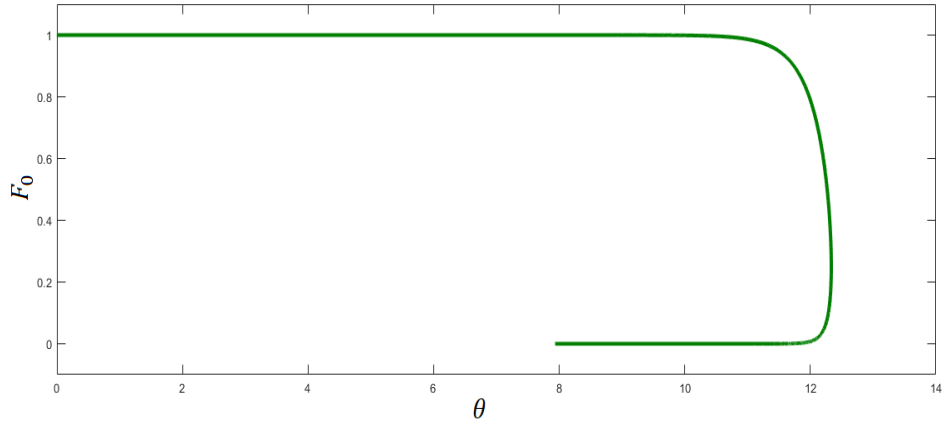

Figure 3.4.3: Travelling wave asymptotic outer solution at leading order when $\phi = 0.5$ where the solution becomes multivalued.

equation (3.4.10) gives

$$2\,\tau\Big(F_0-\gamma\Big)\frac{\mathrm{d}F_1}{\mathrm{d}\theta}+\Big(1-2\,F_0+2\,\tau\,\frac{\mathrm{d}F_0}{\mathrm{d}\theta}\Big)F_1=2\,\tau\,\frac{\mathrm{d}^2\,F_0}{\mathrm{d}\theta^2}-2\,\frac{\mathrm{d}F_0}{\mathrm{d}\theta}, \tag{3.4.16}$$

To solve the $O(\epsilon)$ equation (3.4.16), we consider the integrating factor method. But first let's look for the first and second derivatives of F_0. We recall from equation (3.4.11) that the first derivative of F_0 is

$$\Big(F_0\Big)_\theta=\frac{F_0\big(F_0-1\big)}{2\,\tau\big(F_0-\gamma\big)}. \tag{3.4.17}$$

Therefore, this can be differentiated as follows

$$\begin{aligned}
\Big(F_0\Big)_{\theta\,\theta} &= \frac{\mathrm{d}}{\mathrm{d}\theta}\left(\frac{F_0\big(F_0-1\big)}{2\,\tau\big(F_0-\gamma\big)}\right),\\
&= \frac{\mathrm{d}}{\mathrm{d}F_0}\left(\frac{F_0\big(F_0-1\big)}{2\,\tau\big(F_0-\gamma\big)}\right)\cdot\frac{\mathrm{d}F_0}{\mathrm{d}\theta},\\
&= \frac{{F_0}^2+\gamma-2\,\gamma\,F_0}{2\,\tau\big(F_0-\gamma\big)^2}\cdot\frac{F_0\big(F_0-1\big)}{2\,\tau\big(F_0-\gamma\big)},\\
&= \frac{F_0\big(F_0-1\big)}{4\,\tau^2\big(F_0-\gamma\big)^3}\Big[\big(F_0-\gamma\big)^2+\gamma\big(1-\gamma\big)\Big].
\end{aligned}$$

We put equation (3.4.16) in the standard form of the integrating factor method as follows

$$F_{1\,\theta} + \left(\frac{b(F_0)}{a(F_0)}\right) F_1 \;=\; \frac{c(F_0)}{a(F_0)},$$

where the functions $a\,, b,\, c$ are given by

$$a(F_0) = 2\,\tau\,\Big(F_0 - \gamma\Big), \qquad b(F_0) = 1 - 2\,F_0 + 2\,\tau\,F_{0\,\theta}, \qquad c(F_0) = 2\,\tau\,F_{0\,\theta\,\theta} - 2\,F_{0\,\theta}.$$

Multiplying the PDE with the integrating factor $\exp\big(g(F_0)\big)$, gives

$$\frac{\mathrm{d}}{\mathrm{d}\theta}\Big(\mathrm{e}^{g(F_0)}\;F_1\Big) = \frac{c(F_0)}{a(F_0)}\;\mathrm{e}^{g(F_0)}, \qquad\qquad \text{where} \qquad g(F_0) = \int \frac{b}{a}\,\mathrm{d}\theta. \tag{3.4.18}$$

Now we compute the integrating factor e^{g} by integrating $\frac{b(F_0)}{a(F_0)}$ with respect to F_0 since the function is expressed in terms of $F_0\,.$

$$\begin{aligned}
g(F_0) \;&=\; \int \frac{b\big(F_0\big)}{a\big(F_0\big)}\,\mathrm{d}\theta, \\
&=\; \int \frac{\big(1 - 2\,F_0\big)\big(F_0 - \gamma\big) + F_0\,\big(F_0 - 1\big)}{2\,\tau\,\big(F_0 - \gamma\big)^2}\;\frac{\mathrm{d}\,F_0}{F_{0\,\theta}}, \\
&=\; \int \frac{\big(F_0 - \gamma\big)\big(1 - \;F_0\big) - F_0\big(F_0 - \gamma\big) + F_0\,\big(F_0 - 1\big)}{2\,\tau\,\big(F_0 - \gamma\big)^2}\;\frac{2\,\tau\,\big(F_0 - \gamma\big)}{F_0\big(F_0 - 1\big)}\;\mathrm{d}F_0, \\
&=\; \int \frac{\big(F_0 - \gamma\big)\big(1 - \;F_0\big) - F_0\big(F_0 - \gamma\big) + F_0\,\big(F_0 - 1\big)}{F_0\big(F_0 - 1\big)\big(F_0 - \gamma\big)}\;\mathrm{d}F_0, \\
&=\; \int \left(\frac{1}{F_0 - \gamma} - \frac{1}{F_0} - \frac{1}{F_0 - 1}\right)\;\mathrm{d}F_0, \\
&=\; \ln\left|\frac{F_0 - \gamma}{F_0\big(F_0 - 1\big)}\right|.
\end{aligned}$$

Consequently, the integration factor is

$$\mathrm{e}^{g} = \frac{F_0 - \gamma}{F_0\big(1 - F_0\big)}.$$

Thus the $O(\epsilon)$ PDE of F_1 (3.4.18) can be written as

$$\frac{\mathrm{d}}{\mathrm{d}\theta}\left(\frac{F_0-\gamma}{F_0(1-F_0)}\,.\,F_1\right)=h(F_0), \tag{3.4.19}$$

where the function $h(F_0)$ is

$$\begin{aligned}
h(F_0) &= \frac{c(F_0)}{a(F_0)}\,\mathrm{e}^{g(F_0)},\\
&= \frac{1}{2\,\tau(F_0-\gamma)}\left(2\,\tau\,F_{0\,\theta\,\theta}-2\,F_{0\,\theta}\right)\frac{F_0-\gamma}{F_0(1-F_0)},\\
&= \frac{1}{4\,\tau^2\,F_0(1-F_0)}\left[\frac{F_0(F_0-1)}{(F_0-\gamma)^3}\Big((F_0-\gamma)^2+\gamma(1-\gamma)\Big)-\frac{2\,F_0(F_0-1)}{F_0-\gamma}\right],\\
&= \frac{1}{4\,\tau^2}\,\frac{(F_0-\gamma)^2-\gamma(1-\gamma)}{(F_0-\gamma)^3}.
\end{aligned}$$

We then integrate equation (3.4.19) with respect to θ.

$$\frac{F_0-\gamma}{F_0(1-F_0)}\;F_1=\int h(F_0)\;\mathrm{d}\theta.$$

The integral of the function $h(F_0)$ is

$$\begin{aligned}
\int h(F_0)\;\mathrm{d}\theta &= \frac{1}{4\,\tau^2}\int\frac{(F_0-\gamma)^2-\gamma(1-\gamma)}{(F_0-\gamma)^3}\;\mathrm{d}\theta,\\
&= \frac{1}{4\,\tau^2}\int\left(\frac{(F_0-\gamma)^2-\gamma(1-\gamma)}{(F_0-\gamma)^3}\right)\frac{2\tau\,(F_0-\gamma)}{F_0(F_0-1)}\;\mathrm{d}F_0,\\
&= \frac{1}{2\,\tau}\int\frac{(F_0-\gamma)^2-\gamma(1-\gamma)}{F_0(F_0-1)(F_0-\gamma)^2}\;\mathrm{d}F_0,
\end{aligned}$$

by applying the partial fraction decomposition, the integral of $h(F_0)$ becomes

$$\int h(F_0)\;\mathrm{d}\theta=\frac{(1-2\,\gamma)}{2\,\tau\,\gamma(1-\gamma)}\left[\gamma\,\ln\left(\frac{1-F_0}{F_0}\right)+\ln\left(\frac{F_0}{|F_0-\gamma|}\right)\right]-\frac{1}{2\,\tau(F_0-\gamma)}+C.$$

We can choose to set $C = 0$ as this term can be incorporated into the leading order solution. Hence, the first correction term of the outer solution is

$$F_1 = A\,(F_0)_\theta\,K(F_0), \tag{3.4.20}$$

where $A = \frac{4\,\phi}{\phi^2-1}$ and the function $K(F_0)$ is

$$K(F_0) = \gamma\,\ln\left(\frac{1-F_0}{F_0}\right) + \ln\left(\frac{F_0}{|F_0-\gamma|}\right) + \frac{\phi^2-1}{4\,\phi(F_0-\gamma)}. \tag{3.4.21}$$

We end the analytical derivation of the outer region solution with a figure 3.4.4 showing the $O(\epsilon)$ correction of the outer solution for the three different cases of ϕ. The first case where $\phi > 1$ shown in figure 3.4.4 (a) we see that the function F_1 is bounded and thus the correction $\epsilon\,F_1$ is a small correction throughout the waveform. However, for $\phi = 1$ in 3.4.4 (b), we see $F_1 \to \infty$ as $\theta \to \theta_0$, which indicates a breakdown in the outer solution. In this case some smoothing of the solution occurs close to θ_0 but is not considered further. The third case in figure 3.4.4 (c) where $\phi < 0$, we see also $F_1 \to -\infty$ as $\theta \to \theta_0$, so a breakdown in the outer solution and an inner solution is required which is the analysis presented in the next section.

3.4.4 Asymptotic Solutions: Inner Expansion when $0 < \phi < 1$

We mentioned earlier that in case $\phi < 1$ the outer solution is multivalued due to the unsatisfied boundary conditions and there exists an inner sub-shock. To find this inner sub-shock we deduce the inner solution for the travelling wave equation (3.4.7). We define the re-scaling

$$\hat{\theta} = \frac{\theta-\theta_0}{\epsilon}, \qquad \frac{\mathrm{d}}{\mathrm{d}\theta} = \frac{1}{\epsilon}\frac{\mathrm{d}}{\mathrm{d}\hat{\theta}}, \tag{3.4.22}$$

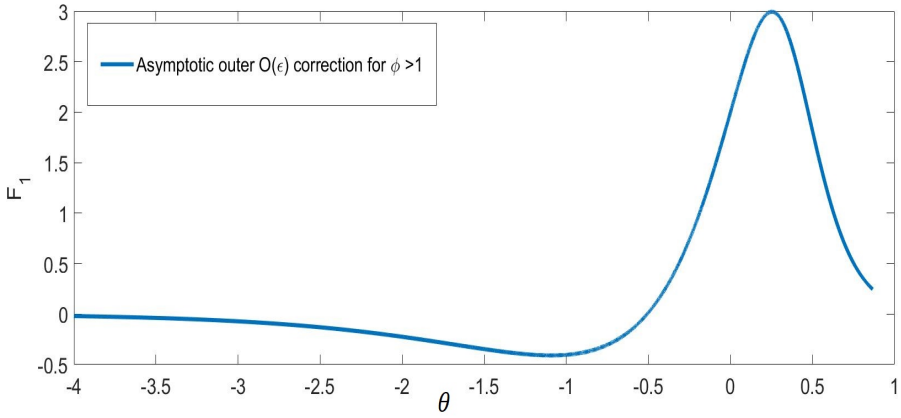

(a) $\phi > 1$

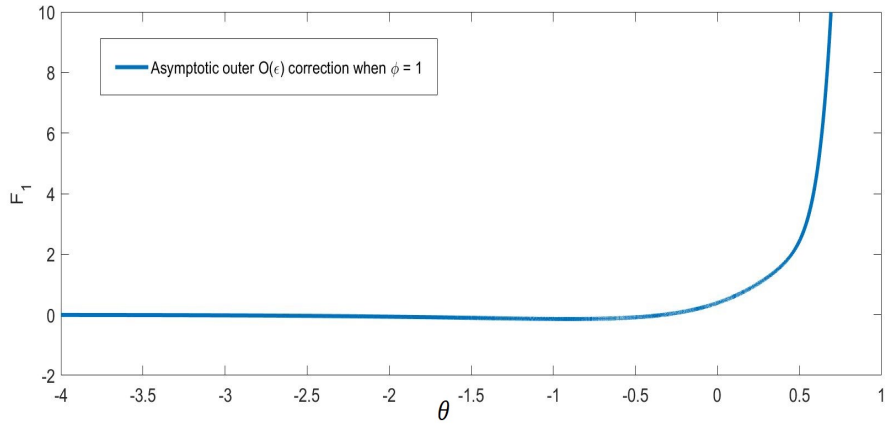

(b) $\phi = 1$

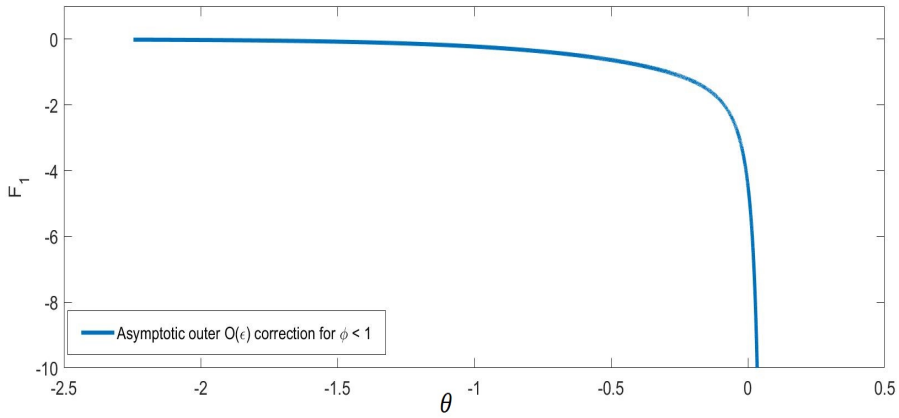

(c) $\phi < 1$

Figure 3.4.4: Travelling wave outer $O(\epsilon)$ correction for $\phi > 1$, $\phi = 1$ and $\phi < 1$ with choosing $\theta_0 = 0$.

where θ_0 will be determined later in the matching analysis. Inserting the inner variable $\hat{\theta}$ in equation (3.4.7) gives

$$2\,\tau\,F_{\hat{\theta}\,\hat{\theta}} - 2\left(\tau\,(F-\gamma)+\epsilon\right)F_{\hat{\theta}} + \epsilon\left(F-1\right)F = 0. \tag{3.4.23}$$

We now consider the inner expansion

$$F_{in}(\hat{\theta}) = f_0(\hat{\theta}) + \epsilon\, f_1(\hat{\theta}) + O(\epsilon^2).$$

Substituting the expansion in (3.4.23) gives the leading order term of the expansion

$$O(1) \qquad \frac{\mathrm{d}^2 f_0}{\mathrm{d}\hat{\theta}^2} - \left(f_0-\gamma\right)\frac{\mathrm{d}f_0}{\mathrm{d}\hat{\theta}} = 0,$$

and the $O(\epsilon)$ correction term

$$O(\epsilon) \quad 2\,\tau\,\frac{\mathrm{d}^2 f_1}{\mathrm{d}\hat{\theta}^2} - 2\,\tau\left(f_0-\gamma\right)\frac{\mathrm{d}f_1}{\mathrm{d}\hat{\theta}} - 2\left(\tau\,f_1+1\right)\frac{\mathrm{d}f_0}{\mathrm{d}\hat{\theta}} + \left(f_0-1\right)f_0 = 0.$$

The limit $F_{in}(\infty) = 0$ whereas when $\hat{\theta} \to -\infty$ the inner solution must match to the outer solution given by (3.4.12), (3.4.20). We begin deriving the inner solution by first integrating the leading order with respect to $\hat{\theta}$ and use the boundary condition $f_0 \to 0$ when $\hat{\theta} \to \infty$ to give

$$\begin{aligned}
\frac{\mathrm{d}f_0}{\mathrm{d}\hat{\theta}} - \frac{1}{2}\left(f_0 - 2\,\gamma\right)f_0 &= 0, \\
\implies \frac{\mathrm{d}f_0}{f_0(f_0-2\,\gamma)} &= \frac{1}{2}\,\mathrm{d}\hat{\theta}, \\
\implies \int\left[\frac{1}{f_0-2\,\gamma} - \frac{1}{f_0}\right]\mathrm{d}f_0 &= \frac{2\,\gamma}{2}\int \mathrm{d}\hat{\theta}, \\
\implies \ln\left(\frac{2\,\gamma - f_0}{f_0}\right) &= \gamma\,(\hat{\theta}-\hat{\theta}_0), \qquad 0 < f_0 < 2\gamma.
\end{aligned} \tag{3.4.24}$$

We define $z = \gamma\,(\hat{\theta} - \hat{\theta}_0)$ and then apply the exponential function to (3.4.24) to arrive at

$$\begin{aligned} f_0 &= \frac{2\,\gamma}{1+\exp(z)}, \\ &= \gamma\,\frac{2\exp(-\frac{z}{2})}{\exp(-\frac{z}{2})+\exp(\frac{z}{2})}, \\ &= \gamma\,\left[1-\frac{\exp(\frac{z}{2})-\exp(-\frac{z}{2})}{\exp(\frac{z}{2})+\exp(-\frac{z}{2})}\right]. \end{aligned}$$

Using the definition of the hyperbolic tangent function $\tanh z$ the inner shock can be expressed as

$$f_0 = \gamma\,\Big(1-\tanh y\Big),$$

where the variable y is

$$y = \frac{\gamma}{2}\,(\hat{\theta} - \hat{\theta}_0). \tag{3.4.25}$$

Recalling that $\gamma = \frac{1}{2}(1-\phi)$, we can write the inner solution as

$$f_0 = \frac{1}{2}\,(1-\phi)\,\left[1-\tanh\Big(\frac{1-\phi}{4}(\hat{\theta}-\hat{\theta}_0)\Big)\right]. \tag{3.4.26}$$

Taking $\hat{\theta} \to -\infty$ gives us the amplitude of the inner shock which is

$$\lim_{\hat{\theta}\to-\infty} f_0 = \lim_{\hat{\theta}\to-\infty} \frac{1}{2}\,(1-\phi)\,\left[1-\tanh\Big(\frac{1-\phi}{4}(\hat{\theta}-\hat{\theta}_0)\Big)\right] = 1-\phi. \tag{3.4.27}$$

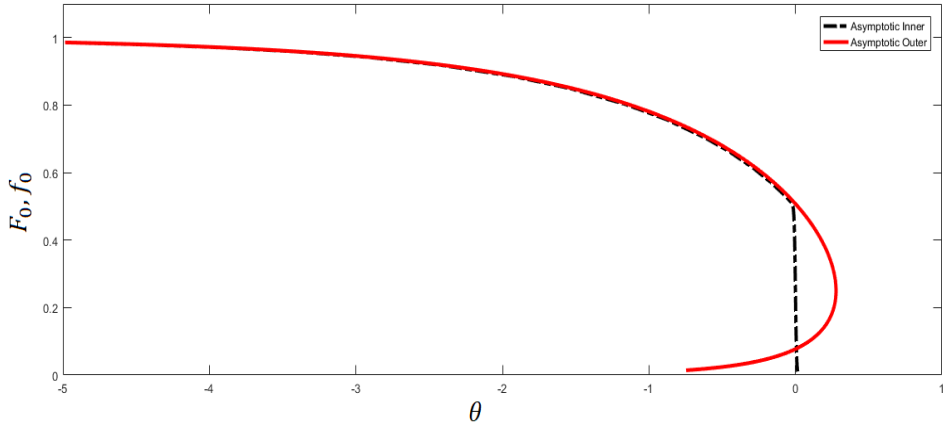

Figure 3.4.5: Asymptotic outer solution (red) and the inserted inner sub-shock (dashed black line) at leading order.

Figure 3.4.26 is an illustration of the partially dispersed shock showing that the outer solution becomes multivalued if defined in $0 < F_0 < 1$. Thus, a sub-shock should be inserted at $1 - \phi$ and the solution (black) becomes single valued.
We next determine $\hat{\theta}_0$, the $O(\epsilon)$ correction to the position of the the inner shock centre. This can be determined by first looking for the $O(\epsilon)$ correction term of the inner expansion then matching the inner to the outer solution. The $O(\epsilon)$ correction to the inner solution, F_{in} is determined by

$$2\,\tau\,\frac{\mathrm{d}^2 f_1}{\mathrm{d}\hat{\theta}^2} - 2\,\tau\,\Big(f_0 - \gamma\Big)\,\frac{\mathrm{d}f_1}{\mathrm{d}\hat{\theta}} - 2\,\Big(\tau\,f_1 + 1\Big)\frac{\mathrm{d}f_0}{\mathrm{d}\hat{\theta}} + \Big(f_0 - 1\Big)\,f_0 = 0.$$

Integrating with respect to $\hat{\theta}$ and using the boundary limit $f_0\,,\, f_1 \to 0$ when $\hat{\theta} \to \infty$ gives

$$\begin{aligned} 2\,\tau\,\frac{\mathrm{d}f_1}{\mathrm{d}\hat{\theta}} - 2\,\tau\big(f_0 - \gamma\big)f_1 &= 2\,f_0 - \int f_0\big(f_0 - 1\big)\;\mathrm{d}\hat{\theta}, \\ \\ \Longrightarrow\; 2\,\tau\,\frac{\mathrm{d}f_1}{\mathrm{d}\hat{\theta}} + 2\,\tau\,\gamma\,\tanh y\,.\,f_1 &= 2\,f_0 - \int f_0\big(f_0 - 1\big)\;\mathrm{d}\hat{\theta}. \end{aligned}$$

Recalling the definition of y in (3.4.25), we will use the scaling $\hat{\theta} = \frac{2}{\gamma}\,y + \hat{\theta}_0$, so $\frac{\mathrm{d}}{\mathrm{d}\hat{\theta}} = \frac{\gamma}{2}\,\frac{\mathrm{d}}{\mathrm{d}y}$. The ODE becomes

$$\tau\,\gamma\,\frac{\mathrm{d}f_1}{\mathrm{d}y} + 2\,\tau\,\gamma\,\tanh y\,.\,f_1 = 2\,f_0 + \frac{2}{\gamma}\int f_0\big(1 - f_0\big)\;\mathrm{d}y. \tag{3.4.28}$$

The integration in the last term can be evaluated as

$$\begin{aligned} \frac{2}{\gamma}\int f_0\big(1 - f_0\big)\;\mathrm{d}y &= 2\int \Big[1 - \tanh y\Big]\,.\,\Big[1 - \gamma\,\big(1 - \tanh y\big)\Big]\;\mathrm{d}y, \\ \\ &= 2\,\gamma\,\tanh y - 2\,\phi\,\ln\big(\cosh y\big) + 2\,\phi\,y + C_1. \end{aligned}$$

The boundary condition $f_0(\infty) = 0$ fixes the integration constant to be $C_1 - 2\,\gamma - 2\,\phi\,\ln 2$. Therefore, equation (3.4.28) can be rewritten as

$$\begin{aligned}\tau\,\gamma\,\frac{\mathrm{d}f_1}{\mathrm{d}y} + 2\,\tau\,\gamma\,\tanh y\,.\,f_1 &= 2\,\gamma\Big(1-\tanh y\Big) - 2\,\gamma\Big(1-\tanh y\Big)\\ &\quad +2\,\phi\Big(y - \ln\big(2\,\cosh y\big)\Big),\end{aligned}$$

which can be rearranged to become

$$\frac{\mathrm{d}f_1}{\mathrm{d}y} + 2\,\tanh y\,.\,f_1 = \frac{2\,\phi}{\tau\,\gamma}\,\Big(y - \ln\big(2\,\cosh y\big)\Big). \tag{3.4.29}$$

Equation (3.4.29) is a first order differential equation and we may use the integrating factor method to solve it. Taking the integrating factor to be $\exp\big(2\int \tanh y\,\mathrm{d}y\big) = \cosh^2 y$, equation (3.4.29) becomes

$$\frac{\mathrm{d}}{\mathrm{d}y}\left(\cosh^2 y\,.\,f_1\right) = \frac{2\,\phi}{\tau\,\gamma}\,\Big(y - \ln\big(2\,\cosh y\big)\Big),$$

integrating with respect to y gives

$$\cosh^2 y\,.\,f_1 = \frac{2\,\phi}{\tau\,\gamma}\int p(y)\,\mathrm{d}y, \tag{3.4.30}$$

where the function $p(y)$ is defined as follows

$$p(y) = \Big(2y - \ln\big(1+\mathrm{e}^{2\,y}\big)\Big)\,\cosh^2 y.$$

For simplicity the integral in equation (3.4.30) is calculated by the Maple program and we arrived at

$$\begin{aligned}\tilde{p}(y) = \int p(y)\;\mathrm{d}y &= \frac{1}{8}\Bigg[4\,y^2 - 2\,y + 2\,\mathrm{diln}\big(1+\mathrm{e}^{2\,y}\big) - \sinh^2 y - \cosh^2 y\\ &\quad + 4\,\sinh y\,\cosh y\Big(2\,y + \frac{1}{2} - \ln\big(1+\mathrm{e}^{2\,y}\big)\Big) + \hat{\theta}_1\Bigg].\end{aligned}$$

Here diln denotes the dilogarithm function, defined in section §2.3.2 by

$$\mathrm{diln}(x) = -\int_1^x \frac{\ln(1-t)}{t}\,\mathrm{d}t.$$

While the integration constant $\hat{\theta}_1$ represents an $O(\epsilon^2)$ correction to the shock location and can be calculated by finding the next term of the inner expansion which we do not wish to consider.

The solution for f_1, the $O(\epsilon)$ correction to the inner solution, can be written as

$$f_1 = \frac{2\,\phi}{\tau\,\gamma}\;\tilde{p}(y)\;\mathrm{sech}^2\,y. \tag{3.4.31}$$

To summarize, we have obtained the solution of the inner sub-shock

$$F_{in}(y) = f_0(y) + \epsilon\, f_1(y) + O(\epsilon^2)$$

where the solution at leading order is given by

$$f_0(y) = \gamma\,\Big(1 - \tanh y\Big), \qquad \text{where} \qquad y = \frac{\gamma}{2}\Big(\hat{\theta} - \hat{\theta}_0\Big).$$

The shock centre is located at $\theta_0 + \epsilon\hat{\theta}_0$ with amplitude $1-\phi$. We also obtained the first correction to this solution

$$\begin{aligned} f_1 \;=\; \frac{\phi}{4\,\tau\,\gamma}\,.\,\Bigg[&\Big(4\,y^2 - 2\,y + 2\,\mathrm{diln}\big(1+\mathrm{e}^{2\,y}\big) + \hat{\theta}_1\Big)\;\mathrm{sech}^2\,y - \tanh^2 y - 1 \\ &+4\;\tanh y\,\Big(2\,y + \frac{1}{2} - \ln\big(1+\mathrm{e}^{2\,y}\big)\Big)\Bigg]. \end{aligned} \tag{3.4.32}$$

We next determine the unknowns $\theta_0\,,\ \hat{\theta}_0\,,$ which fix the position of the inner shock, by matching the inner solution to the outer solution obtained in §3.4.3.

3.4.5 Matching Inner and Outer Expansions of Travelling Wave

When $\phi < 1$ the solution consists of an outer solution which occupies most parts of the domain described in §3.4.3, with an embedded inner solution near $\theta = \theta_0$

described in §3.4.4. We use the matching conditions $\lim_{y\to-\infty} F_{\rm in} = \lim_{\theta\to\theta_0} F_{\rm out}$ to determine the inner shock centre and its $O(\epsilon)$ shift. We recall the inner solution in §3.4.4 is

$$F_{in} = f_0 + \epsilon\, f_1 + O(\epsilon^2),$$

where f_0 and f_1 are determined respectively in equations (3.4.26) and (3.4.32). We derive the $y \to -\infty$ limit of the inner expansion. The $y \to -\infty$ limit of the leading order f_0 is given by

$$\lim_{y\to-\infty} f_0(y) = \lim_{y\to-\infty} \gamma \left(1 - \tanh y\right) = 1 - \phi, \tag{3.4.33}$$

where $y = \frac{\gamma}{2}(\hat{\theta} - \hat{\theta}_0)$. To study the behaviour of the $O(\epsilon)$ correction to the inner solution f_1 when $y \to -\infty$ we notice that

$$\lim_{y\to-\infty} \operatorname{sech}^2 y = 4\,\mathrm{e}^{2\,y}.$$

From equation (3.4.32) we express the behaviour of f_1 as $y \to -\infty$ as follows

$$\begin{aligned}\lim_{y\to-\infty} f_1 \;&=\; \frac{\phi}{4\,\tau\,\gamma}\cdot\Bigg[4\,\mathrm{e}^{2\,y}\Big(4\,y^2 - 2\,y + 2\,\mathrm{diln}\big(1+\mathrm{e}^{2\,y}\big) + \hat{\theta}_1\Big) - 1 - 1 \\ &\qquad - 4\left(2\,y + \frac{1}{2} - \ln\left(1+\mathrm{e}^{2\,y}\right)\right)\Bigg].\end{aligned} \tag{3.4.34}$$

Here the term $(4\,y^2 - 2\,y)\mathrm{e}^{2y} \to 0$ as $y \to -\infty$. The functions $\mathrm{diln}(1+\mathrm{e}^{2\,y})$ and $\ln(1+\mathrm{e}^{2\,y})$ also will vanish when $y \to -\infty$. Therefore, the first correction f_1 is asymptotically

$$f_1(y) \;\sim\; -\frac{\phi}{\tau\,\gamma}\Big(2\,y+1\Big) \qquad\qquad \text{as} \quad y \to -\infty. \tag{3.4.35}$$

Therefore, the $y \to -\infty$ limit of the inner solution is derived as

$$\begin{aligned}\lim_{y\to-\infty} F_{in} \;&=\; \lim_{y\to-\infty}\big(f_0 + \epsilon\, f_1\big) \\ &=\; (1-\phi) - \epsilon\,\frac{\phi}{\tau\,\gamma}\Big(2\,y+1\Big).\end{aligned}$$

In terms of the outer variable θ where $y = \frac{\gamma}{2\epsilon}(\theta - \theta_0 - \epsilon\,\hat{\theta}_0)$ this limit is

$$\lim_{\hat{\theta}\to-\infty} F_{in} = (1-\phi) - \frac{\phi}{\tau}\,\theta + \frac{\phi}{\tau}\,\theta_0 + \frac{\epsilon\,\phi}{\tau}\left(\hat{\theta}_0 - \frac{1}{\gamma}\right). \tag{3.4.36}$$

We next look at the outer solution near the inner region near $\theta = \theta_0$. We recall the outer solution we deduced in §3.4.3

$$F_{out} = F_0 + \epsilon\,F_1 + O(\epsilon^2),$$

where F_0 is expressed implicitly

$$\exp\left[\frac{\theta-\theta_0}{\tau}\right] = \left(\frac{1-F_0}{\phi}\right)^{1+\phi}\left(\frac{F_0}{1-\phi}\right)^{1-\phi}, \qquad 1-\phi < F_0 < 1,$$

and the $O(\epsilon)$ correction is given in terms of F_0 by

$$F_1 = \frac{4\,\phi}{\phi^2-1}\left(F_0\right)_\theta\left[\gamma\,\ln\left(\frac{1-F_0}{F_0}\right) + \ln\left(\frac{F_0}{|F_0-\gamma|}\right) - \frac{1-\phi^2}{4\,\phi(F_0-\gamma)}\right].$$

We obtain the $\theta \to \theta_0$ limit of the outer solution by using Taylor expansions to obtain

$$\begin{aligned}\lim_{\theta\to\theta_0} F_{out} &= \lim_{\theta\to\theta_0}\left[F_0 + \big(\theta-\theta_0\big).\Big(F_0\Big)_\theta + \epsilon\,F_1 + O\Big(\epsilon\,(\theta-\theta_0), (\theta-\theta_0)^2\Big)\right] \\ &= (1-\phi) - \frac{\phi}{\tau}\Big(\theta-\theta_0\Big) \\ &\quad + \epsilon\left[\frac{4\,\phi^2}{\tau\,(1-\phi^2)}.\left(\gamma\,\ln\Big(\frac{\phi}{1-\phi}\Big) + \ln 2 - \frac{1+\phi}{2\,\phi}\right)\right]. \end{aligned} \tag{3.4.37}$$

We see that the first two terms of (3.4.36) and (3.4.37) match automatically. For the $O(\epsilon)$ terms, we see that

$$\frac{4\,\phi^2}{\tau\,(1-\phi^2)}\,\frac{1+\phi}{2\,\phi} = \frac{\epsilon\,\phi}{\tau\,\gamma},$$

then the $O(\epsilon)$ terms match as long as

$$\hat{\theta}_0 = \frac{4\,\phi}{1-\phi^2}\cdot\left(\gamma\ \ln\left(\frac{\phi}{1-\phi}\right)+\ln 2\right). \tag{3.4.38}$$

Composite Solution when $0<\phi<1$

The outer and inner expansions in the partially dispersed shock will overlap in an intermediate region. In this intermediate region $\lim_{y\to-\infty} F_{\text{in}} = \lim_{\theta\to\theta_0} F_{\text{out}}$. A uniformly composite, approximation to $F = F(\theta;\epsilon)$ can be constructed in the form

$$F_{\text{comp}} = \begin{cases} F_{\text{in}} + F_{\text{out}} - F_{\text{inter}}, & \theta < \theta_0 \\ F_{\text{in}}, & \theta \geq \theta_0, \end{cases}$$

where F_{out} and F_{in} are the expansions expressed in equations (3.4.13) and (3.4.26) in terms of θ and $F_{\text{inter}} = 2\,\gamma = 1-\phi\,.$

Figure 3.4.6 shows the continuous composite solutions for the partially dispersed wave plotted for various values of $\phi = 0.2,\ 0.5,\ 0.8$. This solution is a combination of the inner and outer solutions with discarding the overlap region. The asymptotic waveform begins with a very thin thermoviscous sub-shock in which the velocity amplitude is adjusted to $1-\phi\,.$ Followed by region in which the wave is dispersed by the relaxation mechanism. We see that the relaxation process has relatively little effect on the transition when for example $\phi = 0.2$.

3.4.6 Wave Maximum Negative Slope

In capturing the shock wave features, we are interested in looking for the magnitude of the shock and the width. Previously, in studying shocks that are solely controlled by the thermoviscous effects we were able to determine shock width by looking at the x coordinate range where the solution changes from 90% of its amplitude to 10% of its amplitude. However, when considering the

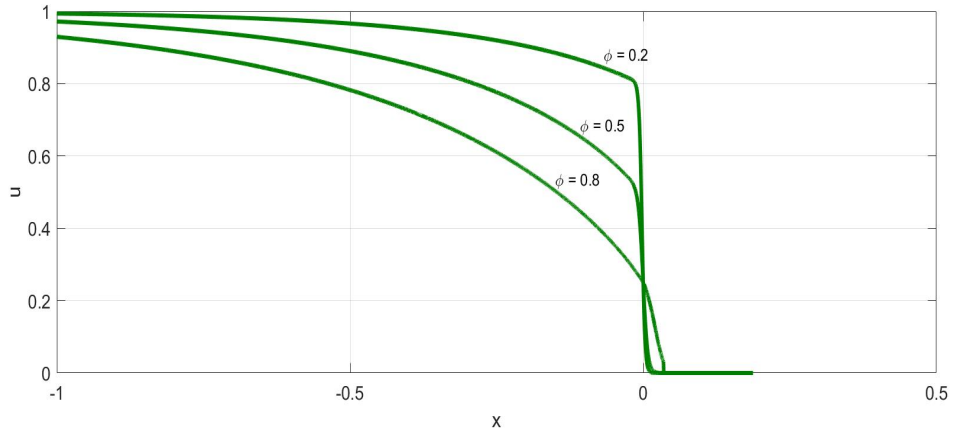

Figure 3.4.6: Partially dispersed travelling wave asymptotic composite solutions for various $\phi = 0.2,\ 0.5,\ 0.8$.

relaxation processes effects on wave propagation, the width of the whole waveform is complicated to study, especially in the partially dispersed case. In general, the shock amplitude will decrease after a certain time and so the molecular concentration parameter Δc, changes through time. Consequently, due to these changes the waveform will reach a point in which it converts from partially dispersed to a fully dispersed wave. Therefore, the wave maximum negative slope (MNS), which looks for the steepest point in the whole waveform is then an easier and practical alternative to describe the key features of the shock. A comparison between asymptotic travelling wave results and the augmented Burgers numerical results using Fourier Pseudospectral methods, will be presented in §3.5.2.

Maximum Negative Slope: $\phi > 1$

We first investigate the case when $\phi > 1$. The outer solution is

$$F_{out} = F_0 + \epsilon F_1.$$

Therefore, the slope can be defined as

$$\begin{aligned} S_{\text{out}} &= \frac{\mathrm{d}F}{\mathrm{d}\theta} \\ &= \frac{\mathrm{d}F_0}{\mathrm{d}\theta} + \epsilon\,\frac{\mathrm{d}F_1}{\mathrm{d}\theta} \\ &= \frac{\mathrm{d}F_0}{\mathrm{d}\theta} + \epsilon\,\frac{\mathrm{d}F_1}{\mathrm{d}F_0}\cdot\frac{\mathrm{d}F_0}{\mathrm{d}\theta} \\ &= \frac{\mathrm{d}F_0}{\mathrm{d}\theta}\left(1+\epsilon\frac{\mathrm{d}F_1}{\mathrm{d}F_0}\right) = S_0 + \epsilon\, S_1. \end{aligned}$$

If we supposed the outer solution reaches its maximum slope at $F_{out} = F_s + \epsilon\, G$, then the maximum negative slope (MNS) can be defined in the form

$$S_{\text{out}}\big(F_s+\epsilon G\big) = S_0\big(F_s+\epsilon G\big) + \epsilon S_1\big(F_s\big) + O(\epsilon^2). \tag{3.4.39}$$

Using Taylor expansion to express MNS yields

$$\max\Big(S_{\text{out}}\Big) = S_0\big(F_s\big) + \epsilon\Big[S_1\big(F_s\big) + G\,S_0'\big(F_s\big)\Big] + O(\epsilon^2). \tag{3.4.40}$$

First, we locate F_s by simply using the usual method to locate any extrema point, which is by differentiating the slope S_0 with respect to F_0 and looking for the roots of the equation $\frac{\mathrm{d}S_0}{\mathrm{d}F_0} = 0$. So, to define the negative slope S_0, let us recall the derivative of the leading order of outer solution which is given in equation (3.4.17) as

$$S_0 = \big(F_0\big)_\theta = \frac{F_0\big(F_0-1\big)}{2\,\tau\big(F_0-\gamma\big)}.$$

Thus, differentiating the slope S_0 with respect to F_0 gives

$$S_0' = \frac{F_0^2 - \gamma\big(2\,F_0-1\big)}{2\,\tau\,\big(\gamma-F_0\big)^2}, \tag{3.4.41}$$

where $'$ denotes the derivative with respect to F_0. Equating equation (3.4.41) to zero results the next two different roots

$$\frac{1}{2}\Big(1-\phi-\sqrt{\phi^2-1}\Big), \qquad \frac{1}{2}\Big(1-\phi+\sqrt{\phi^2-1}\Big).$$

However, since the wave transition is between $0 < F_s < 1$, looking at the first root as $\phi > 1$ and using the definition $\gamma = \frac{1-\phi}{2} < 0$, we find

$$\gamma < 0 \implies \gamma^2 - \gamma > \gamma^2 \implies \gamma - \sqrt{\gamma^2 - \gamma} < 0 \implies \frac{1}{2}\big(1 - \phi - \sqrt{\phi^2 - 1}\big) < 0.$$

Thus, we select F_s to be $F_s = \frac{1}{2}\big(1 - \phi + \sqrt{\phi^2 - 1}\big)$ and so the minimum value of the S_0 which is the leading order term of (3.4.40) is written in the form

$$S_0\big(F_s\big) = -\frac{1}{2\,\tau}\,\big(\phi - \sqrt{\phi^2 - 1}\big). \tag{3.4.42}$$

Next we compute $O(\epsilon)$ correction term $S_1(F_s)$, but notice that S_1 is defined as $S_1 = S_0 \,.\, \frac{\mathrm{d}F_1}{\mathrm{d}F_0}$, where F_1 is the $O(\epsilon)$ correction term of the outer solution given in equation (3.4.20) as

$$F_1 = A \,.\, S_0\big(F_0\big) \,.\, K\big(F_0\big), \tag{3.4.43}$$

where the constant A is $\frac{2\,\phi}{\phi^2 - 1}$ and the function K is defined by

$$K(F_0) = \left[\gamma \,\ln\left(\frac{1 - F_0}{F_0}\right) + \ln\left(\frac{F_0}{F_0 - \gamma}\right) + \frac{\phi^2 - 1}{4\,\phi(F_0 - \gamma)}\right].$$

For a simpler computations of S_1 we write the function S_1 in terms of S_0 and F_1 in (3.4.43) to have

$$S_1 = S_0 \,.\, \frac{\mathrm{d}F_1}{\mathrm{d}F_0} = A\,\Big(S_0\,S_0'\,K + S_0^2\,K'\Big).$$

Inserting $S_0(F_s)$ and $S_1(F_s)$ in (3.4.40) with the use of $S_0'(F_s) = 0$, thus, the expression (3.4.40) for the maximum negative slope reduces to

$$\max\Big(S_{\mathrm{out}}\Big) = S_0\big(F_s\big)\Big[1 + \epsilon\,A\,S_0\big(F_s\big)\,K'\big(F_s\big)\Big]. \tag{3.4.44}$$

To evaluate this, we only need to look for the first derivative of K at F_s which is

$$\begin{aligned} K'\Big|_{F_0=Fs} &= \frac{\Big(F\big(F-2\gamma\big)-\gamma\,\phi\Big)\,\Big(\gamma^2-\gamma\Big)}{\phi\,F\big(1-F\big)\big(F-\gamma\big)^2}\Big|_{F_0=Fs} \\ &= \frac{1}{2}\,\frac{\phi^2-1}{\phi\,F_s\big(1-F_s\big)}. \end{aligned}$$

Hence, the the second term $A\,S_0\,K'$ in (3.4.44) is

$$\begin{aligned} A\,S_0\big(F_s\big)\,K'\big(F_s\big) &= \frac{4\,\phi}{\phi^2-1}\cdot\frac{-F_s\big(1-F_s\big)}{2\tau\big(F_s-\gamma\big)}\cdot\frac{\phi^2-1}{2\phi\,F_s\big(1-F_s\big)} \\ &= -\frac{1}{\tau\,\big(F_s-\gamma\big)} = -\frac{2}{\tau\,\sqrt{\phi^2-1}}. \end{aligned}$$

Inserting S_0 and $A\,S_0\,K'$ in equation (3.4.44) we obtain the MNS for $\phi>1$

$$\max\Big(S_{\text{out}}\Big) = -\frac{1}{2\,\tau}\,\big(\phi-\sqrt{\phi^2-1}\big)\,\left[1-\epsilon\,\frac{2}{\tau\,\sqrt{\phi^2-1}}\right]. \tag{3.4.45}$$

This maximum negative slope is derived for the specific case of unit amplitude. If we define $\max\Big(S_{\text{out}}\Big)$ for a general dimensionless amplitude U_m, we expect the asymptotic maximum slope to be

$$\max\Big(S_{\text{out}}\Big) = -\frac{1}{2\,\tau}\,\big(\phi-\sqrt{\phi^2-U_m^2}\big)\,\left[1-\epsilon\,\frac{2}{\tau\,\sqrt{\phi^2-U_m^2}}\right].$$

Multiplying the above equation with U_m yields

$$\begin{aligned} \max\Big(S_{\text{out}}\Big) &= -\frac{U_m}{U_m}\,\frac{1}{2\,\tau}\,\Big(\phi-\sqrt{\phi^2-U_m^2}\Big)\,\left[1-\epsilon\,\frac{2}{\tau\,\sqrt{\phi^2-U_m^2}}\right] \\ &= -\frac{U_m}{2\,\tau}\,\Big(\frac{\phi}{U_m}-\sqrt{\phi^2/U_m^2-1}\Big)\,\left[1-\frac{\epsilon}{U_m}\,\frac{2}{\tau\,\sqrt{\phi^2/U_m^2-1}}\right]. \end{aligned}$$

Defining $\widehat{\epsilon}=\frac{\epsilon}{U_m}$ and $\widehat{\phi}=\frac{\phi}{U_m}$ as the effective viscous and relaxation absorption parameters, and hence, for a general amplitude U_m the asymptotic MNS for

$\phi > U_m$ is

$$\max\Big(S_{\text{out}}\Big) = -\frac{U_m}{2\,\tau}\left(\widehat{\phi} - \sqrt{\widehat{\phi}^2 - 1}\right)\left[1 - \widehat{\epsilon}\,\frac{2}{\tau\sqrt{\widehat{\phi}^2 - 1}}\right]. \tag{3.4.46}$$

Maximum Negative Slope: $\phi < 1$

We now look in the case when $0 < \phi < 1$, where the maximum negative slope occurs in the inner region $F_{\text{in}} = f_0(y) + \epsilon f_1(y)$ where f_0 and f_1 are expressed in (3.4.26) and (3.4.32) respectively. From 3.4.26) we see that at leading order $\max(S_{\text{in}}) \approx \gamma$ with the maximum negative slope occurring at $y = 0$. Approximating f_0 and f_1 for $|y| \ll 1$, deduces

$$\begin{aligned} F_{\text{in}} \;\sim\; \gamma\left(1 - y + \frac{y^3}{3}\right) + \epsilon\,\frac{\phi}{\gamma\,\tau}\Bigg[&-\frac{1}{24}\Big(\pi^2 + 6 - 6\hat{\theta}_1\Big) - 2y\,\ln 2 \\ &+\frac{1}{24}\Big(\pi^2 + 30 - 6\hat{\theta}_1\Big)\,y^2 - \frac{1}{3}\Big(1 - 2\ln 2\Big)\,y^3\Bigg]. \end{aligned} \tag{3.4.47}$$

The maximum negative slope occurs close to $y = 0$ when

$$\begin{aligned} S_{\text{in}} = \big(F_{\text{in}}\big)_y \;\sim\; \gamma\Big(-1 + y^2\Big) + \epsilon\,\frac{\phi}{\gamma\,\tau}\Bigg[&-2\ln 2 + \frac{1}{12}\Big(\pi^2 + 30 - 6\hat{\theta}_1\Big)\,y \\ &-\Big(1 - 4\ln 2\Big)\,y^2\Bigg] + O(\epsilon^2). \end{aligned}$$

S_{in} is minimum when $y = y_m$. To locate y_m we look for the derivative of S_{in} with respect to y and equate it to zero to have

$$0 = \big(S_{\text{in}}\big)_y \sim 2\gamma\,y + \epsilon\,\frac{\phi}{\gamma\,\tau}\left[\frac{1}{12}\Big(\pi^2 + 30 - 6\hat{\theta}_1\Big) - 2\Big(1 - 4\ln 2\Big)\,y\right] + O(\epsilon^2).$$

Hence, solving the equation for y_m to obtain

$$y_m = -\frac{\epsilon\,\phi}{24\,\gamma^2\,\tau}\Big(\pi^2 + 30 - 6\hat{\theta}_1\Big) + O(\epsilon^2). \tag{3.4.48}$$

In terms of the outer variable θ, we use the definition of y defined in (3.4.25), to express the outer variable as

$$\theta = \theta_0 + \epsilon\,\hat{\theta} = \theta_0 + \frac{2\,\epsilon}{\gamma}\,y + \epsilon\,\hat{\theta}_0.$$

The asymptotic prediction of the negative maximum slope when $\phi < 1$ is

$$\max\big(S_{\rm in}\big) = -\frac{\gamma^2}{2\epsilon}\bigg(1 + \epsilon\,\frac{2\,\phi\,\ln 2}{\gamma^2\,\tau}\bigg) + O(\epsilon^2). \tag{3.4.49}$$

Similar to the $\phi > 1$ case, we will produce a formula for the $\max\big(S_{\rm in}\big)$ with the amplitude U_m, by multiplying equation (3.4.49) with U_m^2 to have

$$\begin{aligned}\max\Big(S_{\rm in}\Big) &= -\frac{U_m^2}{U_m^2}\cdot\frac{\gamma^2}{2\epsilon}\bigg(1 + \epsilon\,\frac{2\,\phi\,\ln 2}{\gamma^2\,\tau}\bigg) + O(\epsilon^2)\\ &= -U_m\,\frac{\gamma^2/U_m^2}{2\epsilon/U_m}\bigg(1 + \big(\epsilon/U_m\big)\,\frac{2\,\big(\phi/U_m\big)\,\ln 2}{\tau\,\big(\gamma^2/U^2{}_m\big)}\bigg) + O(\epsilon^2),\end{aligned}$$

here $\widehat{\gamma} = \frac{\gamma}{U_m} = \frac{1}{2\,U_m}\big(U_m - \phi\big) = \frac{1}{2}\big(1 - \widehat{\phi}\big)$, by inserting the parameters $\widehat{\epsilon}$, $\widehat{\phi}$ and $\widehat{\gamma}$ in the definition for $\max\Big(S_{\rm Inn}\Big)$ yields

$$\max\Big(S_{\rm in}\Big) = -\frac{U_m\,\widehat{\gamma}^2}{2\widehat{\epsilon}}\bigg(1 + \widehat{\epsilon}\,\frac{2\,\widehat{\phi}\,\ln 2}{\widehat{\gamma}^2\,\tau}\bigg) + O(\epsilon^2) \tag{3.4.50}$$

and its position is

$$\theta_0 + \widehat{\epsilon}\,\widehat{\theta}_0 - \widehat{\epsilon}^2\,\frac{\widehat{\phi}}{12\,\widehat{\gamma}^3\,\tau}\,\Big(\pi^2 + 30 - 6\hat{\theta}_1\Big). \tag{3.4.51}$$

This ends the discussion of travelling wave asymptotic solutions and next we consider the travelling wave numerical solutions.

3.4.7 Numerical Solutions of Travelling Wave

The asymptotic solutions derived in §3.4.2 can be verified by comparisons with numerical solutions of the travelling wave. This section is followed by a subsequent explanations in appendix A using phase portraits of the travelling wave numerical solution. We now follow the numerical method proposed by Pierce and Kang [73] to look for a numerical solution of the second order ODE

$$2\,\tau\,\epsilon\,F_{\theta\,\theta} - 2\left(\tau\left(F-\gamma\right)+\epsilon\right)F_{\theta} + \left(F-1\right)F = 0, \qquad \gamma = \frac{1}{2}(1-\phi). \quad (3.4.52)$$

Equation (3.4.52) requires two initial conditions at one end of the spatial range. Thus, for $\theta \to -\infty$, $F \to 1$, then we assume that close to $\theta = 0$ the solution to (3.4.52) takes the form

$$F = 1 - \delta\,\mathrm{e}^{\lambda\,\theta}, \qquad 0 < \delta \ll 1, \qquad \lambda > 0. \quad (3.4.53)$$

Hence, the two initial conditions are

$$F(0) = 1-\delta \qquad \left(F\right)_{\theta}(0) = -\delta\;\lambda. \quad (3.4.54)$$

We look for the eigenvalues $\lambda_{1,2}$ by substituting the first and second derivatives of F, $\left(F\right)_{\theta} = -\lambda\,\delta\,\mathrm{e}^{\lambda\,\theta}$ and $\left(F\right)_{\theta\,\theta} = -\lambda^2\,\delta\,\mathrm{e}^{\lambda\,\theta}$ in equation (3.4.52) to obtain

$$2\,\tau\,\epsilon\,\lambda^2 - 2\left(\tau\left(1-\delta\,\mathrm{e}^{\lambda\,\theta}-\gamma\right)+\epsilon\right)\lambda + \left(1-\delta\,\mathrm{e}^{\lambda\,\theta}\right) = 0.$$

Taking the limit when $\theta \to -\infty$ or equivalently $\delta \to 0$ yields

$$2\,\tau\,\epsilon\,\lambda^2 - 2\left(\tau\left(1-\gamma\right)+\epsilon\right)\lambda + 1 = 0. \quad (3.4.55)$$

This quadratic equation has two solutions for λ. The eigenvalues λ_1 and λ_2 are

$$\lambda_{1,2} = \frac{1}{2\,\tau\,\epsilon}\left(\tau\left(1-\gamma\right)+\;\epsilon\;\mp\;\sqrt{\left(\tau\left(1-\gamma\right)+\;\epsilon\right)^2 - 2\,\tau\,\epsilon}\;\right). \quad (3.4.56)$$

We notice that the eigenvalues are distinct real positive roots, because the discriminant is positive:

$$\big(\tau\,(1-\gamma)+\,\epsilon\big)^2-2\,\tau\epsilon\sim\,-2\epsilon\,\tau\,\gamma+\tau^2\,(1-\gamma)^2>0,\qquad\qquad \epsilon\ll\tau.$$

Thus, the second initial condition $\big(F\big)_\theta(0)\,=\,-\delta\,\lambda_{1,2}$ cannot be determined uniquely for $\theta\,\rightarrow\,-\infty$. Consequently, we cannot march θ in the positive direction from a large negative θ.

Alternatively we look at the solution for $\theta\,\gg\,1$ when F approaches 0 and then march θ in the negative direction of θ. This is simplified by setting $X\,=\,-\theta$ and $F\,=\,F^-$, so the boundary conditions become $F^-\,\rightarrow\,0$ as $X\rightarrow-\infty$ and $F^-\rightarrow1$ when $X\rightarrow\infty$ and the travelling wave becomes

$$2\,\tau\,\epsilon\big(F^-\big)_{XX}+2\,\Big(\tau\,(F^--\gamma)+\epsilon\Big)\big(F^-\big)_X-\Big(1-F^-\Big)\,F^-=0. \tag{3.4.57}$$

Following the same steps of the method described above by assuming the solution to be

$$F^-=\delta\,\mathrm{e}^{\mu\,X}, \tag{3.4.58}$$

with the initial values

$$F^-(0)=\delta\qquad\qquad\big(F^-\big)_X(0)=\delta\;\mu. \tag{3.4.59}$$

The first and second derivatives are $\big(F^-\big)_X\;=\;\mu\,\delta\,\mathrm{e}^{\mu\,X}$ and $F\big(F^-\big)_{XX}\;=\;\mu^2\,\delta\,\mathrm{e}^{\mu\,X}$. Inserting the derivatives in (3.4.57) with the limit $X\rightarrow\infty$ taken, we obtain the quadratic equation for μ

$$2\,\tau\,\epsilon\,\mu^2-\,2\,\big(\tau\,\gamma-\,\epsilon\big)\,\mu-1=0. \tag{3.4.60}$$

The eigenvalues $\mu_{1,2}$ are

$$\mu_{1,2}=\frac{1}{2\,\tau\,\epsilon}\,\Big(\tau\,\gamma-\,\epsilon\mp\sqrt{(\tau\,\gamma-\,\epsilon)^2+2\,\tau\,\epsilon}\;\Big). \tag{3.4.61}$$

In this case we can see that the discriminant is positive and $a\,c < 0,$ which means that only one of the real distinct roots is positive, and so we have a unique choice of positive eigenvalues. Thus, the initial conditions becomes

$$F^{-}(0) = \delta, \qquad \left(F^{-}\right)_{X}(0) = \delta\,.\,\mu_2. \tag{3.4.62}$$

where μ_2 is

$$\mu_2 = \frac{\tau\,\gamma - \epsilon + \sqrt{(\tau\,\gamma - \epsilon)^2 + 2\,\tau\,\epsilon}}{2\,\tau\,\epsilon}, \tag{3.4.63}$$

and $\left(F^{-}\right)_{X}(0)$ is defined uniquely.

We use the fourth-order Runge-Kutta method to march θ in the negative direction, from $\theta = \theta_0 = 0\,.$ Since the vast majority of numerical algorithms are designed for first order ODE systems, to numerically integrate the second order equation we must reduce it to an equivalent first-order system

$$T_1 = \frac{\mathrm{d}F^{-}}{\mathrm{d}X} \qquad T_2 = \frac{1}{2\,\tau\,\epsilon}\left[\left(1 - F^{-}\right)F^{-} - 2\left(\tau\,(F^{-} - \gamma) + \epsilon\right)T_1\right].$$

To forward the system in X where $X = -\theta,$ we use the MATLAB build-in algorithm ODE23bt, fixing only the two end points of the interval $[0, X_{\mathrm{end}}]$ with the default relative and absolute error tolerances. This numerical method is valid for n relaxation modes where $n \geq 1.$ In appendix A we use the phase portraits to show the instability of the travelling wave numerical solution when it is marched forward from the limit $F \to 1$ as $\theta \to -\infty,$ and the stability of the solution if it is marched backward from the other end $F \to 1$ as $\theta \to -\infty,$.

Figure 3.4.7 (a) is an illustration of the numerical solution of the travelling wave given in (3.4.57) for the initial condition $F^{-} = \delta \exp[-\mu\,\theta]$ plotted in terms of X where $X = -\theta$ defined for the range $[0, X_{\mathrm{end}}]$. Here F^{-} approaches 0 as θ decreases therefore, we set $\delta = 0.01,$ while viscosity is fixed at $\epsilon = 0.001$ and $\phi = 0.5\,.$ For this value of ϕ the shock is expected to be partially dispersed. In figure 3.4.7 (b) we take a close-up view showing the inner viscous sub-shock and

its amplitude which is at $1 - \phi = 0.5$.

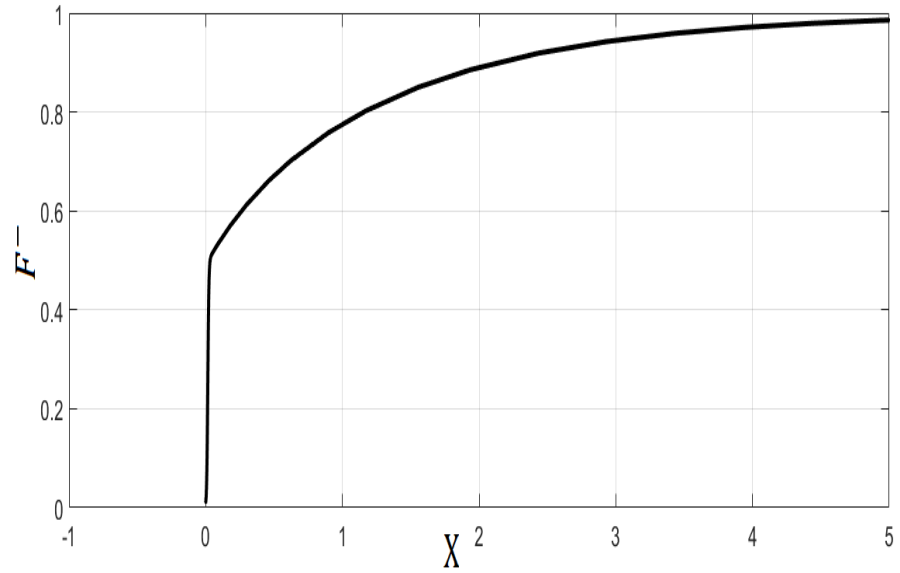

(a) Full view of the partially dispersed wave

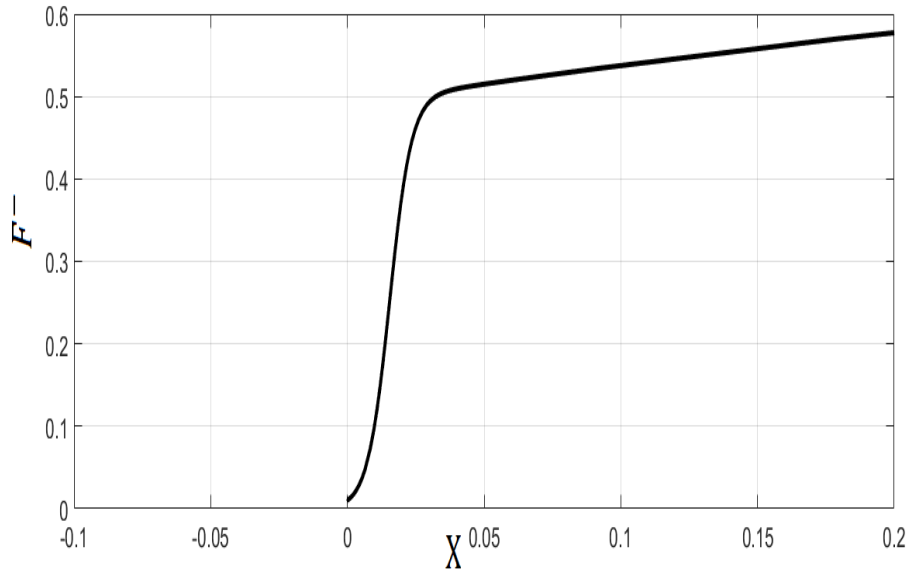

(b) Close-up view of the viscous sub-shock

Figure 3.4.7: Numerical solution of the partially dispersed travelling Wave Equation in (a). Plot (b) is a close-up of the viscous sub-shock

3.4.8 Comparisons of Asymptotic and Numerical Solutions of the Travelling Wave

We present comparison plots of the previously described numerical method to solve the travelling wave and the asymptotic solutions derived in §3.4.2. The asymptotic analysis predicted two cases of wave formation. First case where the waveform consists of one whole region dominated by the relaxation parameters with width $O(\tau)$. Second case which is more complicated in the waveform that consists of two regions. An outer region is governed by the relaxation parameters and has width $O(\tau)$. In addition there is an inner sub-shock controlled by the small viscous parameter of width $(\epsilon/1-\phi)$.

Figure 3.4.8 shows the first case of a wave form for two values of ϕ, $\phi = 2$ in plot(a) and $\phi = 4$ in plot (b). The blue line is the numerical solution and the red-dashed line is the asymptotic solution given by

$$\exp\Big(\frac{\theta-\theta_0}{\tau}\Big) = \Big(1-F\Big)^{1+\phi}\ \Big(F\Big)^{1-\phi}, \qquad \phi = 2\Delta, \tag{3.4.64}$$

which corresponds to the fully dispersed wave. To allow comparison of the numerical and asymptotic solutions, the numerical solution is shifted so that the MNS occurs at $X = 0$ and the asymptotic solution is shifted so that the solution $F(\theta)$ agrees with numerics at $\theta = 0$. After this shift is made we see a good agreement between the two solutions.

Figures 3.4.9 and 3.4.10 show a partially dispersed shock with the plot of the two asymptotic solutions. The blue dashed line marks the outer asymptotic expansion

$$F_{\text{out}} = F_0 + \epsilon\, F_1,$$

where F_0 is expressed implicitly in (3.4.64), and F_1 is defined in (3.4.20). The green dashed line is the inner solution

$$F_{\text{in}} = f_0 + \epsilon\, f_1,$$

where the leading order is the viscous Taylor shock:

$$f_0 = \frac{1}{2}(1-\phi)\left[1 - \tanh\Big(\frac{1-\phi}{4\epsilon}\Big(\theta - \frac{4\,\phi\,\epsilon}{1-\phi^2}\,.\,\big(\gamma\ \ln\big(\frac{\phi}{1-\phi}\big) + \ln 2\big)\Big)\Big)\right]$$

and the correction term f_1 is defined in (3.4.32).

The two solutions are compared to the numerical travelling wave solution (red solid line). In this solution the region governing the transition from 1 to $1-\phi$ can be compared to the outer asymptotic solution. While the region in the wave from $1-\phi$ to 0 is compared with the inner solution. The numerical results is shifted so that $F_N(0) = \gamma$ where $\gamma = \frac{1}{2}(1-\phi)$ and the same shift is made for the asymptotic inner solution so that $F(0) = \gamma$. In each figure, plot (a) shows a full view of the whole wave while plot (b) is close-up view of the inner sub-shock to show the correspondence. These figures are plotted for fixed $\tau = 0.25$ and $\phi = 0.5$ and two values of $\epsilon = 0.01, 0.005$. The decrease in viscosity value results a better agreement in the viscous sub-shock.

Figure 3.4.11 is an illustration of the importance of the $O(\epsilon)$ correction terms obtained in the asymptotic expansions. We can see the better agreement between the numerical and the two-term asymptotic inner solution $f_0 + \epsilon f_1$ (green dashed line) compared to the one-term solution f_0 (black dashed line), in particular the area where the inner and outer expansions meet see figure 3.4.11 (b).

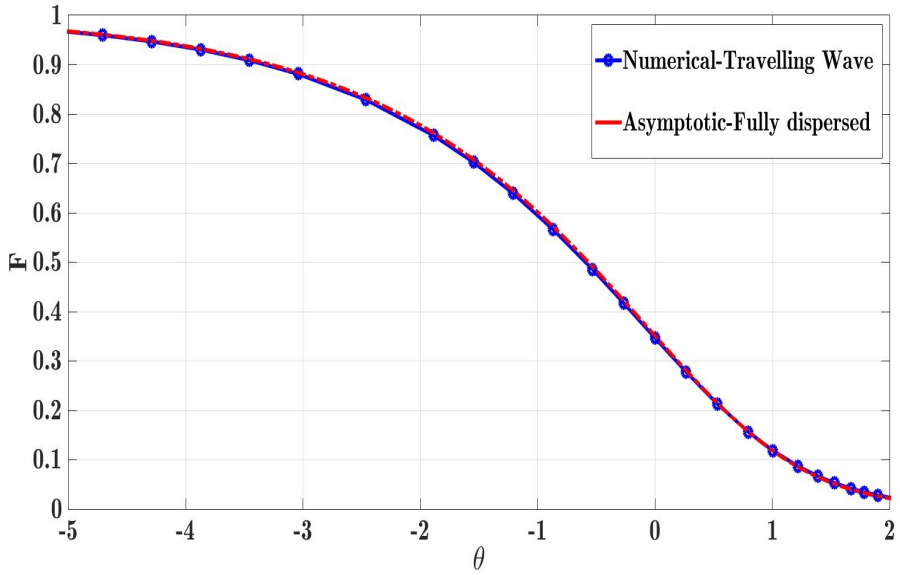

(a) $\phi = 2 \quad \tau = 0.5$

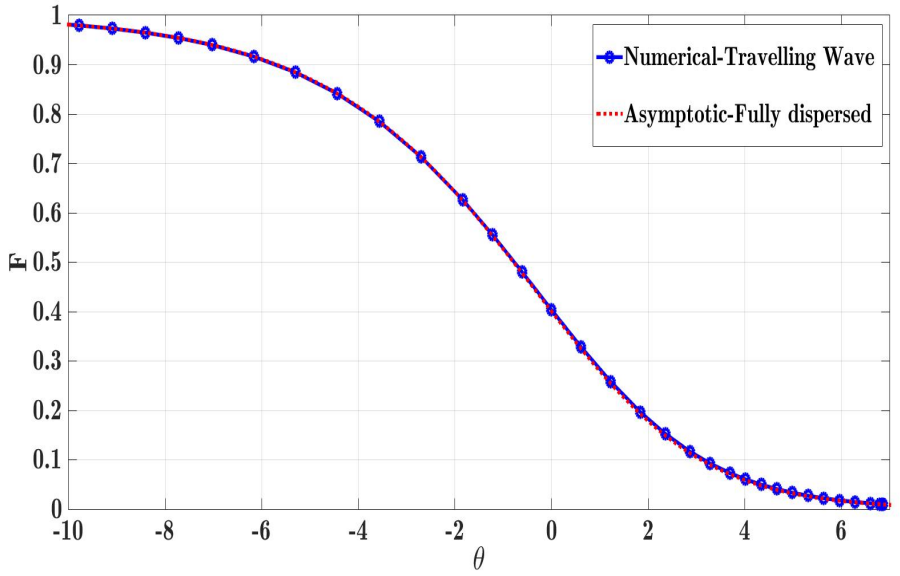

(b) $\phi = 4 \quad \tau = 0.5$

Figure 3.4.8: Comparison of the travelling wave Asymptotic and Numerical solutions when the wave is fully dispersed for the two values $\phi = 2, 4$ and the relaxation time is fixed at $\tau = 0.5$.

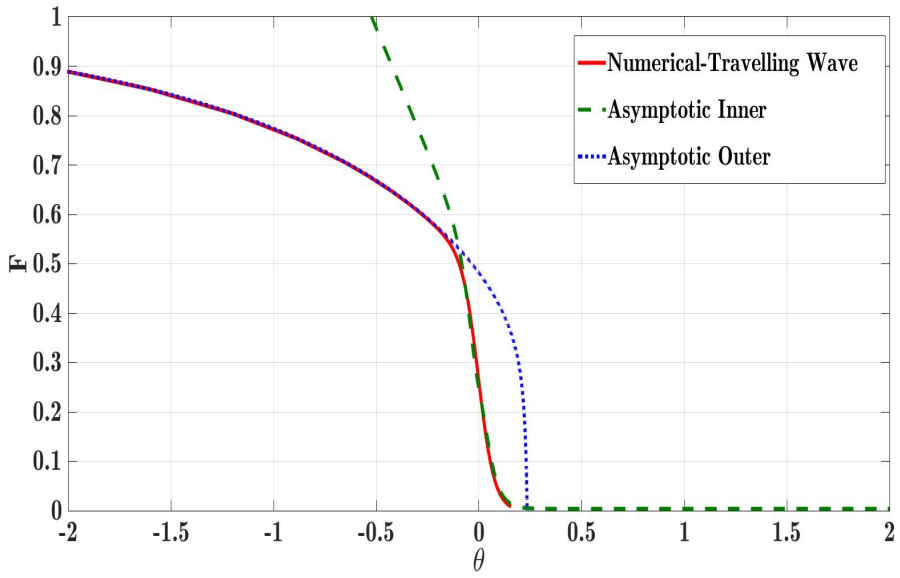

(a) Full view of partially dispersed shock $\epsilon = 0.01$

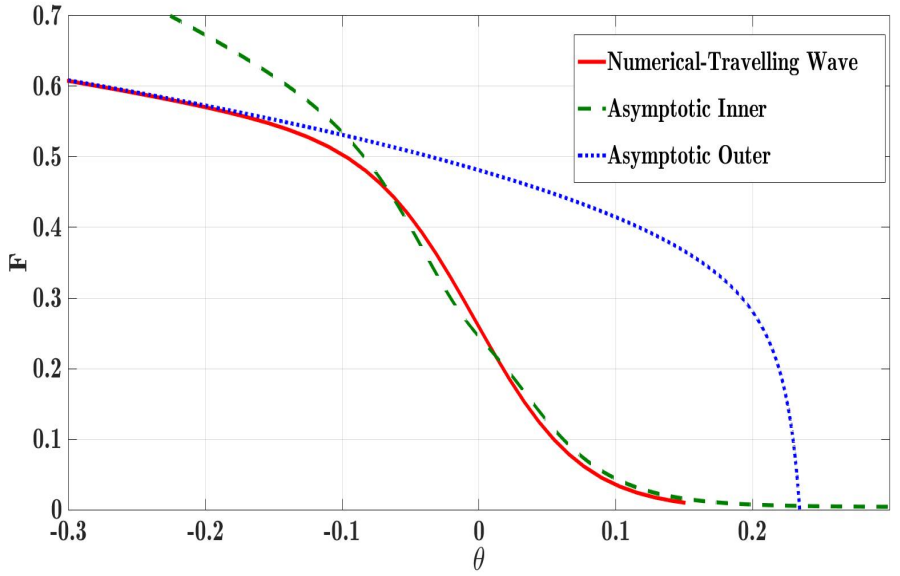

(b) blow up of the inner sub-shock

Figure 3.4.9: Comparison of the travelling wave Asymptotic and Numerical solutions when the wave is partially dispersed for viscosity $\epsilon = 0.01$ and relaxation parameters $\phi = 0.5\,,\ \tau = 0.25\,.$

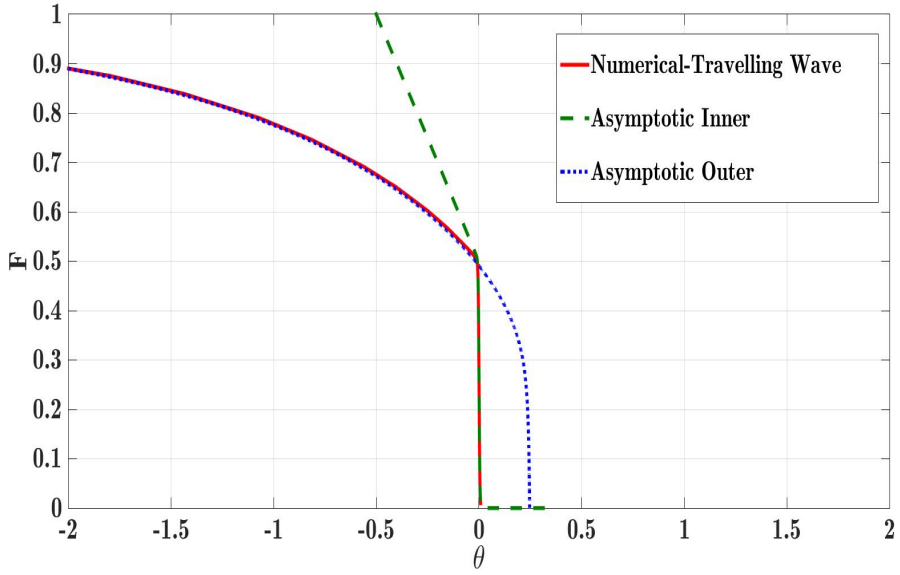

(a) Full view of partially dispersed shock $\epsilon = 0.005$

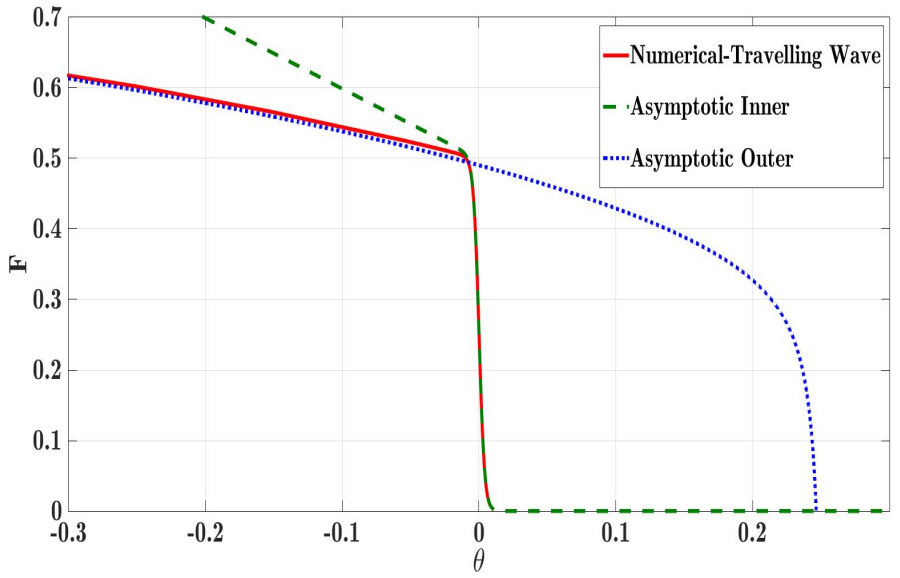

(b) blow up of the inner sub-shock

Figure 3.4.10: Comparison of the travelling wave Asymptotic and Numerical solutions when the wave is partially dispersed for viscosity $\epsilon = 0.005$ and relaxation parameters $\phi = 0.5\,,\ \tau = 0.25\,.$

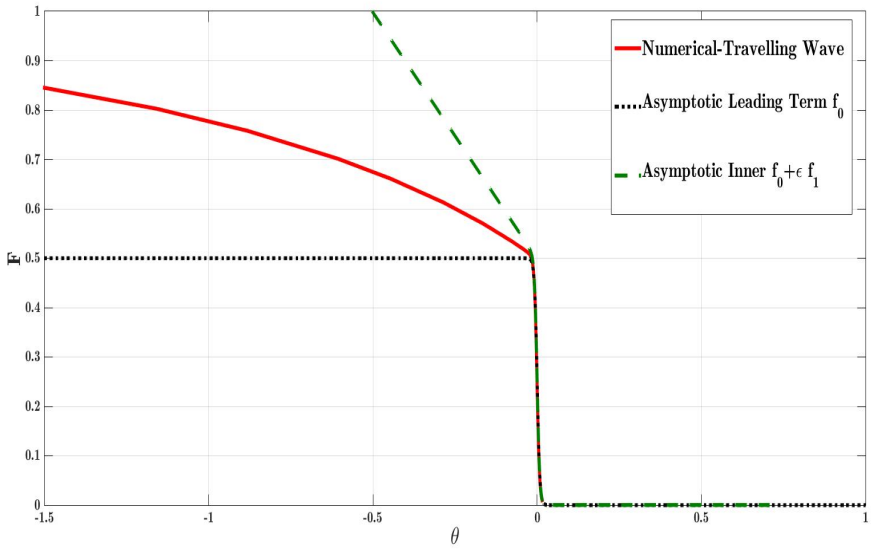

(a) Full view of partially dispersed shock $\epsilon = 0.001$

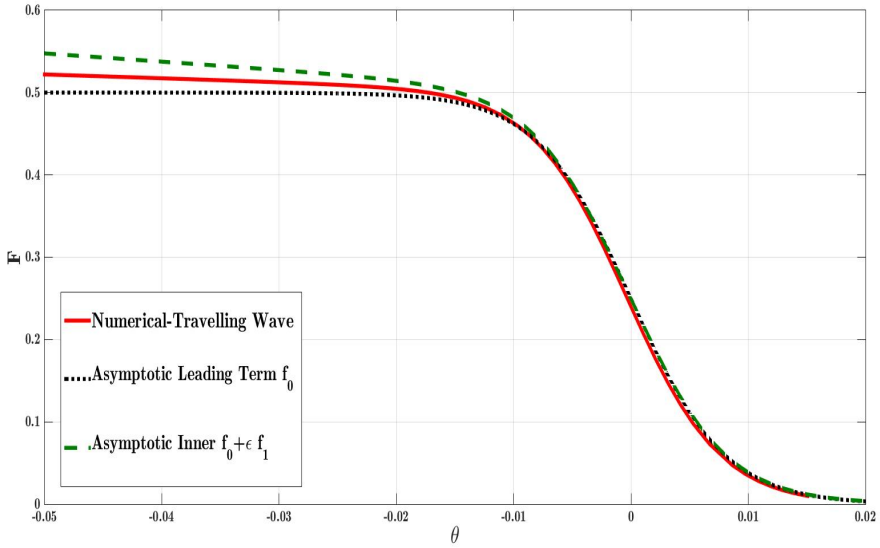

(b) blow up of the inner sub-shock

Figure 3.4.11: Comparison of the travelling wave Asymptotic inner one-term (black) and two-term (green) solutions with Numerical solution (red) when the wave is partially dispersed at $\epsilon = 0.001$ and $\phi = 0.5$, $\tau = 0.25$.

3.4.9 Calculations of the Travelling Wave Inner Shock Width

In §2.3.1 we presented a method to evaluate shock width and we apply this method for the inner sub-shock in the partially dispersed wave. The asymptotic shock width of the embedded shock of amplitude $1-\phi$ can be defined

$$\theta_w = \theta\big(0.1\,(1-\phi)\big) - \theta\big(0.9\,(1-\phi)\big), \tag{3.4.65}$$

The asymptotic shock width at leading order is

$$\theta_w = \frac{1}{\text{Amp}}\,8\,\epsilon\,\tanh^{-1}(0.8), \tag{3.4.66}$$

where Amp is the thermoviscous sub-shock amplitude $1-\phi$, and the width therefore is

$$\theta_{width} = \frac{8}{1-\phi}\,\epsilon\,\tanh^{-1}(0.8) \approx 17.5778\,\epsilon. \tag{3.4.67}$$

In figure (3.4.12) the asymptotic scaled width is compared to the numerical for the range of ϵ from 0.0001 to 0.01 to see the influence of viscosity on two widths. They disagree more as ϵ increases.

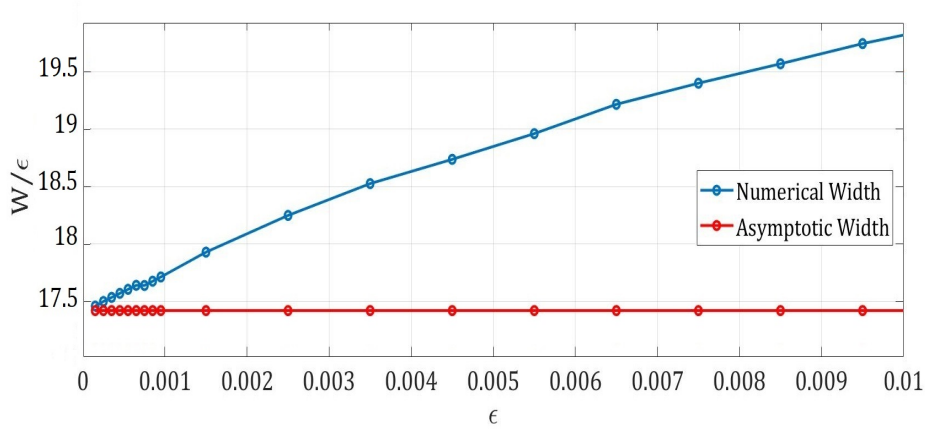

Figure 3.4.12: The scaled width $\frac{W}{\epsilon}$ of numerical (blue) and asymptotic (red) widths at leading order against ϵ.

3.4.10 Comparisons of Wave Maximum Negative Slope

Previously in §3.4.6 we obtained the asymptotic predictions of the maximum negative slope (MNS) for a general amplitude U_m. The asymptotic MNS for the fully dispersed ($\phi > U_m$) and partially dispersed ($\phi < U_m$) shock waves are

$$S_m = \begin{cases} -\dfrac{U_m\,\widehat{\gamma}^2}{2\widehat{\epsilon}}\big(1 + \dfrac{2\,\widehat{\phi}\,\widehat{\epsilon}}{\widehat{\gamma}^2\tau}\log 2\big), & \phi < U_m, \\ \dfrac{U_m}{2\,\tau}\big(\sqrt{\widehat{\phi}^2 - 1} - \widehat{\phi}\big).\big(1 + \widehat{\epsilon}\dfrac{2}{\tau\sqrt{\widehat{\phi}^2 - 1}}\big) & \phi > U_m, \end{cases}$$

where $\widehat{\epsilon} = \frac{\epsilon}{U_m}$, $\widehat{\phi} = \frac{\phi}{U_m}$ and $\widehat{\gamma} = \frac{\gamma}{U_m}$. In figure 3.4.13 (a) the numerical and asymptotic MNS results for travelling wave are compared for a range of values of ϵ for the partially dispersed shock wave, in which the MNS occurs in the inner shock region. The relaxation parameters are fixed at $\tau = 0.25$, $\phi = 0.5$ for the viscosity in the interval $[0.001, 0.01]$ where the amplitude U_m is fixed at one.

On the other hand, figure 3.4.13 (b) shows these comparisons taken for the fully dispersed case as $\phi = 1.5$ with the same range of values of ϵ and τ.

We see in both plots the difference increases with increasing viscosity. Furthermore, we emphasise the importance of the $O(\epsilon)$ correction by considering the leading term of the MNS asymptotic results.

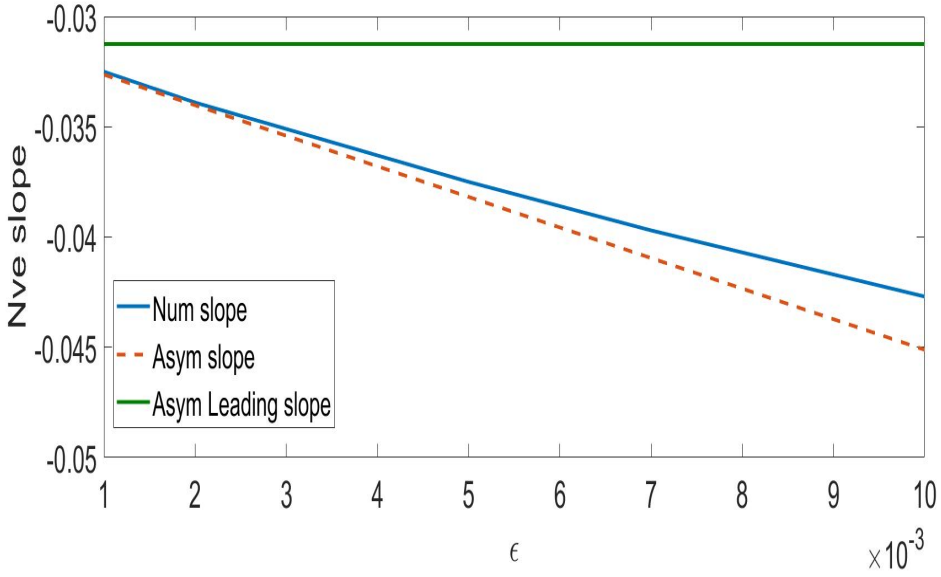

(a) Partially dispersed shock wave $\phi = 0.5$

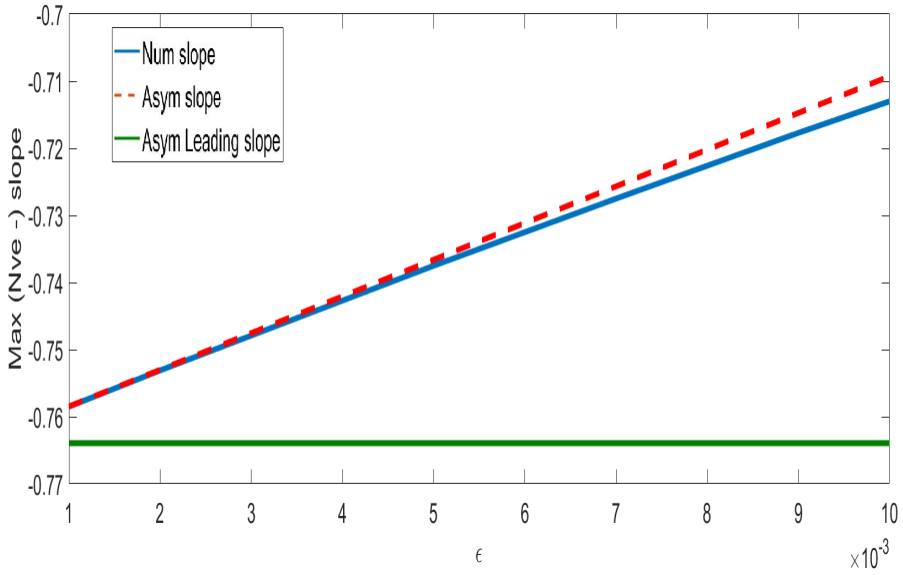

(b) fully dispersed shock wave $\phi = 1.5$

Figure 3.4.13: Wave maximum negative slope for travelling wave numerical solution (blue) compared with the asymptotic solution at leading order (green) and with $O(\epsilon)$ correction (red) when $0.001 < \epsilon < 0.01$, $\tau = 0.25$. Plot (a) is for the partially dispersed shock wave when $\phi = 0.5$, while in plot (b) as $\phi = 1.5$ the wave is fully dispersed .

3.4.11 Summary of Asymptotic and Numerical Approaches of Travelling Wave

We summarize our discussion on the asymptotic and numerical analysis of the travelling wave subject to one relaxation mode

$$2\,\tau\,\epsilon\,F_{\theta\,\theta} - 2\,\Big(\tau\,\big(F-\gamma\big)+\epsilon\Big)F_{\theta} + \Big(F-1\Big)\,F = 0, \qquad \gamma = \frac{1}{2}\big(1-2\Delta\big),$$

with limiting conditions $F(-\infty) = 1\,,\ \ F(\infty) = 0$ and $F_{\theta}(\pm\infty) = 0\,.$ In the case $\epsilon \ll \tau \ll 1,$ we solved the travelling wave for the limit $\epsilon \to 0$ and obtained an implicit equation for F

$$\exp\Big(\frac{\theta-\theta_0}{\tau}\Big) = \Big(1-F\Big)^{1+\phi}\ \Big(F\Big)^{1-\phi}, \qquad \phi = 2\Delta, \tag{3.4.68}$$

which describes waveform transition from $F = 1$ to $F = 0$. We considered the boundary conditions on the implicit solution (3.4.68) for the two cases $\phi > 1$ and $\phi < 1$ corresponding to the cases $\Delta < 1/2$ and $\Delta > 1/2$ respectively. For $\phi > 1\,,$ we saw that F satisfies the required boundary conditions and the waveform of the outer solution remains single-valued. This is known as a fully dispersed relaxing shock of width $O(\tau)$ and represents a physically realistic solution for F. In contrast if $\phi < 1$, we found that one boundary condition is no longer satisfied and the outer solution becomes multi-valued, so, when $\epsilon = 0$ no travelling wave solution exists for $\phi < 1$. For $\phi < 1$ the relaxation effects are insufficient to support the shock, but the small diffusivity ensures a single-valued solution. Thus, an inner sub-shock, controlled by ϵ is inserted inserted at $\theta = 0\,,$ describing the transition from the outer solution for $\theta < 0$ to zero ahead of the inner shock. In this case, the outer relaxed shock wave presented in (3.4.68) with the $O(\epsilon)$ perturbations given in (3.4.20) describes the transition from $F = 1$ to $F = 1-\phi\,.$ In addition to an embedded shock that describes the transition from $F = 1-\phi$ to $F = 0\,,$ this inner viscous

sub-shock comes in the form of the Taylor's shock

$$f_0 = \frac{1}{2}(1-\phi)\ \left[1 - \tanh\left(\frac{1-\phi}{4}(\hat{\theta}-\hat{\theta}_0)\right)\right]$$

presented together with its $O(\epsilon)$ correction term in (3.4.32).

We used the two-term asymptotic series for the outer and inner solutions to derive the maximum negative slope for the travelling wave with amplitude U_m as

$$S_m = \begin{cases} -\dfrac{\mathrm{U}_m\,\widehat{\gamma}^2}{2\widehat{\epsilon}}\Big(1+\widehat{\epsilon}\,\dfrac{2\,\widehat{\phi}}{\widehat{\gamma}^2\tau}\log 2\Big), & \phi < U_m, \\ -\dfrac{\mathrm{U}_m}{2\,\tau}\Big(\widehat{\phi}-\sqrt{\widehat{\phi}^2-1}\Big).\Big(1-\widehat{\epsilon}\dfrac{2}{\tau\sqrt{\widehat{\phi}^2-1}}\Big), & \phi > U_m. \end{cases}$$

This asymptotic MNS was compared with the numerical results.
In the numerical approach for solving the travelling wave, a relationship between F and F_θ was obtained in the linearised shock tail as $\theta \to \infty$. This is then used as the initial condition for a Runge-Kutta solver of the full equation to obtain the waveform for smaller θ.

Next we apply our Fourier pseudospectral scheme, described in §2.5.2, to spatially discretize the Augmented Burgers' equation. A simple modification is included the additional relaxation effects in the numerical code.

3.5 The Rectangular Unit Pulse

In §3.4 we demonstrated an approach to solve the augmented Burgers equation

$$u_t + u\,u_x + \sum_r \Delta_r\, u_{r,x} = \epsilon\, u_{xx}, \tag{3.5.1}$$

$$\Big(\tau\,\frac{\partial}{\partial x} - 1\Big)\, u_r = \tau_r\, u_x, \qquad r = 1, 2, ..., n. \tag{3.5.2}$$

We transferred the augmented Burgers PDE associated with one relaxation mode into the travelling wave ODE (3.4.7) and we conducted asymptotics and a numerical method to obtain solutions. We now present a numerical approach to approximate (3.5.1),(3.5.2) by following the steps of the earlier proposed scheme in §2.5.2 with Fourier pseudospectral differentiation and then forwarding time with fourth order Runge-Kutta method. We also applied the integrating factor method which enables us to enlarge the time steps with stability preserved. The reader can return to §2.5 for more information about the technique, for now we only need to modify the integrating factor to include relaxation effects.

We describe this numerical scheme for n relaxation modes. Let us write the augmented Burgers' equation in the Fourier space

$$\hat{u}_t + \frac{1}{2}\, i\, k\, \widehat{u^2} + i\, k \sum_r \Delta_r\, \hat{u}_r = -\epsilon\, k^2\, \hat{u} \tag{3.5.3}$$

$$(1 - i\, k\, \tau_r)\, \hat{u}_r = -i\, k\, \tau_r\, \hat{u}. \tag{3.5.4}$$

Inserting the values of $\hat{u}_r$ given in (3.5.4) into equation (3.5.3) yields

$$\widehat{u}_t + \frac{1}{2}\, i\, k\, \widehat{u^2} + \Big(\epsilon + \sum_r \Delta_r\, \frac{\tau_r}{1 - i\, k\, \tau_r}\Big) k^2\, \hat{u} = 0. \tag{3.5.5}$$

To apply the Integrating Factor Method we define the new dependent variable

$$\hat{v} = \mathrm{e}^{f(k)\, t}\, \hat{u}. \tag{3.5.6}$$

Differentiating (3.5.6) with respect to time we have

$$\hat{v}_t = f(k)\,\mathrm{e}^{f(k)\,t}\hat{u} + \mathrm{e}^{f(k)\,t}\hat{u}_t. \tag{3.5.7}$$

Returning to equation (3.5.5) and multiplying it by $\exp(f(k)\,t$ gives

$$\hat{u}_t\,\mathrm{e}^{f(k)\,t} + \Big(\epsilon + \sum_r \Delta_r\,\frac{\tau_r}{1 - i\,\tau_r\,k}\Big)\,k^2\,\hat{u}\,\mathrm{e}^{f(k)\,t} + \frac{1}{2}\,i\,k\,\widehat{u^2}\,\mathrm{e}^{f(k)\,t} = 0. \tag{3.5.8}$$

The first two terms of the equation are the right hand side of (3.5.7) as long as the integrating factor is chosen to be

$$f(k) = \Big(\epsilon + \sum_r \Delta_r\,\frac{\tau_r}{1 - i\,\tau_r\,k}\Big)\,k^2. \tag{3.5.9}$$

This integrating factor combines viscous and relaxation effects, since earlier in §2.5 when the described method was for the propagating disturbance influenced by only thermoviscosity, the integrating factor was $f(k) = \epsilon\,k^2$. Using the definition of v_t, equation (3.5.8) then becomes

$$\hat{v}_t = \lambda\,\mathrm{e}^{f(k)\,t}\,\widehat{u^2}, \tag{3.5.10}$$

where $\lambda = -\frac{1}{2}\,i\,k$. The augmented Burgers equation is then discretized in Fourier space in the form

$$\hat{v}_t = \lambda\,\mathrm{e}^{f(k)\,t}\mathcal{F}\left(\Big(\mathcal{F}^{-1}\big(\mathrm{e}^{-f(k)\,t}\hat{v}\big)\Big)^2\right), \tag{3.5.11}$$

where $\mathcal{F}[u] = \hat{u}$ is the Fourier transform operator. We chose the fourth-order Runge-Kutta integration scheme to numerically solve (3.5.11).

3.5.1 Comparisons of Travelling Wave and the Rectangular Pulse

For the comparison purposes with the travelling wave (3.4.7) with the boundary conditions $F(-\infty) = 1$ and $F(\infty) = 0$ we will use the earlier proposed initial wave in §2.5.4. This waveform is the rectangular unit pulse defined on the interval $[-L, L]$ in the form

$$u_0 = \frac{1}{2}\left[1 + \tanh\left(\frac{x-a}{\delta}\right)\right] . \frac{1}{2}\left[1 + \tanh\left(\frac{b-x}{\delta}\right)\right], \tag{3.5.12}$$

where $0 < \delta \ll 1$ fixes the initial wave slope and the two values a and b determines the location and width of the rectangular pulse in the interval $[-L, L]$. We apply the numerical scheme described in §3.5 to numerically approximate the augmented Burgers' equation subject to one relaxation mode with $\epsilon \ll \tau \ll 1$.

Before we discuss the comparisons of the solutions, we would like to describe the propagation of this waveform. Figure 3.5.1 demonstrates the propagation of the unit rectangular wave through time. At the initial time $t = 0$ figure 3.5.1 (a) shows the initial waveform. When the initial waveform is forwarded in time the wave takes the actual form of the solution as in 3.5.1(b) we see the wave at time $t = 12$. The characteristic method predicts a rarefaction wave located at $x_r = a + t$ and a shock at $x_s = b + \frac{1}{2}t$, and we expect them to collide at $t = 2(b - a)$ forming the final triangular-shape shock wave that will decay through later time. Looking at figure 3.5.1(b) we chose $a = -0.5\,L$ and $b = 0.25\,L$ in the interval $[-40, 40]$, thus, the rarefaction wave is positioned at $x_r = -8$ and the shock is at $x_s = 16$ and we expect the two to intersect at $t = 60$. For the choice of a and b we need the pulse to be centred in the interval and the rectangular pulse to be wide, this will give us a longer time before the refraction wave catches up with the shock wave and eventually the two collide.

Figure 3.5.2 is a blow up of the rectangular pulse focusing at the narrow region

of shock front. Figure 3.5.2 (a) captures the fully-dispersed shock at $t = 12$ and figure 3.5.2 (b) captures the partially-dispersed wave. The parameters in figures 3.5.1 and 3.5.2 are taken as $\tau = 0.25$, $\epsilon = 0.005$ and $\delta = 0.0001$ the time step $\Delta t = 0.0001$ with $N = 2^{14}$ Fourier modes.

Figure 3.5.3 compares the numerical solution of the augmented Burgers

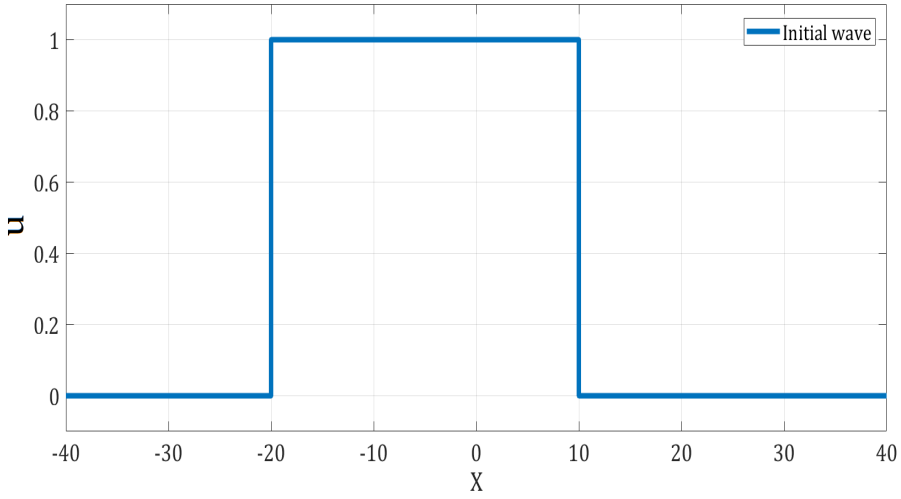

(a) The initial wave $t = 0$

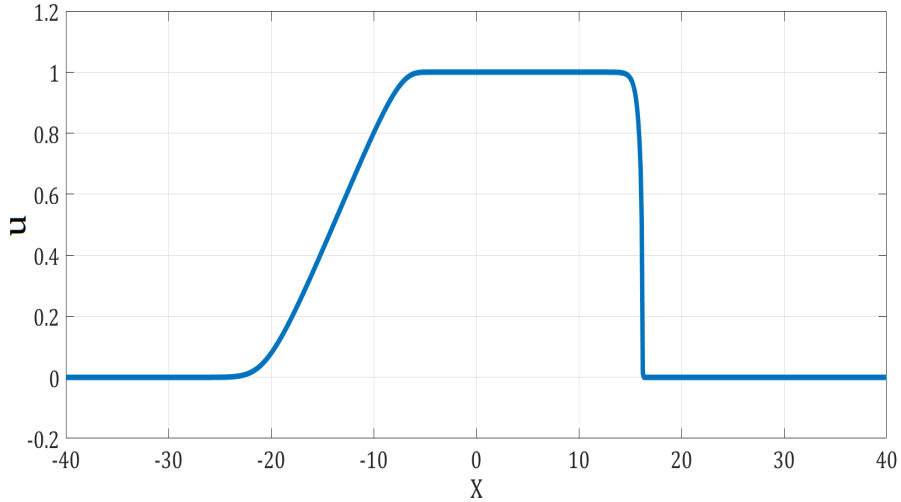

(b) The waveform when time reaches $t = 12$

Figure 3.5.1: Illustration of augmented Burgers numerical solution for the partially dispersed wave $\phi = 0.5 < 1$. The initial waveform at the initial time $t = 0$ is plotted in (a) and in (b) we see the evolution of the rectangular wave when time is marched to $t = 12$. The viscosity is $\epsilon = 0.005$ and the relaxation time $\tau = 0.25$. For $N = 2^{14}$ we chose the time step to be $\Delta t = 10^{-4}$ and the slope of the initial wave was set at $\delta = 10^{-4}$.

equation with the asymptotic travelling wave solution for the fully dispersed transition as $\phi = 1.5$ with width of order $O(\tau)$ where $\tau = 0.1$ and $\epsilon = 0.001$. The above plot of figure 3.5.3 is a view of the full waveform, the generated numerical solution for the augmented Burgers' equation using Fourier Pseudospectral code is marked in blue line along with the travelling wave asymptotic results (red dashed line). The below plot is a blow up of the wave front to show the correspondence of the two solutions. We choose the horizontal

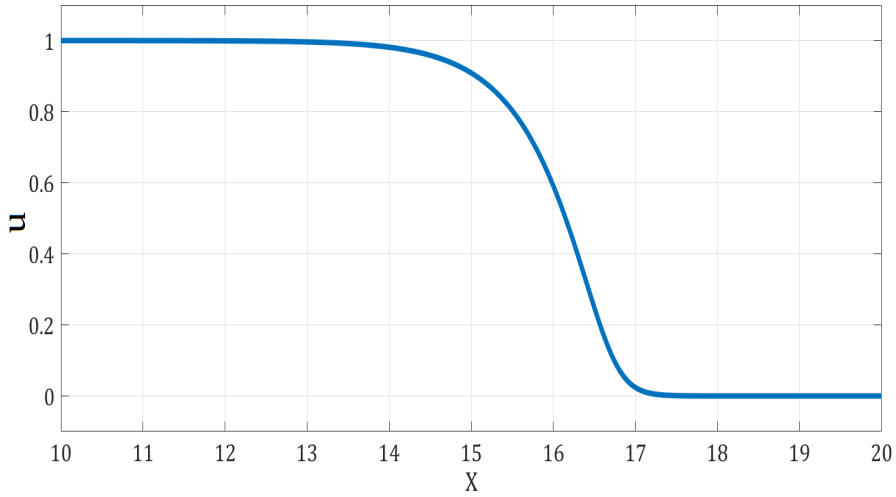

(a) $\phi > 1$

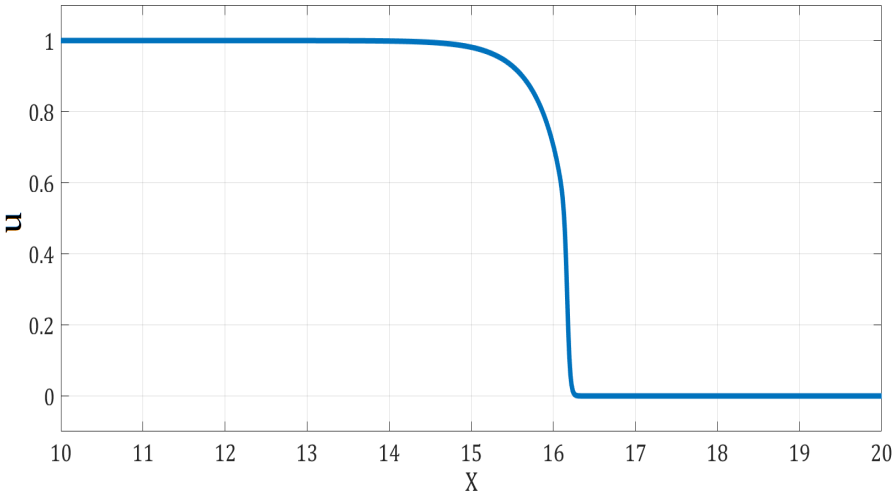

(b) $\phi < 1$

Figure 3.5.2: The evolution of the rectangular wave at the time $t = 12$ showing the numerical Augmented Burgers solution for the fully dispersed wave in (a) and the partially dispersed wave in (b). The plots are taken for viscosity $\epsilon = 0.005$ and relaxation time $\tau = 0.25$ while $\phi = 0.5$ in (b) and $\phi = 1.5$ in (a).

shift in the numerical solution so that the waveform agrees at $u = 0.9$ and no shift is made in the travelling wave.

The next comparison is for the partially dispersed case demonstrated in figure 3.5.4 with $\phi = 0.50$. Figure 3.5.3 (a),(b) and (c) are blow ups showing the very narrow region of the shock front for the values of thermoviscosity $\epsilon = 0.01, 0.005, 0.001$. The numerical solution is marked as the blue line compared to the travelling wave asymptotic outer solution (red) and to the thermoviscous inner shock solution (green). Notice that to capture the correspondence we made a horizontal shift in the numerical (blue) and the asymptotic inner solutions (green) so that the both waveform agrees at the numerical maximum negative slope. It is clearly seen that as the viscous dissipation decreases, the two solutions becomes better, in particular, in the inner sub-shock which is controlled by ϵ.

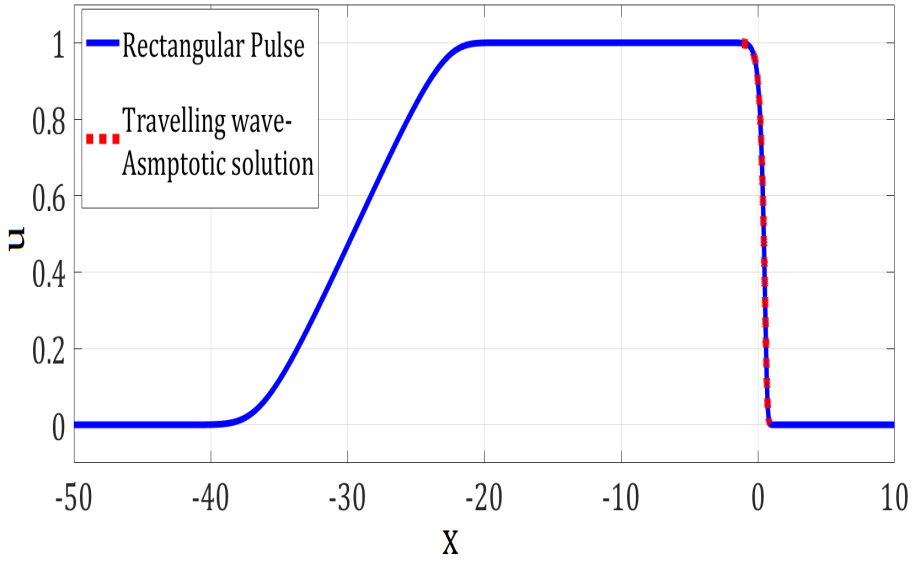

(a) Full view of the rectangular unit pulse

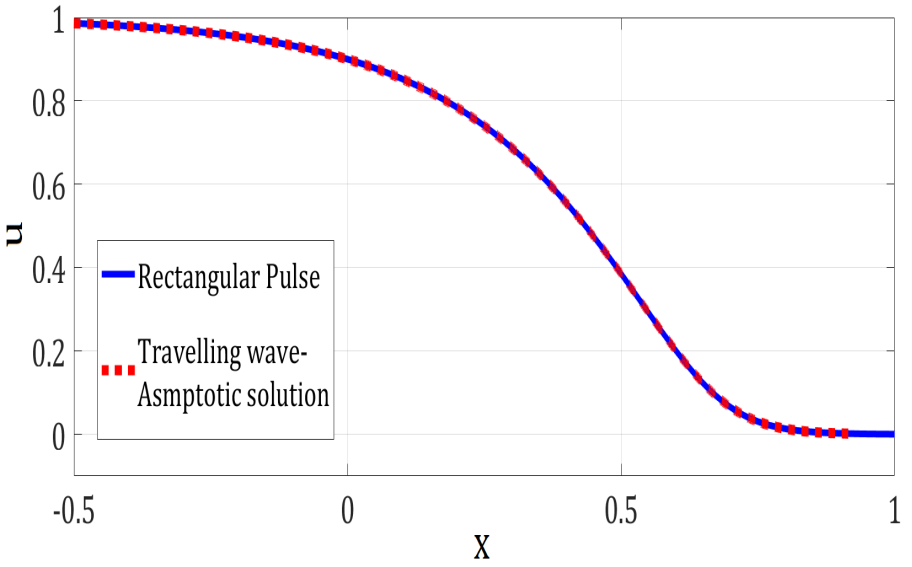

(b) Blow up of the relaxed shock

Figure 3.5.3: Fully dispersed shock wave for the rectangular pulse with viscosity fixed at $\epsilon = 0.001$ and the relaxation parameters $\phi = 1.5, \tau = 0.1$. The numerical solution (blue) is compared to the asymptotic travelling wave solution (red).

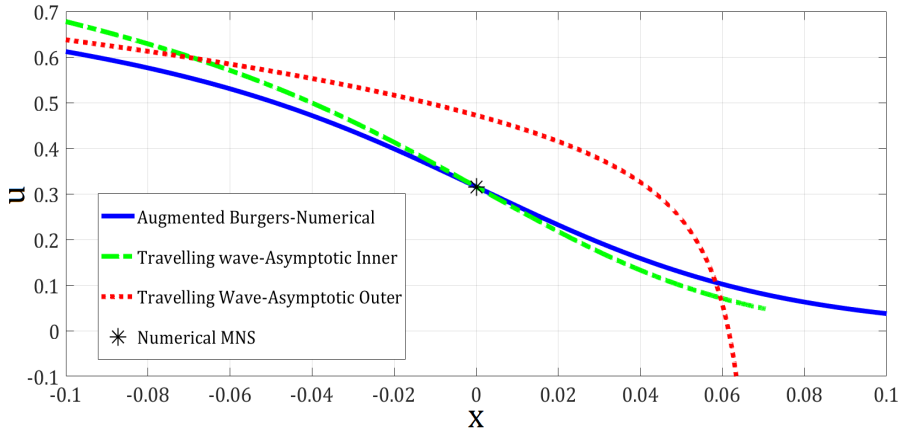

(a) $\epsilon = 0.01$

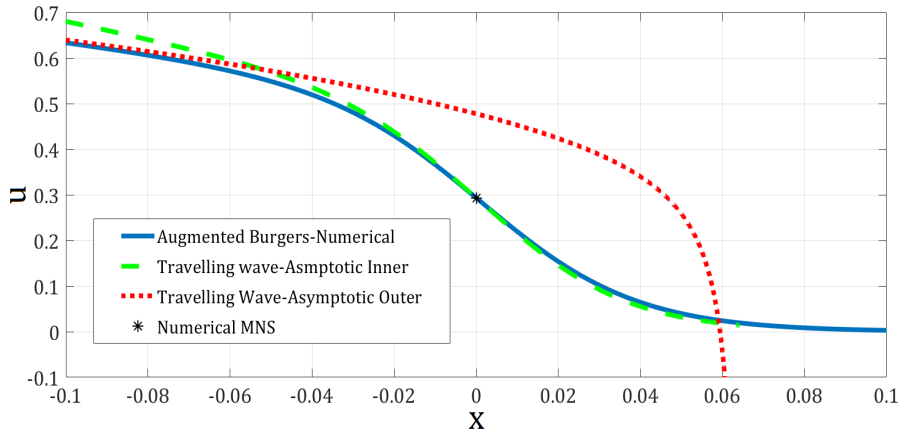

(b) $\epsilon = 0.005$

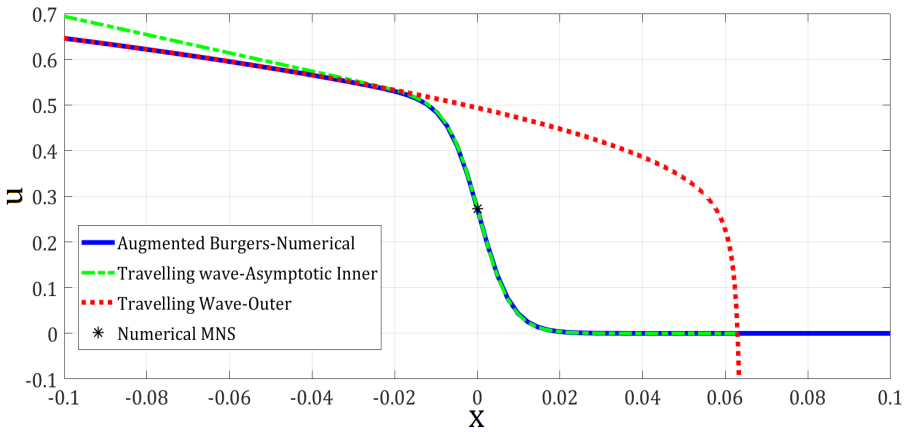

(c) $\epsilon = 0.001$

Figure 3.5.4: Partially dispersed shock wave for the rectangular pulse with viscosity taken at the values $\epsilon = 0.01, 0.005, 0.001$ and the relaxation parameters $\phi = 0.5, \tau = 0.25$. The numerical solution (green) is compared to the first two terms of the relaxation controlled solution (red) and to the inner viscous expansion (blue).

3.5.2 Comparisons of Wave Maximum Negative Slope

In §3.4.6 we described the changes happening in the wave propagation when accounting for the relaxation processes. The amplitude of the rectangular unit pulse decreases after a certain time and so the molecular concentration parameter Δ, changes through time. This change causes the wave to transform from partially to fully dispersed wave. Therefore, the wave maximum negative slope (MNS) is suitable in capturing these changes in the shock structure study.

The calculations of the numerical maximum negative slope (NMNS) over a long period of time depend on the choice of the rectangular pulse dimensions. A reminder of the initial rectangular wave

$$u_0 = \frac{1}{2}\left[1 + \tanh\left(\frac{x-a}{\delta}\right)\right] . \frac{1}{2}\left[1 + \tanh\left(\frac{b-x}{\delta}\right)\right], \tag{3.5.13}$$

defined on the interval $[-L, L]$. Taking $L = 20$, the initial rectangular wave is between $a = -0.75\,L$ and $a = -0.5\,L$ and slope $\delta = 0.0001$. This choice allows us to study the evolution of the rectangular pulse over longer time intervals. Figure 3.5.5 demonstrates the initial wave in (a) and the propagated waveform when it reaches $t = 50$ in (b).

The characteristic method states that the shock is located at $x = b + \frac{1}{2}\,t = -10 + \frac{1}{2}\,t$ and we expect the rectangular wave to transform to its triangular shape at $t = 2\,(b-a) = 2\,(5) = 10$. When the wave propagation

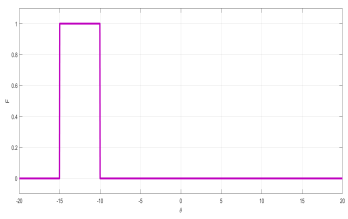

(a) The initial wave at $t = 0$.

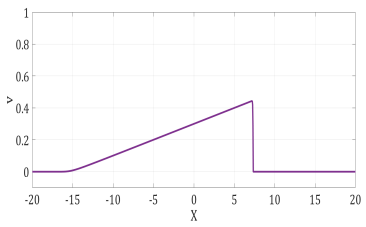

(b) The propagated waveform at $t = 50$

Figure 3.5.5: The initial waveform in (a) and the rectangular pulse after becoming triangular at $t = 50$ in (b). The viscosity is $\epsilon = 0.00013$ and relaxation time $\tau = 0.01$.

reaches this time $t = 10$ the amplitude begins to decay as a result the effective relaxation sound absorption parameter $\widehat{\Delta}$ which is inversely proportional to the amplitude and begins to increase as time advances. We take the molecular relaxation increment to be $\widehat{\Delta} = 0.25$, which puts the parameter $\widehat{\phi} = 2\,\widehat{\Delta} = 0.5$, this value is unchanged as the wave propagates for $0 < t < 10$. Then the wave becomes triangular for $t > 10$ in which $\widehat{\phi}$ increases and then at some fixed time the condition for the shock being partially dispersed changes and the shock becomes fully dispersed. Figure 3.5.6 shows both the numerical (black) and asymptotic amplitudes (green) for the time $0 < t < 50$. We see that both amplitudes are constant at one for $t < 10$, and for $t > 10$ the wave amplitude decays. The amplitude is computed by identifying $\max(u)$ at each time step. The asymptotic amplitude is calculated as one when $t < 10$ and $\sqrt{10/t}$ wile $t > 10$.

Recalling the asymptotic maximum negative slope (AMNS) deduced earlier in

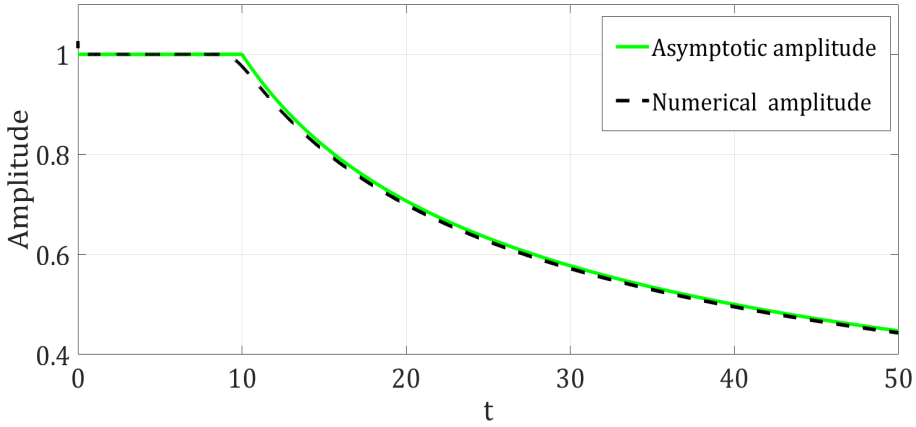

Figure 3.5.6: The asymptotic (green) and numeric (black) amplitude together for the time $0 < t < 50$. Both amplitudes decreases for 10.

§3.4.6

$$S_m = \begin{cases} -\dfrac{\mathrm{U}_m\,\widehat{\gamma}^2}{2\widehat{\epsilon}}\left(1 + \widehat{\epsilon}\,\dfrac{2\,\widehat{\phi}}{\widehat{\gamma}^2\tau}\log 2\right), & \phi < U_m, \\ -\dfrac{\mathrm{U}_m}{2\,\tau}\left(\widehat{\phi} - \sqrt{\widehat{\phi}^2 - 1}\right).\left(1 - \widehat{\epsilon}\,\dfrac{2}{\tau\sqrt{\widehat{\phi}^2 - 1}}\right), & \phi > U_m, \end{cases} \tag{3.5.14}$$

which defines the (AMNS) for the partially and fully dispersed waves, respectively, in the non-dimensional space.

In figure 3.5.7 we plot the asymptotic MNS (AMNS) at leading order while $0 < t < 50$. The relaxation molecular concentration is fixed at $\widehat{\phi} = 2\,\widehat{\Delta} = 0.5$ which corresponds to the partially dispersed case. The relaxation parameter $\widehat{\Delta}$ remains constant for $0 < t < 10$, after which the amplitude begins to decay and subsequently $\widehat{\Delta}$ grows. This growth continues through time until it reaches a stage where the the AMNS switches from the partially dispersed to the fully dispersed region and in between we see a jump discontinuity at $t = 40$. Looking at the behaviour of the AMNS at the discontinuity, we see for the AMNS when $\widehat{\phi} \to 1^{-}$, tends to 0 since

$$-\frac{\mathrm{U}_m\,\widehat{\gamma}^2}{2\widehat{\epsilon}} \to 0 \qquad \text{as} \quad \widehat{\gamma} = 0.5\,(1-\widehat{\phi}) \to 0^{-}.$$

By studying the AMNS for $\widehat{\phi} > 1$ and using the value of $\tau = 0.01$ in figure 3.5.7 we see that when $\widehat{\phi} \to 1^{+}$ the AMNS at leading order

$$\begin{aligned} -\frac{\mathrm{U}_m}{2\,\tau}\big(\widehat{\phi} - \sqrt{\widehat{\phi}^2 - 1}\big) \quad &\to \quad -\frac{\mathrm{U}_m\,\widehat{\phi}}{2\,\tau} \\ &\to \quad -\frac{1}{4\,\tau} = -25 \qquad \text{as} \quad \widehat{\phi} \to 1^{+}. \end{aligned}$$

The next figures demonstrates the two MNS while $0 < t < 50$, the (NMNS)

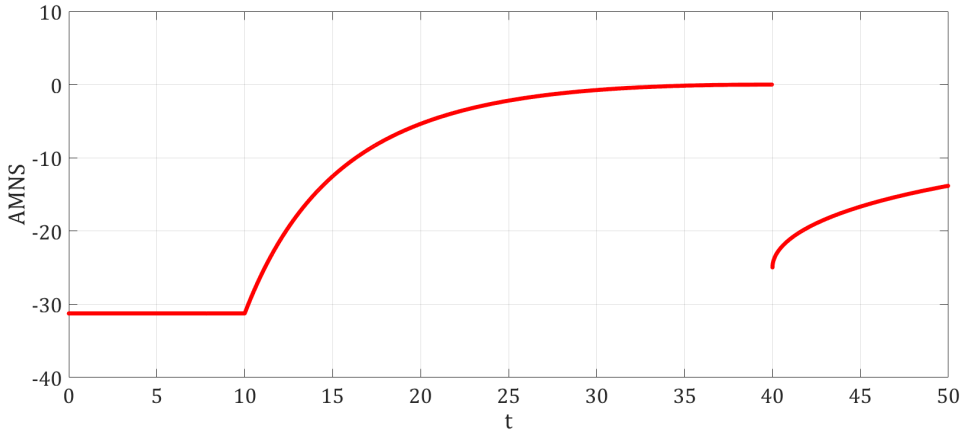

Figure 3.5.7: The asymptotic MNS at leading order for the time $0 < t < 50$ with viscosity $\epsilon = 0.001$ and relaxation time $\tau = 0.01$.

drawn in blue line and the red line presents the (AMNS) defined in equation (3.5.14). The first three figures 3.5.8 , 3.5.9 and 3.5.10 illustrate how a small change in viscosity ϵ has an effect on the two waves MNS correspondence. Each figure contains three plots, (a) a comprehensive view of the (AMNS) and (NMNS), (b) a blow up plot of the area where the shock wave develops to a triangular wave and (c) another blow up showing the area when shock changes from partially to fully-dispersed wave.

Looking at figures 3.5.8, 3.5.10 and 3.5.9, plots (a), we notice by reducing the viscosity from $\epsilon = 0.001$ in plot 3.5.8 to $\epsilon = 0.00013$ in 3.5.10, a relatively good agreement of AMNS for the partially dispersed part. Since in the partially dispersed shock the MNS appears in the inner sub-shock which is controlled by the viscosity. Whereas, in the fully dispersed region the agreement is better for all three values of ϵ as the width depends on τ.

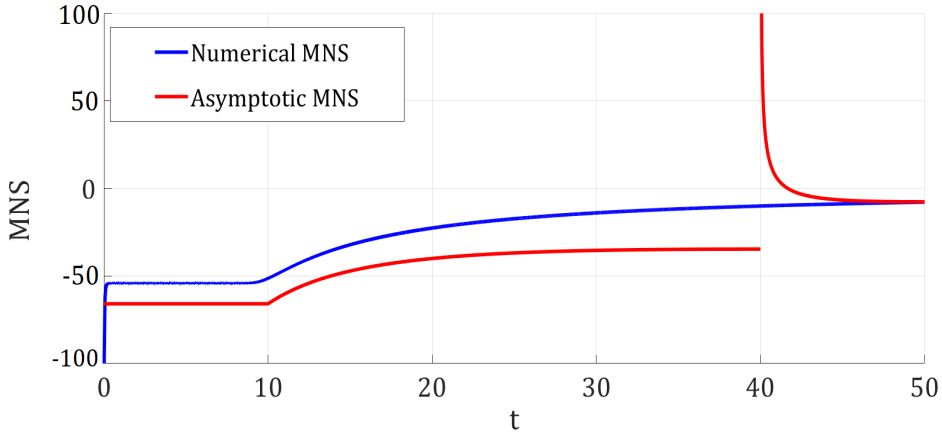

(a) Full view of asymptotic and numeric (MNS)

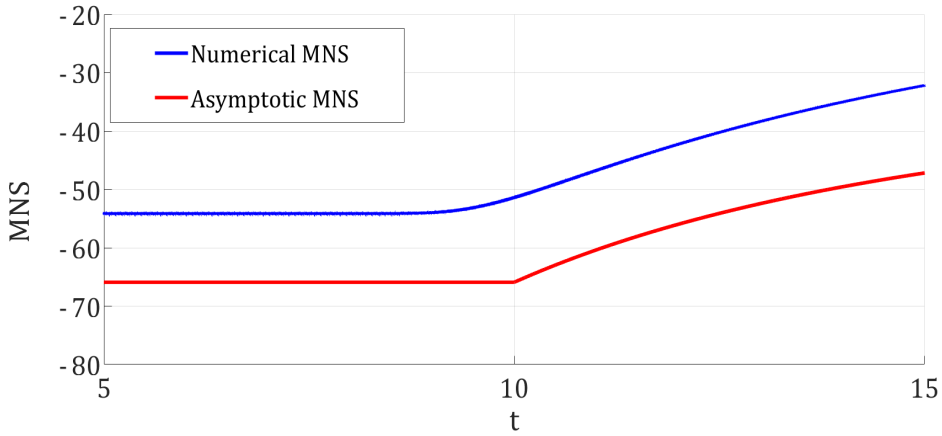

(b) The region where the shock develops to triangular wave

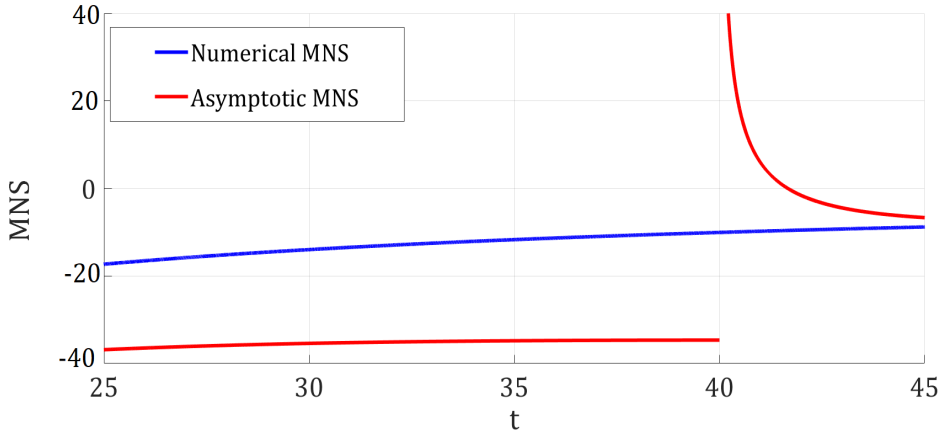

(c) The region where the solution changes from partially to fully dispersed

Figure 3.5.8: Comparison of wave maximum negative slope for the numerical solution (blue) of augmented Burgers equation for $\epsilon = 0.001, \tau = 0.01, \Delta = 0.25$ with asymptotic solutions (red). The shock is predicted to be partly dispersed for $t < 40$ and fully dispersed for $t > 40$.

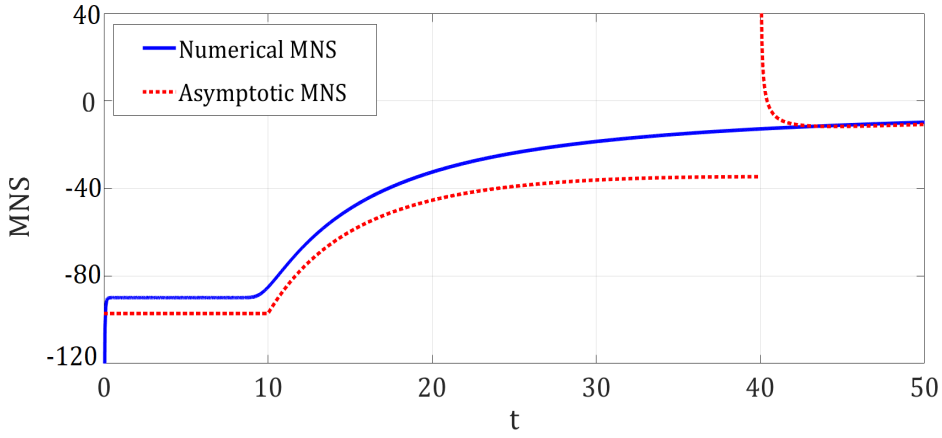

(a) Full view of asymptotic and numeric (MNS)

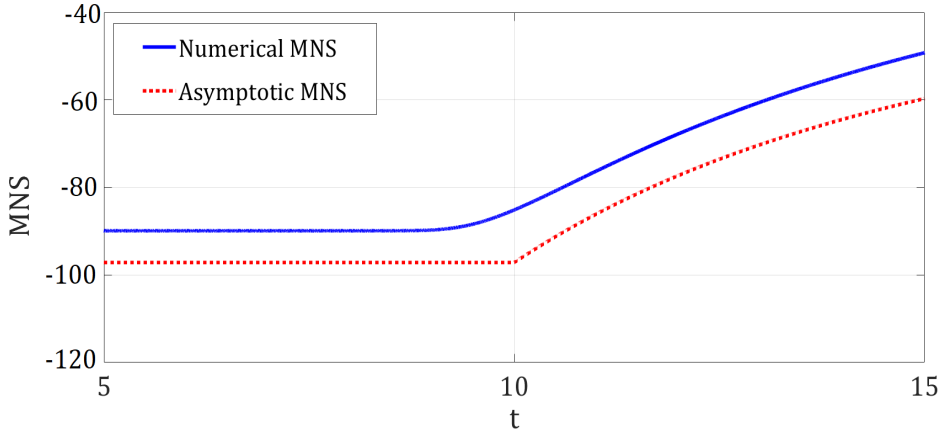

(b) The region where the shock develops to triangular wave

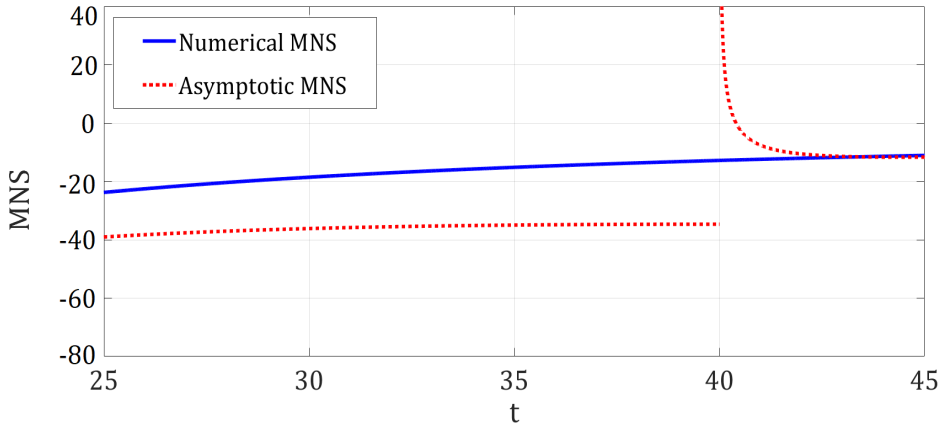

(c) The region where the solution changes from partially to fully dispersed

Figure 3.5.9: Comparison of wave maximum negative slope for the numerical solution (blue) of augmented Burgers equation for $\epsilon = 0.0005, \tau = 0.01, \Delta = 0.25$ with asymptotic solutions (red). The shock is predicted to be partly dispersed for $t < 40$ and fully dispersed for $t > 40$.

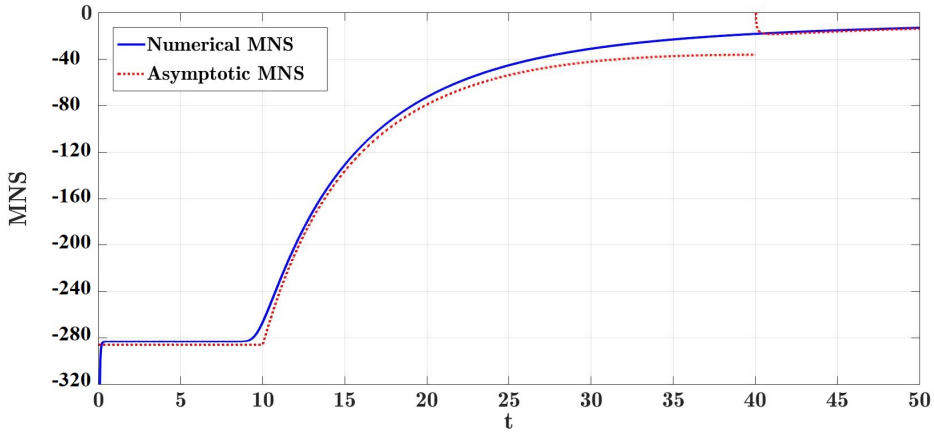

(a) Full view of asymptotic and numeric (MNS)

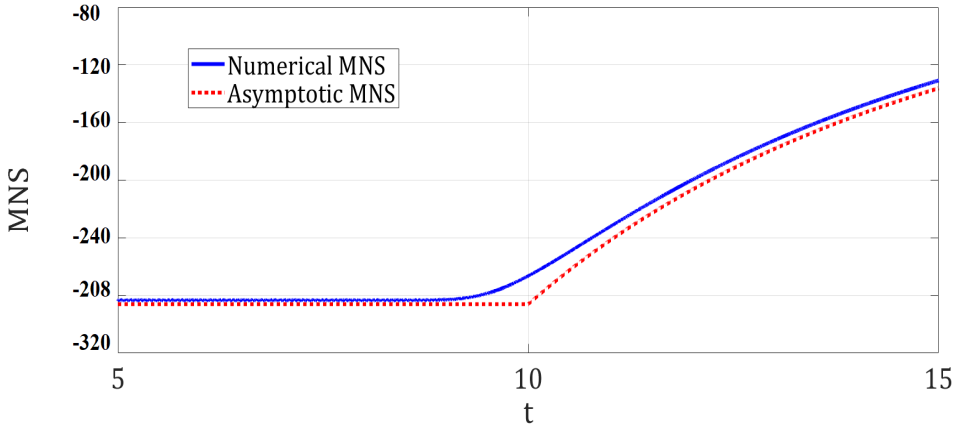

(b) The region where the shock develops to triangular wave

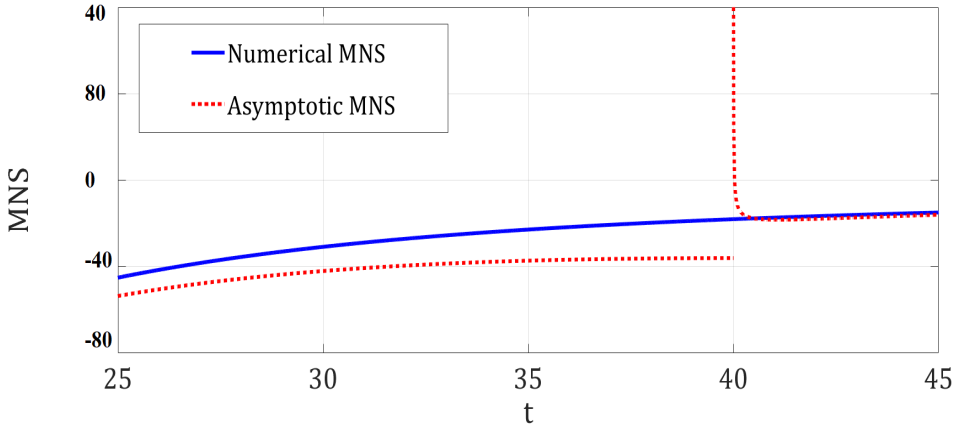

(c) The region where the solution changes from partially to fully dispersed

Figure 3.5.10: Comparison of wave maximum negative slope for the numerical solution (blue) of augmented Burgers equation for $\epsilon = 0.00013, \tau = 0.01, \Delta = 0.25$ with asymptotic solutions (red). The shock is predicted to be partly dispersed for $t < 40$ and fully dispersed for $t > 40$.

3.6 Summary

In this chapter we looked at the propagation of the plane waves of finite amplitudes subject to set of influences consisting of thermoviscosity and relaxation. This investigation was intentioned to the case of one relaxation mode, here the set of the characteristic relaxation parameters are the relaxation time τ, and the increment of the low and hight sound speed frequencies Δc.

We showed that if the wave is propagating with amplitude lower or at the same order of the relaxation frequency $(1 \leq \phi)$, then the whole waveform is controlled by the relaxation mechanism and the viscous effect is neglected. This shock wave is known as fully dispersed. On the contrary, if the amplitude exceeds the relaxation frequency $(1 > \phi)$, then the wave must begin with a discontinuity in which viscosity is significant. This shock is known as partially dispersed, and the discontinuity comes in the form of the Taylor type structure to adjust the amplitude by, $1 - \phi$. Followed by a region where the shock is dissipated due to the relaxation processes.

The augmented Burgers equation is used to model this problem, and we searched for analytical and numerical solutions. We begun by transforming the equation of interest into the travelling wave ODE for a forward facing step transition. We deduced asymptotic solutions via the the method of matched asymptotic expansions and numerical solutions from a numerical integration method of the travelling wave.

We also applied another numerical simulation but this time on the augmented Burgers equation. For a rectangular shaped wave we utilized the Fourier pseudo-spectral method for the discretiziation of the given problem followed by the fourth-order Runge-Kutta method for integration.

The assumption $\epsilon \ll \tau \ll 1$ enabled us to capture the delicate structure of the thin relaxing shock of hight $O(1)$. The results of all approaches described above were compared. We presented a practical method to measure the shock width by looking at the maximum gradient of the velocity, u, and the width can be easily calculated as $\text{width} = \frac{1}{\max u'}$.

4

Augmented Burgers' Model in Multiple Relaxation Modes

4.1 Introduction

The internal vibrational and rotational energies of Nitrogen N_2 and Oxygen O_2 molecules in air dominate the relaxational absorption of sound at moderate frequencies. In seawater, the principal components are Boric acid H_3BO_3 and Magnesium sulphate MgO_4S which contribute the acoustic relaxation absorption by seawater over the range of low frequency of sound [21].

In this chapter, we analyse in depth analytical and numerical solutions representing one-dimensional small amplitude sound wave propagation associated with sonic boom, subject to thermoviscous dissipation and two vibrational relaxation modes. We begin by investigating the travelling wave solutions. Following similar analysis to the earlier work presented in §3.4, we look for asymptotic and numerical solutions for the travelling wave in non-dimensional form. We examine how the shock structure is affected by this combination of thermoviscosity, nonlinearity and the two relaxation processes. Each relaxation mode is characterised by two parameters Δ_r and τ_r, where $r = 1, 2$. In the asymptotic analysis the study is based on the limit $\epsilon \ll \tau_2 \ll \tau_1$ which we will see in §5 is relevant to the propagation in air. In the presence of thermoviscus dissipation and two molecular relaxation modes, the shock may consist of three regimes [44], depending on the the values of the relaxation

parameters. The investigation of shock width will be carried out to study the very thin viscous region by looking at maximum negative wave slope. In §4.3 the Fourier pseudospectral numerical method proposed earlier in §3.5 is used with the inclusion of the second relaxation mode with parameters Δ_2 and τ_2. Following our earlier discussion in solving the augmented Burgers equation with one relaxation mode, we begin with a reminder of the dimensionless augmented Burgers equation (3.3.14) with the relaxation equations (3.3.15) that we derived earlier in §3.3

$$u_t + u\,u_x + \sum_{i=1}^{2} \Delta_i\, u_{i,x} = \epsilon\, u_{xx}, \tag{4.1.1}$$

$$\left(\tau_1 \frac{\partial}{\partial x} - 1\right) u_1 = \tau_1\, u_x, \qquad \left(\tau_2 \frac{\partial}{\partial x} - 1\right) u_2 = \tau_2\, u_x. \tag{4.1.2}$$

We look for the travelling wave solutions of equation (4.1.1) associated with the relaxation equations in (4.1.2) for a step transition of a general non-dimensional amplitude U_m, The boundary conditions then become $u \to U_m$, $u_i \to 0$ as $x \to -\infty$ and $u \to 0$, $u_i \to 0$ as $x \to \infty$.

4.2 Travelling Wave

4.2.1 Asymptotic Waveform

We begin by looking at travelling wave solutions corresponding to a transition of general amplitude U_m

$$u(t,x) = F(\theta) = F(x - st) \qquad u_i(t,x) = G_i(\theta) = G_i(x - st),$$

where $\theta = x - st$ and the boundary conditions become

$$F, F_\theta, G_i, G_{i,\theta} \to 0, \qquad \text{as} \qquad \theta \to \infty, \tag{4.2.1}$$

$$F \to U_m, \qquad F_\theta, G_i, G_{i,\theta} \to 0, \qquad \text{as} \qquad \theta \to -\infty. \tag{4.2.2}$$

Upon replacing the partial derivatives of u and u_i in equations (4.1.1), (4.1.2) with the appropriate derivatives of F and G_i, we get

$$-s\,F_\theta + \Big(\tfrac{1}{2}F^2\Big)_\theta + \quad \textstyle\sum_i \Delta_i\,G_{i,\,\theta} \quad = \epsilon\,F_{\theta\,\theta}, \qquad\qquad \epsilon \ll 1 \tag{4.2.3}$$

$$\Big(\tau_1\,\frac{\mathrm{d}}{\mathrm{d}\theta} - 1\Big)G_1 = \tau_1\,F_\theta, \qquad\qquad \Big(\tau_2\,\frac{\mathrm{d}}{\mathrm{d}\theta} - 1\Big)G_2 = \tau_2\,F_\theta. \tag{4.2.4}$$

The travelling wave (4.2.3) advances to the right with the constant speed s. Integrating (4.2.3) once puts it into the form

$$-s\,F + \frac{1}{2}F^2 - \epsilon\,F_\theta + \sum_i \Delta_i\,G_i = C.$$

The first set of boundary condition (4.2.1) implies the integration constant to be $C = 0$. Applying the second boundary condition requires the shock speed to be $s = \frac{U_m}{2}$. Thus,

$$\frac{1}{2}\Big(F - U_m\Big)\,F - \epsilon\,F_\theta + \Big(\Delta_1\,G_1 + \Delta_2\,G_2\Big) = 0. \tag{4.2.5}$$

To calculate the travelling wave solution we first eliminate $\Delta_1\,G_1 + \Delta_2\,G_2$. Therefore, applying the operator $(\tau_1\,\frac{\mathrm{d}}{\mathrm{d}\theta} - 1)$ to first relaxation equation and $(\tau_2\,\frac{\mathrm{d}}{\mathrm{d}\theta} - 1)$ to second relaxation equation gives

$$\begin{aligned}
\Big(\tau_1\,\frac{\mathrm{d}}{\mathrm{d}\theta} - 1\Big)\,.\,\Big(\tau_2\,\frac{\mathrm{d}}{\mathrm{d}\theta} - 1\Big)\,\Delta_1\,G_1 &= \Big(\tau_2\,\frac{\mathrm{d}}{\mathrm{d}\theta} - 1\Big)\,\tau_1\,\Delta_1\,F_\theta, \\
\Big(\tau_1\,\frac{\mathrm{d}}{\mathrm{d}\theta} - 1\Big)\,.\,\Big(\tau_2\,\frac{\mathrm{d}}{\mathrm{d}\theta} - 1\Big)\,\Delta_2\,G_2 &= \Big(\tau_1\,\frac{\mathrm{d}}{\mathrm{d}\theta} - 1\Big)\,\tau_2\,\Delta_2\,F_\theta.
\end{aligned}$$

Adding them, we have

$$\Big(\tau_1\,\frac{\mathrm{d}}{\mathrm{d}\theta}{-}1\Big)\,\Big(\tau_2\,\frac{\mathrm{d}}{\mathrm{d}\theta}{-}1\Big)\,\Big[\Delta_1\,G_1{+}\Delta_2\,G_2\Big] = \tau_1\,\tau_2\,\Big(\Delta_1{+}\Delta_2\Big)\,F_{\theta\,\theta}{-}\Big(\tau_1\,\Delta_1{+}\tau_2\,\Delta_2\Big)\,F_\theta.$$

Substituting the term $\Delta_1 G_1 + \Delta_2 G_2$ from (4.2.5) yields

$$\left(\tau_1 \frac{\mathrm{d}}{\mathrm{d}\theta} - 1\right)\left(\tau_2 \frac{\mathrm{d}}{\mathrm{d}\theta} - 1\right)\left[\epsilon F_\theta - \frac{1}{2}\left(F - U_m\right)F\right] = \tau_1 \tau_2 \left(\Delta_1 + \Delta_2\right) F_{\theta\theta} - \left(\tau_1 \Delta_1 + \tau_2 \Delta_2\right) F_\theta. \quad (4.2.6)$$

Previously in chapter §3 we considered the propagation of sonic boom for single relaxation mode with $\epsilon \ll \tau \ll 1$. Looking at the unit step we obtained two kinds of relaxing travelling wave solutions depending on the relaxation dispersion. When $\Delta > 1/2$ the waveform was single-valued representing a physically realistic solution. This shock is known as fully-dispersed where the relaxation mode governs the whole waveform at leading order. However, if Δ is below the critical value $\frac{1}{2}$ then the solution becomes multi-valued as one of the boundary conditions is no longer satisfied. For $\Delta < 1/2$ the relaxation mode is insufficient to support the shock and the thermoviscous effects must be considered. This waveform, known as partially-dispersed, consists of an outer relaxation shock and an inner viscous sub-shock of amplitude $1 - 2\,\Delta$.

We now present the asymptotic structure of the travelling wave when two relaxation modes are present. From the previous asymptotic analysis for one relaxation mode, we anticipate the shock profile will take three different types depending on the values of the two relaxation modes. The first type, is a fully-dispersed shock wave controlled by the first relaxation mode. The second type occurs when the first relaxation mode is insufficient to support the shock and a narrower embedded shock controlled by the second relaxation mode arises. Thus, the second type consists of an outer and an inner relaxation shocks, the outer is partially-dispersed whereas the inner is fully-dispersed. The third type is when both the outer and inner relaxation shocks are partially-dispersed and a thermoviscous sub-shock is inserted.

This asymptotic study of the travelling wave structure is conducted in the next section where we assume $\epsilon \ll \tau_2 \ll \tau_1$. We will investigate the travelling wave asymptotic solutions for the general amplitude U_m. Previously in the one relaxation mode analysis §3 we referred to the asymptotic solutions as inner and

outer solutions, in this chapter we will use the terms region 1,2,3 solutions.
Let us first define the two parameters that we will use in our derivation of the three regions

$$\gamma_1 = \frac{U_m}{2} - \Delta_1. \tag{4.2.7}$$

$$\gamma_2 = \frac{U_m}{2} - \Delta_1 - \Delta_2. \tag{4.2.8}$$

We will now begin the derivation of asymptotic expansions at leading order only for each regime of the solution.

Region 1 in Travelling Wave Asymptotic Solution

Taking the $O(\tau_1)$ term in equation (4.2.6) for the first region and neglecting the $O(\tau_2)$ and $O(\epsilon)$ terms gives

$$O(\tau_1) \qquad \left(1 - \tau_1 \frac{\mathrm{d}}{\mathrm{d}\theta}\right) \left[\frac{1}{2}\left(F - U_m\right) F\right] = \tau_1 \Delta_1 F_\theta.$$

which implies the leading order of region 1 satisfies

$$O(\tau_1) \qquad \left(F - U_m\right) F - \tau_1 \left(2F - U_m + 2\Delta_1\right) F_\theta = 0.$$

We rearrange the leading order equation and integrate to arrive at the implicit solution for region 1, so if we let $2\gamma_1 = U_m - 2\Delta_1$ we have

$$\begin{aligned}
\left(F - U_m\right) F &= 2\tau_1 \left(F - \gamma_1\right) \frac{\mathrm{d}F}{\mathrm{d}\theta}, \\
\implies \tau_1 \frac{\mathrm{d}F}{\mathrm{d}\theta} &= \frac{\left(F - U_m\right) F}{2\left(F - \gamma_1\right)}, \\
\implies \frac{1}{\tau_1} \frac{\mathrm{d}\theta}{\mathrm{d}F} &= \frac{2\left(F - \gamma_1\right)}{\left(F - U_m\right) F}, \\
\implies \frac{1}{\tau_1} \frac{\mathrm{d}\theta}{\mathrm{d}F} &= \frac{1}{U_m}\left\{\frac{U_m + 2\Delta_1}{F - U_m} + \frac{U_m - 2\Delta_1}{F}\right\},
\end{aligned}$$

which integrates to

$$U_m\,\theta_1 = \Big(2\gamma_1 + 4\,\Delta_1\Big)\ \ln\Big|F - U_m\Big| + \Big(2\gamma_1\Big)\ \ln\Big|F\Big|. \tag{4.2.9}$$

where $\theta_1 = \frac{\theta - \hat{\theta}_1}{\tau_1}$. This implicit solution is similar to the asymptotic solution obtained earlier in §3. Here Δ_1 plays a critical role in producing either a single-valued or multivalued solution. Thus, if $\gamma_1 < 0$ or in other words $\Delta_1 > \frac{U_m}{2}$ the solution is then a single-valued solution (type A) which describes the transition from $F = U_m$ to 0. Thus, in this case the second relaxation mode and viscosity have little effect on the shape of the waveform. On the other hand, when $\gamma_1 > 0$ or $\Delta_1 < \frac{U}{2}$ the solution is multivalued since the second boundary condition can't be satisfied as

$$\begin{aligned} &\text{for} \qquad F \to U_m \implies \exp\big(\tfrac{\theta}{U_m\,\tau_1}\big) \to 0 \implies \theta \to -\infty, \\ &\text{for} \qquad F \to 0 \implies \exp\big(\tfrac{\theta}{U_m\,\tau_1}\big) \to 0 \implies \theta \to -\infty. \end{aligned}$$

In this case the second relaxation mode ensures a single-valued solution. A new region is inserted and the wave is then one of the other types (B,C). To determine the waveform for all θ, the $O(\tau_2)$ and $O(\epsilon)$ equations must be considered. We now describe this new region that we name region 2.

Region 2 in Asymptotic Travelling Wave Solution, $\gamma_1 > 0$

If $\gamma_1 > 0$ (i.e $\Delta_1 < \frac{U_m}{2}$), we expect the effect of the second relaxation mode to become significant at some point of the waveform. A second relaxation sub-shock is inserted of width $O(\tau_2)$, so we define the rescaling variable for this region

$$\theta_2 = \frac{\theta}{\tau_2}, \qquad \frac{\mathrm{d}}{\mathrm{d}\theta} = \frac{1}{\tau_2}\,\frac{\mathrm{d}}{\mathrm{d}\theta_2}.$$

Neglecting the $O(\epsilon)$ terms and retaining the $O(\tau_2)$, terms in (4.1.1) to become

$$\Big(\frac{\tau_1}{\tau_2}\frac{\mathrm{d}}{\mathrm{d}\theta_2}-1\Big)\,\Big(1-\frac{\mathrm{d}}{\mathrm{d}\theta_2}\Big)\,\left[\frac{1}{2}\,\Big(F-U_m\Big)\,F\right]=\frac{\tau_1}{\tau_2}\,\Big(\Delta_1+\Delta_2\Big)\,F_{\theta_2\,\theta_2}-\Big(\frac{\tau_1}{\tau_2}\,\Delta_1+\Delta_2\Big)\,F_{\theta_2}.$$

Since $\frac{\tau_1}{\tau_2}\gg 1$ the $O(\frac{\tau_1}{\tau_2})$ terms are then dominant. Therefore, we can write the leading order as

$$O(\frac{\tau_1}{\tau_2})\qquad \frac{\mathrm{d}}{\mathrm{d}\theta_2}\,\Big(1-\frac{\mathrm{d}}{\mathrm{d}\theta_2}\Big)\,\left[\Big(F-U_m\Big)\,F\right]-2\,\Big(\Delta_1+\Delta_2\Big)\,F_{\theta_2\,\theta_2}+2\,\Delta_1\,F_{\theta_2}=0, \tag{4.2.10}$$

which integrates to

$$\Big(1-\frac{\mathrm{d}}{\mathrm{d}\theta_2}\Big)\,\left[\Big(F-U_m\Big)\,F\right]-2\,\Big(\Delta_1+\Delta_2\Big)\,F_{\theta_2}+2\,\Delta_1\,F=C. \tag{4.2.11}$$

Using the boundary condition (4.2.2) $F\to 0$ as $\theta_2\to\infty$ fixes the integration constant at $C=0$. The leading order term of this solution is

$$\Big(F-U_m+2\,\Delta_1\Big)\,F-\Big(2F-U_m+2\,\Delta_1+2\,\Delta_2\Big)\,F_\theta=0.$$

We solve for the leading order solution in region 2 in an implicit form,

$$\begin{aligned}
F\,\Big(F-2\,\gamma_1\Big) &= 2\,\Big(F-\gamma_2\Big)\frac{\mathrm{d}F}{\mathrm{d}\theta_2},\\
\Longrightarrow\ \frac{\mathrm{d}F}{\mathrm{d}\theta_2} &= \frac{F\,\Big(F-2\,\gamma_1\Big)}{2\,\Big(F-\gamma_2\Big)},\\
\Longrightarrow\ \frac{\mathrm{d}\theta_2}{\mathrm{d}F} &= \frac{2\,\Big(F-\gamma_2\Big)}{F\,\Big(F-2\,\gamma_1\Big)},\\
\Longrightarrow\ \frac{\mathrm{d}\theta_2}{\mathrm{d}F} &= \frac{1}{2\gamma_1}\left\{\frac{U_m-2\Delta_1+2\Delta_2}{F-2\,\gamma_1}+\frac{U_m-2\Delta_1-2\Delta_2}{F}\right\}.
\end{aligned}$$

Integrating with respect to F gives the implicit form of solution in Region 2

$$2\gamma_1\,\Big(\theta_2-\hat{\theta}_2\Big)=\Big(2\gamma_2+4\Delta_2\Big)\,\ln\Big|F-2\,\gamma_1\Big|+\Big(2\gamma_2\Big)\,\ln\Big|F\Big|. \tag{4.2.12}$$

The same condition on γ_1 addressed earlier in region 1 applies to γ_2. The case $\gamma_2 < 0$ corresponds to a single-valued solution. This solution describes a transition from $F = 2\gamma_1$ to 0 and we call type B shock wave. But if $\gamma_2 > 0$, or we can say $\Delta_1 + \Delta_2 < \frac{U_m}{2}$, then the limiting values becomes

$$\text{for} \qquad F \to 2\gamma_1 \implies \exp\left(\frac{2\gamma_1\theta}{\tau_2}\right) \to 0 \implies \theta \to -\infty,$$

$$\text{for} \qquad F \to 0 \implies \exp\left(\frac{2\gamma_1\theta}{\tau_2}\right) \to 0 \implies \theta \to -\infty,$$

which does not satisfy the boundary condition at $\theta \to \infty$, this rather corresponds to a multi-valued solution. In this case, the second relaxation mode is insufficient to support the transition from $F = 2\gamma_1$ to $F = 0$. Hence, correction terms of $O(\epsilon)$ must be considered and an additional region arises and the wave is of a new type (type C).

Region 3 in Asymptotic Travelling Wave Solution, $\gamma_1, \gamma_2 > 0$

A type C shock wave occurs when $\Delta_1 + \Delta_2 < \frac{U_m}{2}$ consisting of three regimes. The first two (region 1,2) are introduced earlier and controlled by the first and second relaxation modes while region 3 is controlled by the thermoviscous effects. To describe the structure of region 3 which is a viscous sub-shock we first define the re-scaling

$$\theta_3 = \frac{\theta}{\epsilon}, \qquad \frac{\mathrm{d}}{\mathrm{d}\theta} = \frac{1}{\epsilon}\frac{\mathrm{d}}{\mathrm{d}\theta_3}. \tag{4.2.13}$$

Thus, equation (4.1.1) reduces to

$$\left(\frac{\tau_1}{\epsilon}\frac{\mathrm{d}}{\mathrm{d}\theta_3} - 1\right)\left(\frac{\tau_2}{\epsilon}\frac{\mathrm{d}}{\mathrm{d}\theta_3} - 1\right)\left[F_{\theta_3} - \frac{1}{2}\left(F - U_m\right)F\right]$$

$$= \frac{\tau_1\,\tau_2}{\epsilon^2}\left(\Delta_1 + \Delta_2\right)F_{\theta_3\theta_3} - \left(\frac{\tau_1}{\epsilon}\Delta_1 + \frac{\tau_2}{\epsilon}\Delta_2\right)F_{\theta_3}. \tag{4.2.14}$$

Since $\epsilon \ll \tau_2 \ll \tau_1 \ll 1$, then we can say the $O(\frac{\tau_1 \tau_2}{\epsilon^2})$ is the dominant term as $\frac{\tau_1 \tau_2}{\epsilon^2} \gg \frac{\tau_1}{\epsilon} \gg \frac{\tau_2}{\epsilon}$. Thus, we consider only the leading order of the above equation

$$O(\frac{\tau_1\,\tau_2}{\epsilon^2}) \qquad \frac{\mathrm{d}^2}{\mathrm{d}{\theta_3}^2}\left[F_{\theta_3} - \frac{1}{2}\Big(F - U_m\Big)\,F\right] - \Big(\Delta_1 + \Delta_2\Big)\,F_{\theta_3\,\theta_3} = 0.$$

We begin deriving the solution for region 3 sub-shock by first integrating twice the leading order with respect to θ_3 and using the boundary condition (4.2.1) to obtain

$$\frac{\mathrm{d}F}{\mathrm{d}\theta_3} - \frac{1}{2}\,F\,\Big(F - U_m + 2\,\Delta_1 + 2\,\Delta_2\Big) = 0,$$

rearranging this equation for integration

$$\begin{aligned}
\frac{\mathrm{d}F}{F\,\Big(F - 2\,\gamma_2\Big)} &= \frac{1}{2}\,\mathrm{d}\theta_3, \\
\Longrightarrow \int\left[\frac{1}{F - 2\,\gamma_2} - \frac{1}{F}\right]\mathrm{d}F &= \frac{2\,\gamma_2}{2}\int \mathrm{d}\theta_3, \\
\Longrightarrow \ln\left(\frac{2\,\gamma_2 - F}{F}\right) &= \gamma_2\,(\theta_3 - \hat{\theta}_3), \qquad 0 < F < \gamma_2. \quad (4.2.15)
\end{aligned}$$

where γ_2 is defined in equation (4.2.8). We define $z = \gamma_2\,(\theta_3 - \hat{\theta}_3)$ and then apply the exponential function to (4.2.15) to arrive at

$$\begin{aligned}
F &= \frac{2\,\gamma_2}{1 + \exp(z)}, \\
&= \gamma_2\,\frac{2\exp(-\frac{z}{2})}{\exp(-\frac{z}{2}) + \exp(\frac{z}{2})}, \\
&= \gamma_2\,\left[1 - \frac{\exp(\frac{z}{2}) - \exp(-\frac{z}{2})}{\exp(\frac{z}{2}) + \exp(-\frac{z}{2})}\right].
\end{aligned}$$

Using the definition of the hyperbolic tangent function $\tanh z$ the shock can be expressed as

$$F = \gamma_2\,\Big(1 - \tanh y\Big), \qquad (4.2.16)$$

where the variable y is

$$y = \frac{\gamma_2}{2\,\epsilon}\left(\theta_3 - \epsilon\,\hat{\theta}_3\right). \tag{4.2.17}$$

Taking $\theta_3 \to -\infty$ gives us the amplitude of the inner sub-shock which is

$$\lim_{\theta_3\to-\infty} F = \lim_{\theta_3\to-\infty} \gamma_2\,\left[1 - \tanh\left(\frac{\gamma_2}{2\,\epsilon}\big(\theta - \epsilon\,\hat{\theta}_3\big)\right)\right] = 2\,\gamma_2. \tag{4.2.18}$$

Thus, we can say Region 3 describes the change of the solution from $F = 2\gamma_2$ to 0 with width $O(2\epsilon/\gamma_2)$.

In type C wave we can choose the region 3 viscous sub-shock to be centred at $\theta_3 = 0$ (i.e $\hat{\theta}_3 = 0$) and then the values of $\hat{\theta}_1$ and $\hat{\theta}_2$ can be determined by matching at leading order. As $\theta_3 \to -\infty$, $F \to 2\gamma_2$, then the region 2 solution (4.2.12) controlled by the second relaxation mode, matches at leading order to the viscous region 3 solution (4.2.16), if $\hat{\theta}_2$ is given by

$$\hat{\theta}_2 = -\frac{\tau_2}{2\gamma_1}\left[\Big(2\gamma_2 + 4\Delta_2\Big)\ \ln\Big(2\,\gamma_1 - 2\gamma_2\Big) + \Big(2\gamma_2\Big)\ \ln\Big(2\gamma_2\Big)\right]. \tag{4.2.19}$$

Similarly, for the region 2 solution governed by the second relaxation mode, as $\theta_2 \to -\infty$, $F \to 2\gamma_1$, the region 2 solution then matches to the region 1 solution (4.2.9) governed by the first relaxation mode, if $\hat{\theta}_1$ is given by

$$\hat{\theta}_1 = -\frac{\tau_2}{U_m}\left[\Big(2\gamma_1 + 4\,\Delta_1\Big)\ \ln\Big(U_m - 2\gamma_1\Big) + \Big(2\gamma_1\Big)\ \ln\Big(2\gamma_1\Big)\right]. \tag{4.2.20}$$

For the type B case, where the viscous sub-shock is absent, the region 2 solution associated with the second relaxation mode (4.2.12) is centred at $\theta = 0$ by choosing

$$\hat{\theta}_2 = -\frac{\tau_2}{2\gamma_1}\left[\Big(2\gamma_2 + 4\Delta_2\Big)\ \ln\Big(2\,\gamma_1 - \gamma_1\Big) + \Big(2\gamma_2\Big)\ \ln\Big(\gamma_1\Big)\right]. \tag{4.2.21}$$

The first relaxation shock (4.2.9) then matches at leading order to this solution using (4.2.20).

Summary

We have found the travelling wave asymptotic solutions with two relaxation modes. We showed how these two relaxation modes have an effect on the shock front to produce three different forms of solutions, depending on the values of the relaxation parameters $\Delta_{1,2}$.

Assuming that $\epsilon \ll \tau_2 \ll \tau_1$ the travelling step wave of amplitude U_m takes three different types A,B and C depending on the values of the relaxation parameters Δ_1 and Δ_2. In type A solution, the shock wave forms when the first relaxation mode is $2\Delta_1 > U_m$, this wave is fully-dispersed for the first relaxation mode. This type of shock front consists of one region (Region 1) of width $O(\tau_1)$ and describes the transition from $F = U_m$ to $F = 0$. The second class of solutions that we named type B, occurs when $2\Delta_1 < U_m < 2\big(\Delta_1 + \Delta_2\big)$. This shock is covered by two regions, region 1 is the transition from $F = U_m$ to $F = U_m - 2\Delta_1$ governed by the first relaxation mode. While region 2 governed by the second relaxation mode, has width $O(\tau_2)$ with amplitude $F = U_m - 2\Delta_1$. Type B solution describes an outer partially-dispersed shock associated with the first relaxation mode and an inner fully-dispersed shock associated with the second relaxation mode. Finally, type C which is the complicated multilayer solution, consisting of three regions when $2\big(\Delta_1 + \Delta_2\big) < U_m$. The first region is controlled by the first relaxation mode and describes the transition from $F = U$ to $F = U - 2\Delta_1$. While the second region is controlled by the second relaxation mode describes from $F = U_m - 2\Delta_1$ to $F = U_m - 2\Delta_1 - 2\Delta_2$. The third layer is a viscous sub-shock of amplitude $F = U_m - 2\Delta_1 - 2\Delta_2$ and has width $O(2\epsilon/\gamma_2)$. Type C solution describes two partially-dispersed shocks governed by the first and second relaxation modes respectively and a viscous sub-shock.

In figure 4.2.1 we plotted a schematic illustration of Type C shock wave to show the three regions governing the solution.

In §4.2.3 we compare the waveform of the numerical solutions for a travelling

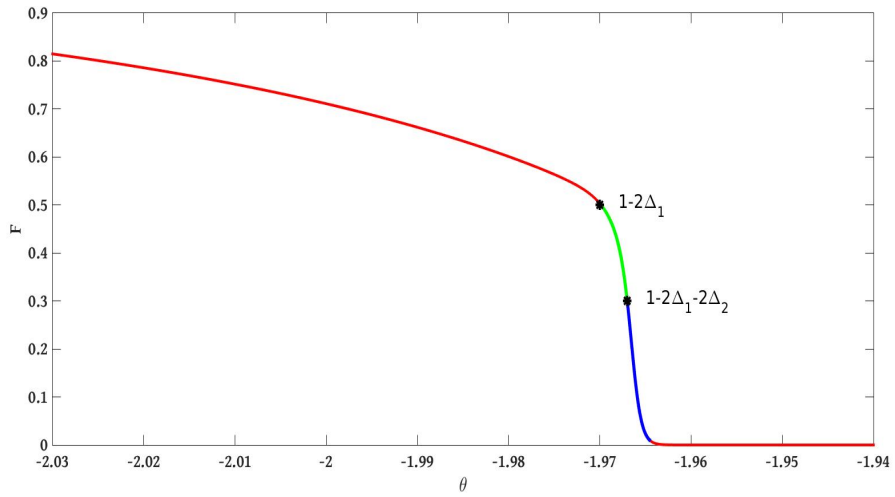

Figure 4.2.1: Schematic illustration of Type C travelling wave solution with two relaxation modes. The wave is of unit amplitude in this case and so a type C solution satisfies the condition $\Delta_1+\Delta_2 < \frac{1}{2}$, and consists of three regions: Region 1(red) with transition from 1 to $1-2\Delta_1$; Region 2 (green) is a transition from $1-2\Delta_1$ to $1-2\Delta_1-2\Delta_2$ of width τ_2 ; and region 3 is a thermoviscous sub-shock (blue).

wave to these asymptotic regions. However another means of comparison is the maximum negative wave slope (MNS). Therefore, in the next section we look for the asymptotic maximum negative slope AMNS for the three shock types.

4.2.2 Asymptotic Values of Maximum Negative Slope

Maximum negative slope for Type A

We first investigate $\gamma_1 < 0$ which is type A, in which region 1 is present. The slope is defined as

$$\begin{aligned} S &= \frac{\mathrm{d}F}{\mathrm{d}\theta} \\ &= \frac{1}{2\,\tau_1} \cdot \frac{\Big(F - U_m\Big)\,F}{F - \gamma_1}. \end{aligned} \tag{4.2.22}$$

Type A solutions are similar to the fully-dispersed shock for one relaxation mode, the maximum negative slope was deduced in section 3.4.6. Thus, the maximum negative slope for type A solutions at leading order when $\gamma_1 < 0$ or when $\Delta_1 > \frac{U_m}{2}$ is

$$\max(S)_A = -\frac{U_m}{\tau_1}\,\Big(\widehat{\Delta}_1 - \sqrt{\widehat{\Delta}_1^2 - \frac{1}{4}}\,\Big), \qquad \text{where} \quad \widehat{\Delta}_1 = \frac{\Delta_1}{U_m}. \tag{4.2.23}$$

Maximum negative slope for Type B

We now consider $\gamma_1 > 0$ the solution is of Type B in which regions 1,2 are present. In the region $2\gamma_1 < F < 1$ the slope is given by (4.2.23), while in Region 2, $0 < F < 2\gamma_1$, the slope is given by

$$S = \frac{1}{2\,\tau_2}\,\frac{F\,\Big(F - 2\gamma_1\Big)}{F - \gamma_2}. \tag{4.2.24}$$

Since $\tau_2 \ll \tau_1$ the maximum negative slope occurs in region 2, so we suppose the solution reaches its maximum slope at $F = F_s$. To locate F_s we look when the

second derivative of F is zero. We now look to see where $\frac{\mathrm{d}S}{\mathrm{d}\theta} = 0$

$$\begin{aligned}
\frac{\mathrm{d}S}{\mathrm{d}\theta} &= \frac{\mathrm{d}S}{\mathrm{d}F} . \frac{\mathrm{d}F}{\mathrm{d}\theta} \\
&= \frac{1}{2\,\tau_2} \frac{1}{\Big(F-\gamma_2\Big)^2} \Big[2\Big(F-\gamma_1\Big)\Big(F-\gamma_2\Big) - F\Big(F-2\gamma_1\Big)\Big] F_\theta \\
&= \frac{S}{2\,\tau_2\Big(F-\gamma_2\Big)^2} \Big[2\,F^2 - 2\Big(\gamma_1+\gamma_2\Big)\,F + 2\gamma_1\gamma_2 - F^2 + 2\,\gamma_1 F\Big] \\
&= \frac{S}{2\,\tau_2\Big(F-\gamma_2\Big)^2} \Big[F^2 - 2\,\gamma_2 F + 2\gamma_1\gamma_2\Big] \\
&= \frac{S}{2\,\tau_2\Big(F-\gamma_2\Big)^2} \Big[F^2 - 2\,\gamma_2 F + {\gamma_2}^2 + 2\gamma_1\gamma_2 - {\gamma_2}^2\Big] \\
&= \frac{S}{2\,\tau_2\Big(F-\gamma_2\Big)^2} \Big[\Big(F-\gamma_2\Big)^2 - \gamma_2\Big(\gamma_2-2\gamma_1\Big)\Big]. \qquad (4.2.25)
\end{aligned}$$

Next we write

$$\gamma_2\Big(\gamma_2-2\gamma_1\Big) = \Big(\gamma_1-\Delta_2\Big)\Big(\gamma_1-\Delta_2-2\gamma_1\Big) = \Big(\Delta_2+\gamma_1\Big)\Big(\Delta_2-\gamma_1\Big) = {\Delta_2}^2 - {\gamma_1}^2,$$

and equation (4.2.25) is then

$$\frac{\mathrm{d}S}{\mathrm{d}\theta} = \frac{F\Big(F-2\gamma_1\Big)}{2\,\tau_2\Big(F-\gamma_2\Big)^3} \Big[\Big(F-\gamma_2\Big)^2 - \Big({\Delta_2}^2 - {\gamma_1}^2\Big)\Big]. \qquad (4.2.26)$$

Equating this expression to zero leads to four roots. The first two roots $F_s = 0$ and $F_s = 2\gamma_1$ are outside Region 2, $0 < F < 2\gamma_1$. The other two roots are $F_s = \gamma_2 \pm \sqrt{{\Delta_2}^2 - {\gamma_1}^2}$. Now if $\gamma_2 < 0$ where $\gamma_2 = \gamma_1 - \Delta_2$, then $\Delta_2 > \gamma_1$ and hence the two roots are real. We chose the positive root as $F_s > 0$ and hence the maximum value is at

$$F_s = \gamma_2 + \sqrt{{\Delta_2}^2 - {\gamma_1}^2}. \qquad (4.2.27)$$

Substituting $F = F_s$ into (4.2.24) gives

$$\begin{aligned} S_B(F_s) &= \frac{1}{2\,\tau_2}\,\frac{F\Big(F-2\gamma_1\Big)}{F-\gamma_2}\,\Bigg|_{F=F_s} \\ &= \frac{1}{2\,\tau_2\,\sqrt{{\Delta_2}^2-{\gamma_1}^2}}\,\Big[\gamma_2+\sqrt{{\Delta_2}^2-{\gamma_1}^2}\Big]\,\Big[\Big(\gamma_2-2\gamma_1\Big)+\sqrt{{\Delta_2}^2-{\gamma_1}^2}\,\Big] \\ &= \frac{1}{2\,\tau_2\,\sqrt{{\Delta_2}^2-{\gamma_1}^2}}\,\Big[\gamma_2\Big(\gamma_2-2\gamma_1\Big)+\Big({\Delta_2}^2-{\gamma_1}^2\Big)+2\Big(\gamma_2-\gamma_1\Big)\sqrt{{\Delta_2}^2-{\gamma_1}^2}\,\Big] \\ &= \frac{1}{2\,\tau_2\,\sqrt{{\Delta_2}^2-{\gamma_1}^2}}\,\Big[2\Big({\Delta_2}^2-{\gamma_1}^2\Big)-2\Delta_2\sqrt{{\Delta_2}^2-{\gamma_1}^2}\,\Big]. \end{aligned}$$

Thus, the asymptotic prediction of the maximum negative slope at leading order for type B solutions is

$$\max(S)_B = -\frac{U_m}{\tau_2}\,\Big(\widehat{\Delta}_2-\sqrt{\widehat{\Delta}_2^2-\widehat{\gamma}_1^2}\,\Big), \tag{4.2.28}$$

where $\widehat{\gamma}_1 = \frac{\gamma_1}{U_m} = \frac{1}{2}\big(1-\widehat{\Delta}_1\big)$ and $\widehat{\Delta}_2 = \frac{\Delta_2}{U_m}$ are the effective relaxation parameters.

Maximum negative slope for Type C

The third predicted maximum negative slope is for the type C solutions where $\gamma_2 > 0$. Three regions are present with maximum slope of order $(1/\tau_1)$ in region 1 defined in (4.2.23) and of order $(1/\tau_2)$ in region 2 in equation (4.2.28). However, the maximum negative slope occurs in region 3, since the MNS in this region is $O(1/\epsilon)$ and $\epsilon \ll \tau_2 \ll \tau_1$. Region 3 is expressed as a Taylor shock, so it is very similar for the maximum negative slope we deduced earlier in §3.4.6 except in this case the viscous shock will have the amplitude $2\gamma_2$

$$\max(S)_C = -\frac{{\gamma_2}^2}{2\epsilon}. \tag{4.2.29}$$

Since $\gamma_2 = \frac{U_m}{2} - \Delta_1 - \Delta_2$, multiplying and dividing by ${U_m}^2$ the maximum negative slope S_c becomes

$$\max(S)_C = -\frac{{U_m}^2}{{U_m}^2} \cdot \frac{{\gamma_2}^2}{2\epsilon} = -\frac{{U_m}^2}{U_m^2} \cdot \frac{\left(\frac{U_m}{2} - \Delta_1 - \Delta_2\right)^2}{2\epsilon} \tag{4.2.30}$$

$$= -\frac{U_m}{2\epsilon/U_m} \cdot \left(\frac{1}{2} - \frac{\Delta_1}{U_m} - \frac{\Delta_2}{U_m}\right)^2. \tag{4.2.31}$$

Thus, the maximum negative slope for Type C solutions at leading order is

$$\max(S)_C = -\frac{U_m\,{\widehat{\gamma}_2}^2}{2\widehat{\epsilon}}, \tag{4.2.32}$$

where

$$\widehat{\gamma}_2 = \frac{\gamma_2}{U_m}, \qquad \widehat{\Delta}_1 = \frac{\Delta_1}{U_m}, \qquad \widehat{\Delta}_2 = \frac{\Delta_2}{U_m}, \qquad \widehat{\epsilon} = \frac{\epsilon}{U_m}, \tag{4.2.33}$$

are the effective relaxation and viscous dissipation that change with amplitude.

To conclude, we presented this asymptotic analysis to obtain the maximum negative slope for the three types of shock wave, shock A, B and C

$$\max(S)_A = -\frac{U_m}{\tau_1}\left(\widehat{\Delta}_1 - \sqrt{\widehat{\Delta}_1^2 - \frac{1}{4}}\right), \tag{4.2.34}$$

$$\max(S)_B = -\frac{U_m}{\tau_2}\left(\widehat{\Delta}_2 - \sqrt{\widehat{\Delta}_2^2 - \widehat{\gamma}_1^2}\right), \tag{4.2.35}$$

$$\max(S)_C = -\frac{U_m\,{\widehat{\gamma}_2}^2}{2\widehat{\epsilon}}. \tag{4.2.36}$$

These findings will be used in §4.3.3 in comparisons with the numerical evolving wave form. Next we illustrate the numerical results for the travelling wave ODE.

4.2.3 Numerical Solution of Travelling Wave

For the study of the numerical solution of travelling waves we adapted the method described in §3.4.7. We define the solution in the limit of large positive X where $X = -\theta$ so that a relationship between F and F_θ is obtained in the linearised shock tail as $X \to \infty$. This is then used as the initial conditions for a Runge-Kutta solver of the full equation to obtain the wave form for smaller θ. If we supposed $X = -\theta$ the boundary conditions become $F \to 0$ as $X \to -\infty$ and $F \to 1$ when $X \to \infty$. We will assume the solution to be

$$F^- = \delta\, \mathrm{e}^{\mu\, X}, \tag{4.2.37}$$

where the coefficient $0 < \delta \ll 1$ and $\mu > 0$. The first and second derivatives are $T = \big(F^-\big)_X = \mu\, \delta\, \mathrm{e}^{\mu\, X}$ and $H = \big(F^-\big)_{XX} = \mu^2\, \delta\, \mathrm{e}^{\mu\, X}$, the functions F^- , T and H satisfy the equivalent first order system

$$\frac{\mathrm{d}F^-}{\mathrm{d}X} = T, \qquad \frac{\mathrm{d}T}{\mathrm{d}X} = H, \tag{4.2.38}$$

$$\begin{aligned} \frac{\mathrm{d}H}{\mathrm{d}X} = \frac{1}{\epsilon\tau_1\tau_2} & \left\{ \frac{1}{2}\Big(1 - F^-\Big)\, F^- - \big(\tau_1 + \tau_2\big) F^-\, T - \tau_1\, \tau_2 \Big(T^2 + F^-\, H\Big) \right. \\ & - \Big(\epsilon - \frac{1}{2}\big(\tau_1 + \tau_2\big) + \tau_1\, \Delta_1 + \tau_2\, \Delta_2\Big) T \\ & - \left. \Big(\epsilon\big(\tau_1 + \tau_2\big) - \tau_1\, \tau_2\, \big(\frac{1}{2} - \Delta_1 - \Delta_2\big)\Big) H \right\}. \end{aligned} \tag{4.2.39}$$

We require three initial values:

$$F^-(0) = \delta, \qquad T(0) = \delta\ \mu, \qquad H(0) = \delta\ \mu^2. \tag{4.2.40}$$

The system (4.2.38),(4.2.39) with the initial conditions (4.2.40) correspond to the work of Pierce and Kang [73]. We now investigate if the ODE has a real positive root. Let us recall the earlier deduced travelling wave defined with respect to X

and the dimensionless amplitude is fixed at $U_m = 1$

$$\begin{aligned}\Big(1+\tau_1\frac{\mathrm{d}}{\mathrm{d}X}\Big)\Big(1+\tau_2\frac{\mathrm{d}}{\mathrm{d}X}\Big)\Big[\frac{F^-}{2}\Big(1-F^-\Big)-\epsilon\,\big(F^-\big)_X\Big] &= \tau_1\,\tau_2\Big(\Delta_1+\Delta_2\Big)\,{F^-}_{XX}\\ &+ \Big(\tau_1\,\Delta_1+\tau_2\,\Delta_2\Big)\,{F^-}_X.\end{aligned}$$

Substituting our assumed solution (4.2.37) and linearising the system gives

$$\Big(1+\tau_1\,\mu\Big)\Big(1+\tau_2\;\mu\Big)\Big[\frac{1}{2}-\epsilon\,\mu\Big]=\tau_1\,\tau_2\Big(\Delta_1+\Delta_2\Big)\,\mu^2+\Big(\tau_1\,\Delta_1+\tau_2\,\Delta_2\Big)\,\mu.$$

We now follow the procedure of Pierce & Kang [73] to show that the cubic equation for μ has only one real positive root and the other two roots are real negative roots.

Rearranging the cubic in μ we find that

$$\begin{aligned}\frac{1}{2} &= \epsilon\,\mu+\frac{1}{\big(1+\tau_1\,\mu\big)\,\big(1+\tau_2\;\mu\big)}\Big[\Delta_1\,\tau_1\,\mu\big(1+\mu\,\tau_2\big)+\Delta_2\,\tau_2\,\mu\big(1+\mu\,\tau_1\big)\Big],\\ \frac{1}{2} &= \epsilon\,\mu+\Delta_1\,\frac{\tau_1\,\mu}{1+\tau_1\,\mu}+\Delta_2\,\frac{\tau_2\,\mu}{1+\tau_2\,\mu}, \qquad (4.2.41)\\ &= f(\mu).\end{aligned}$$

We can see that $f(0)=0$, and $f(\mu)\to\infty$ as $\mu\to\infty$, this is because the terms $\tau_i\,\mu/(1+\tau_i\mu)$ are monotonically increasing for increasing μ. Therefore, the cubic equation has only one positive root μ_+ such that $f(\mu_+)=\frac{1}{2}$. For the other roots, they are either real negative roots or a complex conjugate pair. To look for these roots we can apply Newton's method or we can sketch the cubic equation. The cubic polynomial for μ is

$$g(\mu)=\epsilon\,\tau_1\,\tau_2\,\mu^3+\Big[\epsilon\,\Big(\tau_1+\tau_2\Big)-\tau_1\,\tau_2\,\gamma_2\Big]\mu^2+\Big[\epsilon-\tau_1\,\gamma_1-\tau_2\Big(\gamma_2+\Delta_1\Big)\Big]\mu-\frac{1}{2} \qquad (4.2.42)$$

To look for the roots of $g(\mu)=0$ we sketch $g(\mu)$ for the three wave types defined in §4.2.1, type A when $\gamma_1<0$, type B for $\gamma_1>0$ and $\gamma_2<0$ and thirdly type C when $\gamma_2>0$. For all parameter values considered, we found that we

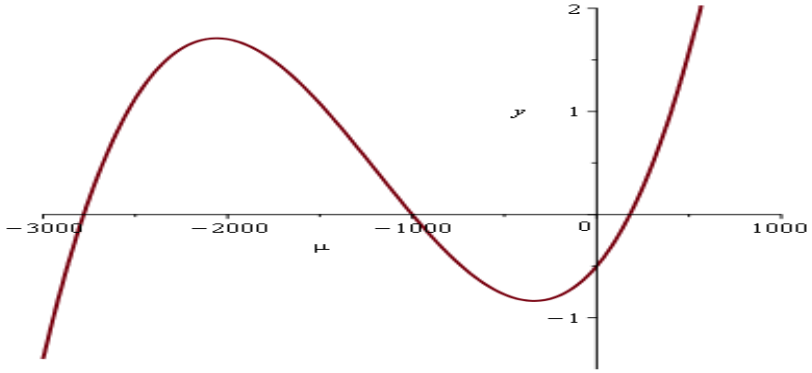

Figure 4.2.2: Plot of $g(\mu)$ defined in (4.2.42) Type A solutions $\gamma_1 < 0$ taking the parameters to be $\Delta_1 = 0.75$, $\Delta_2 = 0.00$, $\tau_1 = 0.01$, $\tau_2 = 0.001$ and viscosity $\epsilon = 0.0001$.

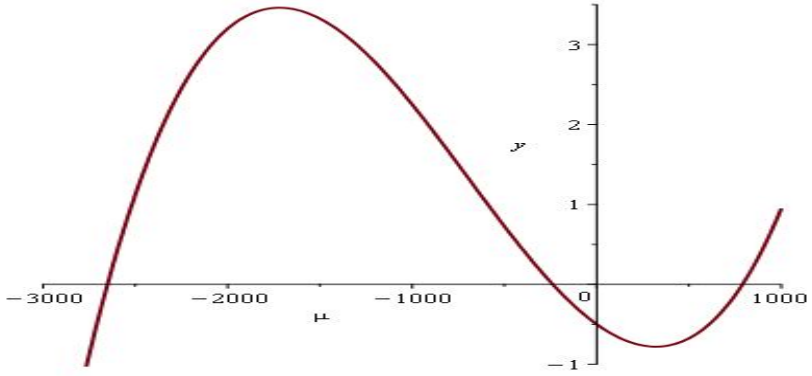

Figure 4.2.3: Plot of $g(\mu)$ defined in (4.2.42) for Type B solutions $\gamma_1 > 0$ and $\gamma_2 < 0$ taking the parameters to be $\Delta_1 = 0.35$, $\Delta_2 = 0.25$, $\tau_1 = 0.01$, $\tau_2 = 0.001$ and viscosity $\epsilon = 0.0001$.

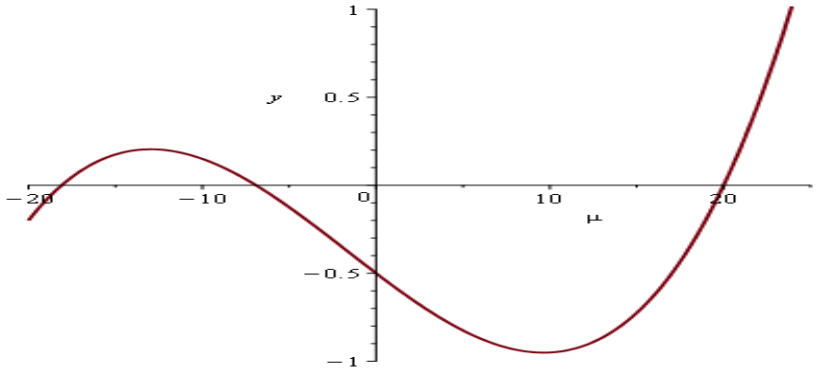

Figure 4.2.4: Plot of $g(\mu)$ defined in (4.2.42) for Type C solutions $\gamma_2 > 0$, taking the parameters to be $\Delta_1 = 0.25$, $\Delta_2 = 0.10$, $\tau_1 = 0.2$, $\tau_2 = 0.1$ and viscosity $\epsilon = 0.01$.

have three real roots, consisting of a pair of negative roots and one positive root (see figures 4.2.2, 4.2.3, 4.2.4). We will not proceed to verify analytically that

there are two negative real roots for all parameters as this is not needed for the following results.

Figures 4.2.2, 4.2.3, 4.2.4 show plots of $g(\mu)$ defined in (4.2.42). First figure 4.2.2 is an example of type A shock waves $\gamma_1 < 0$ the positive eigenvalue was $\mu_+ \approx 179.9$. Figures 4.2.3, 4.2.4 are for type B, and C travelling waves with positive eigenvalues $\mu_+ \approx 790$ and $\mu_+ = 20$ respectively. We noticed that the positive root μ_+ in plot 4.2.2 is smaller compared to the value in plot 4.2.3, we will see later how this value shows in the tail in front the shock. We now focus on how the value of the positive root varies with the parameters.

In figure 4.2.5 we plot the relation between the second relaxation mode Δ_2 and the positive eigenvalue μ_+ for a fixed values of the other parameters. We can say that the root μ_+ is inversely proportional to Δ_2. As Δ_2 increases μ decreases slightly which means that the shock tail will be longer. Notice that for $\Delta_2 = 0$ it becomes the case of single relaxation mode where equation (4.2.42) becomes a quadratic equation for μ_+. In that case $\mu_+ = 179.9$ which is validated by the quadratic equation (3.4.63). We can also see that $\mu = 179.9$ matches the positive root in figure 4.2.2.

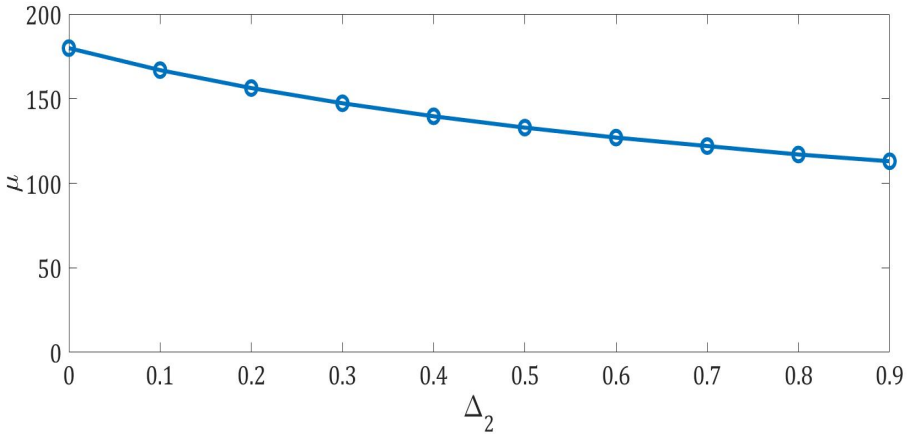

Figure 4.2.5: The real positive eigenvalue μ_+ against the second relaxation mode Δ_2 for the set of relaxation parameters $\Delta_1 = 0.75$, $\tau_1 = 0.01$, $\tau_2 = 0.001$ and viscosity $\epsilon = 0.0001$.

In figures 4.2.6, 4.2.7 and 4.2.8 we demonstrate the numerical representation of travelling wave covering the three different types A,B,C respectively. For a given set of relaxation parameters Δ_1, Δ_2, τ_1, τ_2 and viscosity ϵ, we solve $g(\mu) = 0$ given in equation (4.2.42) to find its real positive root then substitute this root in the three initial conditions (4.2.40) to solve the system of ODE's (4.2.38), (4.2.39) by a Matlab built-in ODE solver ode23tb, fixing the beginning and end points of the interval $[0, X_{\text{end}}]$, and the relative and absolute error tolerances are setted at default.
These plots are taken for the set of parameters $\tau_1 = 0.1$, $\tau_2 = 10^{-3}$ and $\epsilon = 10^{-5}$ for various $\Delta_{1,2}$. The arbitrary horizontal shift is chosen so that the maximum negative slope MNS is fixed at $\theta = 0$.

Figure 4.2.6 shows a type A wave, in which both $\gamma_1, \gamma_2 < 0$ as described in §4.2.1. This shock type corresponds to the first relaxation mode controlling the transition from $F = 1$ to $F = 0$. Fixing the first relaxation $\Delta_1 = 0.60$, this shock is totally controlled by the first relaxation mode and the other mode does not have that much of impact on the shock front except in the shock tail area. As the value of Δ_2 increases the value of the positive root μ_+ decreases resulting a longer tail for the fully dispersed shock. This shock has width of order τ_1, so a smaller value of τ_1 results a narrower shock. In figure 4.2.6 (a) we plotted the type A shock wave with two relaxation modes (red) for $\Delta_2 = 0$, together with the shock wave for one relaxation mode (green) described earlier in §3.4.7. The reason for the comparison is to verify the validity of the ODEs (4.2.38), (4.2.39), and we can see in 4.2.6 (a) the two solutions are indistinguishable.

Figure 4.2.7 where $\gamma_1 > 0$ and $\gamma_2 < 0$ represents type B wave. The solution describes the change of solution from $F = 1$ to $2\gamma_1$ in region 1 which is controlled by the first relaxation mode and region 2 controlled by the second relaxation mode is the change from $F = 2\gamma_1$ to 0. Comparing to type A shock we see that the type B shock wave is narrower, due to the existence of the inner

shock of width $O(\tau_2)$. For this type of shock (type B), we plotted the wave for $\Delta_1 > \Delta_2$, in plot 4.2.7(a) and $\Delta_1 < \Delta_2$ in plot 4.2.7(b), we see that for the fixed value of Δ_1 when $\Delta_1 < \Delta_2$ the inner shock becomes slightly wider.

Type C shock illustrated in figure 4.2.8 for the wave that is propagating with frequency higher than both relaxation frequencies Δ_1 and Δ_2 (i.e. $\gamma_1, \gamma_2 > 0$). Thus, this thin relaxing shock will be consisting of three regions. The shock profile begins with region 3, the viscous sub-shock which describes the transition $0 < F < 2\gamma_2$. Followed by region 2 in which the second relaxation mode becomes important where F transits from $2\gamma_1$ to $2\gamma_2$. Finally region 1 which is the change $1 < F < 2\gamma_1$, the wave in this region is dispersed due to the first relaxation mode. We plotted for the two cases Δ_1 $\Delta_1 > \Delta_2$ in plot(a) and $\Delta_1 < \Delta_2$ in plot(b) which represents the cases when the value of the first relaxation frequency is higher or lower than that for the second relaxation mode. So, for fixed $\Delta_1 = 0.15$, we took two values of $\Delta_2 = 0.10, 0.20$. We see that region 1 is unchanged, however, region 2 is changed, since for smaller Δ_2 as figure 4.2.8 (a) a larger adjustment required for the velocity. Thus, we see the viscous sub-shock (region 3) is of amplitude higher than that in figure 4.2.8 (b).

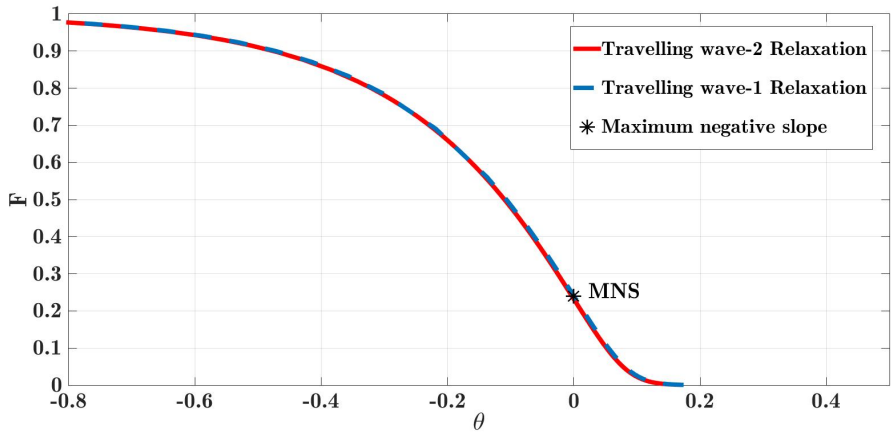

(a) $\Delta_1 = 0.60 \quad \Delta_2 = 0.00$

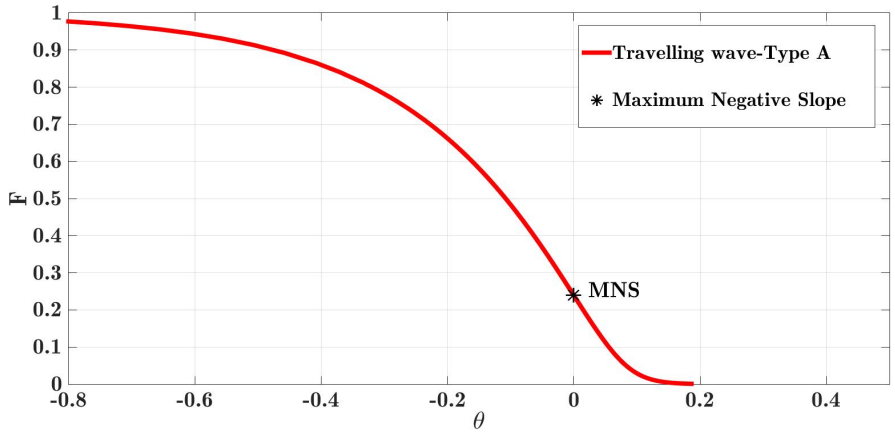

(b) $\Delta_1 = 0.60 \quad \Delta_2 = 0.40$

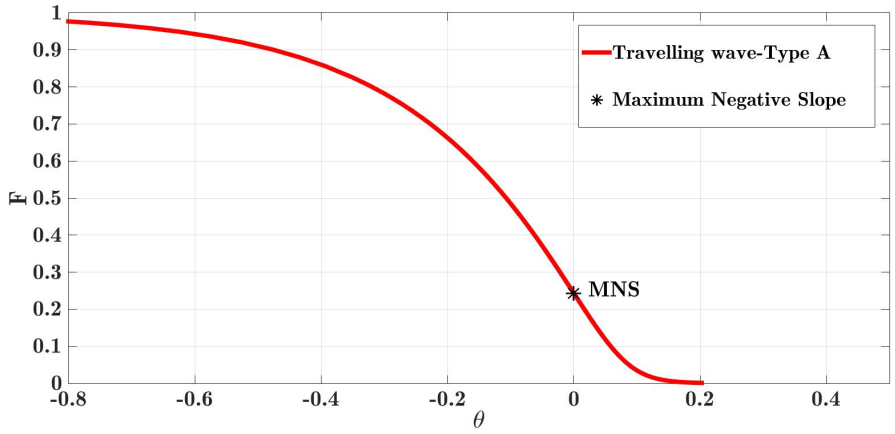

(c) $\Delta_1 = 0.60 \quad \Delta_2 = 0.80$

Figure 4.2.6: Plots (b), (c) show the numerical solution of type A travelling shock wave with two relaxation modes. Type A travelling wave is a fully-dispersed shock wave and the first relaxation mode $\Delta_1 = 0.60$ and $\tau_1 = 0.1$ has a full control of the shock wave. The second relaxation time is fixed at $\tau_2 = 10^{-3}$ for various values of Δ_2 and viscosity is at $\epsilon = 10^{-5}$. In plot (a) the second relaxation mode is neglected, type A solution then becomes the fully-dispersed solution described in §4.2.

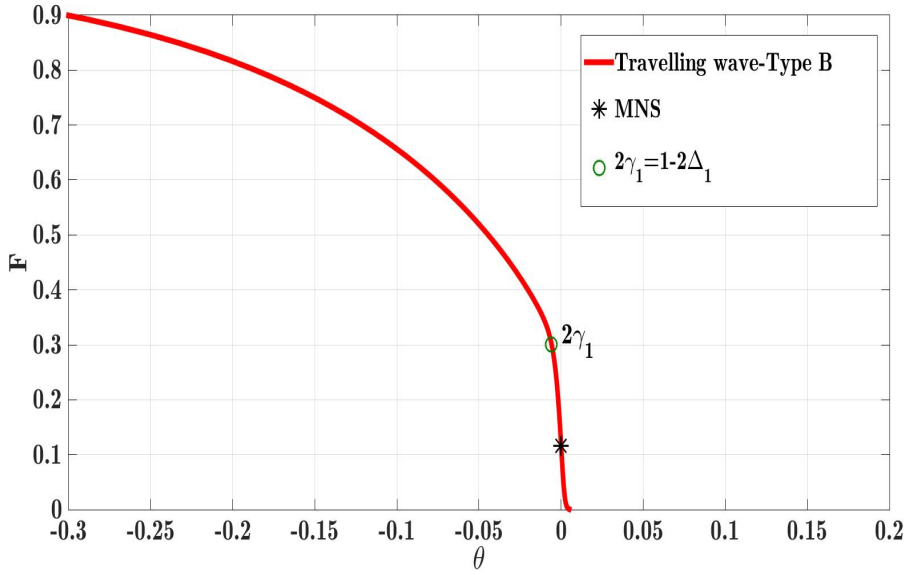

(a) $\Delta_1 = 0.35 \quad \Delta_2 = 0.25$

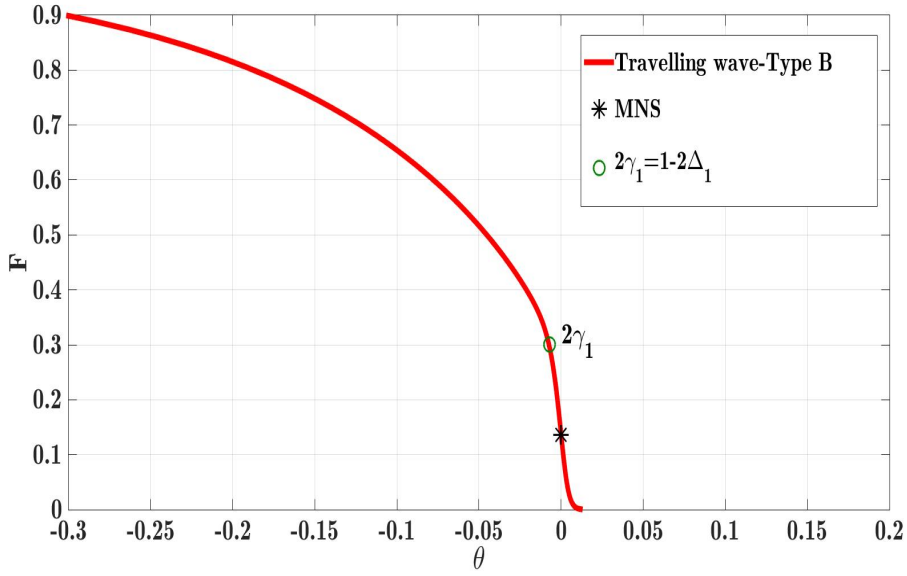

(b) $\Delta_1 = 0.35 \quad \Delta_2 = 0.45$

Figure 4.2.7: The numerical solution of type B travelling shock wave with two relaxation modes. Type B travelling wave consists of two regions, region 1 is the solution change from $F = 1$ to $F = 2\gamma_1 = 1 - 2\Delta_1$ controlled by the first relaxation mode $\Delta_1 = 0.35$ and $\tau_1 = 0.1$. While region 2 controlled by the second relaxation mode Δ_2 and $\tau_2 = 10^{-3}$, is the solution change from $F = 2\gamma_1$ to $F = 0$. Viscosity is fixed at $\epsilon = 10^{-5}$.

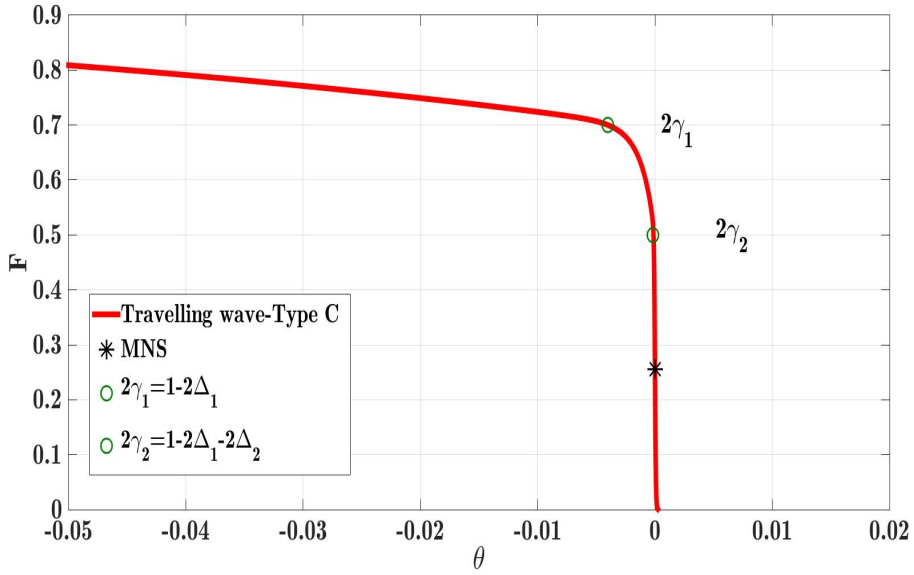

(a) $\Delta_1 = 0.15 \quad \Delta_2 = 0.10$

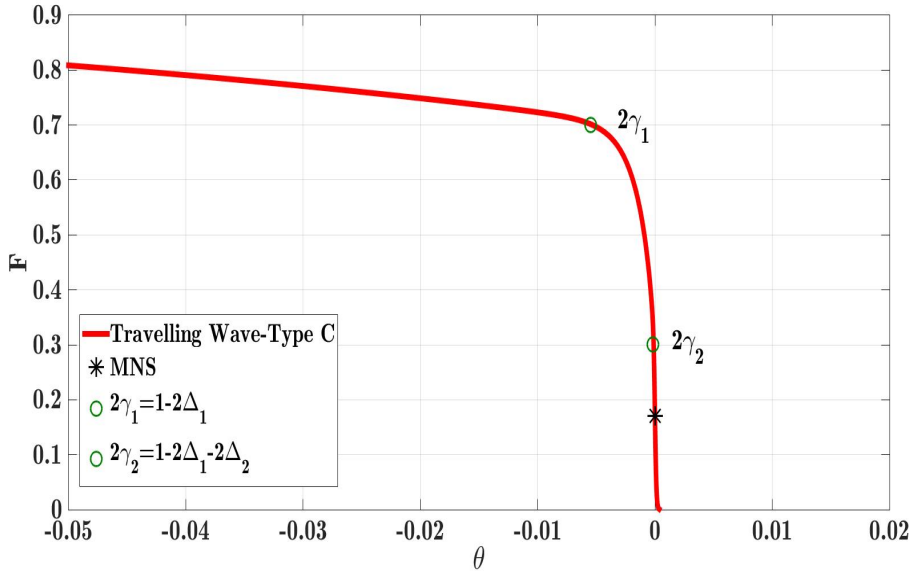

(b) $\Delta_1 = 0.15 \quad \Delta_2 = 0.20$

Figure 4.2.8: The numerical solution of type C travelling shock wave with two relaxation modes. Type C travelling wave consists of three regions, region 1 is the solution change from $F = 1$ to $F = 2\gamma_1 = 1 - 2\Delta_1$ controlled by the first relaxation mode $\Delta_1 = 0.15$ and $\tau_1 = 0.1$. While region 2 controlled by the second relaxation mode Δ_2 and $\tau_2 = 10^{-3}$, is the solution change from $F = 2\gamma_1$ to $F = 2\gamma_2 = 1 - 2\Delta_1 - \Delta_2$. The final third region controlled by $\epsilon = 10^{-5}$ is a fine viscous sub-shock of amplitude $2\gamma_2$.

4.2.4 Comparison of Numerical and Asymptotic Waveforms

We end the travelling wave discussion with the next two figures showing comparisons between asymptotic and numerical solutions of the travelling wave. Figure 4.2.9 represents type B solution with relaxation modes being $\gamma_1 > 0$ and $\gamma_2 < 0$, this type of solution consists of two regions controlled by the first and second relaxation modes respectively. This travelling wave is plotted for the unit amplitude, i.e $U_m = 1$ for the vibrational relaxation parameters $\Delta_1 = 0.35$ and $\Delta_2 = 0.20$ with the relaxation times $\tau_1 = 0.01$, $\tau_2 = 0.001$. Figure 4.2.9 (a) is an illustration of the two asymptotic and numeric solutions for this set of parameters, while figure 4.2.9 (b) is a blow up of plot (a). The numerical solution is marked with blue line where we applied a shift to the X-axis so that $F_{\text{Num}}(0) = \gamma_1$ where $\gamma_1 = 0.5(1 - 2\Delta_1)$.

For the asymptotic solutions, we plotted region 1 solution (red dashed line) defined in §4.2.1 as

$$\theta - \hat{\theta}_1 = \tau_1 \left[\left(2\gamma_1 + 4\,\Delta_1\right)\ \ln\left(1 - F_1\right) + \left(2\gamma_1\right)\ \ln\left(F_1\right) \right], \tag{4.2.43}$$

where $\hat{\theta}_1$ is defined in (4.2.20), thus, the implicit solution of region 1 is

$$\theta = \tau_1 \left[\left(2\gamma_1 + 4\,\Delta_1\right)\ \ln\left(\frac{1 - F_1}{1 - 2\gamma_1}\right) + \left(2\gamma_1\right)\ \ln\left(\frac{F_1}{2\gamma_1}\right) \right], \tag{4.2.44}$$

The region 1 asymptotic solution $1 > F_1 > 2\gamma_2$ is defined for $\theta < 0$. We apply a horizontal shift on this solution so that the asymptotic solution for region 1 agrees with the numerics at $F = 2\,\gamma_1$ which occurs at $\theta \approx -0.002$. Region 2 asymptotic solution marked in green line in which we plotted the solution defined earlier in §4.2.1 as

$$\theta - \hat{\theta}_2 = \frac{\tau_2}{2\gamma_1} \left[\left(2\gamma_2 + 4\Delta_2\right)\ \ln\left(2\,\gamma_1 - F_2\right) + \left(2\gamma_2\right)\ \ln\left(F_2\right) \right], \tag{4.2.45}$$

where $\hat{\theta}_2$ is defined in (4.2.21). The region 2 solution is then

$$\theta = \frac{\tau_2}{2\gamma_1}\left[\left(2\gamma_2 + 4\Delta_2\right)\ \ln\left(\frac{2\,\gamma_1 - F_2}{2\,\gamma_1 - \gamma_1}\right) + \left(2\gamma_2\right)\ \ln\left(\frac{F_2}{\gamma_1}\right)\right]. \tag{4.2.46}$$

The above equation defines the transition $2\gamma_1 > F_2 > 0$ for $\theta < 0$.

One can notice in the blow up figure 4.2.9 (b), the poor agreement between the two asymptotic and numeric approaches specially in the region 2. The apparent reasons for this are firstly, the values of the length-scales tau_1 and τ_2 are not small enough and for reduced values we would expect a better agreement. The other is due to the asymptotic expansions which are obtained only at leading order, with no correction terms, so we would expect these unsatisfactory results when comparing the asymptotic solutions either with the travelling wave numerical solution or with the Fourier pseudosperctral solutions shown later in §4.3.2. We also would expect that the agreement will become much poorer in the very thin viscous inner-shock that we referred to as region 3. Since we assume $\epsilon \ll \tau_2 \ll \tau_1$, the solutions of region 2, region 3 which have widths τ_2 and ϵ, respectively, are very sensitive to small changes. This emphasises the critical role of the solutions' perturbations.

Figure 4.2.10 shows the type C asymptotic and numeric travelling wavesolutions that satisfy the condition $\gamma_1, \gamma_2 > 0$. In type C there is an additional finer region to regions 1 and 2 described above, which is the region 3 viscous sub-shock. Type C travelling wave is plotted for the set of relaxation and thermoviscous quantities: $\Delta_1 = 0.25,\ \tau_1 = 0.01,\ ,\ \Delta_2 = 0.10\ \tau_2 = 0.001$ and $\epsilon = 10^{-4}$. Similarly to the previous figure, plot 4.2.10 (a) is full view of the wave while plot 4.2.10 (b) shows a blow-up of the inner regions 1 and 2.

The region 1 asymptotic solution (4.2.44), is plotted in red dashed line, and to make this solution agree with numerics at $2\gamma_1$ we made a horizontal shift so that the region 1 transition $1 > F_1 > 2\gamma_1$ is defined for $\theta < -0.002$. For region 2 asymptotic solution, $\hat{\theta}_2$ is defined in (4.2.19). Therefore, the region 2

asymptotic solution is given by

$$\theta = \frac{\tau_2}{2\gamma_1}\left[\left(2\gamma_2 + 4\Delta_2\right)\ \ln\left(\frac{2\,\gamma_1 - F_2}{2\,\gamma_1 - 2\gamma_2}\right) + \left(2\gamma_2\right)\ \ln\left(\frac{F_2}{2\gamma_2}\right)\right]. \tag{4.2.47}$$

This solution is plotted in green solid line with a shift in θ so that $F_1(-0.0005) = 2\gamma_2,$. The final asymptotic solution is for region 3 (yellow) which we defined earlier in §4.2.1 as

$$F = \gamma_2\ \left[1 - \tanh\frac{\gamma_2}{2\epsilon}\left(\theta - \epsilon\,\hat{\theta}_3\right)\right],$$

with letting the centre of viscous-sub shock $\theta = 0$.

The calculated numerical approximation of type C travelling wave solution is plotted in blue line, and this solution is shifted so that it agrees with the asymptotic viscous sub-shock (yellow) at the shock centre. Therefore, we applied the shift $F_{\mathrm{Num}}(0) = \gamma_2$.

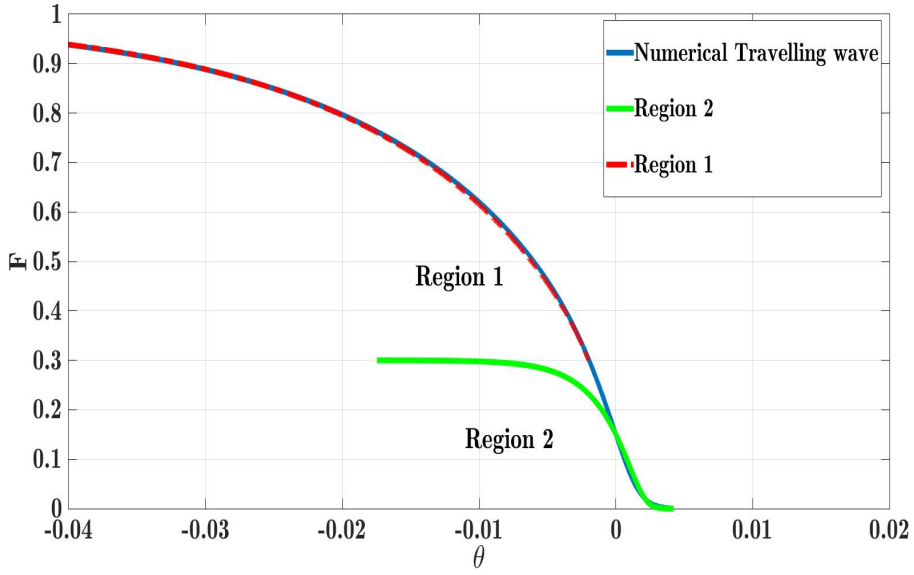

(a) Type B wave

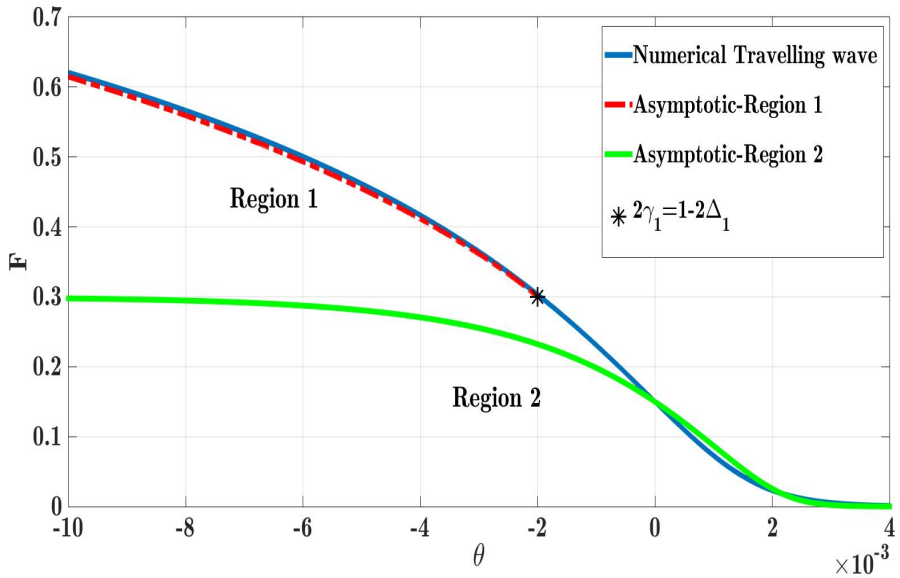

(b) Blow up of the shock focusing on the correspondence of the solutions

Figure 4.2.9: Type B travelling wave of the predicated asymptotic solutions together with the numerical approximations. This travelling wave is coupled with two relaxation modes $\Delta_1 = 0.35$, $\tau_1 = 0.01$, and $\Delta_2 = 0.20$, $\tau_2 = 0.001$. The asymptotic solution consists of two regions: region 1 in red dashed line, region 2 in green line and the numerical solution is marked in blue line. The lower plot (b) is a blow up of plot (a)to show the match of the two solutions.

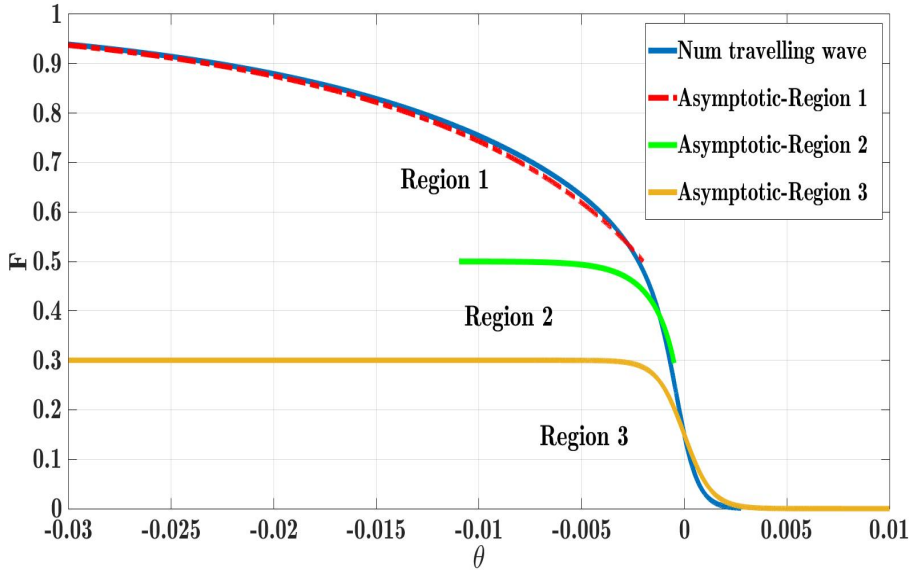

(a) $\epsilon = 0.0001$ $\tau_1 = 0.01$, $\tau_2 = 0.001$

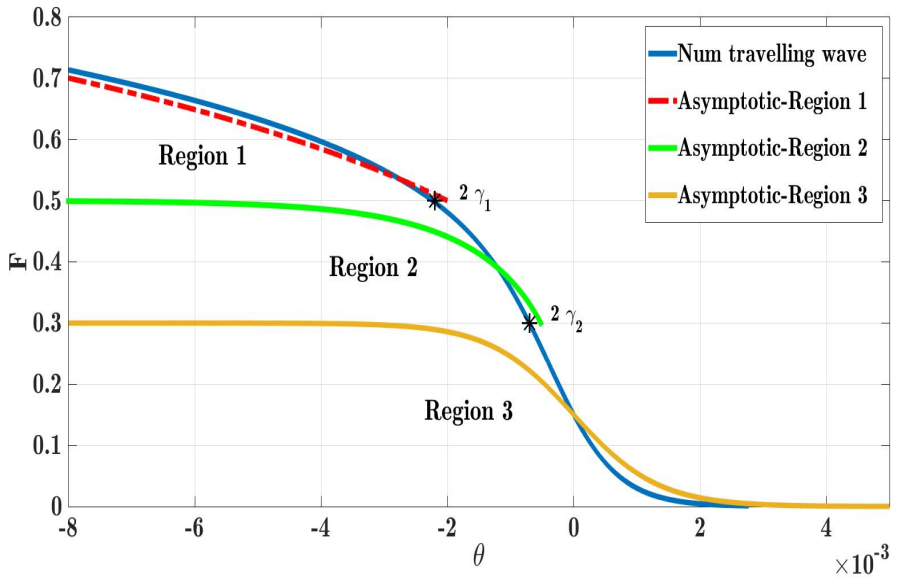

(b) Blow up of the shock front

Figure 4.2.10: Type C travelling wave of the predicated asymptotic solutions together with the numerical approximations. This travelling wave is coupled with two relaxation modes $\Delta_1 = 0.25$, $\tau_1 = 0.01$, and $\Delta_2 = 0.10$, $\tau_2 = 0.001$ for the thermoviscous parameter $\epsilon = 0.0001$. The asymptotic solution consists of three regions: region 1 in red dashed line, region 2 in green line and finally region 3 in yellow line. The numerical solution is marked in blue line. The lower plot (b) is a blow up of plot (a) to show the match of the two solutions.

4.2.5 Summary of Travelling Wave Analysis

We presented an approach to solve the augmented Burgers equation coupled with two relaxation modes by transforming to a travelling wave equation. We first derived the asymptotic travelling wave with two relaxation modes

$$\Big(\tau_1 \frac{\mathrm{d}}{\mathrm{d}\theta} - 1\Big)\Big(\tau_2 \frac{\mathrm{d}}{\mathrm{d}\theta} - 1\Big)\Big[\epsilon\, F_\theta - \frac{F}{2}\Big(F-1\Big)\Big] = \tau_1\,\tau_2 \quad \Big(\Delta_1 + \Delta_2\Big) F_{\theta\,\theta} - \Big(\tau_1\,\Delta_1 + \tau_2\,\Delta_2\Big) F_\theta.$$

Depending on the relaxation modes Δ_1 and Δ_2 three types of solutions are derived assuming $\tau_1 \geq \tau_2 \geq \epsilon$. We gave these solutions the names type A, B and C shock waves. Type A shock wave consists of one region governed by the first relaxation mode describing the transition from $F = U_m$ to $F = 0$ which is defined implicitly as

$$U_m\,\theta_1 = \Big(2\gamma_1 + 4\,\Delta_1\Big)\ \ln\Big|F - U_m\Big| + \Big(2\gamma_1\Big)\ \ln\Big|F\Big|. \tag{4.2.48}$$

This type of shock is of width $O(\tau_1)$ and forms when both $\gamma_1, \gamma_2 < 0$ and where $\gamma_1 = \frac{U_m}{2} - \Delta_1$. If $\gamma_1 > 0$ and $\gamma_2 < 0$ then the shock is of the second type, type B. This shock is covered by two regions, region 1 controlled by the first relaxation mode where solution in equation(4.2.48) changes from $F = U_m$ to $F = 2\gamma_1$. Second region is region 2 governed by the second relaxation mode of width $O(\tau_2)$ where the transition from $F = 2\gamma_1$ to 0 defined in

$$2\gamma_1\,\theta_2 = \Big(2\gamma_2 + 4\Delta_2\Big)\ \ln\Big|F - 2\,\gamma_1\Big| + \Big(2\gamma_2\Big)\ \ln\Big|F\Big|. \tag{4.2.49}$$

The final type, Type C shock wave forms when both $\gamma_1, \gamma_2 > 0$ and is covered by three regions. First region is the transition from $F = U_m$ to $F = 2\gamma_1$ defined in equation (4.2.48). Second region governed by the second relaxation mode of width $O(\tau_2)$ describes the transition from $F = 2\gamma_1$ to $F = 2\gamma_2$ defined in equation (4.2.49). Third region is a viscous sub-shock of amplitude $F = 2\gamma_2$ as

follows

$$F = \gamma_2 \left[1 - \tanh \frac{\gamma_2}{2\epsilon} \left(\theta_3 - \epsilon\hat{\theta}_3\right)\right],$$

We used the asymptotic expansions for type A, B and C travelling wave solutions to obtain three formulas of the maximum negative slope for each type of travelling wave as follows

$$S_m = \begin{cases} -\dfrac{U_m}{\tau_1}\left(\widehat{\Delta}_1 - \sqrt{\widehat{\Delta}_1^2 - \dfrac{1}{4}}\right), & \frac{1}{2}U_m < \Delta_1, \\ -\dfrac{U_m}{\tau_2}\left(\widehat{\Delta}_2 - \sqrt{\widehat{\Delta}_2^2 - \widehat{\gamma}_1^2}\right), & \Delta_1 < \frac{1}{2}U_m < \Delta_1 + \Delta_2, \\ -\dfrac{U_m\,\widehat{\gamma}_2{}^2}{2\widehat{\epsilon}}, & \Delta_1 + \Delta_2 < \frac{1}{2}U_m. \end{cases}$$

Secondly, we attempted to solve the travelling wave numerically. We followed the method of Pierce & Kang [73] to obtain a relationship between F and F_θ in the linearised shock tail as $\theta \to \infty$. This has then used as the initial condition for a Runge-Kutta method to solve the full equation to obtain the wave form for smaller θ. We summed up the travelling wave analysis with comparison between the asymptotic and numerical approaches. The difference between the results of the two approaches could be improved if the small perturbations were included in the asymptotic expansions.

4.3 The Rectangular Unit Pulse

We simulate the propagation of finite amplitude acoustics in a relaxing medium. For this simulation we use the initial waveform (2.5.23) which is a composition of hyperbolic tangent functions resembling a unit rectangular pulse smoothed by δ in the interval $[a, b]$.

We use the Fourier pseudospectral method to discretize the augmented Burgers equation for multiple relaxation modes described earlier in §3.5. Results from §3.5 showed that the model for a single relaxation mode can provide satisfactory predications of shock structure and shock width, and we hope a similar satisfactory results for the two relaxation modes.

4.3.1 Numerical Methods

Let us recall the augmented Burgers equation associated with the two relaxation modes, defined in §3.5 as

$$u_t + u\,u_x + \quad \textstyle\sum_i \Delta_i\, u_{i,x} \quad = \epsilon\, u_{xx},$$

$$\left(\tau_1 \frac{\partial}{\partial x} - 1\right) u_1 = \tau_1\, u_x, \qquad\qquad \left(\tau_2 \frac{\partial}{\partial x} - 1\right) u_2 = \tau_2\, u_x.$$

The augmented Burgers equation is discretized in a Fourier space in the form

$$\hat{v}_t = \lambda\, \mathrm{e}^{f(k)\,t}\, \mathcal{F}\left(\left(\mathcal{F}^{-1}\left(\mathrm{e}^{-f(k)\,t}\hat{v}\right)\right)^2\right), \tag{4.3.1}$$

where $\hat{v} = \mathrm{e}^{f(k)\,t}\,\hat{u}$, $\lambda = -\frac{1}{2}\,i\,k$, $\mathcal{F}[u] = \hat{u}$ is the Fourier transform operator and $f(k)$. The integrating factor was obtained in §3.5 as

$$f(k) = \left(\epsilon + \sum_r \Delta_r \frac{\tau_r}{1 - i\,\tau_r\,k}\right) k^2 \qquad\qquad r = 1, 2. \tag{4.3.2}$$

The fourth-order Runge-Kutta scheme is employed to advance the equation (4.3.1) in time.

We next present results of the numerical model in contrast with the travelling wave numerical and asymptotic solutions. More results of maximum negative slope numerically computed by the FPS model are compared to the asymptotic maximum negative slope.

4.3.2 Comparisons of Travelling Step Wave and the Rectangular Unit Pulse

Previously in §4.2 we presented asymptotic and numerical approaches for finding the travelling wave solutions. For the travelling wave asymptotic solution, we predicted three different cases depending on the values of $\Delta_{1,2}$. We then compared these asymptotic solutions for each case with the numerical calculated solutions of the travelling wave.
We now conduct another comparison. This comparison is for the travelling wave asymptotic and numerical solutions together with the rectangular pulse numerical solutions generated using Fourier Pseudo-Spectral (FPS) technique. For $\epsilon \ll \tau_2 \ll \tau_1 \ll 1,$ we begin showing figures of the FPS numerical solutions and the travelling wave solutions.

Using the initial wave (2.5.23) in the interval $[-L, L]$, we set the initial rectangular wave parameters at $L = 10$ $\delta = 10^{-5}$, $a = -0.75\,L$, $b = -0.50\,L$. Thus, the wave remains in the defined domain for a long period of time. Earlier in §2.5.1 we discussed that in order to properly resolve the shock, the sampling rate needs to be adequately high. Thus, the number of Fourier modes taken high was at $N = 2^{17}$. This ensures enough data points within the shock. However, FFT requires this sampling rate to be applied over the whole waveform, and when large FFT calculations are preformed $\big(O(N \log N)\big)$, the FFT algorithm produces some numerical errors. It is therefore necessary to reduce the time step so that the numerical error associated with FFT is treated when capturing steep shocks. Experimenting on the ideal time step Δt which is proportional to ϵ, yielded to this value of time step $\Delta t = 0.00006$.

The characteristic method in §2.2, suggests that the shock of the pulse is located at $x_s = b + \frac{1}{2}t$, so when the time is at $t = 1$ the shock positioned at $x_s = -4.5$. For $t = 3$ the shock is at $x_s = -3.5$ and using the formula $t = 2(b - a)$ we expect the shock to become a triangular shaped wave at $t = 5$.

Figure 4.3.1 illustrates the rectangular unit pulse numerical solution at time $t = 1$ with the travelling wave type B asymptotic solutions. At $t = 1$ the rectangular pulse amplitude remains at one, so we choose the travelling wave amplitude $U_m = 1$ and the relaxation parameters are $\Delta_1 = 0.35$, $\tau_1 = 0.01$ and $\Delta_2 = 0.25$, $\tau_2 = 0.001$, where the shock wave satisfies the condition $\gamma_1 = 0.5(1 - 2\Delta_1) > 0$ and $\gamma_2 = 0.5(1 - 2\Delta_1 - 2\Delta_2) < 0$. The type B shock wave combines two regions: region 1 is the solution transition $1 > F > 2\gamma_1$; and region 2 is the transition $2\gamma_1 > F > 0$. The FPS generated solution is marked in black line with a shift in the x-axis chosen so that the maximum slope is fixed at $x = 0$. For the asymptotic solutions, we plotted region 1

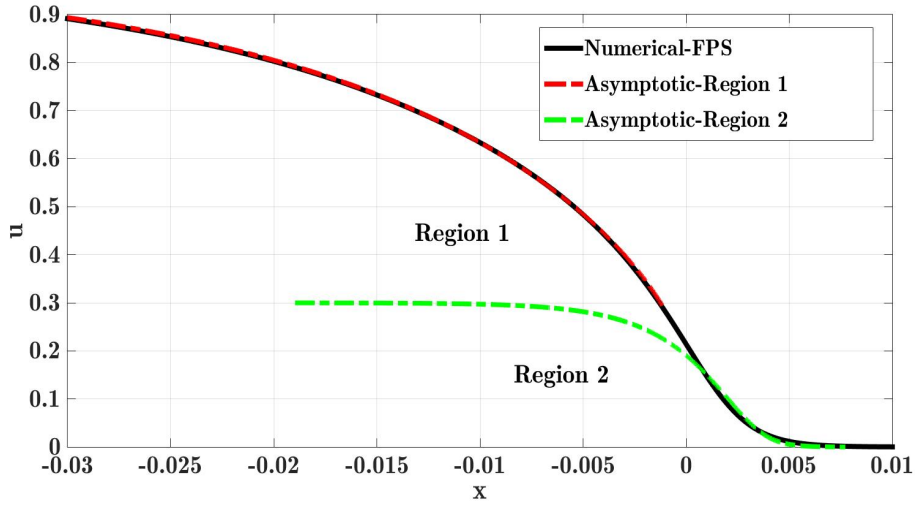

Figure 4.3.1: The rectangular pulse FPS numerical solution plotted when the time is at $t = 1$ and the type B travelling wave asymptotic solutions for two relaxation modes $\Delta_1 = 0.35$, $\tau_1 = 0.01$, and $\Delta_2 = 0.25$, $\tau_2 = 0.001$. The asymptotic solution consists of two regions: region 1 in red dashed line, region 2 in green dashed line and the FPS numerical solution is marked in black line.

solution (red dashed line) defined in §4.2.1 as

$$\theta - \hat{\theta}_1 = \tau_1 \left[\left(2\gamma_1 + 4\,\Delta_1\right)\ \ln\left(1 - F_1\right) + \left(2\gamma_1\right)\ \ln\left(F_1\right) \right].$$

the above equation describes the solution $1 > F_1 > 2\gamma_1$ and $\hat{\theta}_1$ is defined in (4.2.20), inserting the formula for $\hat{\theta}_1$ yields

$$\theta = \tau_1 \left[\left(2\gamma_1 + 4\,\Delta_1\right)\ \ln\left(\frac{1 - F_1}{1 - 2\gamma_1}\right) + \left(2\gamma_1\right)\ \ln\left(\frac{F_1}{2\gamma_1}\right) \right]. \tag{4.3.3}$$

We shifted this solution so that it agrees with numerics at $F = 2\gamma_1$ which occurs at $\theta \approx -0.002$.

Region 2 asymptotic solution marked in green dashed line describes the solution defined earlier in §4.2.1 as

$$\theta - \hat{\theta}_2 = \frac{\tau_2}{2\gamma_1} \left[\left(2\gamma_2 + 4\Delta_2\right)\ \ln\left(2\,\gamma_1 - F_2\right) + \left(2\gamma_2\right)\ \ln\left(F_2\right) \right], \tag{4.3.4}$$

Substituting the value of $\hat{\theta}_2$ given in (4.2.21) and the above solution will then become

$$\theta = \frac{\tau_2}{2\gamma_1} \left[\left(2\gamma_2 + 4\Delta_2\right)\ \ln\left(\frac{2\,\gamma_1 - F_2}{2\,\gamma_1 - \gamma_1}\right) + \left(2\gamma_2\right)\ \ln\left(\frac{F_2}{\gamma_1}\right) \right]. \tag{4.3.5}$$

we choose a shift in θ so that the asymptotic region 2 solution agrees with numerics at $F = \gamma_1$ which occurs at $\theta \approx 0.002$.

Figure 4.3.2 shows the rectangular unit pulse numerical solution at the time $t = 3$ with the travelling wave type C asymptotic solutions. For $t = 3$ the rectangular pulse amplitude remains at one, so we choose the travelling wave amplitude $U_m = 1$, the molecular relaxation parameters are fixed at the values $\Delta_1 = 0.25$, $\tau_1 = 0.01$ and $\Delta_2 = 0.10$, $\tau_2 = 0.001$ and thermoviscosity is at $\epsilon = 0.0001$. This shock wave satisfies the condition $\gamma_1 = 0.5(1 - 2\Delta_1) > 0$ and $\gamma_2 = 0.5(1 - 2\Delta_1 - 2\Delta_2) > 0$, with an additional third region. Each parameter $\tau_1 \gg \tau_2 \gg \epsilon$ determines the width of the regions 1,2 and 3 respectively. Region

1 is the transition $1 > F > 2\gamma_1$ and region 2 is $2\gamma_1 > F > 2\gamma_2$ and finally region 3 is the transition $2\gamma_2 > F > 0$. Similarly to figure 4.3.1 we plot the FPS numerical solution of the rectangular unit pulse in black line with the same shift chosen above in type B solution.

Region 1 asymptotic solution defined in (4.3.3) is plotted in red dashed line with the same shift chosen above in type B solution. Region 2 asymptotic solution given in the form

$$\theta = \frac{\tau_2}{2\gamma_1}\left[(2\gamma_2 + 4\Delta_2)\ \ln\left(\frac{2\,\gamma_1 - F_2}{2\,\gamma_1 - 2\gamma_2}\right) + (2\gamma_2)\ \ln\left(\frac{F_2}{2\gamma_2}\right)\right]. \tag{4.3.6}$$

This equation describes the region 2 solution $2\gamma_1 > F_2 > 2\gamma_2$ for $\theta < 0$. The final region, in which the solution in region 3 is defined as

$$F = \gamma_2\left[1 - \tanh\frac{\gamma_2}{2\epsilon}\left(\theta - \epsilon\,\hat{\theta}_3\right)\right],$$

where the viscous sub-shock center is located at $\theta = 0.0005$.

Next we look at the other comparison between the travelling wave numerical

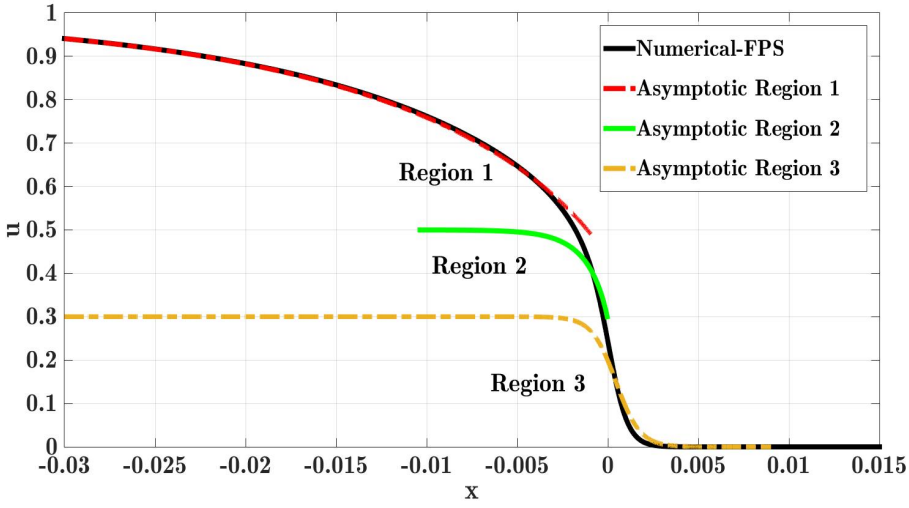

Figure 4.3.2: The rectangular pulse FPS numerical solution (black) plotted when the time is at $t = 3$ and the type C travelling wave asymptotic solutions for two relaxation modes $\Delta_1 = 0.25$, $\tau_1 = 0.01$, and $\Delta_2 = 0.10$, $\tau_2 = 0.001$ and viscosity $\epsilon = 0.0001$. The asymptotic solution consists of three regions: region 1 in red dashed line, region 2 in green line and region 3 in yellow dashed line.

solution derived earlier in §4.2.3 marked in red, and the rectangular pulse marked either in blue or green. This comparison is focusing only on the type C shock which contains the inner thermoviscous shock.

For $\epsilon \ll \tau_2 \ll \tau_1 \ll 1$, figures 4.3.3, 4.3.4 are blow up of the shock front to show the matching in this thin area. The two figures are plotted for the following set of parameters' values:

$$\begin{array}{lll} \text{1st} & \text{Relaxation} & \Delta_1 = 0.25, \quad \tau_1 = 0.1 \\ \text{2nd} & \text{Relaxation} & \Delta_2 = 0.10, \quad \tau_2 = 0.05, \\ & & \epsilon = 0.005, \quad 0.0001, \quad 0.00005. \end{array}$$

In figure 4.3.3, a horizontal shift is made to the travelling wave numerical solution so that the maximum negative slope is at $\theta = 0$. While the rectangular pulse solution is shifted so that the solution agrees with travelling wave at $\theta = 0$. We see that as ϵ reduces the MNS for the rectangular pulse approaches the MNS for the travelling wave. In the other hand, the second figure 4.3.4, the shift is different where the maximum negative slope for both solutions are at $\theta = 0$. figure 4.3.4 shows that this measurement is sensitive to the change in ϵ.

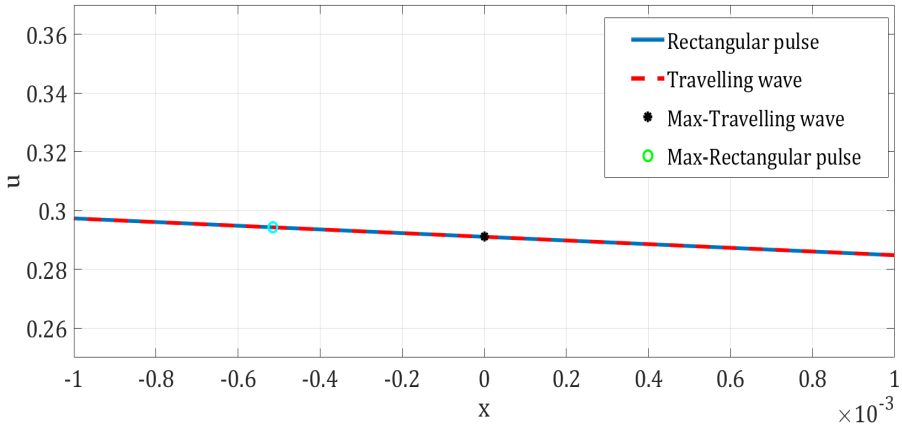

(a) $\epsilon = 0.005$

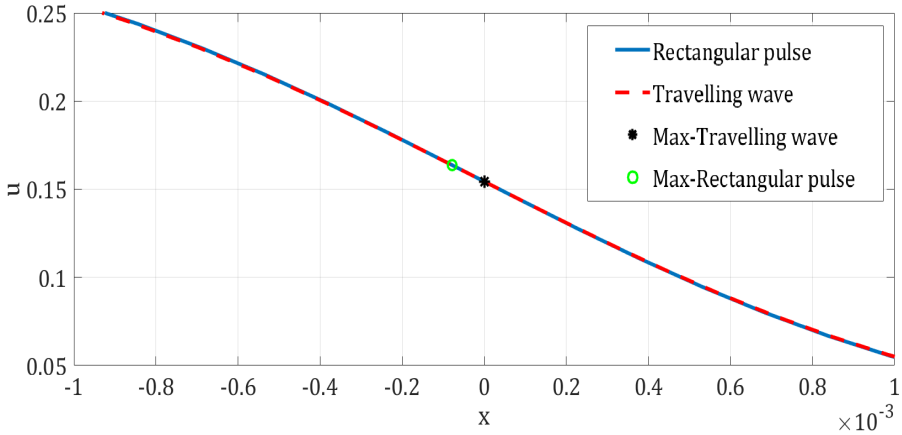

(b) $\epsilon = 0.0001$

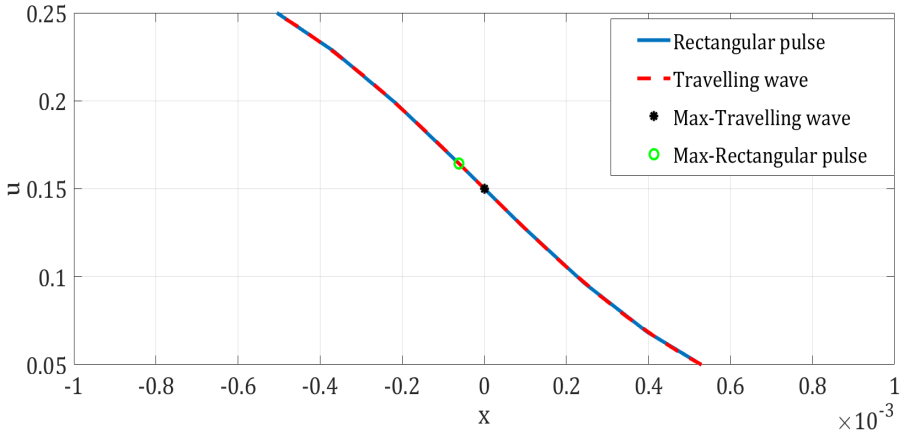

(c) $\epsilon = 0.00005$

Figure 4.3.3: Comparison for the numerical shock wave solution of the travelling wave and the numerical solution of the rectangular pulse at time $t = 3$ with two relaxation modes.The viscosity is taken for $\epsilon = 0.005, 0.0001, 0.00005$, while the relaxation parameters fixed at $\Delta_1 = 0.25$, $\Delta_2 = 0.10$, $\tau_1 = 0.1$, $\tau_2 = 0.05$. A horizontal shift is made to the travelling wave numerical solution so that the maximum negative slope is at $\theta = 0$. While the rectangular pulse solution is shifted so that the solution agrees with travelling wave at $\theta = 0$.

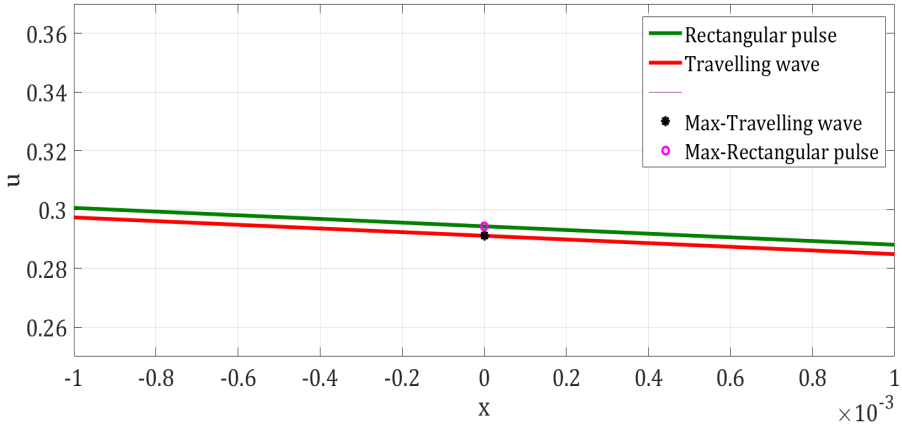

(a) $\epsilon = 0.005$

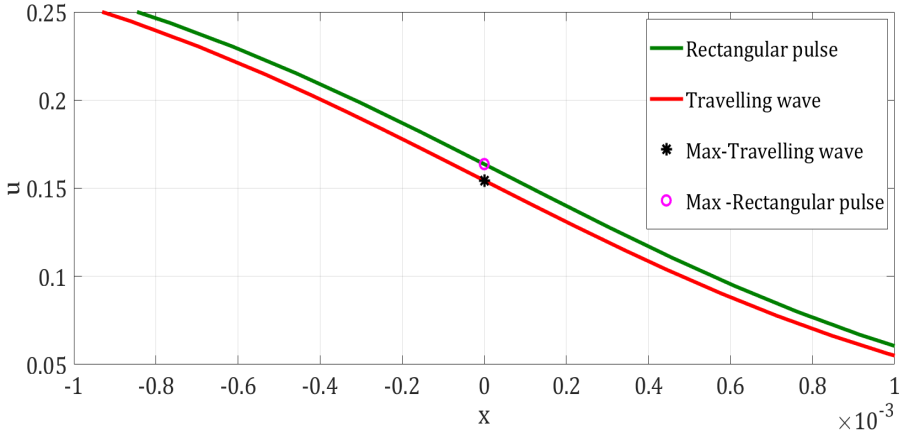

(b) $\epsilon = 0.0001$

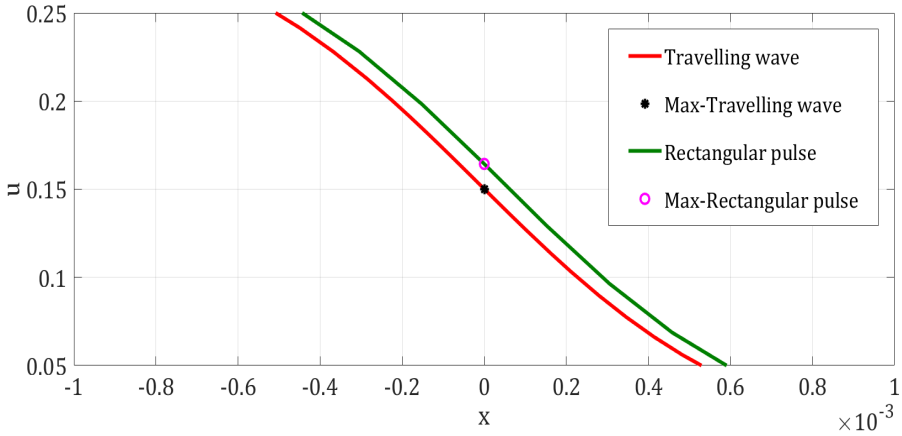

(c) $\epsilon = 0.00005$

Figure 4.3.4: Comparison for the numerical shock wave solution of the travelling wave and the numerical solution of the rectangular pulse at time $t = 3$ with two relaxation modes.The viscosity is taken for $\epsilon = 0.005,\ 0.0001,\ 0.00005$, while the relaxation parameters fixed at $\Delta_1 = 0.25,\ \Delta_2 = 0.10,\ \tau_1 = 0.1,\ \tau_2 = 0.05$. This figure differs from figure 4.3.3 in the horizontal shift, in this figure the maximum negative slope for both solutions are at $\theta = 0$.

4.3.3 Comparison Plots of Wave Maximum Slope

The wave maximum negative slope is another procedural method to measure the shock width. This method is based on locating the steepest gradient, which determines the position of the shock. Larger values of maximum slope indicate a narrower shock. The shock wave under investigation is facing forward to the right, we therefore look for peak value of the negative slope $\max\left(\frac{\mathrm{d}u}{\mathrm{d}x}\right)$.

We now conduct a parametric study on the predicated asymptotic maximum negative slope with the abbreviation (AMNS) and the simulated numerical maximum negative slope (NMNS). This study is similar to that carried out in §3.5.2 for the propagation with one relaxation mode. When two vibrational relaxation states are present we investigate the effect of these two molecular states on the shock front over time. We also examine how the shock develops from one type to another of the three types A, B and C described earlier in §4.2.1.

We begin this parametric analysis with a demonstrative description provided with illustrative plots in figure 4.3.5. The main purpose of this example is to show how the variations in the quantities $U_m,\ \gamma_1,\ \gamma_2$ controls the formation of the shock profile.

Figure 4.3.5 (a) shows numerical (purple) and asymptotic (green) amplitudes for $0 < t < 30$. For the initial waveform defined in §3.5.1, the initial pulse is located in the interval $[-7.5, -5]$. The characteristic theory in §2.2 suggests that the breaking time where this rectangular wave develops to a triangular wave is $t_b = 2(-5 + 7.5) = 5$, after which the waves' peak value begins decreasing from one. The asymptotic amplitude is calculated as

$$U_m(t) = \begin{cases} 1, & 0 < t < 5 \\ \sqrt{\frac{5}{t}}, & 5 \leq t < 30. \end{cases}$$

We notice in figure 4.3.5 (a) the smoothing in the numerical amplitude (purple) when $t = 5,$ compared to the instant change in the asymptotic amplitude (green) which is calculated using the inviscid theory, whereas the numerical calculation involves the effect of viscosity which smooths sharp changes in gradient. This is also due to the rounding made on the initial rectangular wave for the FPS algorithm which causes a gradual change in amplitude. Figure 4.3.5 (b) shows the change of the parameters $\gamma_1,\ \gamma_2$ where these two parameters are $\gamma_1 = \frac{U_m}{2} - \Delta_1$ and $\gamma_1 = \frac{U_m}{2} - \Delta_1 - \Delta_2$.

Previously in §4.2.1 we described in detail the conditions on the quantities γ_1 and γ_2 to preserve a specific shock type of the three types A,B and C which are as follows

$$\begin{aligned} \gamma_1,\ \gamma_2 < 0, &\qquad \text{Type A shock,} \\ \gamma_1 > 0,\ \gamma_2 < 0, &\qquad \text{Type B shock,} \\ \gamma_1,\ \gamma_2 > 0, &\qquad \text{Type C shock.} \end{aligned}$$

We study this change for $0 < t < 30,$ and the set of values for the first and second relaxation states are $\Delta_1 = 0.25,\ \tau_1 = 0.01$ and $\Delta_2 = 0.10,\ \tau_2 = 0.001$ and $\epsilon = 0.00005.$ Thus, for the amplitude $U_m = 1$ the quantities γ_1 and γ_2 have the values $\gamma_1 = 0.25$ and $\gamma_2 = 0.15,$ and as U_m gradually decreases, the pair γ_1 and γ_2 also decrease.

We see in figure 4.3.5 (b), for $0 < t < 5,$ since $U_m = 1$ $\gamma_1,\ \gamma_2$ are then constant values and for $5 < t < 30$ both quantities decrease as long as U_m is declining. For $0 < t < 10,$ the pair $\gamma_1,\ \gamma_2$ have positive signs indicating that the shock profile is of type C consisting of three regions described earlier in §4.2.1. For $10 < t < 20,$ γ_2 changes its positive sign to a negative sign so we have $\gamma_1 > 0,\ \gamma_2 < 0$ and hence the shock becomes type B which includes two regions. Finally, for $20 < t < 30,$ γ_1 changes its sign so that both $\gamma_1,\ \gamma_2$ are negative values and the developed shock front is then of type A which is fully-dispersed shock controlled by the first relaxation mode.

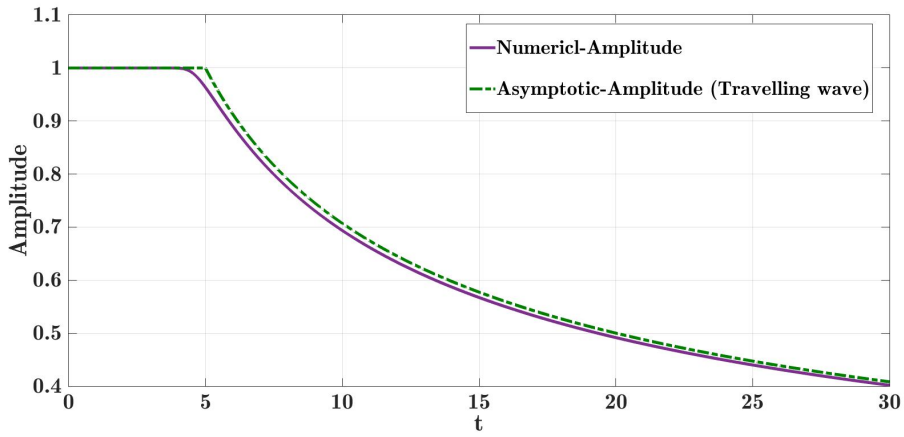

(a) Amplitude

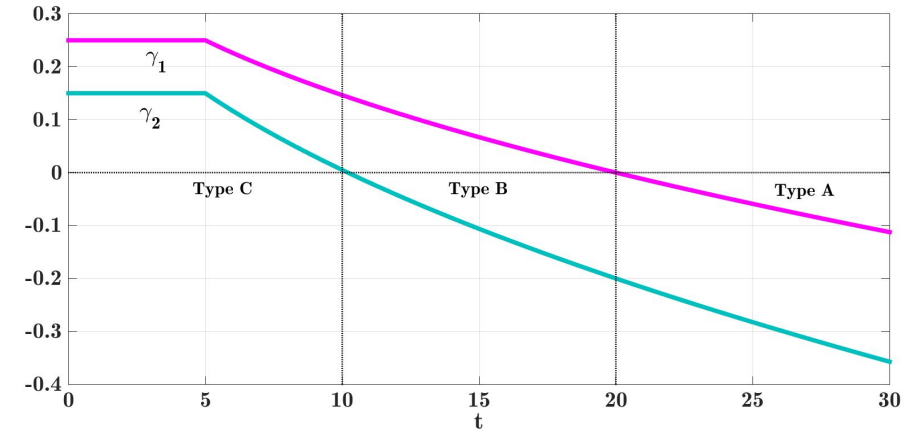

(b) γ_1, γ_2

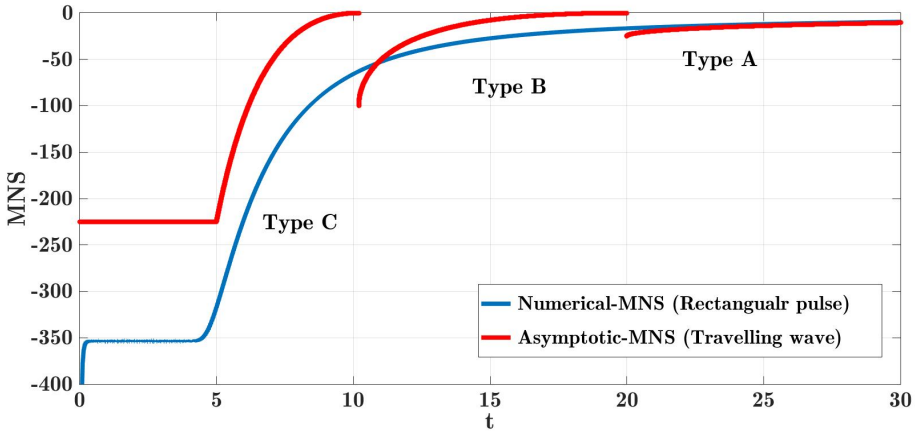

(c) Maximum Negative Slope

Figure 4.3.5: The wave asymptotic and numerical maximum negative slope in (c) and amplitude (a). Plot (b) is the change in γ_1 and γ_2. The figures are taken for the relaxation modes $\Delta_1 = 0.25$, $\tau_1 = 0.1$ and $\Delta_1 = 0.10$, $\tau_1 = 0.001$ and viscosity $\epsilon = 0.00005$.

Figure 4.3.5 (c) shows the AMNS of type A, B and C shocks (red) defined in (4.2.34), (4.2.35) and (4.2.36) and the FPS numerical computations of NMNS marked in blue line for the range of time $0 < t < 30$. Looking closely at the asymptotic MNS, we see that for $0 < t < 10$ the maximum negative slope (MNS) represents type C shock wave. When the time reaches $t \approx 20$ the MNS converts to type B shock, and for $20 < t < 30$ the MNS is formed for type A waves. A more detailed discussion will be carried out later in figure 4.3.7 for a range of parameters. In figure 4.3.5 (c) we mainly focus on the jump discontinuities that appear in the AMNS.

We see in figure 4.3.5 (c) the type C wave asymptotic MNS approaches 0 as γ_2 tends to zero from the left, since

$$\text{AMNS}_C = \frac{U_m\,\widehat{\gamma}_2^2}{2\widehat{\epsilon}} \to 0, \qquad \text{as} \quad \widehat{\gamma}_2 \to 0^-.$$

The AMNS for type B begins to emerge when $\gamma_2 \to 0^+$ approximately at

$$\begin{aligned} \text{AMNS}_B &= \frac{U_m}{\tau_2}\left(\widehat{\Delta}_2 - \sqrt{\widehat{\Delta}_2^2 - \widehat{\gamma}_1^2}\,\right) \qquad \text{as } \widehat{\gamma}_2 = \left(\widehat{\gamma}_1 - \Delta_2\right) \to 0^+ \\ &= -\frac{U_m}{\tau_2}\,\widehat{\Delta}_2, \end{aligned}$$

and since $\widehat{\Delta}_{1,2} = \frac{\Delta_{1,2}}{U_m}$ we can estimate in this case of the selected parameters, that type B wave MNS is at 20. When the time reaches $t \approx 20$ the condition on $\widehat{\Delta}_1$ changes from $\widehat{\Delta}_1 < 1/2$ to $\widehat{\Delta}_1 > 1/2$. The type B wave MNS approaches zero as $\widehat{\Delta}_1 \to 1/2^-$

$$\text{AMNS}_B = \frac{U_m}{2\,\tau_2}\left(2\widehat{\Delta}_2 - \sqrt{\left(2\widehat{\Delta}_2\right)^2 - \left(1 - 2\widehat{\Delta}_1\right)^2}\,\right) \to 0 \quad \text{as } \widehat{\Delta}_1 \to \frac{1}{2}^-.$$

When $\widehat{\Delta}_1 = 1/2^+$, the type A MNS approaches approximately at

$$\begin{aligned} \max(S)_A &= -\frac{U_m}{\tau_1}\left(\widehat{\Delta}_1 - \sqrt{\widehat{\Delta}_1^2 - \frac{1}{4}}\right) \qquad \text{as } \widehat{\Delta}_1 \to \frac{1}{2}^+ \\ &= -\frac{U_m}{\tau_1}\,\left(\frac{\Delta_1}{U_m}\right) \\ &= -\frac{\Delta_1}{\tau_1} = \frac{0.25}{0.01} = -25, \end{aligned}$$

This ends the analytical discussion of figure 4.3.5 and next we move to another discussion on the validation of the asymptotic MNS.

We produce figure 4.3.6 to show the consistency of asymptotic predictions of wave maximum negative slope for travelling wave governing two relaxation modes. We plotted travelling wave asymptotic MNS of one relaxation mode (red) and the case of two relaxation modes when $\Delta_2 \to 0$ (blue), as expected the one and two relaxation modes agreed (see figure 4.3.6 (a)). In the case of two relaxation modes, if Δ_2 is neglected the parameter τ_2 is meaningless. Thus, the solution change from Type C to Type A as conditions changes from $\gamma_1 < 0$ to $\gamma_1 > 0$. When we slightly increased the second relaxation mode $\Delta_2 = 0.02$ (green), Type B solutions arise governing solutions where $\gamma_1 > 0$ and $\gamma_2 < 0$ (see plot 4.3.6(b)). Notice that for the small size of $\Delta_2 = 0.02$, a large change in the AMNS is seen for type B and C. Because the meaningless effect of the second relaxation increment in type A grows as the wave changes its shape from one type to another and this effect becomes significantly high in type C as the amplitude γ_2 is scaled by the very little value of ϵ.

Figure 4.3.7 illustrates the asymptotic maximum negative slope of travelling wave for the three types A, B and C marked in red line and numerical maximum negative slope for the rectangular pulse marked in blue line.
We study the evolution of the unit rectangular pulse over longer time intervals, the wave becomes triangular at some fixed time after which the shock amplitude decreases causing changes in the relaxation parameters $\Delta_{1,2}$ and the shock may transform from being one type of the three(type A,B,C) to another type. The most complex case arises when the shock is initially of type C (i.e $U_m > 2\big(\Delta_1 + \Delta_2\big)$) in the period of time $0 < t < 10$. Looking closely at both MNSs we can see that for $0 < t < 5$ the NMNS along with the AMNS are constants, because the wave has not transformed to a triangular wave yet. At

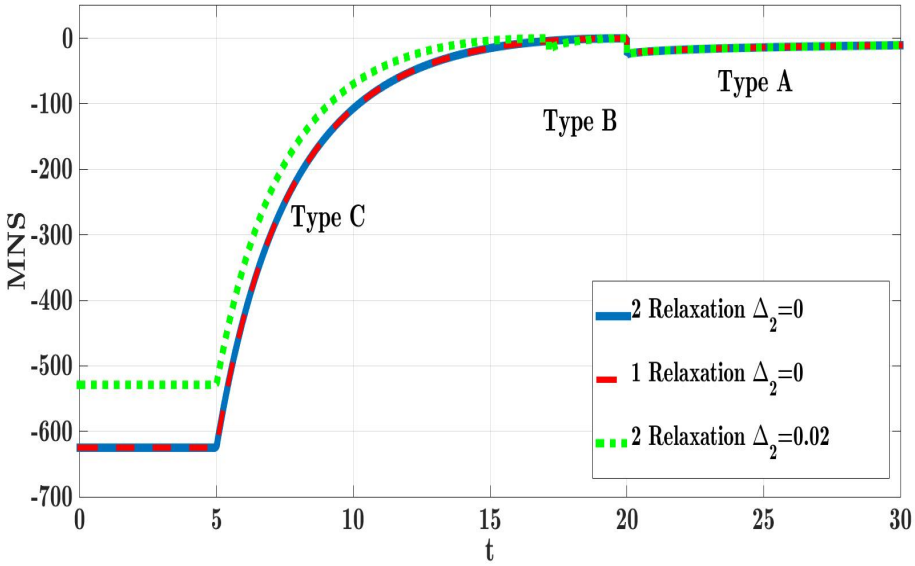

(a) AMNS for $0 \geq t \geq 30$

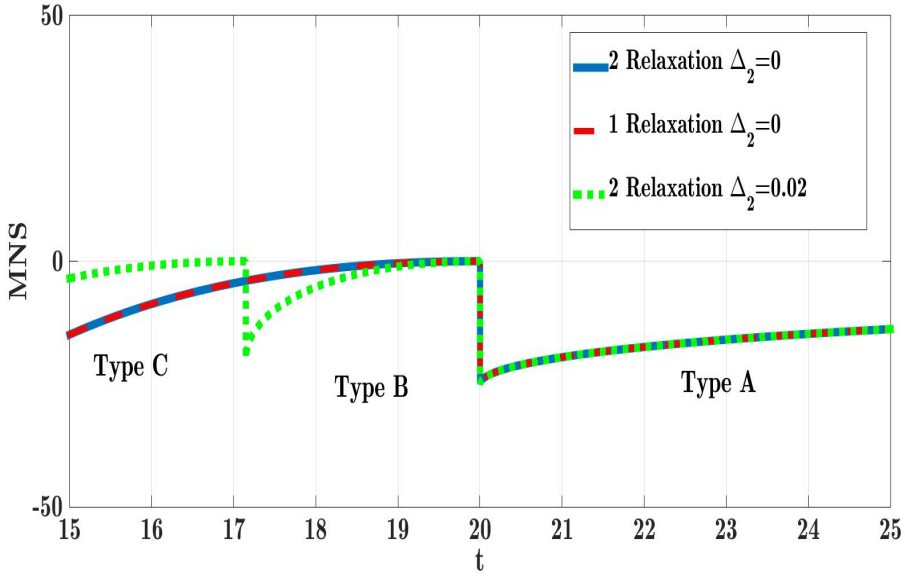

(b) Blow up of plot a showing type B wave AMNS

Figure 4.3.6: Plot (a) shows the asymptotic wave maximum negative slope (AMNS) for two relaxation modes when the second relaxation mode is neglected (i.e $\Delta_2 = 0$) (blue). This is compared to the AMNS for the case of one relaxation mode (red) in the time range $0 \geq t \geq 30$. We also plot the two relaxation AMNS for a little amount of $\Delta_2 = 0.02$ (green). The other relaxation parameters are $\Delta_1 = 0.25$, $\tau_1 = 0.01$, $\tau_2 = 0.001$ for thermoviscosity $\epsilon = 0.00005$. Plot (b) is a blow-up of plot (a) showing type B wave AMNS.

$t = 5$ the wave then reaches the triangular form after which the amplitude decreases and the shock widens (see figure 4.3.5 (a) showing the decline in the asymptotic and numerical amplitudes as time increases). At $t \approx 10$ the amplitude has decreased to the level where the amplitude $U_m < 2\big(\Delta_1 + \Delta_2\big)$ but still greater than $2\Delta_1$, the waveform then converts from type C to type B shock. The amplitude continues decreasing and becomes less than $2\Delta_1$ once more the shock will change this time from type B to type A shock at $t \approx 20$.

In figure 4.3.7 we set the first relaxation parameters to $\Delta_1 = 0.25$, $\tau_1 = 0.01$ and the second relaxation parameters are $\Delta_2 = 0.10$, $\tau_2 = 0.001$ with the values of viscosity $\epsilon = 0.0005,\ 0.0001,\ 0.00005$. The purpose of this figure is to examine the effect of the viscosity on the waveform in particular the type C where thermoviscosity plays a significant role. Additional purpose is to experiment if the viscosity reduction could lead to a a closer agreement between the AMNS and NMNS. We notice in the plots a close correspondence between the asymptotic and numerical MNS for type A wave. However, agreement reduces in the other types and become very poor in type C shock wave. This is an expected consequence of obtaining the asymptotic expansions at only leading order, we recall that the expansions in equations (**??**), (**??**) and (**??**) do not include correction terms. This limitation shows obviously in type C wave which involves the viscous sub-shock that is sensitive to small perturbations. Another reason for inaccuracy is the significant rounding of the triangular wave compared to sharp triangular wave that the inviscid characteristic theory predicts.

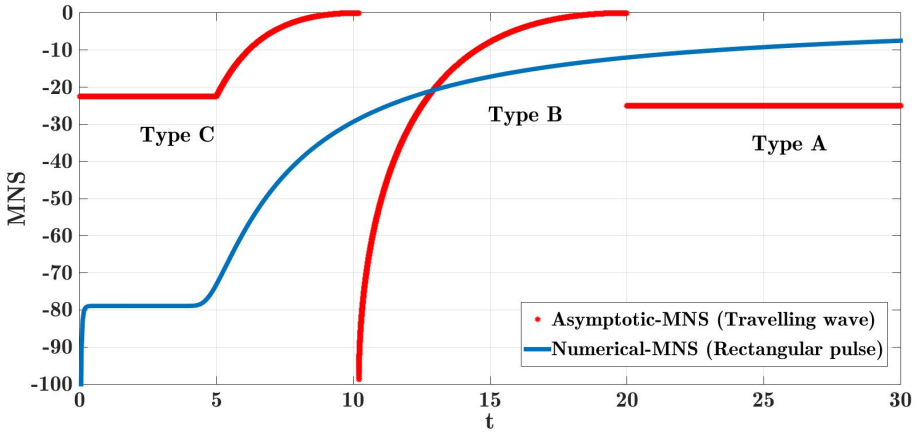

(a) $\epsilon = 0.0005$

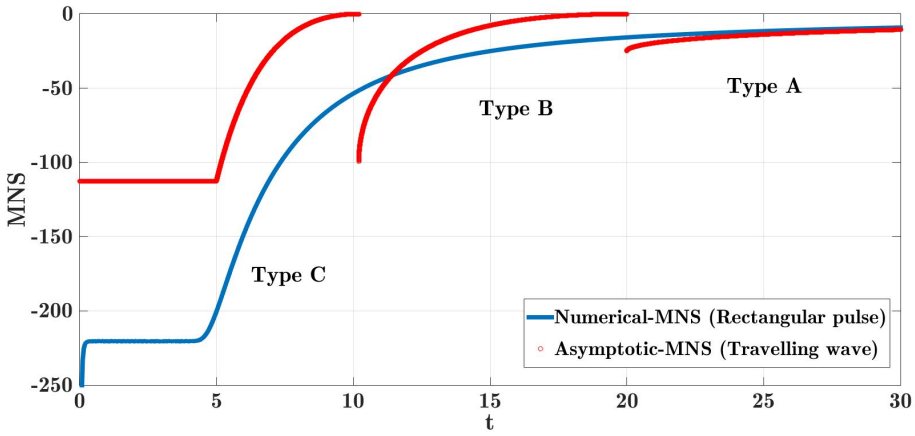

(b) $\epsilon = 0.0001$

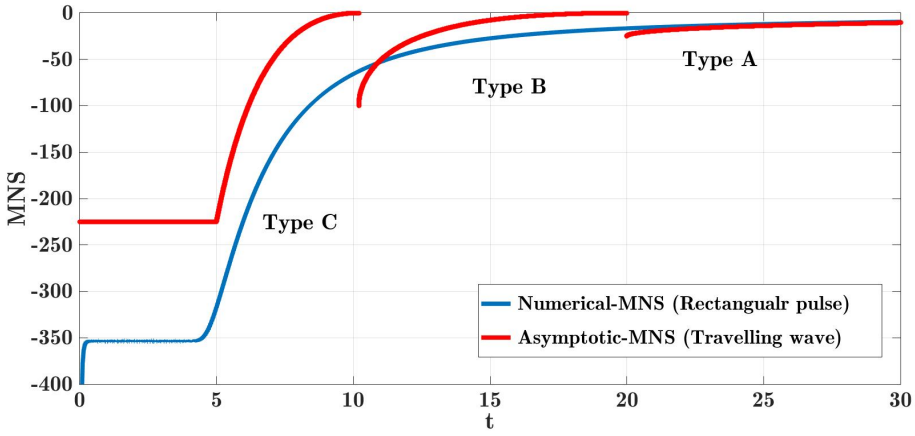

(c) $\epsilon = 0.00005$

Figure 4.3.7: A comparison of wave maximum negative slope for the numerical results of FPS and asymptotic travelling wave solutions. The relaxation modes $\Delta_1 = 0.25$, $\tau_1 = 0.01$ and $\Delta_1 = 0.10$, $\tau_1 = 0.001$. Viscosity is for $\epsilon = 0.005, 0.0001, 0.00005$. The wave begins as Type C shock, changes to Type B when the time is $10 < t < 20$ and to Type A for $t > 20$

4.4 Summary

This chapter discussed the propagation of small-amplitude plane acoustical waves subject to thermoviscous dissipation and two vibrational relaxation modes. Looking for different analytical and numerical solutions in which the two relaxation states are present. In this chapter, once again, we follow the analysis presented in chapter §3 to bring asymptotic and numerical solutions for the travelling wave in the nondimensional form. We examine how the shock structure is affected by this combination of thermoviscosity, nonlinearity and the two relaxation processes. Each relaxation mode is characterised by the two parameters Δ_r and τ_r where $r = 1, 2$. In the asymptotic analysis the study is based on the limit $\epsilon \ll \tau_2 \ll \tau_1$ which is relevant to the propagation in air. In the presence of thermoviscous dissipation and two molecular relaxation modes, the shock may consist of three regimes depending on the relaxation parameters. The shock width with this multiple layers is studied by looking at the negatively highest value of the pressure's gradient. In §4.3 the Fourier pseudospectral numerical method (FPS) proposed in §3.5 is used with the inclusion of the second set of relaxation parameters Δ_2 and τ_2. This chapter was concluded by a parametric study, comparing the maximum gradient of the FPS and the asymptotics.

5

Physical Example

5.0.1 Introduction

In this chapter we present the numerical method proposed by Pierce and Kang [73] to estimate the shock profile of sonic boom shocks on the ground. We then use the atmospheric measured values in Pierce and Kang's example to compare with our predictions of pressure waveform.

For propagation through earth's atmosphere, the molecular relaxation modes associated with Nitrogen N_2 and Oxygen O_2 molecules are significant in controlling the sonic boom shock. The relative humidity has a considerable impact on the molecular absorption in air. Since the relative humidity and the relaxation absorption are changing with altitude. Thus, the sonic boom width varies considerably as the boom propagates to the ground [2]. The parameters associated with relaxation and diffusion are considered constant in the atmosphere. The analysis is based on the limit $\epsilon \ll \tau_1 \ll \tau_2 \ll 1$ which is relevant to the propagation through air. Here τ_1 is the relaxation time associated with molecules O_2, and τ_2 is the relaxation time associated with N_2 molecules, and ϵ is the thermoviscous diffusion coefficient. It is found that the shock structure can take three possible forms depending on the quantities Δ_1 and Δ_2, the sound speed increments associated with N_2 and O_2 molecules respectively. These three possible shock forms were discussed earlier in §4.2.1.

The governing equation for the one-dimensional nonlinear propagation, subject to thermoviscous diffusion and N_2 , O_2 molecular relaxation is the augmented

Burgers equation associated with the relaxation equations

$$\frac{\partial \tilde{p}}{\partial \tilde{t}} + c\frac{\partial \tilde{p}}{\partial \tilde{x}} + \Big(\frac{\beta\,\tilde{p}}{\rho\,c}\Big)\,\frac{\partial \tilde{p}}{\partial \tilde{x}} + \sum_r \tilde{\Delta}_r\,\frac{\partial \tilde{p}_r}{\partial \tilde{x}} = \tilde{\epsilon}\,\frac{\partial^2 \tilde{p}}{\partial \tilde{x}^2}, \tag{5.0.1}$$

$$\Big(1 + \tilde{\tau}_r\,\frac{\partial}{\partial \tilde{t}}\Big)\,\tilde{p}_r = \tilde{\tau}_r\,\frac{\partial \tilde{p}}{\partial \tilde{t}}. \tag{5.0.2}$$

Here p represents the acoustic pressure and p_r are the partial pressures associated with the relaxation modes. Equations (5.0.1) and (5.0.2) are recast in the dimensionless form

$$u_t + u\,u_x + \sum_r \Delta_r\,u_{r,x} = \epsilon\,u_{xx}, \tag{5.0.3}$$

$$\Big(1 - \tau\,\frac{\partial}{\partial x}\Big)u_r = -\tau_r\,u_x, \qquad r = 1, 2, ..., n. \tag{5.0.4}$$

The dimensionless quantities that appear in the above equations were introduced earlier in §3.3 as

$$u = \frac{\beta\,\tilde{p}}{\rho\,c\,V_\infty}, \qquad x = \frac{\tilde{x} - c\,\tilde{t}}{L}, \qquad t = \frac{\tilde{t}}{K},$$
$$\epsilon = \frac{\tilde{\epsilon}}{V_\infty\,L}, \qquad \Delta_r = \frac{\tilde{\Delta}_r}{V_\infty}, \qquad \tau_r = \frac{c\,\tilde{\tau}_r}{L},$$

where V_∞, L and K are velocity distance and time units with choosing the distance $L = K\,V_\infty$.

5.0.2 The Pierce-Kang Numerical Example

Pierce and Kang [73] developed a scheme to account easily for nonlinearity, absorption, and dispersion, using atmospheric conditions at the ground. In the absence of turbulence the shock width is controlled by the contradicting effects of waveform operational steepening and absorption and dispersion. Kang and Pierce assumed the problem in a simplified form in which the step shock propagating in relaxing gas is modelled by a set of coupled ordinary differential equations. The equations were integrated numerically and the result provided

the pressure shock profile.

In the parametric example proposed by Pierce and Kang [73], they presented the following measured values of thermoviscous dissipation and molecular relaxation quantities associated with the O_2 and N_2 vibrational relaxation in air at 20° C and relative humidity of 50%

$$\tilde{\tau}_1 = 4.42 \times 10^{-6} s, \quad \tilde{\tau}_2 = 4.73 \times 10^{-4} s \quad , \qquad \frac{\tilde{\epsilon}}{c^2} = 1.58 \times 10^{-10} s, \tag{5.0.5}$$

$$\frac{\tilde{\Delta}_1}{c} = 3.36 \times 10^{-4}, \qquad \frac{\tilde{\Delta}_2}{c} \;\; = \;\; 6.27 \times 10^{-5}. \tag{5.0.6}$$

Pierce and Kang recast the partial differential equations (5.0.1), (5.0.2) in the non-dimensional form

$$\begin{aligned} \frac{1}{N}\,\frac{\partial p}{\partial t} + \Big(\frac{1}{N} + 2p\Big)\frac{\partial p}{\partial x} + \sum_r \Delta_r \,\frac{\partial p_r}{\partial x} \;\; &= \;\; \epsilon\,\frac{\partial^2 p}{\partial x^2}, \\ \Big(1 + \tau_r\,\frac{\partial}{\partial t}\Big)\, p_r \;\; &= \;\; \tau_r\,\frac{\partial p}{\partial t}, \end{aligned}$$

and defined the dimensionless quantities that appear in the above equations in the form

$$t = \frac{\tilde{t}}{t_{\text{ref}}}, \quad x = \frac{\tilde{x}}{c\,t_{\text{ref}}}, \quad p = \frac{\tilde{p}\beta}{2N\rho c^2}, \quad \tau_r = \frac{\tilde{\tau}_r}{t_{\text{ref}}}, \quad \Delta_r = \frac{\tilde{\Delta}_r}{Nc}, \quad \epsilon = \frac{\tilde{\epsilon}}{Nc^2 t_{\text{ref}}}, \tag{5.0.7}$$

here t_{ref} and ct_{ref} are the characteristic time and distance and the characteristic acoustic pressure is $p_{\text{ref}} = 2N\rho c^2/\beta$ where N is a dimensionless quantity.

Pierce and Kang [73] used the values in (5.0.6) and reached these relevant dimensionless parameters

$$\tau_1 = 9.39, \quad \tau_2 = 1006, \quad \epsilon = 1, \quad \Delta_1 = 1, \quad \Delta_2 = 0.1865, \tag{5.0.8}$$

Pierce and Kang [73] presented a parametric table showing the numerical data of the shock pressure p where it rises from 0.05 of its maximum overpressure to 0.95 of its maximum overpressure. In figure 5.0.1 we plot the non-dimensional

pressure profile that corresponds to the parameter values given by Pierce and Kang, the pressure waveform in plot 5.0.1 is presented in non-dimensional units.

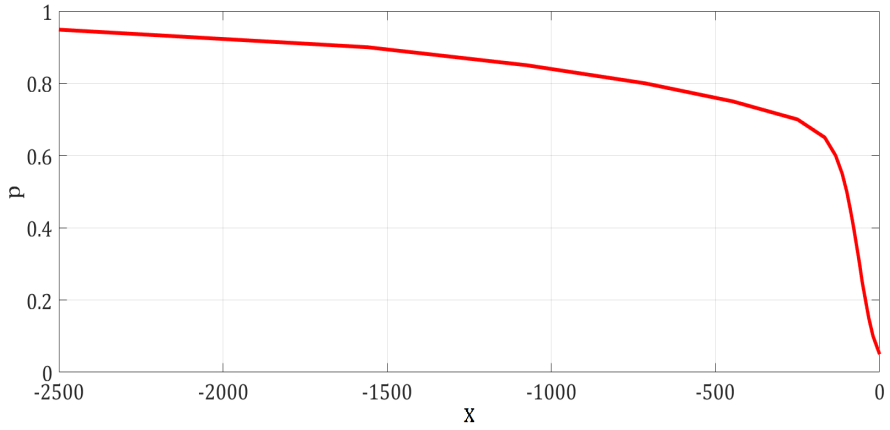

Figure 5.0.1: Pressure profile corresponding to the numerical data presented by Pierce and Kang in their experiment.

5.0.3 Comparison Results

The travelling wave equation presented by Pierce and Kang [73] is consistent with the travelling wave equation (4.2.5) in §4.2.1 provided we put $p = \frac{1}{2}F$.
Choosing the distance unit L equal to ct_{ref} and the velocity unit V_∞ equal to $N\,c$ give the relevant non-dimensional quantities which correspond to Pierce and Kang's results in (5.0.9). Pierce and Kang fixed $t_{\text{ref}} = 4.70 \times 10^{-7}$, and $N = 3.36 \times 10^4$. Table 5.1 is a demonstration of air properties at sea level at temperature 20° C and relative humidity of 50%.

$$\epsilon = \frac{39.71\text{Pa}}{P_s}, \qquad \Delta_1 = \frac{39.71\text{Pa}}{P_s}, \qquad \Delta_2 = \frac{7.41\text{Pa}}{P_s}. \tag{5.0.9}$$

The asymptotic analysis suggested that for the parametric values above the shock profile takes one of the previous illustrated three forms. For $P_s < 14.82\,\text{Pa}$, the shock is fully-dispersed, governed by N_2, of width $O(c\tau_1)$ that is $O(16\,\text{cm})$. For $14.82\,\text{Pa} < P_s < 94.25\,\text{Pa}$ the shock is partially-dispersed, controlled by N_2, with an embedded fully-dispersed shock

Temperature	T	20°	C
Pressure	p	101.325	Pa
Density	ρ	1.2041	kgm^{-3}
Sound speed	c	343.21	ms^{-1}
Ratio of specific heats	α	1.4	-
Volume expansion coefficient	$\beta = \frac{1+\alpha}{2}$	1.2	-

Table 5.1: Standard properties of air at sea level at 20°C.

controlled by O_2 of width $O(0.15\,\mathrm{cm})$. Finally, for $94.25\,\mathrm{Pa} < P_s$ we have an outer, N_2 partially-dispersed relaxed shock and an inner O_2 partially-dispersed relaxed in addition to very thin viscous sub-shock of width less than $O(0.0068\,\mathrm{cm})$. Table 5.2 demonstrates the overpressure range at which each shock type reforms. Pierce and Kang presented their numerical

Dimensionless range	Peak overpressure range	shock Type
$1 - 2\Delta_2 < 0$	$P_s < 14.82\,\mathrm{Pa}$	fully-dispersed shock controlled by N_2.
$1 - 2\Delta_2 > 0$ & $1 - 2\Delta_2 - 2\,\Delta_1 < 0$	$14.82\,\mathrm{Pa} < P_s < 94.25\,\mathrm{Pa}$	partially-dispersed N_2 shock & O_2 fully-dispersed shock.
$1 - 2\Delta_2 - 2\,\Delta_1 > 0$	$94.25\,\mathrm{Pa} < P_s$	partially-dispersed N_2 shock & O_2 partially-dispersed shock & viscous inner sub-shock

Table 5.2: Asymptotic analysis of shock waveform depending on overpressure value.

example for the parameters in (5.0.9) with the value of overpressure being $P_s = 39.71\,\mathrm{Pa}$. The asymptotic analysis suggests that this should correspond to a type B wave. In this case, the wave consists of partially-dispersed relaxed shock wave controlled by Nitrogen, with an embedded fully-dispersed shock of amplitude $(1 - 2\Delta_2)P_s = 24.90\,\mathrm{Pa}$ controlled by Oxygen.

Figure 5.0.2 shows the pressure profile for the set of relaxation and viscous

parameters given in (5.0.8) in comparison with the numerical data reported by Pierce and Kang. The waveform is presented in non-dimensional units in (a) and dimensional units in (b). For the value of overpressure $P_s = 100\,\mathrm{Pa}$, we

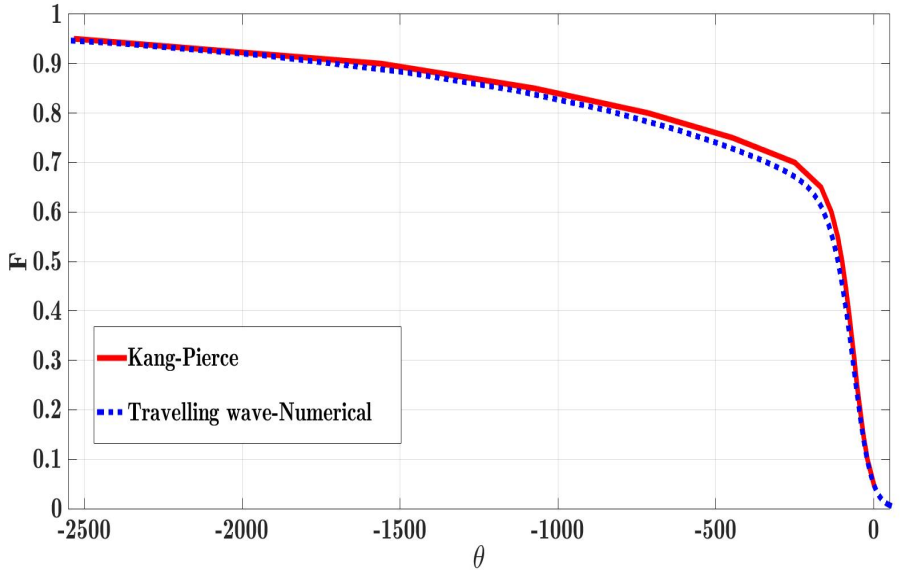

(a) Shock waveform in non-dimensional units

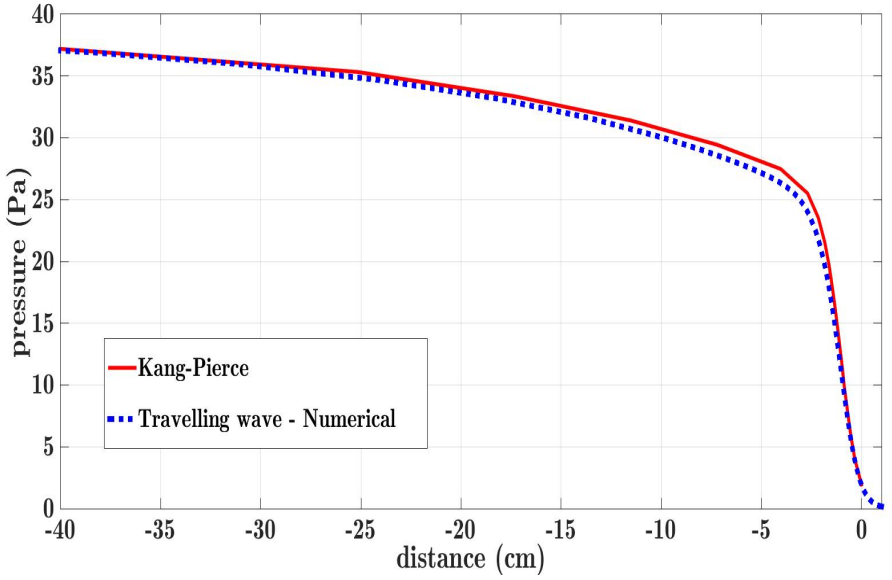

(b) Shock waveform in dimensional units

Figure 5.0.2: Comparisons of shock profile with Pierce-Kang results.

insert it in (5.0.9), in this case, this corresponds to a type C wave. This wave consists of partially-dispersed shock wave controlled by Nitrogen together with another partially-dispersed sub-shock of amplitude $(1 - 2\Delta_2)P_s = 86\,\mathrm{Pa}$

controlled by Oxygen and a narrower viscous sub-shock of amplitude $(1 - 2\Delta_2 - 2\Delta_1)P_s = 6\,\mathrm{Pa}$. Figure 5.0.3 represents this pressure profile in dimensional units for the parameter values $\tau_1 = 1006$, $\Delta_1 = 0.4$, $\tau_2 = 9.39$, $\Delta_1 = 0.07$, and viscosity 0.4.

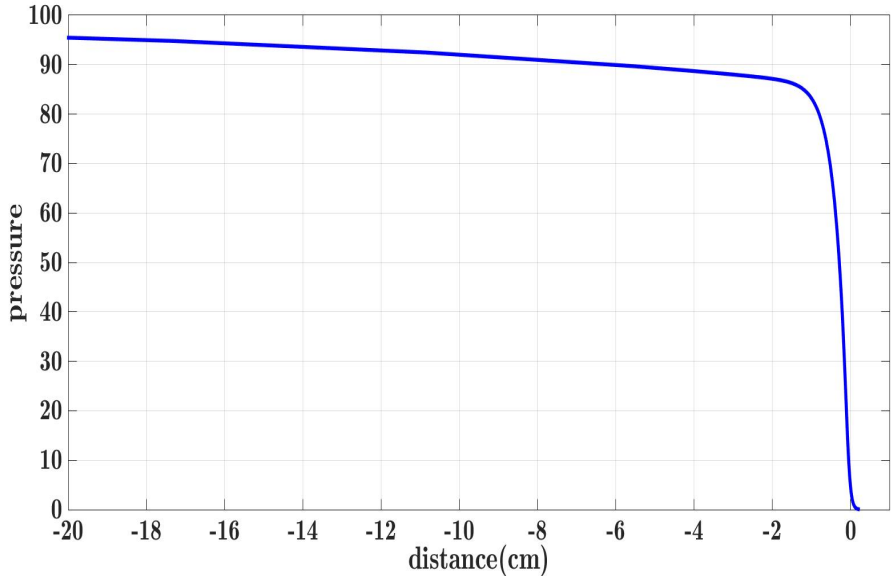

Figure 5.0.3: Pressure profile taken when overpressure is 100 Pa, which results in a type C shock wave.

6

Conclusions and Future Work

6.1 Conclusions

This thesis was devoted to the investigation of the shock structure of acoustic waves associated with sonic booms. The augmented Burgers equation is used to model the propagation of sonic booms. The effect of nonlinear steepening, dissipation and absorption due to thermoviscosity and relaxation processes were considered. To begin with, in the second chapter we ignored relaxation processes and conducted a comprehensive study on different schemes to produce exact and numerical solutions of Burgers' equation when only viscous losses are included. These schemes varied from the lossless characteristic theory, the Cole-Hopf transformation, the method of matched asymptotic expansions and the Fourier pseudospectral algorithm for numerical solutions. We also examined the efficiency and practicality of each method. In each approach we managed to produce a well behaved solution that compared very well to the other solutions. However, while the Cole-Hopf provided an exact solution for the plane Burgers equation, considerable care was needed in evaluating the solution for small viscosity and the computations were time consuming. On the other hand, the asymptotic analysis and the Fourier pseudospectral method proved to be a better choice. Characteristic theory together with the Rankine-Hugoniot jump condition determines the position and amplitude of the shock discontinuity. The method also estimates critical times at which the wave profile changes its shape. These predication were utilized in the asymptotic analysis. The only small

defect of the characteristic method is the over estimated shock amplitude, that can be noticed in the calculated asymptotic shock amplitude and width when they are compared to the Fourier pseudospectral results. The reason for that is because the characteristic theory treats the shock as a discontinuity, which does not fully describe the physical shock.

A full study of this propagation in a relaxing medium is discussed in chapters three and four extending some of the techniques outlined in chapter two. We began by determining the travelling shock wave solutions for the augmented Burgers equation associated with the relaxation rate equations. The asymptotic analysis gives a description of the shock shape which can be comprised of several regions of contrasting magnitude. The shock can be controlled by different physical mechanisms over various regions of the propagation. The analysis clarified that for a particular values of the relaxation parameters, the relaxation modes do not fully control the shock and a finer sub-shock controlled by viscosity arises.

The time domain algorithm that we called FPS implements the Fourier pseudospectral method for the discreatization and the fourth order Runge-Kutta for the time marching. It is developed to solve the augmented Burgers' equation including the dissipative and relaxation absorption terms. For small thermoviscosity, a large number of mesh points are required to capture shock details. For sharp shocks, smaller time step are necessary for the stability, and utilizing the integrating factor method is efficient for reasonable calculating. The code outputs agreed very well with both asymptotic and numerical solutions of the travelling wave. This code can be easily modified to include other physical mechanisms, such as geometrical spreading or the stratification of the atmosphere. We may look in future at the extended Burgers equation when these additional effects are accounted for, and examine how they impact the shock waveform.

Since the shock is actually not a discontinuity, there is a characteristic length scale in which the pressure increment rises from 10% of its amplitude (or peak value) to 90% of its amplitude [74]. This small portion is termed as shock thickness or as we referred in this thesis, the shock width. Much effort in this thesis was devoted to investigate the magnitude of the shock and the width. In the second chapter, in studying the shocks that are solely controlled by the thermoviscous effects, we were able to determine shock width by looking at the length range in which the pressure increment rises from 10% of its amplitude to 90% . However when considering the relaxation processes effects on wave propagation, the width of the whole waveform is complicated to study as the wave involves several regions and each region is governed by a different mechanism. Therefore, we implemented an alternative procedure to measure the shock width. This method known as the wave maximum negative slope, looks for the steepest point in the whole waveform and so is an easier and practical alternative to compute these physical quantities. The shock width is inversely proportional to the Maximum negative slope (i.e width=1/MNS).
When two relaxation states are included, the shock structure depends on five parameters (two for each relaxation state in addition to the thermoviscosity) and the effect of these parameters on the shock profile were analysed for a propagating disturbance. In this thesis the relaxation parameters are taken to be constant. However, in the atmosphere, the parameters will depend upon the altitude and future work will consider how this could be incorporated.

This thesis was concluded with a comparison study with the numerical example of Kang and Pierce [73]. The comparison was made for the propagation of sound disturbance associated with two relaxation modes. Using numerical data suggested as relevant to the atmosphere [73], our numerical travelling wave results were compared for the set of relaxation and viscous parameters proposed by Kang and Pierce.

6.2 Future Work

In this thesis, we presented asymptotic and numerical calculations of the shock width throughout its propagation path in a viscous relaxing gas. Asymptotic conditions were delivered for the relaxing shock wave and predications of the shock width over long course of propagation were presented for different values of viscosity. However, there was a particular value of the shock width that was not fully covered by the asymptotic theory. This particular value is when the wave amplitude U_m is of the same order as the relaxation frequency, for example, in one relaxation mode $\Delta = \frac{1}{2}U_m$ and in two relaxation modes there were two values when $\Delta_1 = \frac{1}{2}U_m$ and $\Delta_1 + \Delta_2 = \frac{1}{2}U_m$. These values appear in the figures capturing the velocity maximum gradient as jump discontinuities, but the behaviour on the left and the right of these discontinuities is studied. A more asymptotic investigation is needed to better understand the behaviour of the maximum gradient at these values.

In future we may conduct an analytical and numerical study using the augmented Burgers equation to predict the sonic boom propagation and signature at the ground. The study should take into account the effects of non-linearity, geometrical spreading, inhomogeneity of atmosphere, absorption and dissipation due to thermoviscosity and molecular vibration relaxation of Nitrogen and Oxygen. The Fourier pseudo-spectral method can by performed, since any modifications to the augmented Burgers model can be easily applied for this scheme. We look for developing an investigation to examine the effects of these influences on shock structure, in particular, shock width and amplitude. An other suggested numerical simulation is the Semi-Lagrangian finite difference discretization method. This scheme that consists of the finite difference approximation that counts for backward time integration can be applied to the non-linear Burgers' equation.

A

Appendix: Phase Plane of Travelling Wave Solutions

This appendix is a subsequent discussion of §3.4.7 using phase portraits to show the instability of the numerical solutions of the travelling wave ODE obtained in §3.4.2 equation (3.4.7) in the limit $F \to 1$ as $\theta \to -\infty$. Consequently, we look for the solutions in the other end $F \to 0$ as $\theta \to \infty$ and we mange to find stable solutions. Since most nonlinear models are complicated to analytically solve, to overcome this complication one can try instead to predict the behaviour of a differential equation's solution without solving it. The equilibrium states in which the system settles in an equilibrium (steady) state after some time and this indicates for the qualitative behaviour of the system after a long time.

The basic idea in this discussion is to classify the equilibrium points for the given travelling wave which are $(0, 0)$ and $(1, 0)$. Investigating whether these points are stable or unstable by looking at the eigenvalues of the linearized system. Locating the eigenvector associated with each eigenvalue determines the long term behaviour of the system in the neighbourhood of each equilibrium point. We aid this discussion with plots of the numerical solution obtained by the use of the build in MATLAB algorithm ODE45, the behaviour of the governing system is demonstrated.

Let us recall the travelling wave given in §3.4.7

$$F'' = \frac{1}{2\,\tau\,\epsilon}\left[\Big(1 - F\Big)\,F + 2\,\Big(\tau\,(F - \gamma) + \epsilon\Big)F'\right]. \tag{A.0.1}$$

where $\prime$ denotes the derivative with respect to θ. Putting the nonlinear ODE in the system form with defining $y_1 = F$ and $y_2 = F'$ gives

$$\frac{\mathrm{d}Y}{\mathrm{d}\theta} = G(Y,\theta), \qquad \text{where} \quad Y = \begin{pmatrix} y_1 \\ y_2 \end{pmatrix} \tag{A.0.2}$$

An equilibrium $\tilde{Y}$ for (A.0.2) is when $G(\tilde{Y},\theta) = 0$ and for this case the equilibrium points are $(0,0)$ and $(1,0)$.

The linearized ODEs of the travelling wave in the neighbourhood of $(1,0)$, can be written in the system

$$\begin{aligned} \frac{\mathrm{d}y_1}{\mathrm{d}\theta} &= \frac{\mathrm{d}F}{\mathrm{d}\theta}, \\ \frac{\mathrm{d}y_2}{\mathrm{d}\theta} &= \frac{1}{2\,\epsilon\,\tau}\Big(- y_1 + 2\,\big(\tau(1-\gamma)+\epsilon\big)\,y_2\Big). \end{aligned}$$

We can write the system in the matrix form

$$\frac{\mathrm{d}Y}{\mathrm{d}X} = \begin{bmatrix} 0 & 1 \\ -\dfrac{1}{2\,\tau\,\epsilon} & \dfrac{\tau\,(1-\gamma)+\epsilon}{\tau\,\epsilon} \end{bmatrix} Y, \qquad \text{where} \quad Y = \begin{pmatrix} y_1 \\ y_2 \end{pmatrix}.$$

We study this matrix that we call A of this system to know the behaviour of the system. To locate the eigenvalues we usually solve $\det\big(A - I\,\lambda\big) = 0$ or we can look at the determinant and the trace of A to have a sense about the eigenvalues since

$$\lambda^2 - \mathrm{tr}A\,\lambda + \det A = 0.$$

In this case we have $\det A = 1/2\tau\epsilon > 0$ and $\mathrm{tr}A = \big(\tau(1-\gamma)+\epsilon\big)/\tau\epsilon > 0$. Thus, both roots $\lambda_{1,2}$ are real roots as $\big(\mathrm{tr}A\big)^2 > 4\det A$ and of the same positive sign as $\det A > 0$. Therefore, we expect the equilibrium point $(1,0)$ to be unstable node.

Let us continue with this analysis to show that the solution for any initial condition is an unstable. The two eigenvalues

$$\lambda_{1,2} = \frac{1}{2\,\tau\,\epsilon}\Big(\tau\,(1-\gamma) + \,\epsilon\, \mp \,\sqrt{\big(\tau\,(1-\gamma)+\,\epsilon\big)^2 - 2\,\tau\,\epsilon}\,\Big), \tag{A.0.3}$$

which are similar to those earlier obtained in §3.4.7 equation (3.4.56) and the eigenvectors respectively

$$\nu_1 = \begin{pmatrix} \tau\,(1-\gamma) + \epsilon - \sqrt{\left(\tau\,(1-\gamma) + \epsilon\right)^2 - 2\,\tau\,\epsilon} \\ 1 \end{pmatrix},$$

$$\nu_2 = \begin{pmatrix} \tau\,(1-\gamma) + \epsilon + \sqrt{\left(\tau\,(1-\gamma) + \epsilon\right)^2 - 2\,\tau\,\epsilon} \\ 1 \end{pmatrix}.$$

The general solution of the system is

$$Y(\theta) = c_1\,\nu_1\,\mathrm{e}^{\lambda_1\,\theta} + c_2\,\nu_2\,\mathrm{e}^{\lambda_2\,\theta}. \tag{A.0.4}$$

.

We have exponential growth in both directions given by $\nu_{1,2}$ for the eigenvalues $\lambda_2 > \lambda_1 > 0$, and this growth is faster in the direction defined by ν_2 and so trajectories starting close to the equilibrium point $(1, 0)$ tend to move away from the equilibrium in this direction. Consequently, $Y \to \infty$ as $\theta \to -\infty$ for any initial condition regardless of the values of c_1 and c_2.

In figure A.0.1 we plot the two-dimensional phase plane showing trajectories about the equilibrium point $(1, 0)$. We see the red trajectories diverging from the point $(1, 0)$ since both eigenvalues for the linearized travelling wave are positive and hence the point $(1, 0)$ is unstable node. The eigenvectors ν_1 (magenta) and ν_2 (cane) intersecting at the equilibrium $(1, 0)$. We plot the vector solution Y of the travelling wave (A.0.1) for the initial data $[y_1(0), y_2(0)] = [1 - \delta, -\delta\,\lambda_1]$ marked by the blue dashed line and $[1 - \delta, -\delta\,\lambda_2]$ given by the green line, with setting $\delta = 0.01$. As expected for both initial conditions the solution $Y \to \infty$ as $\theta \to -\infty$ instead of tending to zero. The viscous and relaxation parameters were set at $\epsilon = 0.1$, $\phi = 0.5$ and $\tau = 0.25$.

Alternatively we look for the solution in the other end so we define the new variable $X = -\theta$ so that the boundary condition $F_- \to 1$ when $X \to \infty$ so that

the travelling wave (A.0.1) becomes

$$F''_{-} = \frac{1}{2\,\tau\,\epsilon}\Big[\Big(1 - F_{-}\Big)\,F_{-} - 2\,\Big(\tau\,(F_{-} - \gamma) + \epsilon\Big)F'_{-}\Big], \tag{A.0.5}$$

where $'$ this time denotes the derivative with respect to X. We construct the solution in the neighbourhood of the equilibrium point $(0, 0)$, by linearization of the governing equation in (A.0.5) to become the system

$$\begin{aligned} \frac{\mathrm{d}\hat{y}_1}{\mathrm{d}X} &= \frac{\mathrm{d}F_{-}}{\mathrm{d}X}, \\ \frac{\mathrm{d}\hat{y}_2}{\mathrm{d}X} &= \frac{1}{2\,\epsilon\,\tau}\Big(\hat{y}_1 + 2\,(\tau\,\gamma - \epsilon)\,\hat{y}_2\Big), \end{aligned}$$

or in the matrix form

$$\frac{\mathrm{d}\hat{Y}}{\mathrm{d}X} = \begin{bmatrix} 0 & 1 \\ \dfrac{1}{2\,\tau\,\epsilon} & \dfrac{\tau\,\gamma - \epsilon}{\tau\,\epsilon} \end{bmatrix}\hat{Y}, \qquad \text{where} \quad \hat{Y} = \begin{pmatrix} \hat{y}_1 \\ \hat{y}_2 \end{pmatrix}.$$

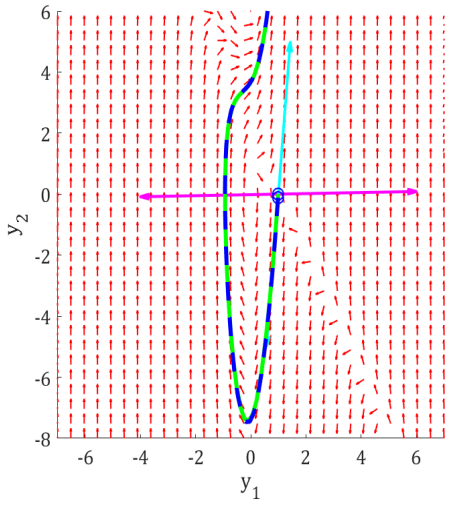

Figure A.0.1: Phase plane of the trajectories (red) in the neighbourhood of the equilibrium $(1, 0)$ with the eigenvectors ν_1 (magenta) and ν_2 (cane) intersecting at $(1, 0)$. The solution to the travelling wave (A.0.1) plotted for the initial condition $[1 - \delta, -\delta\,\lambda_1]$ (blue) and $[1 - \delta, -\delta\,\lambda_2]$ (green).

The eigenvalues of the system are obtained by solving the determinant

$$\det \begin{bmatrix} -\mu & 0 \\ \dfrac{1}{2\,\tau\,\epsilon} & \dfrac{\tau\,\gamma - \epsilon}{\tau\,\epsilon} - \mu \end{bmatrix} = 0.$$

This gives the same eigenvalues we obtained earlier in §3.4.7 equation (3.4.61)

$$\mu_{1,2} = \frac{1}{2\,\tau\,\epsilon}\Big(\tau\,\gamma - \epsilon \mp \sqrt{(\tau\,\gamma - \epsilon)^2 + 2\,\tau\,\epsilon}\Big),$$

and the eigenvectors respectively

$$\kappa_1 = \begin{pmatrix} \tau\,\gamma - \epsilon - \sqrt{(\tau\,\gamma - \epsilon)^2 + 2\,\tau\,\epsilon} \\ 1 \end{pmatrix}, \qquad \kappa_2 = \begin{pmatrix} \tau\,\gamma - \epsilon + \sqrt{(\tau\,\gamma - \epsilon)^2 + 2\,\tau\,\epsilon} \\ 1 \end{pmatrix}.$$

The eigenvalues $\mu_{1,2}$ are real with $\mu_1 < 0 < \mu_2$ as $(\tau\,\gamma - \epsilon)^2 < (\tau\,\gamma - \epsilon)^2 + 2\,\tau\,\epsilon$. Thus, in this case we have exponential growth in the direction represented by μ_2 but exponential decay in the direction represented by μ_1. This is called a saddle point and we see in the phase portrait in figure A.0.2 showing the trajectories represented by the eigenvector κ_1 moves towards the equilibrium in the direction of μ_1, but the trajectories given by the eigenvector κ_2 moves away from the equilibrium in the the direction of μ_2. The solution Y of the travelling wave (A.0.5) is plotted for the initial data $[y_1(0), y_2(0)] = [\delta, \delta\,\mu_1]$ marked by the blue dashed line and $[\delta, \delta\,\mu_2]$ given by the green line, with setting $\delta = 0.01$ and for both initial conditions the solution tend to the other equilibrium state i.e $Y = [y_1, y_2] \to [1, 0]$ as $X \to \infty$.

Based on the initial condition, if the solution is defined in the stable subspace where the trajectories converge to the equilibrium then the solution always tend to $(1, 0)$. However, if the solution is defined in the unstable subspace where the trajectories diverge from the equilibrium here the solution will go to infinity. This is clear in figure A.0.3 (a), we plot the solution for four initial conditions $[y_1(0), y_2(0)] = [\delta, \delta\,\mu_i]$ where μ is given respectively as $\mu = \mu_1$, μ_2, $50, -20$ we see for the first three values of μ when initial value is defined in the stable subspace we have three solutions, whereas in the fourth case as the initial

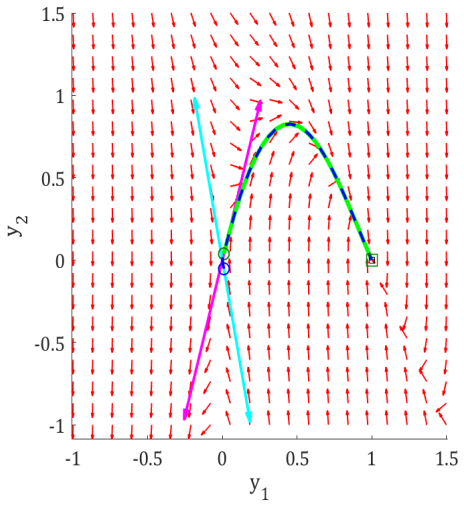

Figure A.0.2: Phase plane of the trajectories (red) in the neighbourhood of the equilibrium $(0, 0)$ with the eigenvectors κ_1 (magenta) and κ_2 (cane) intersecting at $(0, 0)$. The solution to the travelling wave (A.0.5) plotted for the initial condition $[\delta, \delta\,\mu_1]$ (blue) and $[\delta, \delta\,\mu_2]$ (green).

condition is defined in unstable subspace the solution $Y \to -\infty$ (see figure A.0.3 (b)). Therefore, we should be careful in choosing the initial condition and μ_2 is an ideal choice for the solution. The parameters were set at $\epsilon = 0.1$, $\phi = 0.5$ $\tau = 0.25$ and $\delta = 0.01$.

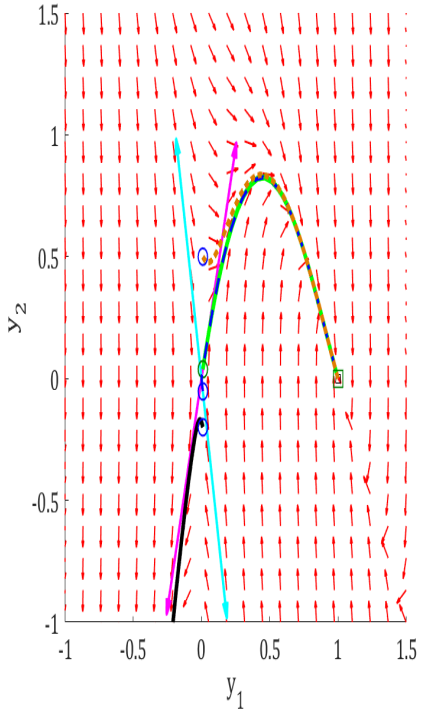

(a) Phase portrait

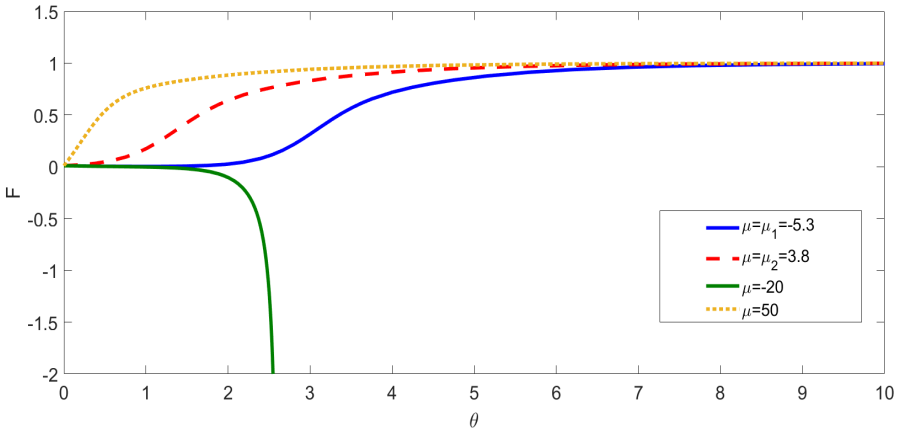

(b) Travelling wave solution

Figure A.0.3: Phase plane of the trajectories (red) in the neighbourhood of the equilibrium $(0,0)$ with the eigenvectors κ_1 (magenta) and κ_2 (cane) intersecting at $(0,0)$. The solution to the travelling wave (A.0.5) plotted for the initial conditions $[\delta, \delta\,\mu]$ when $\mu = \mu_1 = -5.2846$ (blue), $\mu = \mu_2 = 3.7846$ (red), $\mu = 50$ (yellow) and $\mu = -20$ (green).

Bibliography

[1] M. Abramowitz and I. A. Stegun. *Handbook of mathematical functions: with formulas, graphs, and mathematical tables*, volume 55. United States Department of Commerce, National Institute of Standards and Technology, 1964.

[2] H. E. Bass, L. C. Sutherland, A. J. Zuckerwar, D. T. Blackstock, and D. Hester. Atmospheric absorption of sound: Further developments. *The Journal of the Acoustical Society of America*, 97(1):680–683, 1995.

[3] H. Bateman. Some recent researches on the motion of fluids. *Monthly Weather Review*, 43(4):163–170, 1915.

[4] E. R. Benton and G. W. Platzman. Table of solutions of one-dimensional Burgers equation. *Quarterly of Applied Mathematics*, 30(2):195, 1972.

[5] C. Bernardi and Y. Maday. Spectral methods. *Handbook of numerical analysis*, 5:209–485, 1997.

[6] D. T. Blackstock. Thermoviscous attenuation of plane, periodic, finite-amplitude sound waves. *The Journal of the Acoustical Society of America*, 36(3):534–542, 1964.

[7] D. T. Blackstock. Connection between the Fay and Fubini solutions for plane sound waves of finite amplitude. *The Journal of the Acoustical Society of America*, 39(6):1019–1026, 1966.

[8] N. Bleistein and R. A. Handelsman. Asymptotic expansions of integrals. *Holt, Rinehart and Winston, New York*, 1975.

[9] P. Blythe. Non-linear wave propagation in a relaxing gas. *Journal of Fluid Mechanics*, 37(1):31–50, 1969.

[10] J. P. Boyd. Hyperviscous shock layers and diffusion zones: Monotonicity, spectral viscosity, and pseudospectral methods for very high order differential equations. *Journal of Scientific Computing*, 9(1):81–106, 1994.

[11] J. P. Boyd. *Chebyshev and Fourier spectral methods*. Courier Corporation, 2001.

[12] J. M. Burgers. Mathematical examples illustrating relations occurring in the theory of turbulent fluid motion. *Trans. Roy. Neth. Acad. Sci*, 17:1–53, 1939.

[13] J. M. Burgers. A mathematical model illustrating the theory of turbulence. *Adv. in Appl. Mech.*, 1:171–199, 1948.

[14] J. C. Butcher. *The numerical analysis of ordinary differential equations: Runge-Kutta and general linear methods*. Wiley-Interscience, 1987.

[15] J. Caldwell and P. Smith. Solution of Burgers' equation with a large Reynolds number. *Applied Mathematical Modelling*, 6(5):381–385, 1982.

[16] J. Caldwell, P. Wanless, and A. Cook. A finite element approach to Burgers' equation. *Applied Mathematical Modelling*, 5(3):189–193, 1981.

[17] J. R. Cannon. *The one-dimensional heat equation*. Cambridge University Press, 1984.

[18] T. Carlton and D. Blackstock. Propagation of plane sound waves of finite amplitude in inhomogeneous fluids. *The Journal of the Acoustical Society of America*, 56(S1):S42–S42, 1974.

[19] I. Christie and A. Mitchell. Upwinding of high order Galerkin methods in conduction-convection problems. *International Journal for Numerical Methods in Engineering*, 12(11):1764–1771, 1978.

[20] J. F. Clarke and J. Rodgers. Shock waves in a gas with several relaxing internal energy modes. *Journal of Fluid Mechanics*, 21(4):591–610, 1965.

[21] R. O. Cleveland. *Propagation of sonic booms through a real, stratified atmosphere*. PhD thesis, The University of Texas at Austin, 1995.

[22] W. J. Cody. Rational Chebyshev approximations for the error function. *Mathematics of Computation*, 23(107):631–637, 1969.

[23] J. D. Cole. On a quasi-linear parabolic equation occurring in aerodynamics. *Quarterly of applied mathematics*, 9(3):225–236, 1951.

[24] S. Cox and P. Matthews. Exponential time differencing for stiff systems. *Journal of Computational Physics*, 176(2):430–455, 2002.

[25] D. Crighton and J. F. Scott. Asymptotic solutions of model equations in nonlinear acoustics. *Philosophical Transactions of the Royal Society of London A: Mathematical, Physical and Engineering Sciences*, 292(1389):101–134, 1979.

[26] D. G. Crighton. Model equations of nonlinear acoustics. *Annual Review of Fluid Mechanics*, 11(1):11–33, 1979.

[27] S. Dhawan, S. Kapoor, S. Kumar, and S. Rawat. Contemporary review of techniques for the solution of nonlinear Burgers equation. *Journal of Computational Science*, 3(5):405–419, 2012.

[28] R. S. Earnshaw and M. Sheffield. On the mathematical theory of sound. In *Classic Papers in Shock Compression Science*, pages 83–108. Springer, 1998.

[29] G. Emanuel. *Gasdynamics: theory and applications*. American Institute of Aeronautics and Astronautics, 1986.

[30] L. Euler. Sur la force des colonnes. *Memoires de l'Academie des Sciences de Berlin*, pages 252–282, 1759.

[31] D. J. Evans and A. Abdullah. The group explicit method for the solution of Burger's equation. *Computing*, 32(3):239–253, 1984.

[32] B. Fornberg and T. A. Driscoll. A fast spectral algorithm for nonlinear wave equations with linear dispersion. *Journal of Computational Physics*, 155(2):456–467, 1999.

[33] V. Fridman. Propagation of a strong sound-wave in a plane-layered medium. *SOVIET PHYSICS ACOUSTICS-USSR*, 22(4):349–350, 1976.

[34] J. Gazdag. Numerical convective schemes based on accurate computation of space derivatives. *Journal of Computational Physics*, 13(1):100–113, 1973.

[35] D. Gottlieb and J. S. Hesthaven. Spectral methods for hyperbolic problems. *Journal of Computational and Applied Mathematics*, 128(1-2):83–131, 2001.

[36] D. Gottlieb and S. A. Orszag. *Numerical analysis of spectral methods: theory and applications*, volume 26. Siam, 1977.

[37] E. Hairer and G. Wanner. Solving ordinary differential equations. ii, volume 14 of springer series in computational mathematics, 1996.

[38] W. D. Hayes. The basic theory of gasdynamic discontinuities. *Fundamentals of Gas dynamics*, 3:426, 1958.

[39] J. Hodgson. Vibrational relaxation effects in weak shock waves in air and the structure of sonic bangs. *Journal of Fluid Mechanics*, 58(1):187–196, 1973.

[40] E. Hopf. The partial differential equation $u_t + uu_x = \mu u_x x$. *Communications on Pure and Applied Mathematics*, 3(3):201–230, 1950.

[41] H. Hugoniot. Propagation du Mouvement dans les Corps. *J. Ec. Polyt. Paris*, 57:1–125, 1889.

[42] P. Jain and D. Holla. Numerical solutions of coupled Burgers' equation. *International Journal of Non-Linear Mechanics*, 13(4):213–222, 1978.

[43] P. Jain and B. Lohar. Cubic spline technique for coupled non-linear parabolic equations. *Computers & Mathematics with Applications*, 5(3):179–185, 1979.

[44] M. Johnson and P. Hammerton. Effect of molecular relaxation processes on travelling wave solutions of sonic boom waveforms. *Wave Motion*, 38(3):229–240, 2003.

[45] A.-K. Kassam and L. N. Trefethen. Fourth-order time-stepping for stiff PDEs. *SIAM Journal on Scientific Computing*, 26(4):1214–1233, 2005.

[46] J. Katz and M. Green. A Burgers model of interstellar dynamics. *Astronomy and Astrophysics*, 161:139–141, 1986.

[47] W. Keck and R. T. Beyer. Frequency spectrum of finite amplitude ultrasonic waves in liquids. *The Physics of Fluids*, 3(3):346–352, 1960.

[48] S. Kida. Asymptotic properties of Burgers turbulence. *Journal of Fluid Mechanics*, 93(2):337–377, 1979.

[49] L. Kofman and A. Raga. Modeling structures of knots in jet flows with the Burgers equation. *The Astrophysical Journal*, 390:359–364, 1992.

[50] H.-O. Kreiss and J. Oliger. Stability of the Fourier method. *SIAM Journal on Numerical Analysis*, 16(3):421–433, 1979.

[51] J. D. Lambert. *Numerical methods for ordinary differential systems: the initial value problem*. John Wiley & Sons, Inc., 1991.

[52] L. Landau and E. Lifshitz. Fluid mechanics. *Course of Theoretical Physics*, 1987.

[53] S. Leibovich and A. Seebass. Examples of dissipative and dispersive systems leading to the Burgers and the Korteweg-deVries equations(dissipative gas dynamics and shallow water waves). *Nonlinear waves.(A 74-20717 07-23) Ithaca, N. Y., Cornell University Press, 1974,*, pages 103–138, 1974.

[54] H. W. Liepmann and A. Roshko. *Elements of gasdynamics*. Courier Corporation, 2001.

[55] M. J. Lighthill. Viscosity effects in sound waves of finite amplitude. *Surveys in mechanics*, 250, 1956.

[56] T.-P. Liu. Hopf-Cole transformation. *Bulletin of the Institute of Mathematices Academia Sinica New Series*, 12(1):71–101, 2017.

[57] B. Lohar and P. Jain. Variable mesh cubic spline technique for N-wave solution of Burgers' equation. *Journal of Computational Physics*, 39(2):433–442, 1981.

[58] A. M. Loske. *Medical and biomedical applications of shock waves*. Springer, 2017.

[59] E. Mach and P. Salcher. *Photographische Fixirung der durch Projectile in der Luft eingeleiteten Vorgänge*. K. k. Hof-u. Staatsdruckerei, 1887.

[60] E. Mach, O. Tumlirz, and C. Kögler. *Über die Fortpflanzungsgeschwindigkeit der Funkenwellen*. Kk Hof-und Staatsdruckerei, 1878.

[61] Y. Maday, A. T. Patera, and E. M. Rønquist. An operator-integration-factor splitting method for time-dependent problems: application to incompressible fluid flow. *Journal of Scientific Computing*, 5(4):263–292, 1990.

[62] Y. Maday and A. Quarteroni. Legendre and Chebyshev spectral approximations of Burgers' equation. *Numerische Mathematik*, 37(3):321–332, 1981.

[63] Y. Maday and A. Quateroni. Approximation of Burgers' equation by pseudo-spectral methods. *ESAIM: Mathematical Modelling and Numerical Analysis-Modélisation Mathématique et Analyse Numérique*, 16(4):375–404, 1982.

[64] C. Mavriplis. Adaptive mesh strategies for the spectral element method. *Computer methods in applied mechanics and engineering*, 116(1-4):77–86, 1994.

[65] J. Mendousse. Nonlinear dissipative distortion of progressive sound waves

at moderate amplitudes. *The Journal of the Acoustical Society of America*, 25(1):51–54, 1953.

[66] P. A. Milewski and E. G. Tabak. A pseudospectral procedure for the solution of nonlinear wave equations with examples from free-surface flows. *SIAM Journal on Scientific Computing*, 21(3):1102–1114, 1999.

[67] J. P. Moran and S. Shen. On the formation of weak plane shock waves by impulsive motion of a piston. *Journal of Fluid Mechanics*, 25(04):705–718, 1966.

[68] H. Nguyen and J. Reynen. A space-time finite element approach to Burgers' equation. *Numerical Methods for Non-Linear Problems*, 2:718–728, 1982.

[69] H. Ockendon and D. Spence. Non-linear wave propagation in a relaxing gas. *Journal of Fluid Mechanics*, 39(2):329–345, 1969.

[70] H. Ockendon and A. B. Tayler. *Inviscid fluid flows*, volume 43. Springer Science & Business Media, 2013.

[71] R. Peyret. *Spectral methods for incompressible viscous flow*, volume 148. Springer Science & Business Media, 2013.

[72] A. D. Pierce. *Acoustics: an introduction to its physical principles and applications*, volume 20. McGraw-Hill New York, 1981.

[73] A. D. Pierce and J. Kang. Molecular relaxation effects on sonic boom waveforms. *Frontiers of nonlinear acoustics: Proceedings of the 12th ISNA*, pages 165–170, 1990.

[74] A. D. Pierce and V. W. Sparrow. Relaxation and turbulence effects on sonic-boom signatures. In *Proceedings, 1st Annual HSR Workshop*, pages 14–16, 1992.

[75] S. D. Poisson. Memoir on the theory of sound. *J. Ecole Polytech. Paris*, 7:319–370, 1808.

[76] A. Polyakova, S. Soluyan, and R. Khokhlov. Propagation of finite disturbances in a relaxing medium. *Sov. Phys. Acoust*, 8:78–82, 1962.

[77] W. J. M. Rankine. XV. On the thermodynamic theory of waves of finite longitudinal disturbance. *Philosophical Transactions of the Royal Society of London*, (160):277–288, 1870.

[78] L. Rayleigh. CXII. The problem of the whispering gallery. *The London, Edinburgh, and Dublin Philosophical Magazine and Journal of Science*, 20(120):1001–1004, 1910.

[79] M. Renardy and R. C. Rogers. *An introduction to partial differential equations*, volume 13. Springer Science & Business Media, 2006.

[80] B. Riemann. *Über die Fortpflanzung ebener Luftwellen von endlicher Schwingungsweite*. Verlag der Dieterichschen Buchhandlung, 1860.

[81] J. Schofield and P. Hammerton. Numerical and asymptotic solutions of generalised Burgers' equation. *Wave Motion*, 51(6):919–934, 2014.

[82] Z.-S. She, E. Aurell, and U. Frisch. The inviscid Burgers equation with initial data of Brownian type. *Communications in Mathematical Physics*, 148(3):623–641, 1992.

[83] L. M. Smith and F. Waleffe. Transfer of energy to two-dimensional large scales in forced, rotating three-dimensional turbulence. *Physics of Fluids*, 11:1608–1622, 1999.

[84] L. M. Smith and F. Waleffe. Generation of slow large scales in forced rotating stratified turbulence. *Journal of Fluid Mechanics*, 451:145–168, 2002.

[85] G. G. Stokes. LIV. On a difficulty in the theory of Sound. *The London, Edinburgh, and Dublin Philosophical Magazine and Journal of Science*, 33(223):349–356, 1848.

[86] E. Tadmor. Convergence of spectral methods for nonlinear conservation laws. *SIAM Journal on Numerical Analysis*, 26(1):30–44, 1989.

[87] T. Tatsumi and S. Kida. Statistical mechanics of the Burgers model of turbulence. *Journal of Fluid Mechanics*, 55(4):659–675, 1972.

[88] G. I. Taylor. The conditions necessary for discontinuous motion in gases. In *Classic Papers in Shock Compression Science*, pages 409–420. Springer, 1998.

[89] J. W. Thomas. *Numerical partial differential equations: conservation laws and elliptic equations*, volume 33. Springer Science & Business Media, 2013.

[90] L. N. Trefethen. *Spectral methods in MATLAB*, volume 10. SIAM, 2000.

[91] G. Whitham. On the propagation of weak shock waves. *Journal of Fluid Mechanics*, 1(3):290–318, 1956.

[92] G. B. Whitham. *Lectures on wave propagation*, volume 61. Tata Institute of Fundamental Research Bombay, 1979.

[93] G. B. Whitham. *Linear and nonlinear waves*. John Wiley & Sons, 2011.

[94] G. Zemplén. Über die theorie der stoßwellen. *Physik. Z*, 13:498–501, 1912.